Naval Research Laboratory
Washington, DC 20375-5320 NRL/PU/5230--93-235 May 1993

Original contains color plates: All DTIC reproductions will be in black and white

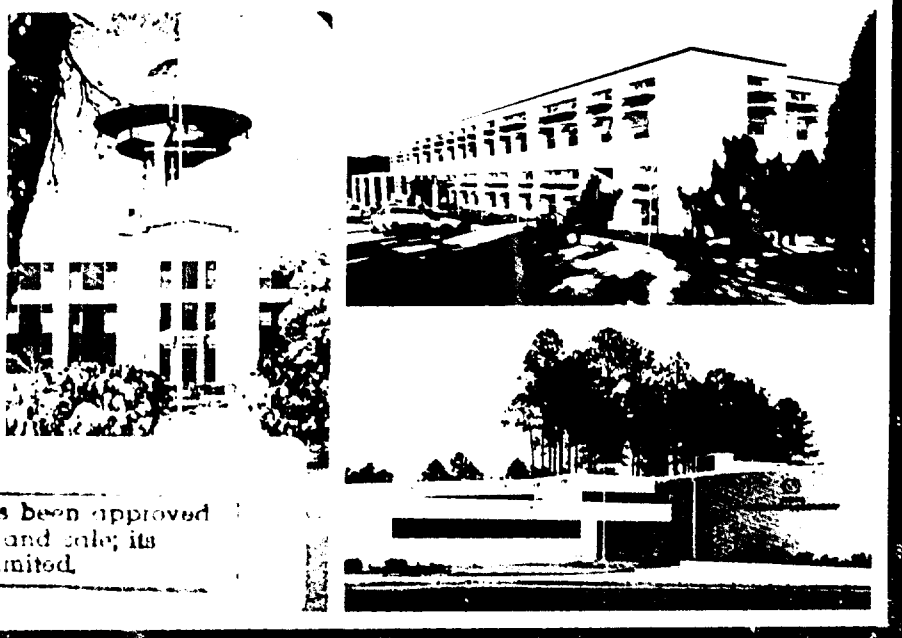

1993 NRL Review

In this *1993 NRL Review*, we present highlights of the unclassified research and development programs for fiscal year 1992. This book fulfills a dual purpose: it provides an exchange of information among scientists, engineers, scholars, and managers; it is also used in recruiting science and engineering professionals. As you read this *1993 NRL Review*, you will become even more aware that the Naval Research Laboratory is a dynamic team working together to promote the programs, progress, and innovations that will continue to foster discoveries, inventiveness, and scientific advances for the Navy of the future.

Cover: This year officially marks the consolidation of NRL and the Naval Oceanographic and Atmospheric Research Laboratory with campuses at Stennis Space Center, Bay St. Louis, Mississippi (NRL-SSC), and Monterey, California (NRL-MRY). The background multicolor image shows a satellite cloud classification from the visible and thermal channels of a NOAA weather satellite. This automated form of cloud classification is being implemented at NRL-MRY into the Tactical Environmental Support System (TESS), a shipboard environmental diagnostic/forecast system. The photo inset shows facilities at NRL-MRY (top right), NRL-SSC (bottom right), and NRL in Washington, DC.

DISCLAIMER NOTICE

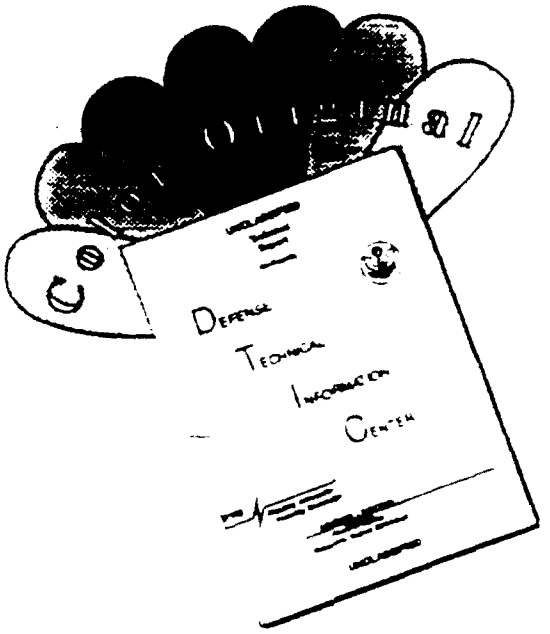

THIS DOCUMENT IS BEST QUALITY AVAILABLE. THE COPY FURNISHED TO DTIC CONTAINED A SIGNIFICANT NUMBER OF COLOR PAGES WHICH DO NOT REPRODUCE LEGIBLY ON BLACK AND WHITE MICROFICHE.

Contents

Mission

To conduct a broadly based multidisciplinary program of scientific research and advanced technological development directed toward maritime applications of new and improved materials, techniques, equipment, systems, and ocean, atmospheric, and space sciences and related technologies.

The Naval Research Laboratory provides

- **Primary in-house research for the physical, engineering, space, and environmental sciences**
- **Broadly based exploratory and advanced development programs in response to identified and anticipated Navy needs**
- **Broad multidisciplinary support to the Naval Warfare Centers**
- **Space and space systems technology development and support**

Preface

Naval Focus—National Impact

"...NRL's strength lies in its broad, multidisciplinary character and the willingness of great scientists and engineers from diverse fields to work together towards the best solution."

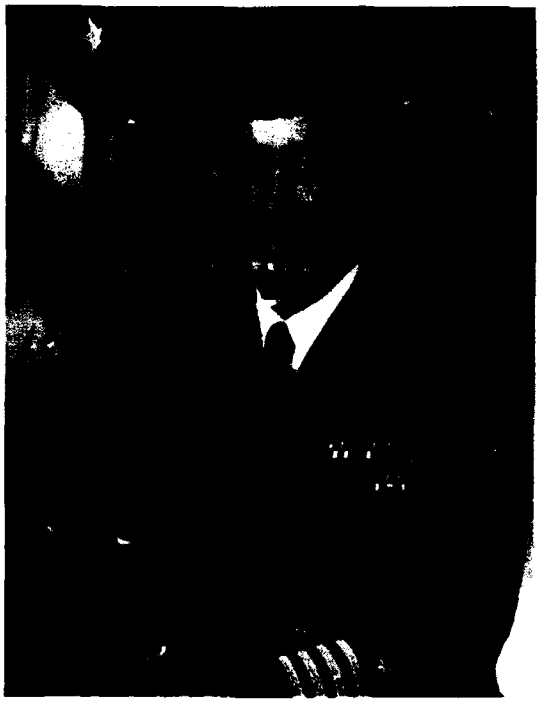

CAPT Paul G. Gaffney II, USN
Commanding Officer

There will always be debate about Service roles and missions and force structure. There is no debate, that in this maritime nation of ours, the Department of the Navy will be called upon continually to represent national interests globally. In peace, crisis or war, American leaders have always turned to the Sea Services first to demonstrate our resolve. To carry out that responsibility, the Navy and Marine Corps must stay technologically up to the task.

The Naval Research Laboratory has for 70 years, this year, been the centerpiece of science and technological innovation in the Department of the Navy. Our history is rich in contributions to a world-class Navy. Our unique capability to corporately address naval problems—a capability that Thomas Edison designed into NRL and one which the Navy leadership recently endorsed again seven decades later—ensures open-minded approaches to problem solving.

In the Laboratory's recent review of its strategic vision, we agreed that NRL's strength lies in its broad, multidisciplinary character and the willingness of great scientists and engineers from diverse fields to work together towards the best solution.

That broad, multidisciplinary capability, undeniably a Navy and Defense resource, is also a national treasure created to serve the American taxpayer. Domestic technology transfer legislation over the past several years now makes it easy, even attractive, for American industry to work with great Federal laboratories like NRL. We have committed to search out every opportunity to assist American commerce and industry to increase its technological edge through "partnership" vehicles, such as Cooperative R&D Agreements and joint licensing agreements.

While NRL is the Department of the Navy's Corporate Laboratory, it can continue to contribute in several areas as America's corporate laboratory, as well. We intend to ensure that the Navy of the future is technologically world-leading. At the same time, we intend to bring more of NRL's talent to bear on American industry's technical challenges.

During the past 70 years the Naval Research Laboratory has had many distinguished achievements, including the early discovery and development of radar in the United States, project Vanguard, and the technology program and satellite prototypes that resulted in the Global Positioning System (GPS). It is important to note that the Laboratory accomplished its long history of achievements over a period during which the world has changed remarkably. This was done by adhering to a basic set of principles regarding the advancement of science and technology in a mission-oriented activity, while at the same time adapting to a dramatically changing world. We are once again in a period of great change, and the Laboratory will adapt as it has during previous periods of great change. Part of that adaptation has always involved taking an inventory of what we have accomplished within our existing program to eliminate activities that have run their course and to identify those undertakings that are not going to pan out, either for technical reasons or because the marketplace that was driving their pursuit no longer exists. This must be done to impedance-match the Laboratory into the new world and to make the resources available to deal with the new problems that are arising. This is a time to build upon our many strengths and to establish partnerships, both inside and outside of the Laboratory, so that we may most rapidly accommodate the coming changes and most expeditiously respond to the many opportunities that lie ahead.

As we look to the future, there are a number of things that we must strive to do. We must ensure that the Laboratory maintains a broad base of competence in the physical, engineering, and environmental sciences and technologies. We must strive to maintain the Laboratory's independence while ensuring the relevance of its programs. We must find methods to provide quick response funding for new concept exploration. We must be prepared to identify a few winning concepts and run with them. And finally, we must constantly search for vehicles for transitioning NRL-developed technology to industry or to the Navy's Warfare Centers. A positive synergistic relationship between NRL and the Navy's Warfare Centers will be especially important in the coming years. These institutions must work together and work with American industry if the Navy is to have the technology it needs when the need is there.

Dr. Timothy Coffey
Director of Research

"This is a time to build upon our many strengths and to establish partnerships, ... so that we may most rapidly accommodate the coming changes and most expeditiously respond to the many opportunities that lie ahead."

The Naval Research Laboratory

NRL—Our Heritage

Today, when government and science seem inextricably linked, when virtually no one questions the dependence of national defense on the excellence of national technical capabilities, it is noteworthy that in-house defense research is relatively new in our Nation's history. The Naval Research Laboratory (NRL), the first modern research institution created within the United States Navy, began operations in 1923.

Thomas Edison's Vision—The first step came in May 1915, a time when Americans were deeply worried about the great European war. Thomas Edison, when asked by a *New York Times* correspondent to comment on the conflict, argued that the Nation should look to science. "The Government," he proposed in a published interview, "should maintain a great research laboratory.... In this could be developed...all the technique of military and naval progression without any vast expense." Secretary of the Navy Josephus Daniels seized the opportunity created by Edison's public comments to enlist Edison's support. He agreed to serve as the head of a new body of civilian experts—the Naval Consulting Board—to advise the Navy on science and technology. The Board's most ambitious plan was the creation of a modern research facility for the Navy. Congress allocated $1.5 million for the institution in 1916, but wartime delays and disagreements within the Naval Consulting Board postponed construction until 1920.

The Laboratory's two original divisions, Radio and Sound, pioneered in the fields of high-frequency radio and underwater sound propagation. They produced communications equipment, direction-finding devices, sonar sets, and, perhaps most significant of all, the first practical radar equipment built in this country. They also performed basic research, participating, for example, in the discovery and early exploration of the ionosphere. Moreover, the Laboratory was able to work gradually toward its goal of becoming a broadly based research facility. By the beginning of World War II, five new divisions had been added: Physical Optics, Chemistry, Metallurgy, Mechanics and Electricity, and Internal Communications.

The War Years and Growth—Total employment at the Laboratory jumped from 396 in 1941 to 4400 in 1946, expenditures from $1.7 million to $13.7 million, the number of buildings from 23 to 67, and the number of projects from 200 to about 900. During WWII, scientific activities necessarily were concentrated almost entirely on applied research. New electronics equipment—radio, radar, sonar—was developed. Countermeasures were devised. New lubricants were produced, as were antifouling paints, luminous identification tapes, and a sea marker to help save survivors of disasters at sea. A thermal diffusion process was conceived and used to supply some of the ^{235}U isotope needed for one of the first atomic bombs. Also, many new devices that developed from booming wartime industry were type tested and then certified as reliable for the Fleet.

NRL Reorganizes for Peace—Because of the major scientific accomplishments of the war years, the United States emerged into the postwar era determined to consolidate its wartime gains in science and technology and to preserve the working relationship between its armed forces and the scientific community. While the Navy was establishing its Office of Naval Research (ONR) as a liaison with and supporter of basic applied scientific research, it was also encouraging NRL to broaden its scope and become, in effect, its corporate research laboratory. There was a transfer of NRL to the administrative oversight of ONR and a parallel

Dignitaries watch as Secretary Josephus Daniels breaks ground for Building 1 on December 6, 1920. NRL was known then as the U.S. Naval Experimental and Research Laboratory.

shift of the Laboratory's research emphasis to one of long-range basic and applied investigation in a broad range of the physical sciences.

However, rapid expansion during the war had left NRL improperly structured to address long-term Navy requirements. One major task—neither easily nor rapidly accomplished—was that of reshaping and coordinating research. This was achieved by transforming a group of largely autonomous scientific divisions into a unified institution with a clear mission and a fully coordinated research program. The first attempt at reorganization vested power in an executive committee composed of all the division superintendents. This committee was impracticably large, so in 1949 a civilian director of research was named and given full authority over the program. Positions for associate directors were added in 1954.

The Breadth of NRL—During the years since the war, the areas of study at the Laboratory have included basic research concerning the Navy's environments of Earth, sea, sky, and space. Investigations have ranged widely from monitoring the Sun's behavior, to analyzing marine atmospheric conditions, to measuring parameters of the deep oceans. Detection and communication capabilities have benefited by research that has exploited new portions of the electromagnetic spectrum, extended ranges to outer space, and provided means of transferring information reliably and securely, even through massive jamming. Submarine habitability, lubricants, shipbuilding materials, fire fighting, and the study of sound in the sea, have also been steadfast concerns.

The Laboratory has pioneered naval research into space, from atmospheric probes with captured V-2 rockets, through direction of the Vanguard project—America's first satellite program—to involvement in such projects as the Navy's Global Positioning System. As part of the SDI program, the Low-Power Atmospheric Compensation Experiment (LACE) satellite was designed and built by NRL. Today, NRL is the Navy's lead laboratory in space systems research, fire research, tactical electronic warfare, microelectronic devices, and artificial intelligence. NRL has also evaluated new issues, such as the effects of intense radiation and various forms of shock and vibration on aircraft, ships, and satellites.

NRL's innovative research tradition in science and technology continued during this past year. A team of American and Russian scientists, working under the aegis of the 1987 U.S.-U.S.S.R. Civil Space Agreement, reported the discovery of a new belt of radiation trapped in the Earth's magnetic field. The belt is formed from the *anomalous* component of cosmic radiation. In another joint venture, NRL and Russian scientists studied the distribution of the cosmic ray produced isotope Beryllium-7.

These on-going ventures are exciting examples of cooperative scientific research in the post-cold war world.

NRL's Oriented Scintillation Spectrometer Experiment (OSSE) completed its initial set of observations to study a high-energy, variable point source of galactic radiation. One aim of the experiment is to determine the origin of diffuse high-energy emissions from the central region of the Milky Way galaxy. In other space and atmosphere related research, NRL scientists cooperated in developing a radiation-hardened space processor, the RH-3000; developed a new system to allow astronauts to determine the latitude and longitude of Earth features from photographic images; helped design and build a sensor to measure the global structure of the stratosphere and its chemical composition; and produced separate optical instrumentation for remote sensing of weather and atmospheric conditions from the National Oceanic and Atmospheric Administration's (NOAA) TIROS satellite and the platforms of the Defense Meteorological Satellite Program.

NRL scientists have also been active in the ocean environment. Researchers at the Laboratory cooperated with colleagues at NOAA to develop a specially modified sonar system that produces three-dimensional images of plumes from high-temperature seafloor springs. The sonar will facilitate studies of the dispersal of chemicals and heat from the springs. Additionally, scientists here developed a Central Atmosphere Measuring System (CAMS-II) to detect developing atmospheric conditions on U.S. atomic submarines. The analyzer detects and provides early warning of developing atmospheric conditions, which could pose a danger to the submarine crew or equipment. The CAMS-II is a modified and enhanced version of an earlier detector produced at NRL.

In other work, Laboratory chemists came up with a new technique for the deposition of thin films of biocompatible ceramics. The new technique is especially suited to the deposition of coatings of bonelike ceramics onto metal, ceramic, semiconductor, or polymer substrates. NRL scientists have been involved in providing modeled data in the form of digital realizations of complex scenes for strategic and theater missile defense applications. The so-called Strategic Scene Generation Model provides a physics-based, computer-aided design tool for use in system engineering applications. NRL researchers have also developed a new class of computer-vision operators that can be used to quickly identify and locate objects in range-finder images. The operators are mathematical structures that measure surface shape features for free-form shapes. The measurements are independent of the viewpoint from which the rangefinder observes the surface.

Finally, the Laboratory has continued to remain very active in the area of cooperative research and development agreements (CRADAs). CRADAs provide for the transfer of publicly funded technology to the commercial sector and allow for the government to cooperate in the commercialization process. During this calendar year, NRL entered into a half dozen such agreements with a wide range of industries, covering the fields of energy, analytical instruments, electronics, and laser manufacturing.

CAPT Paul G. Gaffney II (right) and CDR Larry R. Elliott cut the cake following the NRL/NOARL change of command ceremony. CAPT Gaffney officially received command of NRL Stennis and Monterey from CDR Elliott on January 14, 1992.

NRL Today

ORGANIZATION AND ADMINISTRATION

The position of NRL within the Navy is that of a field command under the Chief of Naval Research.

Heading the Laboratory with joint responsibilities are the naval commanding officer, CAPT Paul G. Gaffney II, USN, and the civilian director of research, Dr. Timothy Coffey. Line authority passes from the commanding officer and the director of research to five associate directors of research and an associate for business operations. Research is performed in the following areas:

- General Science and Technology
- Warfare Systems and Sensors Research
- Materials Science and Component Technology
- Ocean and Atmospheric Science and Technology
- Naval Center for Space Technology.

Further details of the Laboratory's organization that includes NRL-Stennis Space Center (NRL-SSC) in Mississippi and NRL-Monterey (NRL-MRY) in California are given on the organizational chart appearing in the "General Information" section. NRL-SSC and NRL-MRY are the result of a merger with NRL and the Naval Oceanographic and Atmospheric Research Laboratory (NOARL).

Through FY 92, NRL operated as a Navy Industrial Fund (NIF) activity. As a NIF activity, all costs, including overhead, were charged to various research projects. Funding in FY 92 came from the Chief of Naval Research, the Naval Systems Commands, and other government agencies, such as the Defense Advanced Research Projects Agency, the Department of Energy, and the National Aeronautics and Space Administration as well as several nongovernment activities. NRL's relationship with its sponsoring agencies, both inside and outside DoD, is defined by a comprehensive policy on interagency support agreements.

Besides funding for scientific work, NRL receives Navy monies for general construction, maintenance, and operations.

PERSONNEL DEVELOPMENT

At the end of FY 92, NRL employed 4051 personnel—36 military officers, 70 enlisted men

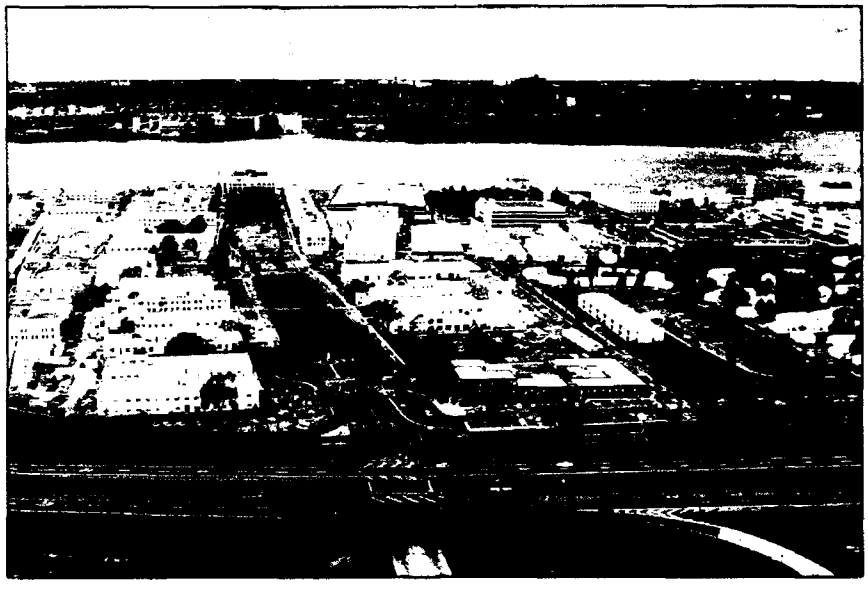

NRL today as viewed from the east

and women, and 3945 civilians. In the research staff, there are 878 employees with doctorate degrees, 465 with masters degrees, and 673 with bachelors degrees. The support staff assists the research staff by providing administrative, computer-aided designing, machining, fabrication, electronic construction, publication, personnel development, information retrieval, large mainframe computer support, and contracting and supply management services.

Opportunities for higher education and other professional training for NRL employees are available through several programs offered by the Employee Development Branch. These programs provide for graduate work leading to advanced degrees, advanced training, college course work, short courses, continuing education, and career counseling. Graduate students, in certain cases, may use their NRL research for thesis material.

For non-NRL employees, several postdoctoral research programs exist. There are also cooperative education agreements with several universities, summer and part-time employment programs, and various summer and interchange programs for college faculty members, professional consultants, and employees of other government agencies.

NRL has active chapters of Women in Science and Engineering, Sigma Xi, Toastmaster's International, and the Federal Executive and Professional Association. Four computer clubs meet regularly—NRL IBM-PC, Mac, NeXT, and Sun NRL Users Groups. An amateur radio club, a drama group (the Showboaters), and several sports clubs are also active. NRL has a recreation club that provides swimming, saunas, whirlpool bath, gymnasium, and weight-room facilities. The recreation club also offers classes in martial arts, aerobics, swimming, water-walking, and cardiopulmonary resuscitation.

A community outreach program at NRL provides tutoring for local students, science fair judging, participation in high school and college career day programs, an art and essay contest during Black History Month, student tours of NRL, and a Christmas party for disadvantaged children, with gifts donated by Laboratory employees. Through this program NRL has active partnerships with four District of Columbia public schools.

NRL has an active, growing Credit Union with assets of almost $150 million and a membership numbering over 18,000. Public transportation to NRL is provided by Metrobus.

For more information, see the *NRL Review* chapter entitled, "Programs for Professional Development."

SCIENTIFIC FACILITIES

In addition to its Washington, DC campus of about 130 acres and 152 buildings, NRL maintains 14 other research sites including a vessel for fire research and a Flight Support Detachment. The many diverse scientific and technological research and support facilities are described in the following paragraphs.

Research Facilities

- Radar

NRL has gained worldwide renown as the "birthplace of radar" and has maintained its reputation as a leading center for radar-related research and development for a half century.

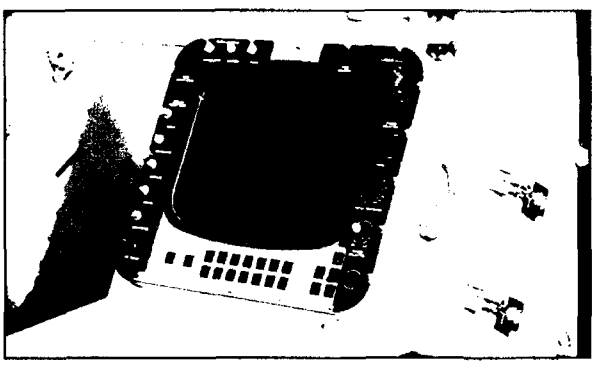

In its recent active operations dealing with drug interdiction, search and rescue, general law enforcement, and the Haitian exodus, the Coast Guard has been assisted by NRL-developed radar display equipment installed under the radar and distribution system (RADDS) program. The Radar Division's RADDS program has led to the development of the new SPA-25G raster-scan display as shown here. The SPA-25G has received widespread acceptance, and hundreds of models that have been produced are being deployed on surface ships and submarines.

An impressive array of facilities managed by NRL's Radar Division continues to contribute to this reputation. These include airborne and laboratory radar cross section measurement systems; two Ultrahigh-Resolution Inverse Synthetic Aperture Radars (ISAR), one for airborne installation and the other for shipboard installation; and a rooftop space-time adaptive array laboratory. Also, the division manages and maintains a radar display testbed, an IFF ground station, a digital signal processing facility, and a radar cross section prediction facility. A radar research and development activity is located at the Chesapeake Bay Detachment (CBD), Randle Cliffs, Maryland. It has separate facilities for specific types of systems that range from high-frequency, over-the-horizon systems to millimeter wave radars. The SENRAD radar testbed, a flexible and versatile system for demonstrating new developments in radar, and a point defense radar testbed are also located at CBD.

• Information Technology

The Information Technology Division is at the forefront of DoD research and development in artificial intelligence, telecommunications, computer networking, human-computer interaction, information security, parallel computation, and computer science.

The division maintains a local area computer network to support its research. This network interconnects about 400 machines, including personal computers (primarily Apple Macintosh), workstations (Sun/DTC-2, Hewlett-Packard/TAC-3, Silicon Graphics, NeXT, IBM RISC), file and computational servers, terminal servers, and printers. Major shared resources on the network include several Sun multiprocessor servers, a Convex minisupercomputer, and a Connection Machine with 16,384 processors and a 10-gigabyte parallel disk array. The network provides access to NRL's NICENET, the regional SURANET, MILNET, TWBNET, and the rest of the Internet system. The division also maintains comparable isolated facilities for classified processing. Other special facilities include an information security testbed network and an experimental facility

Scientists in the Information Technology Division are researching computer interface designs that may help to reduce automation deficit. Here is demonstrated the method used to select a tactical target (touchscreen in the left window), while using a joystick to simultaneously track a target in the right window.

with special displays, eye and gesture trackers, and speech I/O devices for research in human-computer interaction.

• Optical Sciences

Ultralow-Loss, Fiber-Optic Waveguides—NRL has developed record-setting ultrahigh transparency infrared waveguides. These fluoride glass materials offer the promise of long-distance communications without the need of signal amplification or repeaters.

Focal Plane Evaluation Facility—This facility has extensive capabilities to measure the optical and electrical characteristics of infrared focal plane arrays being developed for advanced Navy sensors.

IR Missile-Seeker Evaluation Facility—This facility performs open-loop measurements of the susceptibilities of infrared tracking sensors to optical countermeasures.

Large Optic, High-Precision Tracker—NRL has developed a tracker system with an 80-cm primary mirror for atmospheric transmission and target signature measurements. By using a quadrant detector, the servo system has demonstrated a 12-mrad tracking accuracy. An optical correlation tracker system tracks objects without a beacon.

High-Energy Pulsed Hydrogen Fluoride, Deuterium Fluoride Laser—NRL has constructed a pair of pulsed chemical lasers each capable of producing up to 30 J of laser energy at 2.7 to 3.2 mm and 3.8 to 4.5 mm in a 2-ms pulse. This facility is used to investigate a variety of research areas including stimulated Brillouin scattering, optical phase conjugation, pulsed laser amplification, propagation, and beam combining.

Fiber-Optic Sensors—The development and fabrication of fiber-optic sensor concepts, including acoustic, magnetic, and rate-of-rotation sensors, are conducted in several facilities within the Laboratory's Optical Sciences and Acoustics Divisions. Equipment includes facilities for evaluating optical fiber coatings, fiber splicers, an acoustic test cell, a three-axis magnetic sensor test cell, a rate table, and various computers for concept analysis.

Digital Processing Facility—This facility is used to collect, process, analyze, and manipulate infrared data and imagery from several sources.

Emittance Measurements Facility—NRL routinely performs measurements of directional hemispheri al reflectance from 2 to 16 mm in the infrared by using a diffuse gold integrating sphere and a Fourier Transform Spectrophotometer (FTS). Sample temperatures can be varied from room temperature to 250°C and incidence angles from 0° to 60°.

• Electronic Warfare

The scope of research and development at NRL in the field of electronic warfare covers the entire electromagnetic spectrum, from basic technology research, component and subsystem development, to system design and effectiveness evaluation. Major emphasis is placed on providing the methods and means to counter enemy hostile actions in all battle phases, from the beginning—when enemy forces are mobilized for an attack—through the final engagement stages. For this purpose, NRL has constructed special research and development laboratories,

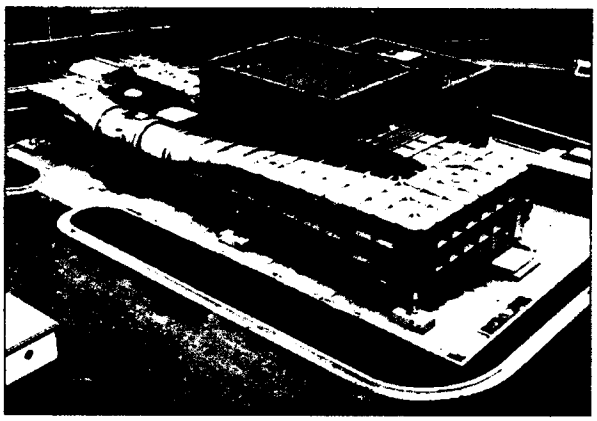

The Tactical Electronic Warfare's Offboard Test Platform (OBTP) is a continuous flow, low-speed wind tunnel that is optimized for testing small, expendable decoy air vehicles. The facility is especially well suited for the study of subsonic low Reynolds number aerodynamics because of its low turbulence intensity. Research includes studying the flowfield around various bodies of interest, obtaining force and moment data on the bodies, and dynamic testing of deployment systems and propulsion devices.

anechoic chambers, and facilities for modeling and simulation. NRL has also added extensive new facilities where scientists can focus on the coordinated use of all organic defensive and offensive resources now present in the Fleet.

• Structure of Matter

The Laboratory investigates the atomic arrangement of matter to improve old materials or to invent new materials. Various diffraction methodologies are used to make these investigations. Subjects of interest include the structural and functional aspects of energy conversion, ion transport, device materials, and physiologically active substances such as drugs, antibiotics, and antiviral agents. Theoretical chemistry calculations are used to complement the structural research. A real-time graphics system aids in modeling and molecular dynamics studies.

• Chemistry

NRL has been a major center for chemical research in support of naval operational requirements since the late 1920s. The Chemistry Division continues its tradition with a broad spectrum of basic and applied research programs concerned with controlled energy release

(fuels, fire, combustion, countermeasure decoys, explosives), surface chemistry (corrosion, adhesion, tribology, adsorbents, film growth/etch), advanced polymeric materials (high strength/low weight structures, drag reduction, damping, special function), and advanced detection techniques (environment, chemical/biological, surveillance). Facilities for research include a wide range of the modern photon electron, magnetic and ion-based spectroscopic/microscopic techniques for bulk and surface analysis; multiple facilities for materials synthesis and physical/chemical characterization; a 325-M^3 (11,400 ft^3) fire research chamber (Fire I), and a 475-ft ex-USS *Shadwell* (LSD-15) advanced fire research ship.

- Materials

NRL has capabilities for X-ray and electron diffraction analyses and for electron and Auger spectroscopy. It has a secondary ion mass spectrometer for surface analysis that significantly extends the diagnostic capability of the technique. A high-resolution, reverse-geometry mass spectrometer is used to probe reactions between ions and molecules. The Laboratory has a fully equipped fatigue and fracture laboratory, a modern vacuum arc melting furnace for reactive metals, an ultrasonic gas atomization system for making metal powders, and hot isostatic press facilities. The Laboratory's cryogenic facilities include dilution refrigerators and superconducting magnetic sensors for measuring ultrasmall magnetic fields. Also available are two molecular beam epitaxy devices for growing thin films.

- Laboratory for Computational Physics and Fluid Dynamics

The Laboratory for Computational Physics and Fluid Dynamics (LCP&FD) is a participant in the DARPA Touchstone Scalable Parallel Processing Project. An Intel IPSC/860 Touchstone Gamma supercomputer provides the environment necessary to develop, debug, and benchmark parallel simulations. With multi-MFLOP processors as building blocks, the computer is configured as a hypercube and is an MIMD distributed memory machine. This 32-node machine is expected to attain a computational speed of several hundred MFLOPS. Access to the 518-node Touchstone Delta machine at Cal Tech is also available.

LCP&FD has also developed a Graphical and Array Processing System (GAPS), which is an MIMD shared memory system. This system provides a significant computational engine for parallel computations, with real-time, high-resolution visualization, and simulation-steering capabilities.

Two IBM RS/6000 high-capacity workstation class-compute-server computers will provide LCP&FD with medium- to large-scale memory and computational power enabling the division to perform calculations, algorithm development, diagnostic, and evolution postprocessing for large simulations.

A 64-million word Convex C210 currently provides LCP&FD with medium performance scalar and vector capability for jobs that require large amounts of memory.

A high-quality video studio has been created that uses digital recording techniques to create graphical representations of simulation data for analysis and presentation.

Graphical workstations, including IRIS 4D vector display, Sun Microsystems, Tektronics, Metheus, and Macintosh are used.

- Condensed Matter and Radiation Sciences

The Condensed Matter and Radiation Sciences Division is the primary Navy center studying the effects of radiation on material items including electronic equipment, satellites, etc., and the condensation of materials (thin films) on other objects through the use of charged-particle radiation. The division approaches these activities from both the theoretical and applied aspects, including application to environmental as well as military situations. The facilities for production and employment of photons, electrons, ions, and hypervelocity projectiles available to the division include:

High-Powered Microwave (HPM) Facility—This facility is used to investigate the response of systems and components to pulsed high-

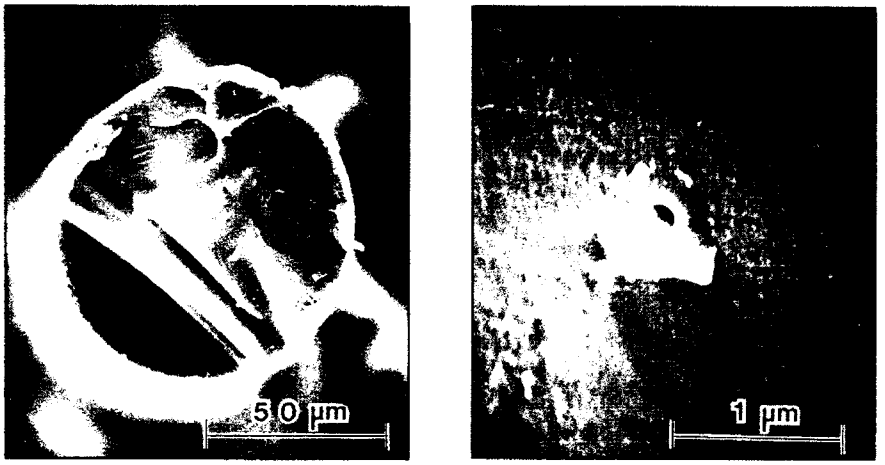

Co-investigators from NRL's Condensed Matter and Radiation Sciences Division and from the Carnegie Institute of Washington for the first time obtained useful X ray structure data from single crystals with submicrometer dimensions. Shown here is the end of a glass fiber with a fine Bi core. Scanning electron micrographs show cross section of the glass-enshrouded filament (left) and closeup of the bismuth (right). The ultrathin bismuth filaments were made by a researcher in the Materials Science and Technology Division.

power radiation. Effects, susceptibility, and survivability are the major research areas of interest. The large anechoic chamber (4.9 m × 4.9 m × 9.8 m long) can be used for frequencies ranging from 0.6 to 94 GHz.

Laser Facilities—The ultrafast lasers provide a broad range of capabilities by bringing together an extensive array of laser sources for the study of condensed matter interactions. Pulses of up to several joules are available from one system, while time resolutions down to 100 femtoseconds are produced by another. Synchronized, Q-switched oscillators are configured for pump-probe experiments. A range of optical, laser, and soft X-ray spectroscopes are used to study nonlinear optical effects, time response, and laser-target interactions.

X-ray Facility—Laboratory X-ray sources, monochromators, detectors, and related equipment are available for X-ray energies from 0.7 to 25 keV and the dose rates up to 10^5 rads/s.

Synchrotron Radiation Facility—Intense, monochromatic X-ray photon beams, tunable from 10 eV to 12 keV, are available from the three beam lines developed by NRL at the National Synchrotron Light Source at the Brookhaven National Laboratory. Standard measurements include X-ray diffraction, absorption, reflectance, and photoelectron emission. Environmental target chambers can span a pressure range from 10^{-12} to 10^5 atmospheres and temperatures from 10 to 1500 K.

60-MeV Electron Linear Accelerator (LINAC)—The LINAC produces intense electron beams that are used to study radiation effects on microelectronics and materials for DoD satellite and missile programs. It is also used to study radiation effects on the new, high-critical temperature superconductors.

Ion Implantation Facility—The facility consists of a 200-keV ion implanter with specialized ultrahigh vacuum chambers and associated in situ specimen analysis instrumentation. The facility is used to develop advanced surface treatments of materials to modify their properties and improve corrosion and wear resistance.

3-MeV Tandem Van de Graaff—This facility is used to study charged-particle radiation

damage effects such as occur in space, to perform Rutherford backscattering spectroscopy and nuclear reaction analysis, to provide high-sensitivity composition depth profiles, and to perform MeV energy implants in materials.

Hypervelocity Impact Facilities—Three facilities are used for ballistics research at speeds exceeding 6 km/s with toxic and explosive targets while measuring projectile velocity, orientation, and dynamic projectile-target interaction.

• Plasma Physics

The Plasma Physics Division is the major center for in-house Navy and DoD plasma physics research. The division conducts a broad experimental and theoretical program in basic and applied research in plasma physics, which includes laboratory and space plasmas, pulsed-power sources, electric mass launchers, intense electron and ion beams, atomic physics, laser physics, and numerical simulations. The facilities include an extremely high-power laser, Pharos III, for the laboratory simulation of space plasmas and high-latitude nuclear explosion effects studies. The division has developed a variety of pulsed-power sources to generate electron and ion beams, powerful discharges, and various types of radiation. The largest of these pulsers, GAMBLE II, is used to study the production of megampere electron beams and for producing very hot, high-density plasmas. Other generators are used to produce particle beams that are injected into magnetic fields and/or cavities to generate intense microwave pulses. A charged-particle-beam (CPB) propagation facility exists for testing advanced CPB propagation (both endo- and exoatmospheric) concepts. A 5-MW generator injects pulses of electron current into preheated ionization channels to study the effectiveness of propagation under various conditions.

• Electronics Science

In addition to specific equipment and facilities to support individual scientific and technology programs in electronics and electronic-materials growth and analysis, NRL operates the Nanoelectronics Processing Facility. The

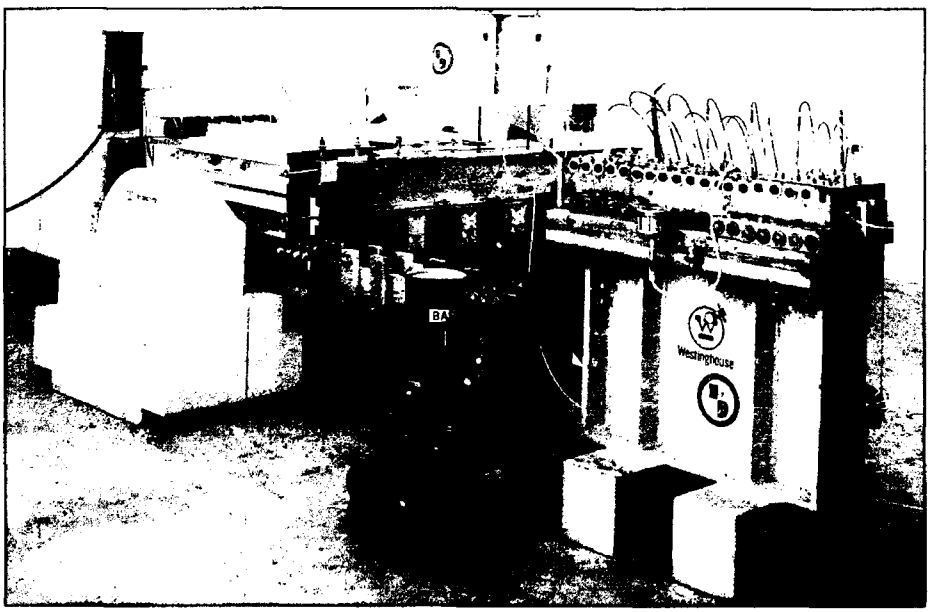

Plasma Physics Division's new facility, the Railgun Electric Launcher (a 1-m long railgun (front right)) is powered by a 0.5 MJ capacitor bank (rear). The railgun uses electric current to accelerate a projectile to very high velocities ($v > 2$ km/s). Applications include antiship missile defense, antitank weapons, long-range artillery, theater missile defense, and ultimately, space launch.

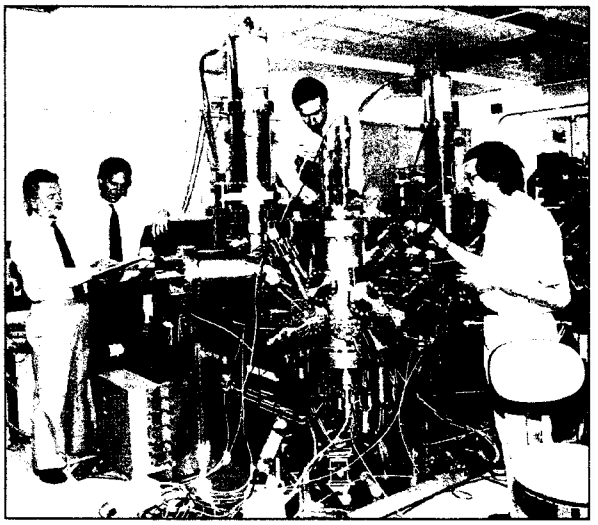

Scientists from the Electronics Science and Technology Division have developed a technique to fabricate silicon-on-insulator materials. Here the research team attends the Silicon Molecular Beam Epitaxy Facility, where this technique takes place.

Scientists from the Center for Bio Molecular Science and Engineering have developed a novel fiber optic biosensor that uses long fibers for analysis remote from the optical components. The fiber-optic biosensor is being developed to detect biological warfare agents, explosives, pathogens, and toxic materials that pollute the environment. Here a researcher prepares for operation of the biosensor system.

facility provides services to electronics programs throughout the Laboratory and to external organizations. This facility provides support for NRL programs that require microelectronics processing skills and equipment. The facility includes a nanowriter that can be used to fabricate nanoscale (80 Å) structures and, in general, supplies NRL programs with a range of items from discrete structures and devices to complete integrated circuits with very large scale integration (VLSI) complexity based on silicon metal oxide semiconductors (MOS) submicrometer technology.

- Bio/Molecular Science and Engineering

The Center for Bio/Molecular Science and Engineering conducts interdisciplinary research and development using modern biotechnology to solve problems for the Navy, the Department of Defense, and the nation at large. The approach to these problems involves long-term research of complex material systems, coupled with an integrated exploratory and advanced development program. Basic research programs focus on structure/function studies of biologically derived systems and may involve the engineering of molecules, characterizing submicron molecular systems, studying interactions of the systems with the environment, and assessing the applicability of these systems to the solution of Navy problems. Problems currently being addressed include biological warfare defense, combat casualty care, environmental quality (including pollution clean-up and control), and advanced material development (for electronic and structural applications). Center staff are drawn from the disciplines of biochemistry, biophysics, molecular biology, organic chemistry, solid-state and theoretical physics, and electronics and materials engineering. The center also has extensive interactions with external industrial and academic laboratories and other government facilities.

- Acoustics

NRL's facilities in support of acoustical investigations are located at the main Laboratory site; at Stennis Space Center in Bay St. Louis, Mississippi; and at the Underwater Sound Reference Detachment (USRD) in Orlando, Florida. At the main Laboratory site, there are three research tanks instrumented to study echo characteristics of targets and to develop devices. The most significant of the three is located in

the NRL Laboratory for Structural Acoustics in Building 5, which includes a state-of-the-art acoustic pool for conducting scale-model scattering and radiation studies. Capabilities include near-field acoustic holography for studying complex 3-D sound fields near a target and the vibrations of the target itself. NRL has successfully produced the first near-field acoustical-scattered hologram in this facility. Among the benefits of the holographic capability is that near-field measurements can be projected to the far field, and target strengths can be obtained in any desired direction. In general, the pool complex permits model studies and demonstrations to be carried out at scales ranging from about 30:1 to several hundred to one. Projects involving modeling include, but are not limited to, target strength, radiation, signature reduction, classification, and structural acoustics. Advanced hull sensor technologies can be studied at any scale. There is also an underwater acoustic holography facility for research in acoustic fields and a water tunnel having a large blow-down channel with a 15-m test section used for acoustic and flow-induced vibration studies of towed line arrays and flexible cables.

The division also has several acoustic receiver array systems used to collect data for coherent signal processing. The primary system consists of a 64-element, towed, seismic-type receiver array with the associated tow cable, winch, and electrical components. The towed array component can be replaced with a 64-element, fixed bottomed array or 64-element vertical array. There are also two radio telemetered, buoyed, acoustic receiver array systems with 20-element arrays capable of being vertically or horizontally deployed. All receiver arrays are interfaced into the At-sea Data Acquisition, Recording, and Real-time Processing System.

The high-frequency (up to 200 kHz) acoustic measurement systems obtain scattering, target strength, and propagation data by using facilities such as four large bottom-moored instrumentation towers and a high-speed, remotely operated vehicle. These data are used to simulate the performance of weapons and mine countermeasures in shallow-water environments. The mid-frequency (30-1000 Hz) towed horizontal array system is used to conduct studies leading to an understanding of the three dimensional characteristics of the acoustic ambient noise field; these will be used to develop tactics and advanced systems to exploit these characteristics. An acoustic simulation that is based on multiple workstations linked to a CRAY supercomputer provides benchmark simulations of acoustic performance based on high-resolution oceanographic and atmospheric environmental information.

- Remote Sensing

The Remote Sensing Division conducts a program of basic research, science, and applications to develop new concepts for sensors and imaging systems for objects and targets on the Earth and in the near-Earth environment, as well as in deep space. The research, both theoretical and experimental, leads to discovering and understanding the basic physical principles and mechanisms that give rise to the background environmental emissions and targets of

NRL-SSC researchers from the Remote Sensing Branch, along with researchers from the Navy/National Oceanic and Atmospheric Administration Joint Ice Center successfully located and tracked an Antarctic iceberg that eventually threatened shipping traffic. Iceberg A 24 (upper left-hand corner) is visibly portrayed in the remote sensing image taken on April 2, 1992.

interest and to absorption and emission mechanisms of the intervening medium. Accomplishing this research requires the development of sensor systems technology. The development effort includes active and passive sensor systems used for the study and analysis of the physical characteristics of phenomena that evolve from naturally occurring background radiation, such as that caused by the Earth's atmosphere and oceans and man-made or induced phenomena, such as ship/submarine hydrodynamic effects. The research includes theory, laboratory, and field experiments leading to ground-based, airborne, or space systems for use in remote sensing, astrometry, astrophysics, surveillance, nonacoustic ASW, and improved meteorological/oceanographic support systems for the operational Navy. Special emphasis is given to developing space-based platforms and exploiting existing space systems.

• Oceanography

The Oceanography Division is the major center for in-house Navy research and development in oceanography. It is known nationally and internationally for its unique combination of theoretical, numerical, and experimental approaches to oceanographic problems. Theoretical research makes extensive use of the Maury Oceanographic Library (jointly operated by NRL-Stennis Space Center (NRL-SSC) and the Naval Oceanographic Office), which is recognized as one of the best and most comprehensive oceanographic libraries in the world. The division numerically models the ocean on the Navy's most powerful supercomputer, the Primary Oceanographic Prediction System (POPS, operated by the Naval Oceanographic Office for both operational and research needs). The division operates a number of highly sophisticated graphics systems to visualize ocean models. The seagoing experimental programs of the division are particularly well supported. Unique measurement systems include towed sensor and advanced microstructure profiler systems for studying micro- and fine-scale ocean structure. The division uses a number of self-contained, multichannel in situ recording systems for acoustic and oceanographic measurements. The division deploys an integrated absorption cavity and optical profiler system for studying ocean optical characteristics. In the laboratory, the division operates an environmental scanning electron microscope for detailed studies of biocorrosion in naval materials.

• Marine Geosciences

The Marine Geosciences Division is the major center for in-house Navy research and development in marine geology, geophysics, geoacoustics, and geotechnology. It is also the Navy lead activity for mapping, charting, and geodesy research and development. The division has acquired unique instrumentation suites for its studies of the seafloor and its subbottom. These include side-scan sonar systems; deep-towed, low-frequency acoustic reflection systems; and parametric acoustic swath subbottom mapping systems. These systems allow studies ranging from sediment classification to mapping of inclusions and changes in the seafloor subbottom structure. The division deploys ocean bottom and subbottom seismometer systems for use in studies ranging from tectonic noise to studies of whale migration. Specialized seafloor probes allow measurement of the water pressure

As part of sample preparation for sediment fabric studies, a scientist from the Marine Geosciences Division advances the diamond knife toward the epoxy-embedded sample mounted in the ultramicrotome. The ultramicrotome cuts the sample into 500 to 1000 Å thick slices for viewing on the transmission electron microscope.

in sediment pores, acoustic compression, and shear wave velocity and attenuation. Laboratory equipment includes a transmission electron microscope with an environmental cell to carry out sediment-fabric and sediment-pollution absorption studies. The Map Data Formatting Facility, a collection of computers and work stations with associated graphics manipulation software, is used to compress map information onto compact disk read-only memory for Navy and Marine Corps aircraft digital moving maps. The division also operates the NRL Magnetic Observatory at SSC. This facility includes two specially built wood buildings with minimal ferrous content and arrays of magnetometers that extend radially from the building. The Magnetic Observatory measures the ambient magnetic field, its changes, and other magnetic phenomena. The Observatory is part of a worldwide observing system.

• Marine Meteorology

The Marine Meteorology Division of NRL is located in Monterey, California. NRL-Monterey (NRL-MRY) performs both basic and applied research in meteorology, in applications relevant to both central-site and shipboard meteorological analysis and forecasts. Located adjacent to the Fleet Numerical Oceanography Center (FNOC), the Navy's operational forecast center, NRL-MRY has developed both the global and regional forecast systems that are run at FNOC and that provide worldwide Navy forecasts. NRL-MRY is also the technical direction agent for TESS(3), a minicomputer-based environmental diagnosis/forecast system designed for shipboard use. Advanced technologies in use include satellite meteorology, advanced numerical techniques, and artificial intelligence.

NRL scientists in the Marine Meteorology Division developed shipboard environmental support using the AN/SMQ-11 satellite receiver and the Tactical Environmental Support System (TESS). NRL-MRY is the lead laboratory for TESS(3), third phase of a system currently being deployed for bringing environmental data and software aboard our large combatants.

• Space Science

NRL is the Navy's main laboratory for conducting basic research and development in the space sciences. The Space Science Division has a number of commitments for space experiments in the areas of upper atmospheric, solar, and astronomical research aboard NASA, DoD, and other space projects. Division scientists are involved in major research thrusts that include ultraviolet remote sensing of the upper atmosphere, studies of the solar atmosphere by using spectrographic techniques, and studies of astronomical radiation ranging from the ultraviolet through cosmic rays. This includes the mission operations and data analysis facilities for NRL's OSSE experiment on NASA's Compton Observatory. The division maintains facilities to design, construct, assemble, and calibrate space experiments. A network of VAX computers, super minicomputers, image processing hardware, a PDS microdensitometer, and Cray and Connection Machine accesses are used to analyze and interpret space data. The division also operates the SDIO Background Data Center, which is a repository and analysis center for experimental data pertaining to natural backgrounds.

• Space Technology

In its role as a center of excellence for space systems research, the Naval Center for Space Technology (NCST) designs, builds, analyzes, tests, and operates spacecraft, as well

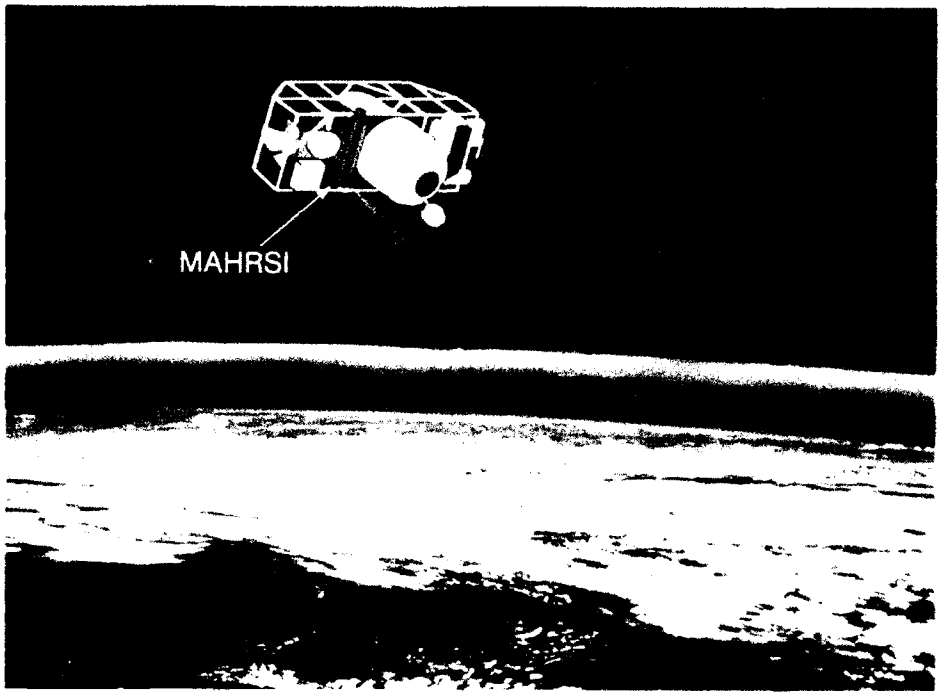

Scientists from the Space Science Division have developed a high resolution spectrograph that will be used to obtain data to help scientists gain a better understanding of the processes that create and destroy ozone in the atmosphere. Shown is an artist's concept of the middle atmosphere high resolution spectrograph investigation (MAHRSI) experiment. The MAHRSI is scheduled to fly in October 1994 on a mission sponsored by the German Space Agency in conjunction with NASA's ATLAS 3 flight.

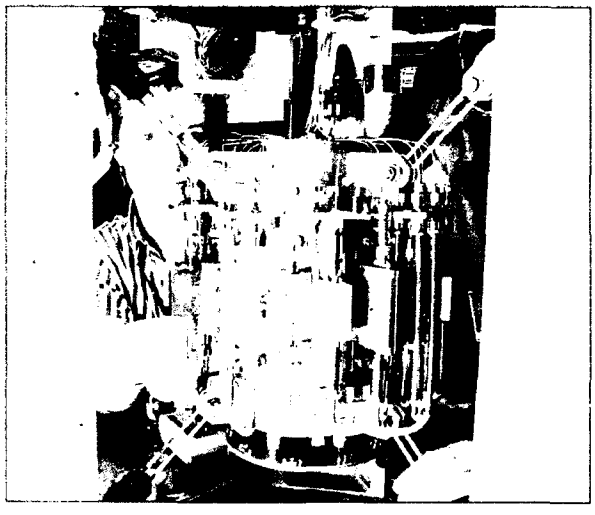

Researchers from the Space Systems Development Department observe the HTSSE I Flight Experiment Deck during cryogenic assembly.

as identifies and conducts promising research to improve spacecraft and their support systems. NCST facilities that support this work include large and small anechoic radio frequency chambers, clean rooms, shock and vibration facilities, an acoustic reverberation chamber, large and small thermal-vacuum test chambers, control system interaction laboratory, satellite command and control ground stations, fuels test facility, and modal analysis test facilities. NCST has a facility for long-term testing of satellite clock time/frequency standards under thermal-vacuum conditions linked to the Naval Observatory; a 5-m optical bench laser laboratory; and a hologram research laboratory to conduct research in support of the development of space systems.

Research Support Facilities

- Technical Information Services

The Ruth H. Hooker Research Library and Technical Information Center contains more than one million items, including current journals. Its collections can be searched by computer-based catalogs. The Library also

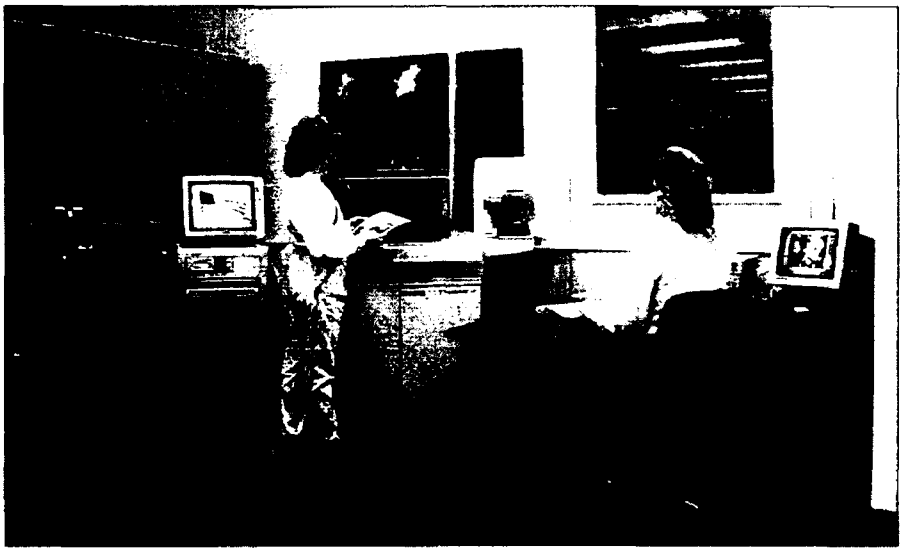

This photograph of the Technical Information Division's new Electronic Imaging Center was captured with a state-of-art digital camera

provides interlibrary loans, on-line literature searches, access to CD-ROM databases, loans of microcomputer software and laptops, and a full range of reference services, including assistance in selecting and using microcomputer software. Library resources that include an online catalog and a number of CD-ROM databases can be accessed from offices and laboratories through the InfoNet campus-wide information system.

Publication services include writing, editing, composition, phototypesetting, and publications consultation. The primary focus is on using computer-assisted publishing technology to produce scientific and technical information containing complex artwork, equations, and tabular material.

The research conducted at NRL requires a diversity of graphic support, such as technical and scientific illustrations, computer graphics, design services, photographic composites, calligraphy, display panels, sign making, and framing. A high-end workstation provides and delivers a new level of electronic airbrushing and photographic retouching.

Photographic services include high-speed motion picture, video, and still-camera coverage for data documentation both at NRL and in the field. A photographic laboratory offers custom processing and printing of black and white and color films. Photographic images can also be captured with state-of-the-art digital cameras and still video. Video services include producing video reports of scientific and technical programs. A video studio and editing facility with 3/4 in. and VHS editing equipment support video production.

The Electronic Imaging Center offers high-quality output from computer-generated files in PostScript, PICT, TIFF, and DICOMED DDC formats. The DICOMED film recorder produces high-resolution 35-mm slides, viewgraphs, and negatives. Photographic-quality color prints and viewgraphs are available from the Kodak XL7700. The Canon CLC500 scans color photographs to a Macintosh or PC disk. The Linotron Imagesetter produces gray-scale prints and transparencies at 1293 dpi.

- Central Computing Facility

The Central Computing Facility (CCF) features a Cray Y-MP EL/2-512 two-processor system with 512 megabytes of memory. The dual CPUs run on a clock cycle of 30 nanoseconds. The EL is configured with three VME-based I/O subsystems, providing a total bandwidth of 120 megabytes/second. Storage for the EL system is provided by eight DD-4 disk drives, each with 2.7 gigabytes of disk storage.

Together they provide over 21 gigabytes of disk storage. The DD-4 disk drives operate at sustained data transfer rates of 6 to 7 megabytes per second.

The EL system runs UNICOS, Cray Research Inc.'s UNIX-based operating system. Scientific, statistical, and mathematical software packages (including NAG, IMSL, and DISSPLA) are available to solve a wide range of problems. The primary programming languages for the Cray are FORTRAN, PASCAL, and C. Programs can be debugged locally on the EL and then scaled up easily to run on larger Cray Y-MP systems. The EL system provides a convenient platform for users to convert their Cray X-MP COS programs and data to UNIX. Software tools are available on the EL system to allow users to read COS PDSDUMP and ARCHIVE format tapes.

In addition to the Cray, the CCF also provides support for general-purpose computing, such as text editing, e-mail, etc. VMS users work on a cluster of VAXes, while UNIX users work on the CCF Sun, a Sun SPARCserver 470 system. The CCF is integrated with the NRL File Server/Archiver (FS/A), which provides 64 gigabytes of online storage in the form of CDC Disk Array Subsystems and 1.5 terabytes of nearline storage featuring advanced robotics from Storage Technology in an automated tape cartridge system. A CDC 4680 RISC processor functions as the FS/A file server.

The RCD Visualization Lab functions as an information center, video production unit, and training center for the latest tools in scientific visualization. Using either Macintoshes or UNIX workstations from Silicon Graphics, Sun, IBM, Hewlett Packard, or Stardent, scientists can turn the results of their computations into color prints, 35mm slides, or a video tape. Supported software includes AVS, IRIS Explorer, Wavefront Advanced Visualizer, and various tools from NCSA, FAST, and Khoros.

All of the CCF facilities listed above are accessed through the NRL local area network, NICENET, which includes a new local FDDI network. Through NICENET, the CCF has access to the Internet both through the DDN MILNET and through SURAnet to the NSFnet backbone. Dial-in modem access is also available.

FIELD STATIONS

NRL has acquired or made arrangements over the years to use a number of major sites and facilities for research. The largest facility is located at the Stennis Space Center (SSC) in Bay St. Louis, Mississippi. Others include a facility at the Naval Postgraduate School in Monterey, California, the Chesapeake Bay Detachment (CBD) in Maryland, and the Underwater Sound Reference Detachment (USRD) in Orlando, Florida. Additional sites are located in Maryland, Virginia, Alabama, and Florida.

One of NRL's specially configured P-3 aircraft at NRL FSD

- Flight Support Detachment (NRL FSD)

Located on the Patuxent River Naval Air Station at Lexington Park, Maryland, NRL's FSD operates and maintains four uniquely modified P-3 Orion turboprop aircraft that are used as airborne research platforms. The detachment has a flawless safety record, having amassed 46,000 hours of accident-free flying over a 29-year period. These aircraft annually log over 1200 flight hours worldwide and are the sole airborne platforms for numerous projects such as bathymetry, electronic countermeasures, gravity mapping, and radar development research.

- Chesapeake Bay Detachment (CBD)

CBD occupies a 168-acre site near Chesapeake Beach, Maryland, and provides facilities

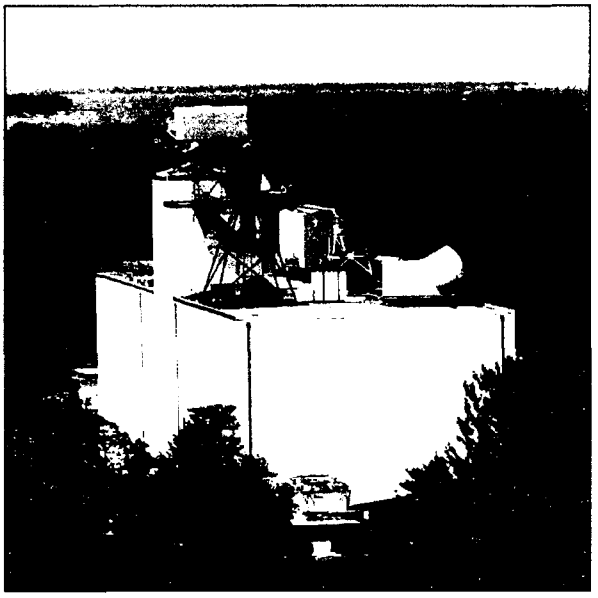

This laboratory at CBD is located on the cliff overlooking the Chesapeake Bay and was specifically constructed to bear the load of numerous radar antennas. The laboratory houses a Shipboard Radar Display Facility built around the AN/SPA-25G, which provides a brighter, more controllable and more easily read radar display. The facility includes not only SPA-25G displays but also large-screen displays, small-screen plasma status boards, a new solid-state switchboard, a radar-output recorder, a display-output recorder, and a fiber-optic data link.

and support services for research in radar, electronic warfare, optical devices, materials, communications, and fire research. Because of its location high above the Chesapeake Bay on the western shore, unique experiments can be performed in conjunction with the Tilghman Island site 16 km across the bay from CBD. Some of these experiments include low clutter and generally low background radar measurements. By using CBD's support vessels, experiments are performed involving dispensing chaff over water and radar target characterizations of aircraft and ships. Basic research is also conducted in radar antenna properties, testing of radar remote sensing concepts, use of radar to sensor ocean waves, and laser propagation. CBD also hosts facilities of the Navy Technology Center for Safety and Survivability, which conducts fire research on simulated carrier, surface, and submarine platforms.

- Underwater Sound Reference Detachment (USRD)

Located at Orlando, Florida, USRD functions as a link in the traceability of underwater sound measurements to the National Institute of Standards and Technology and also performs R&D for sonar transducers and related acoustic materials. Its semitropical climate and clear, quiet lakes (nearly circular and 11-m deep) is a distinct asset to its research and development on sonar transducers and underwater reference standards and to its improvement of techniques to calibrate, test, and evaluate underwater acoustic devices. USRD has two large, high-pressure tanks for simulating ocean depths to approximately 700 m and 2100 m. Smaller pressure tanks simulate depths to approximately 7000 m. A spring-fed lake, located in a remote area about 40 miles north of USRD (the Leesburg Facility), provides a natural tank for water depths to 52 m with an ambient noise level 10 dB below that for sea state zero; larger objects can be calibrated here. A 15-cm shock tube simulates 60 pounds of high explosive at a range of 20 ft for shock testing small sonar transducers. The detachment provides acoustic equipment and calibration services not only to hundreds of Navy activities and their contractors but also to private firms and universities not engaged in DoD contracts.

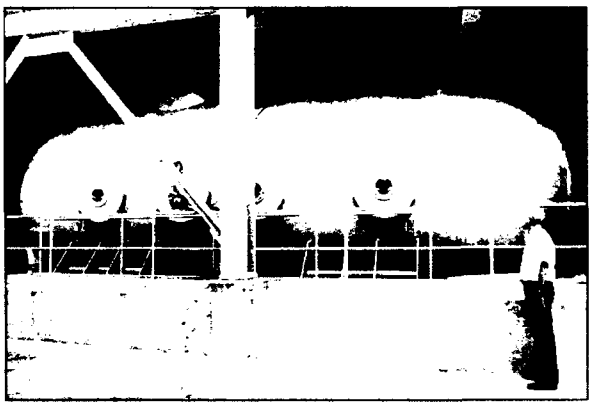

USRD's new acoustic measurement tank is capable of testing transducers or materials to 3000 psi at temperatures from 2° to 40°C

- Marine Corrosion Test Facility

Located on Fleming Key at Key West, Florida, this facility offers an ocean-air environment and clear, unpolluted, flowing seawater for studies of environmental effects on materials. Equipment is available for experiments involving weathering, general corrosion, fouling, and electrochemical phenomena, as well as coatings, cathodic protection devices, and other means to combat environmental degradation.

- Naval Research Laboratory-Stennis Space Center (NRL-SSC)

NRL-SSC, a tenant activity at NASA's Stennis Space Center (SSC) is located in the southwest corner of Mississippi about 50 miles northwest of New Orleans, Louisiana, and 30 miles from the Mississippi Gulf Coast. SSC encompases over 200 square miles of land area including a perimeter *buffer* zone to insulate surrounding civilian communities from the noise of rocket engine testing by NASA. Other Navy tenants at SSC include the Commander, Naval Oceanography Command, and the Naval Oceanographic Office, who are major operational users of the oceanographic and atmospheric research and development performed by NRL. The Naval Oceanographic Office provides access for NRL researchers to the Navy's largest supercomputer. This unique concentration of operational and research oceanographers makes SSC the center of naval oceanography and the largest such grouping in the world.

NRL-SSC provides administrative and business operations support for NRL's Center for Environmental Acoustics, Remote Sensing Applications Branch, Oceanography Division, and Marine Geosciences Division. NRL-SSC occupies over 200,000 square feet of research, computation, laboratory, administrative, warehouse, and other facilities at SSC. Facilities include a number of large antennas to receive available oceanographic and meteorological satellite data, a Magnetic Observatory building constructed of nonferrous materials in an electromagnetically quiet area of SSC, a Pattern Analysis Laboratory, a Map Data Formatting Facility, a water-wave channel, and numerous laboratories for acoustic and oceanographic computation, instrumentation, analysis, and testing. Special areas are available for construction, staging, refurbishment, and storage of seagoing equipment.

- Marine Meteorology Division Monterey, California (NRL-MRY)

Located in Monterey, California, as a tenant activity of the Naval Postgraduate School, this facility is collocated with the Fleet Numerical Oceanography Center (FNOC) to support development and upgrades of numerical atmospheric forecast systems and related user products. NRL-MRY's mission has broadened considerably to include basic research and support to other customers. Collocation with FNOC has the return benefit to NRL of making available state-of-the art mainframe computer resources and real-time and archived global atmospheric and oceanographic databases for research on site and at other NRL locations.

NRL-MRY's experience extends to prototype distributed (regional and shipboard) database management and prediction systems. A prototype third-generation system, the Tactical Environmental Support System (TESS(3)), has been developed for SPAWAR and is undergoing various upgrades on site. TESS(3) is functioning as an R&D testbed for new tactical/environmental decision aids (TDA's/EDA's). Environmental components of future systems for the Navy and other agencies are being developed within a system rooted in commercially available database management software; this system, the Naval Environmental Operational Nowcasting System (NEONS), creates an environment that allows new products for weather and ocean forecasters to be developed from a blending of satellite and conventional data. Both orbiting and geostationary satellite data receivers are located at NRL-MRY.

• Other Sites

Some field sites have been chosen primarily because they provide favorable conditions to operate specific antennas and electronic subsystems and are close to NRL's main site. Maryland Point, south of NRL, operates two radio telescopes (25.6 and 26 m in diameter) for radio astronomy research. Pomonkey, a field site south of NRL, has a free-space antenna range to develop and test a variety of antennas. The antenna model measurement range in Brandywine, Maryland, has a 4.6-m diameter turntable in the center of a 305-m diameter ground plane for conducting measurements on scale-model shipboard and other antenna designs.

• Advanced Space Sensing

The Midway Research Center (MRC), located in Virginia, is now an operational facility dedicated solely to space-related applications in naval communications, navigation, and basic research.

• Research Platforms

NRL uses ships and aircraft to conduct some of its research. Ocean-going research ships are obtained from a pool of vessels maintained by the Naval Oceanographic Office, Stennis Space Center, Mississippi.

NRL in the Future

To continue its growth and provide preeminent research for tomorrow's Navy, NRL must maintain and upgrade its scientific and technological facilities at the forefront. Its physical plant to house these facilities must also be adequate. NRL has embarked on a Corporate Facilities Investment Plan (CFIP) to renew its physical plant. This plan and future facility plans are described below.

THE CORPORATE FACILITIES INVESTMENT PLAN (CFIP)

The CFIP is a financial spending plan to provide modern research facilities at NRL by the year 2000. The plan calls for both Congressional and Laboratory investment and is updated and altered as changes occur in scientific emphasis and Congressional attitude. Over the past several years, Congressionally approved military construction (MILCON) funds were used to construct the new Electro-Optics Laboratory and to complete the final phase of the Tactical Electronic Warfare Facility. At this time, funds have been provided to build a second wing to the Electro-Optics Building, and funds have been requested for a facility to house the Naval Center for Space Technology and an advanced Materials Research Building.

In the past years, NRL's general and administrative (G&A) funds were used to renovate Buildings 16, 32, 34, 35, 46, 47, 56, 58, 72, 101, A-11, and A-13 and major portions of several other buildings. Approximately $4 million of Laboratory funding is budgeted for modernization each year.

• Radar

The Radar Division and the Naval Center for Space Technology have jointly established a new microwave test facility located in Building A-59. This compact range facility will allow test and evaluation of antennas and radar targets over a frequency range of 1 to 100 GHz. The indoor range and supporting laboratories occupy approximately 6000 ft^2 of space. Test objects up to 8-ft diameter can be accommodated. This facility obviates the need for an outdoor test range several thousand feet in length, achieving far-field radiation conditions from a large, prime focus, parabolic reflector.

• Optical Sciences

In FY 91, NRL began construction of the second phase of the Electro-Optics Research Laboratory (MILCON Project P-115). This will

be a 50,000-ft^2 addition to the existing Building 215 and will accommodate approximately 120 scientists and engineers and their research facilities. Completion and occupancy should occur during the second and third quarter of FY 93. This will allow activities currently in Buildings 12 and 30 to be consolidated with those already in Building 215 and the adjacent Building A-50. In addition to putting all fiber optics and glass materials under one roof, it will accomplish replacement of obsolete silica glass facilities with new state-of-the-art facilities. It will also allow closer coordination between the infrared detector development activity and sensor system activities. The new structure contains spaces specially designed for testing and modelling sensors.

- Shock Test Facility

A new facility for shock testing small transducers has been introduced at the Underwater Sound Reference Detachment. The present capability of the shock tube duplicates the MILSTD open-water shock tests but with a size limitation that the test object fit inside a 6-in. diameter cylinder. An extension of the shock tube to 10-in. diameter is under construction and should become operational sometime in FY 93.

- Center for Materials Research

The Department of the Navy is in the process of programming construction of a special-purpose laboratory. This special facility will provide stringently clean laboratories with carefully controllable temperature, humidity, vibration isolation, ambient dust, and power for investigations in the rapidly evolving fields of electronic technology and nanometrics.

- Plasma Physics

A major 2-kJ KrF-laser facility will be established in the Plasma Physics Division by the end of FY 94. This facility is being initiated to provide intense radiation for studying inertial confinement fusion target heating at short wavelengths. A large-volume (2-m diameter by 5-m long) space chamber facility was completed in FY 92 to do space plasma physics research in the laboratory. A uniform axial magnetic field up to 1 kG and adjustable plasma density and temperature allow great flexibility to study laboratory simulation of space phenomena under controlled conditions.

- Electronics Science and Technology

Important division emphasis is focused on the continual upgrading of the Nanoelectronics Processing Facility and expanding activities in the nanoelectronics physics and vacuum electronics programs. A new penthouse facility has been planned for Building 208, which will consolidate and upgrade existing facilities for processing III-V semiconductor material devices. The penthouse facility will serve the research needs of individual scientists within the division.

- Center for Bio/Molecular Science and Engineering

Beginning in January 1993, Building 30 will be renovated to accommodate the growing and diverse research programs of the Center for Bio/Molecular Science and Engineering. When completed, the center will have over 32,000 ft^2 of modern laboratory and office space. These facilities will include laboratories for biochemistry, organic synthesis, surface chemistry, and spectroscopy. Specialized facilities will include controlled-environment rooms, an advanced computer graphics laboratory, electron and scanning microprobe laboratories, and a submicron and nanostructure fabrication and characterization laboratory. Ample space is provided in which the center's interdisciplinary staff can meet and discuss joint projects. Renovations are expected to be complete in the third quarter of FY 94.

- Vacuum Ultraviolet Space Instrument Test Facility

The Space Science Division has installed a new vacuum ultraviolet space instrument test facility. This facility is capable of housing space instrumentation up to 2 m in diameter and

5 m in length. While exposed to high vacuum (10^{-7} torr), instruments can be illuminated by a simulated solar spectrum for alignment and verification tests. The facility also includes a 13-m evacuated extension containing sources to simulate the solar corona. An externally mounted 1-m diameter heliostat will be employed to project a beam from the Sun directly into the vacuum chamber. In the near future, the facility will be used to test space instruments that are presently under development for flight on the European Space Agency's Solar and Heliospheric Observatory spacecraft.

• Midway Research Center

NRL's newest field site, the Midway Research Center (MRC), is located on a 158-acre site in Stafford County, Virginia. Located adjacent to the Quantico Marine Corp Base's Combat Development Command, the MRC will have approximately 10,000 ft^2 of operations and administration area and three precision 18.5-m diameter parabolic antennas housed in 100-ft radomes. When completed, the MRC, under the auspices of the Naval Center for Space Technology, will provide NRL with additional state-of-the-art facilities dedicated solely to space communications and research.

REHABILITATION OF SCIENTIFIC FACILITIES

Specialized facilities are being installed or upgraded in several of the research and support divisions.

• Flight Support Detachment

Currently, NRL's Flight Support Detachment's aircraft Bureau number 154589 is undergoing a major aircraft modification and service life extension and is scheduled to be operationally ready by June 1993. This aircraft will expand NRL's capabilities for airborne research projects well into the next century.

• Radar

The Radar Division has installed a computer aided engineering (CAE) facility to aid in digital system design. The system has seven full-color graphics workstations to provide capabilities for circuit design and simulation and printed circuit board layout. The facility has been used to design systems based on commercially available components as well as advanced systems incorporating VHSIC and gate array technologies. It has proven to be a valuable tool in evaluating new technologies for radar signal-processing requirements. The facility is currently being expanded to include Sun workstations and IDAS software, which will allow designs to be modeled and simulated at the system level. VHDL (VHSIC Hardware Description Language) software has been acquired for the workstations. This provides designers with an integrated toolset to model and simulate their designs from the system level down to the device level.

• Information Technology

The Information Technology Division continues to expand and upgrade its local area network and high-speed networking capabilities (including SONET/ATM technology), as well as its massively parallel and other computational resources. Personnel and facilities in Buildings 29 and 54 are moving to Building 34. In addition, specific facility upgrades are planned or in progress. An upgrade for the Human-Computer Interaction Laboratory will integrate and enhance its video and audio presentation and recording capabilities. A state-of-the-art head-coupled, boom-mounted, stereoscopic display will be used for research in man-machine dialog and virtual environments.

• Underwater Sound Reference

Installation of a new precision measurement system (PMS) is near completion in each of four facilities—at the Lake Facility, the Leesburg Facility, and the two large high-pressure tank facilities. PMS is a sophisticated, computer-controlled, signal-generation and data-acquisition system that provides significantly increased accuracy, dynamic range, and signal to noise than was previously available. It allows the use of new, sophisticated signal-processing techniques being developed for making lower frequency measurements on sonar transducers and

related acoustical coating materials under reverberation limited conditions, such as in the large, high-pressure tank facilities. PMS will also process acquired data very rapidly so that most results can be presented to customers at the time of the measurements.

• Materials Science and Technology

Renovation is proposed for Building 3, which is now made up of two of the original five buildings at NRL, to contain modern laboratories for studies of thin-film deposition and characterization, superconducting materials, magnetic materials, and other materials science projects. The new space will feature the most modern molecular beam epitaxy and other materials synthesis and processing equipment, an up-to-date fatigue and fracture laboratory and state-of-the-art diagnostic equipment, including electron microscopes, spectrometers, and electron and X-ray diffraction equipment. The renovated building will also contain office and laboratory space for approximately 70 technical personnel.

• Plasma Physics

A state-of-the-art short-pulse (< 1 ps) high-intensity (> 1 TW) Table-Top Terawatt (T^3) laser has been procured for a variety of physics studies. The T^3 laser will be integrated into the Pharos III Nd-laser facility to boost its power into the 10 to 100 TW range. This will provide a facility to do fundamental physics experiments in intense laser-plasma interactions and intense laser-electron beam interactions.

A low-frequency (300 MHz to 10 GHz), high-power microwave facility, which uses a relativistic klystron concept, is being upgraded to produce multigigawatt coherent radiation pulses. A new laser facility is also planned. It will use a powerful KrF laser and a target chamber to conduct inertial confinement fusion research.

A new electric mass launcher facility has been established to investigate the evolution of the plasma armature in a high-velocity railgun.

• Electronics Science and Technology

In a move to further meet existing safety standards, potentially hazardous III-V semiconductor processes and associated chemicals will be moved to the new penthouse facility in Building 208. This facility employs a single-pass air-ventilation system to minimize hazards to personnel.

Highlights of NRL Research in 1992

Point Defense Demonstration System

A problem with shipboard radar is the detection and tracking of low observable, sea skimmer threats while distinguishing between large numbers of nuisance targets (such as birds, insects, and sea spikes) and the target of interest. Scientists in the Radar Division have developed a new technique based on doppler measurements for distinguishing between these nuisance targets and sea skimmer threats. The premise for this technique is that all targets that are detectable using the full sensitivity of the radar will be detected and their velocities measured. Slow moving targets will be distinguished from the high-speed targets. This technique has been implemented into the advanced radar signal processor of the Point Defense Demonstration System. This accomplishment demonstrates that low observable skimmer threats can be detected at adequate ranges to support ship self-defense.

***

High-Power Semiconductor Broad Area Amplifiers

Researchers in the Optical Sciences Division have developed a new method for generation of high-power, diffraction-limited radiation through the use of traveling wave broad area diode amplifiers. These amplifiers generate diffraction limited emission at power levels up to 21 W, a factor 10 times greater than conventional laser diodes, and have an electrical-to-optical conversion efficiency much larger than that of other types of lasers. These amplifiers will improve the performance and practicality of many systems that previously had to rely on low-power laser diodes or inefficient solid-state lasers. They are well suited for use in optical printers, visual displays, surgery, remote sensing, satellite communications, and military applications such as optical target designators and illuminators, optical communication transmitters, and optical beacons.

***

Development of a Calibrator for Long-Line Underwater Acoustic Arrays

Navy towed arrays are presently calibrated one channel at a time to a plane wave sound field. The actual array sensitivity pattern that gives its through-the-beamformer response is never measured, and the arrays are never tested under environmental conditions because no facility exists in which these measurements can be made. A new calibration concept that measures actual array beam patterns has been successfully prototyped by the Underwater Sound Reference Detachment, and a facility incorporating this technique with environmental testing is under development. This new calibrator provides measurement capabilities not previously possible. Using this system, beam patterns of long arrays will actually be measured rather than theoretically calculated from individual channel data. Measurements made under an anticipated operating environment and where the entire array is exposed to the sound field could indicate potential array problems prior to fleet installation.

***

Structural Mapping of Ultrathin Films

As a reduction in film thickness generates new phenomena and as thinner films become utilized in technological applications, the detailed morphology of these films becomes increasingly important. As films become ultrathin, they can exhibit unique and extraordinary behavior. In many cases the film structure, interface abruptness, and thickness uniformity determine the film behavior. To understand the basis for this behavior, a detailed and complete structural description of the film/substrate system must be determined to avoid erroneous conclusions as to the physical mechanisms underlying the observed behavior. To completely characterize the structure and growth mode of ultrathin films and overlayers, Auger electron diffraction and X-ray photoelectron diffraction measurement techniques have been developed by researchers in the Materials Science and Technology Division. These techniques have been applied to ultrathin magnetic films and to semiconductor heterostructures to assist in completely describing the film structure that allows for accurate film synthesis and comparison with theoretical predictions.

***

Microwave Power Module

Increasingly sophisticated electronic systems require high specific transmitter power (watts/unit volume or weight) in the frequency bands of interest. This requirement of needed size and weight reduction is being met by the continuing development for near-term applications of a Microwave Power Module (MPM) by the Electronics Science and Technology Division as part of a Tri-Service/DARPA Vacuum Electronics Initiative. The MPM consists of a solid-state driver, a vacuum electronics power booster, and integrated power conditioning; the near-term applications include phased arrays, electronic decoys, and missile seekers. At its current stage of development, the MPM represents a significant size reduction (a transmitter hardware package of 20 $in.^3$ or less) and at least a four-fold improvement in specific power, providing 100 W CW over 6 to 18 GHz. In addition, the MPM target specifications support a common module for electronic warfare and radar applications.

***

Detection Systems for Biological Warfare Agents

Based on technology from ONT-supported development of a fiber-optic-based sensor using antibodies as a generic ultrasensitive detection method, a system for detecting biological warfare agents was developed by the Center for Bio/Molecular Science and Engineering to support the troops of Desert Storm/Shield. The system was composed of a DNA probe, a supporting fiber-optic-based sensor, and an antibody-based detection system. Immunoassays were worked out with a response time of < 1 min and sensitivities in the ng/ml range, and various DNA probes were prepared that recognized toxins and very small numbers of pathogenic organisms. The DNA probes were used successfully in the Desert Storm theater. Rapid, automated sensors employing antibodies and DNA as the detection elements can also be used for pollution control, process monitoring, detection of environmental hazards and drugs, and in clinical diagnosis.

***

Flow Immunosensor for Detection of Drugs of Abuse and Explosives

Federal agencies have an urgent need for ultrasensitive detection systems to monitor the environment for the presence of drugs and explosives. Responding to this need, an antibody-based biosensor was developed by the Center for Bio/Molecular Science and Engineering for rapid, ultrasensitive detection of small molecules present in environmental samples. These can be examined rapidly since there is no incubation period, and the system can be used for multiple analyses without the need for additional reagents. Analysis time is < 1 min. The laboratory prototype can detect TNT, cocaine, and other small molecular weight compounds present in aqueous samples at the ng/ml range within seconds of sample injection. Response is specific and proportional to the number of unknown molecules present. In collaboration with U.S. Alcohol Testing, Inc., a commercial instrument is being developed that will be used to detect the presence of drugs of abuse in urine.

***

Array Deconvolution Acoustic Transients in an Acoustic Waveguide

When an acoustic signal propagates in the ocean, it is distorted by the environmental characteristics of the bounding waveguide. The signal contains useful information about the sound source. The purpose of this work by the Acoustics Division was to locate the source within the waveguide and reconstruct its uncorrupted signature, given a set of passively received time series on a vertical array. Signal processors were developed successfully on the Connection Machine to solve this problem. Acoustic sources were accurately located up to 100 km from the array in a deep-ocean, multipath environment, and source signatures were accurately reconstructed by using real ocean data over a bandwidth of 25 to 110 Hz. The distortive nature of waveguide propagation makes it difficult to accurately classify acoustic sounds using pattern recognition techniques. By minimizing this distortion, the data passed to a classification scheme has high integrity, and the result should be a lower probability of classification error.

***

NRL'S OSSE Experiment on NASA'S Compton Observatory

The Oriented Scintillation Spectrometer Experiment (OSSE) is one of four gamma ray instruments on NASA's Compton Gamma Ray Observatory mission (launched in April 1991). The OSSE instruments that consists of four large scintillation detectors is conducting a broad-based program of gamma ray observations in the 50 keV to 10 MeV energy range in which high-energy nuclear processes occurring in very energetic sources—ranging from solar flares to massive black holes—can be studied. To date, observations have been made of active galactic nuclei, two recent supernovae (SN1987a and SN1991t), positron-annihilation radiation from the galactic center region, and several discrete galactic sources. Also observed was an intense period of solar activity, a radio flare from Cyg X-3, and three X-ray transients believed to contain stellar mass black holes. The technology relates to Navy and DoD interests in surveillance of nuclear materials, energetic solar phenomenon, monitoring atmospheric nuclear weapons tests, and tracking test debris.

***

Multimission Advanced Tactical Terminal (MATT)

The MATT system is a Space Systems Development Department technology development program for miniaturized communications products oriented towards tactical intelligence data reception and processing. The MATT system is the first miniaturized, ruggedized, and airborne qualified UHF communications terminal available to the U.S. military for intelligence data reception and processing. Multiple communications channels, embedded cryptographic devices, and processing capacity provide the capability to receive and process data from a multitude of links, and the MATT system makes near-real-time intelligence information available to a wide variety of military platforms that were previously prohibited from direct reception of this data because of the size and weight of earlier equipment.

***

Radar Sensing of Petroleum Seepage Gases

For several years oil exploration groups have considered the use of radar to sense the presence of petroleum seepage gases. Recently, the Radar Division has completed an initial investigation of this claimed technique. Experimental data indicate that unique radar returns were detected. Distinctive signal characteristics include: return signals from weak, distributed targets; signal amplitude variations of ≥ 10 dB and range changes of ± 60 ft, within time periods of one-third second; radar echoing volumes observed at ranges of < 2000 ft and at elevation angles $< 1°$. The range and amplitude varying radar returns were suppressed by rain and/or the presence of wet ground and during local nighttime conditions.

***

Compensating Digital Sidelobe Canceler Demonstration

Radars in a wartime scenario must contend with enemy jamming interference intentionally directed at the receiving antenna and entering the antenna sidelobes. The Radar Division has significantly advanced the state-of-the art in jammer suppression with new sidelobe canceler technology that is tolerant of a wide range of system imperfections. Techniques have been developed that significantly increase a radar's sensitivity in a jamming environment. These new techniques, which more than double the detection range of fleet radars, have been successfully demonstrated on the SPS-49 radar and are being transitioned to the fleet.

***

Measurement of the Dynamic Transfer Function and Polarization Matrix for Scattering Elements on a Water Surface

A major obstacle in establishing the basic physics of sea scatter is the need to measure the scattering properties of transient surface features that change their form rapidly during brief lifetimes. Data taken with wavetank instrumentation consisting of an ultrashort pulse radar and a scanning laser slope gauge have been used by the Radar Division to derive two basic scattering descriptors over the duration of a measured surface event—the dynamic scattering function and the polarization matrix. This laboratory capability shows great promise for disclosing the nature of sea scatter processes at a fundamental level and is expected to influence the future development of the physics of sea scatter, including scattering from rapidly changing natural targets.

***

Bayesian Reasoning Tool

Military personnel often have to sift through a complex flow of information to solve problems and make critical decisions in short periods of time. Rapid identification of relevant information and flexible interpretation of partial results are required for effective computer-based decision making. Motivated by the problem of ship classification, a Bayesian Reasoning Tool (BaRT) has been developed by the Center for Applied Research in Artificial Intelligence, which provides software for the management of uncertain evidence. Suited to the support of probabilistic reasoning in target classification problems, BaRT has broader applicability to any domain where evidence must be combined in support of high-level hypotheses. BaRT is an innovative mix of classical probabilistic reasoning and research in artificial intelligence.

***

Fiber-Optic Electric Field and Voltage Sensors Based on the Electrostrictive Effect

Electric field sensors based on conventional electric field technology are limited in resolution and require large antenna lengths while fiber-optic, low-frequency electric field sensors can provide significantly higher resolution and shorter baselines. Such high resolution fiber-optic dc and low frequency voltage sensors based on the electrorestrictive effect have been demonstrated by the Radar Division. The self noise of the fiber-optic device rivals that of conventional voltage sensors, and it has the potential to achieve self noise at least 10 times lower than that of the conventional sensors. When such high-resolution, low-frequency voltage sensors are integrated with underwater antennas, they form compact electric field sensor modules that can be used to detect extremely faint dc and low-frequency electric signals.

***

Broadband, Low Drive Voltage Optical Modulator

Optical modulators are used as optical microwave transducers for fiber-optic transmission applications, but broadband devices using traveling electrode structures are limited by phase mismatch between the optical and microwave waves. Mismatch is limited by keeping devices short; this results in a high drive voltage. A 40 GHz integrated optical modulator with a 5V drive voltage was fabricated in the Optical Sciences Division reducing drive voltage requirements of previous devices by a factor of 3. The low drive voltage devices will impact broadband optical links used for optical delay lines, antenna remoting, and RF electric field sensors.

***

Computer Modeling for the Evaluation of Spaceborne Surveillance Concepts

Spaceborne electro-optical and infrared sensors play a key role in real-time intelligence, surveillance, and reconnaissance. The Optical Sciences Division has developed a set of comprehensive computer models for the evaluation of various spaceborne system concepts. These models incorporate experimental and synthetic background data for the evaluation of system performance. They are used to perform utility analysis on these concepts in specific threat scenarios on a deterministic basis and optimize the configuration of satellite constellations. This software is based on the use of a custom three-dimensional, animated graphics package developed in-house. These models have been key in

driving the design requirements for spaceborne sensors and their associated real-time processors, and have provided for the timely and cost-effective evaluation of various spaceborne sensor concepts.

***

11.2 W Multiple Q-Switched, Diode-Pumped Ho:Tm:YAG Laser at 2.09 μm

Laser diode-pumped, solid-state lasers are emerging as an important new technology for compact, efficient laser sources for moderate to high average power applications. Researchers in the Optical Sciences Division have constructed a laser diode-pumped Ho:Tm:YAG laser producing 11.2 W of average power at 2.09 μm in a multiple Q-switched pulsed format at 30 Hz repetition rate. Overall laser efficiency is >2%. This is the first demonstration of a pulsed diode-pumped Ho:Tm:YAG laser, and it firmly establishes this laser as an important new coherent source in the infrared. It has important significance to the Navy, particularly in the area of infrared countermeasures for defeating IR-guided missiles.

***

Reconstruction Module

The Reconstruction Module, developed in the Tactical Electronic Warfare Division, provides the capability to recreate tactical events for display on a geographic map in a dynamic environment. The module allows the playback of historical track data annotated with operational comments provided during the events (real time) to include environmental conditions, emission control, and weapons and equipment readiness. Analytical tools available for use during real time can be applied to the reconstructed events. The Reconstruction Module provides a near real-time playback capability for analyzing events, enables a full-scale reconstruction of fleet exercises or other operational events, and provides an enhanced reconstruction capability to establish the ground truth of a past situation.

***

Multipath Signal Modeling for Electroacoustic Transducer Calibration

As lower frequency electroacoustic transducers are developed, calibration in a confined environment using standard techniques becomes more difficult because boundary echos arrive at the hydrophone before the transient response dies out thereby interfering with the acoustic signal before the calibration information can be acquired. Thus, a new signal modeling technique was devised at the Underwater Sound Reference Detachment for evaluating the low frequency performance of a transducer where echo interference is a problem. The signal model contains multiple arrivals of weighted sums of exponential functions. By adjusting the model parameters so that the predicted waveforms match with measured data, parameter estimates are obtained that characterize both the direct signal and the echoes. This allows extraction from the data of steady state information for the direct signal. Using this method, transducers can be evaluated at lower frequencies than previously possible in existing facilities simulating ocean conditions.

***

The Development of a Portable, Self-Contained, and Easily Deployed Hydrophone System for Recording Deep-Ocean Ambient Noise

A portable hydrophone system has been developed by the Underwater Sound Reference Detachment that can be easily deployed from a ship to a maximum depth of 5000 m, receive, measure, and record

ambient noise (in the 8 to 20 kHz range), and be remotely returned to the surface for recovery. The system's key component is a four-element hydrophone array and self-contained electronics that can be programmed to control a digital audio tape recorder. Two hours of ambient noise can be recorded over a period of several hours or days. The Deep Deployable Ambient Recording System has been successfully deployed in waters depths of 275 to 4880 m and can be used to survey future underwater tracking range areas to determine if adequate signal-to-noise ratios can be achieved.

***

Low Cost, Nonmetallic Mounting Brackets for Sonar Transducers

Spherical array sonar transducers require mounting brackets for installation, however, the seawater environment within sonar domes is highly corrosive to metal fasteners—even those fabricated from corrosion-resistant metals. The solution is to use reinforced, nonmetallic brackets. Such have been designed and tested by the Underwater Sound Reference Detachment. Candidate high-strength materials were laboratory-screened for strength, toughness, environmental resistance, and ease of molding and used to prepare mounting brackets for the TR-317 spherical array transducer. The materials were impact tested. Brackets of the two best materials were successfully exposed to very harsh explosive shock testing. These brackets will be evaluated at sea on a full-scale sonar sphere. Beside cost reduction, these nonmetallic brackets will provide a weight savings of 1900 lb on the nose of a submarine.

***

Development and Testing of Algorithms for Three-Dimensional Magnetic Reconnection

Classical rates for magnetic reconnection are too slow to account for many solar phenomena, such as coronal heating and two-ribbon flares. Turbulence has often been invoked as a process that could help speed up the rate of magnetic energy release via reconnection. Three spectral computer codes (ORRMAG, SEC3D, MHDFSL) for simulating various aspects of three-dimensional magnetic reconstruction have been developed by the Laboratory for Computational Physics and Fluid Dynamics. These codes have been used to simulate the transition to turbulence of a neutral sheet, hypothesized to exist in the solar corona following the eruption of a prominence. These simulations indicate that magnetic reconnections can become turbulent in three spacial dimensions, and that turbulence enhances the rate at which magnetic energy is transformed into heat and kinetic energy. Magnetic reconnection can explain fast energy release processes in the upper solar atmosphere.

***

Numerical Simulation of Transient Flows Around Accelerating Objects

The effect of transient flows around accelerating objects is an important issue in developing missiles, torpedos, ram accelerators and other systems that have to sustain large accelerations. To aid in the design of such systems, numerical capabilities are needed to simulate the development of flow fields around accelerating objects. An algorithm has been developed by the Laboratory for Computational Physics and Fluid Dynamics to simulate these highly transient, chemically reactive flows. This algorithm couples the acceleration of the object into the fluid dynamics and is capable of accurately calculating the pressure distribution on the accelerating object and the acceleration of the object as well as other performance parameters. The computational results show that this approach yields smooth changes in the flow field for objects of very high acceleration (up to approximately 10^8 m/s^2).

***

Agile Mirror—A New Concept in High-Frequency Microwave Beam Steering

The Navy uses airborne and seaborne radar systems to detect, locate, and identify objects; provide targeting information for weapons systems; and perform other electronic warfare functions. Electronically steered, phased array radars perform many of these functions, but they have certain technical limitations and are costly. A device that could steer high-frequency, wideband microwave pulses from single or multiple high-power tubes while maintaining the electronic steering capability of a phased array would be advantageous for some applications. A low-inertia plasma mirror for directing high-frequency radars could provide this capability, and it is under development in the Plasma Physics Division. This microwave beam director uses a plasma distribution to reflect microwaves from a single, high-power source towards a target. The orientation of the plasma distribution can be determined electronically, and initial experiments show that a plasma mirror can be established in 10 μs and maintained for >70 μs. The rapid turn-on and electronic control could lead to high-power, high-frequency radar systems with broadband capabilities.

***

Control of Proximity Effect in Electron Beam Lithography Using Multilayer Approaches

X-ray lithography is a promising technology for the fabrication of integrated circuits of 0.25 μm design rules. Tungsten is slated as the absorber of choice for future X-ray masks, however, this element gives rise to a loss of resolution and critical dimension control due to a proximity effect. A method has been developed by the Electronics Science and Technology Division for reducing this effect in high-resolution electron beam patterning of high atomic weight materials such as tungsten. The method involves interposing a thin (50 to 400 nm) layer of SiO_2 between the resist and the underlying high-Z substrate. The optimum layer thickness for the best resolution of the gratings is 200 nm. Empirical results and the Monte Carlo modeling of e-beam exposure on tungsten absorbers for electron scattering and energy loss indicate that having the low atomic number SiO_2 layer between the resist and the tungsten prevents the fast secondary electrons being generated at the surface of the tungsten from propagating back into the resist, thus providing a mechanism for proximity effect reduction. These results have important practical application for X-ray mask making.

***

Interface Trap Creation in MOS Devices

All metal oxide semiconductor (MOS) devices degrade when subjected to various types of stress because traps are created at the oxide-silicon interface, and the basic chemistry of this degradation process remained uncertain. The problem has been difficult to resolve because the standard techniques for determining impurity concentrations in the oxide lack the required sensitivity. Researchers in the Electronics Science and Technology Division have since identified this basic chemistry of interface trap (D_{it}) creation in MOS devices after their exposure to radiation by studying its time-dependence in oxides annealed in deuterium or hydrogen. The growth rate is significantly retarded in the deuterium-annealed oxide. Since deuterium is an isotope of hydrogen and undergoes the same chemical reactions, the only possible reason for this difference is related to deuterium's greater mass that reduces its drift rate. This result provides the first incontrovertible proof that the rate-limiting step in the D_{it} creation process must be drift of radiation-induced hydrogen ions in the oxide.

***

Analog VLSI High-Frequency Adaptive Filter

Until recently, the most advanced method of implementing high-frequency adaptive filters using monolithic analog circuits has been by a switched capacitor circuit. This circuit was limited to speeds of approximately 100 kHz. A new approach for implementing these filters has been demonstrated by the Electronics Science and Technology Division. This approach utilizes continuous-time analog VLSI circuits, and an adaptive filter circuit that operates at 80 MHz with 32 dB cancellation of CW signals has been demonstrated. The advantages of the continuous-time analog circuit are the potential for a large number of adaptive learning elements (>200), small size, low-power dissipation, low cost, and high frequency of operation (>80 MHz). This work demonstrates that high-frequency (>50 MHz) adaptive filters can be implemented in a small volume and with low-power dissipation using a monolithic integrated circuit.

***

Variations in Substrate Temperature Induced by Molecular Beam Epitaxial (MBE) Growth

An accurate method for measuring the substrate temperature is needed during the growth of GaInSb/InAs superlattices on GaAs for infrared detector applications, and the inability to obtain an accurate and reproducible determination of substrate temperature hinders reliable, high-quality MBE growth. Large changes in substrate temperature were observed to occur during MBE growth of materials with energy gaps smaller than that of the substrate. These temperature changes, not detected by the conventional thermocouple used for temperature control, have been measured by the Electronics Science and Technology Division by observing changes in the IR transmission spectrum of the radiatively heated substrate. Although the effect is very strong when GaSb or InAs is grown on GaAs substrates, it is also expected to occur for growth of InGaAs on InP, SiGe on Si, and HgCdTe on CdTe. This method of temperature determination allows the reproducible growth of high-quality GaInSb/InAs lattices and also the accurate transfer of substrate temperature among different laboratories.

***

Numerical Methods for Assessing Low-Frequency Active System Performance in Realistic Shallow Water Environments

An evaluation of low-frequency acoustic system performance in shallow water ocean environments was undertaken by the Acoustics Division to determine the dependence and significance of source, receiver, target, and environmental parameter values upon system performance. Numerical and analytical methods were developed that significantly enhanced ability to accurately and rapidly assess system performance in these environments. Significant improvements were made through the development of a more efficient method for specifying ocean environmental data; a more rapid method for computing signal excess, ocean bottom-induced reverberation and target echo; and a method for qualitatively assessing the change in system performance as parameter values are varied.

***

Enhancements of a Massively Parallel Wave Simulator

Close engagement scenarios require the integration of acoustic propagation and scattering into a single computational model capable of displaying bounded, shallow water environments for making tactical

decisions. These engagement arenas involve boundaries and time-dependent changes that are computationally intractable in current computational models. Thus, researchers in the Acoustics Division have developed a fast, massively parallel wave simulator that can compute and display efficiently and accurately the time evolution of an acoustic field. The simulations cast finite difference solutions in a cellular automaton architecture for efficiency and incorporate multiple, independently driven sources arranged as array elements or in various positions of either a two- or three-dimensional field. Specific accomplishments include: 3-D simulation and rendering of acoustic waves, attenuation, smooth barriers between cells, analysis and compensation for grid dispersion, elastic boundaries, and the beginnings of an X-window interface.

***

New Algorithm for Characterizing Low-Frequency Acoustic Backscatter from the Sea Surface

Previously, the Navy has relied on an empirical algorithm to characterize acoustic sea surface backscatter at frequencies below 1000 Hz. Measurements have been made by the Acoustics Division of the fraction of incoming acoustic energy that is backscattered by the sea surface as a function of the incident grazing angle, the frequency of the acoustic energy, and the sea surface conditions. Using broadband explosive charges as sound sources, surface scattering strength measurements were made at frequencies from 70 to 1000 Hz, at grazing angles as low as 5°, and at wind speeds of 1.5 to 14 m/s. Three regimes were identified in the frequency-wind speed parameter space in which various backscattering mechanisms dominated the scattering process. These regimes (relatively calm seas at all frequencies and rougher seas at lower frequencies, rougher seas at higher frequencies, and a transitional region) have been codified into an algorithm that provides a significant improvement over the standard Navy scattering model.

***

Strategic Scene Generation Model—Baseline Development

A computerized system was developed by the Space Science Division to generate simulated line-of-sight radiometry and time-sequenced digital images in support of the design, development, and test of electro-optical surveillance systems and for engagement simulations of strategic and theater ballistic missile defense concepts. The system integrates state-of-science knowledge, databases, and validated phenomenological models, thereby serving as an accessible, traceable, physics-based standard for the Strategic Defense Initiative community. Sensor-perspective radiance maps are derived from an ensemble of the best available government standard models and authenticated databases. The phenomenology consists of quiescent and enhanced natural and perturbed backgrounds. The backgrounds include a number of environmental parameters, and target phenomena include a wide variety of space objects and debris. This system is used for digital simulations, hardware demonstration, system design and evaluation, and evaluation of system performance predictions.

***

HERCULES: Hand-Held, Earth-Oriented, Real-Time Cooperative, User-Friendly Location Targeting and Environmental System

Images taken from the space shuttle usually do not contain enough information to determine their location on Earth, and the need for a system that can geolocate these image was identified. HERCU-

LES—developed by the Space Systems Development Department jointly with the Army, Air Force, and NASA—will supply this need. It will allow a shuttle astronaut in space to point a camera at a place of interest on Earth that has no distinguishing geographical features, record the image digitally, and know the latitude and longitude of the center of the image within 2 nmi. A ring-laser gyro provides attitude reference and the NASA-developed, charge-coupled device camera stores the image digitally. Any Nikon compatible lens system can be used, and, in darkness, an Army-developed, night-vision image intensifier can be added. The camera system will provide a valuable Earth observational system for military, environmental, oceanographic, and meteorologic applications.

***

The Development and Space Demonstration of a High Reliability, Long-Life 77°K Cryogenic System for the High-Temperature Space Superconducting Experiment (HTSSE 1)

HTSSE 1 is the first spaceflight carrying high-temperature superconducting devices that must be cooled to 77°K for 6+ months. To provide this cooling, a long-life clearance seal Stirling cycle mechanical cryocooler was employed because this device offered the best near-term potential to meet the long-life, high reliability requirements needed for space systems. A 77°K cryogenic bus has been developed by the Spacecraft Engineering Department and integrated with the Stirling cryocooler for the HTSSE. Accomplishments pertaining to the cryogenic bus include: development and utilization of a low thermal conductivity RF coax cable; space-qualified helium gas gap thermal switches; and a high-flexibility, high-conductivity thermal link for coupling the cold finger of the cryocooler with the cryogenic cold bus. The cryocooler was instrumented to obtain orbit diagnostic performance evaluations.

Meet the Researchers

Dr. Brenda Little is a supervisory research chemist in the Ocean Sciences Branch of the Oceanography Division at NRL-Stennis Space Center, Mississippi. For the past 12 years, Dr. Little has investigated interactions between microcroorganisms and metal surfaces, including biodeterioration, in the marine environment.

"The study of microbiologically influenced corrosion is truly multidisciplinary. NRL has provided an environment for collaboration with metallurgists, materials scientists, surface chemists, electrochemists, microbiologists, and oceanographers. I have also had the opportunity to work with both applied and basic research problems related to microbe/metal interactions."

Dr. Little holds adjunct faculty positions in the Department of Chemical Engineering at Montana State University and in the Marine Sciences Department at the University of Southern Mississippi.

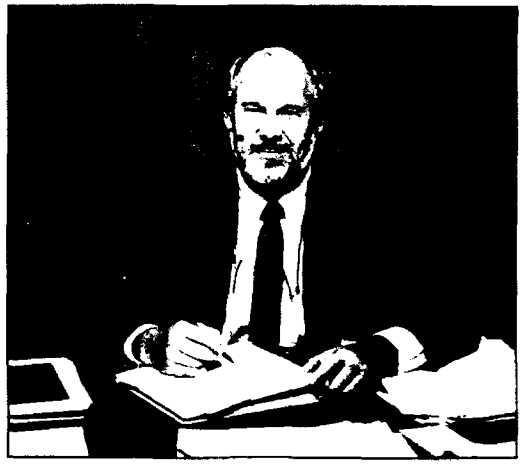

Dr. Eric O. Hartwig came to NRL in October 1992 as the Associate Director of Research in the Ocean and Atmospheric Science and Technology Directorate. Dr. Hartwig is "honored to head an S&T organization that has the broadest scientific and technological coverage of environmental sciences in DoD." Expertise in space sciences, remote sensing, acoustics, oceanography, marine geology and geophysics, and marine meteorology provides NRL with a potent edge in addressing Navy, DoD, and national environmental issues. He adds, "The interaction and sharing of scientific and technological ideas and concepts across these fields create tremendous scientific and programmatic opportunities for those involved. The environmental sciences promote interdisciplinary interaction and teamwork as these sciences seek to understand how a natural system functions as a whole rather than as isolated components."

Dr. Hartwig concludes, "NRL's working environment enables its gifted scientists and engineers to perform research not only on the most fundamental concepts and ideas but also encourages the translation of these basic advances into useful products. This combination of gifted S&T talent, interaction and teamwork on basic to applied research issues, and the expectation of excellence and impact has led NRL to its international reputation for creativity, innovation, and discovery."

CDR Steven S. Smith, officer in charge of NRL's Flight Support Detachment at the Patuxent River Naval Air Station in Lexington Park, Maryland, leads the river-based unit responsible for all airborne research activities. The Detachment provides technical assistance during project installation and conducts flights worldwide in support of a wide spectrum of projects that range from electronic warfare and advanced radar designs to magnetic/gravinometric and airborne laser technology.

"NRL is an exhilarating assignment! The daily challenges are varied so nothing becomes routine, making work exciting and enjoyable. I feel that my greatest responsibilities rest in the support of the outstanding people I work with and the important contributions made by each sailor, engineer, scientist, or technician—military or civilian."

Dr. Norman C. Koon of the Materials Science and Technology Division leads a program on magnetic materials that has achieved national and international recognition for scientific and technological developments. He was recognized for originating a new class of high-performance permanent magnet materials based on rare earths, iron, and boron—an achievement for which he received numerous awards, including the American Physical Society International Prize for new materials, the Federal Laboratory Consortium Award for excellence in technology transfer, and the Washington Technology Magazine Award as one of the Washington area's top high-tech talents.

"Research is a long-term investment in the future, and I am particularly proud in my own work to be associated with NRL, one of the premier research institutions in the country. It has been very satisfying to see some of the things discovered here find application in the real world. In the final analysis that is the return on investment, which justifies our existence."

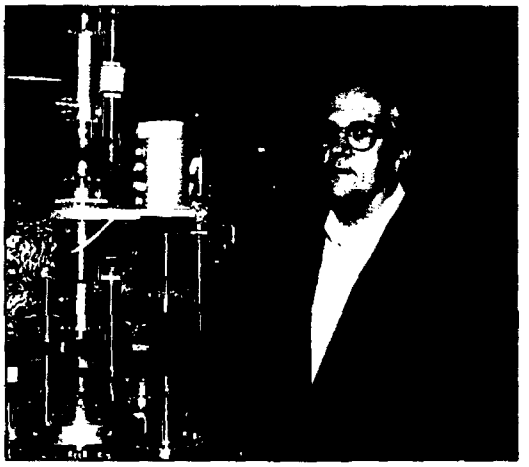

Dr. James D. Kurfess is Head of the Gamma and Cosmic Ray Astrophysics Branch in the Space Science Division. Branch scientists undertake observational and theoretical investigations related to the high-energy particle and radiation environment in space and of the sources that produce these radiations throughout the universe.

"Contributing to the rich tradition that NRL has established in the space sciences is a wonderful professional experience. I am particularly interested in applying nuclear physics to investigations of some of the most powerful and interesting objects in the universe. Much of our work, studying solar flare phenomena and the effects of energetic particles, has direct application to DoD. However, one of the rewards of working at NRL is the opportunity to undertake basic research that relates to fundamental questions about the origin and evolution of the universe. I believe that global pursuit of such knowledge and conveying this knowledge to the lay public is of great importance for societies in general."

Color Presentation

For visual interest, we present some of NRL's latest scientific achievements.

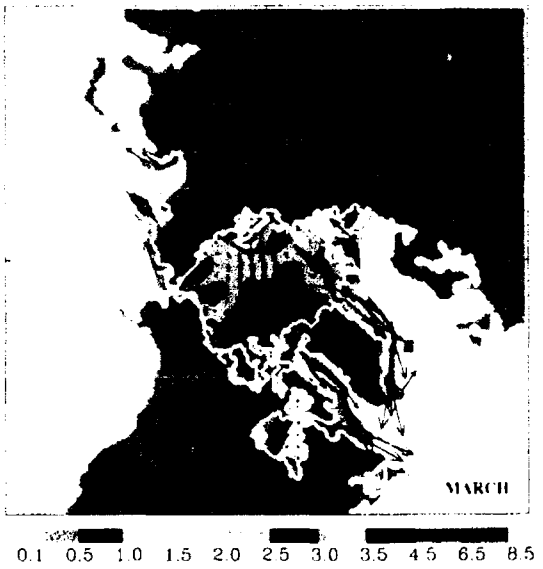

Ice thickness and ice drift derived from NRL's ice-ocean model, the Polar ice Prediction System 2.0 (PIPS 2.0) for the ice-covered regions of the northern hemisphere in winter
(R. Preller, Code 7322)

Color-coded surface of a magnetic field generated by a sheared ion flow in a weakly collisional plasma.
(J.D. Huba, Code 6780)

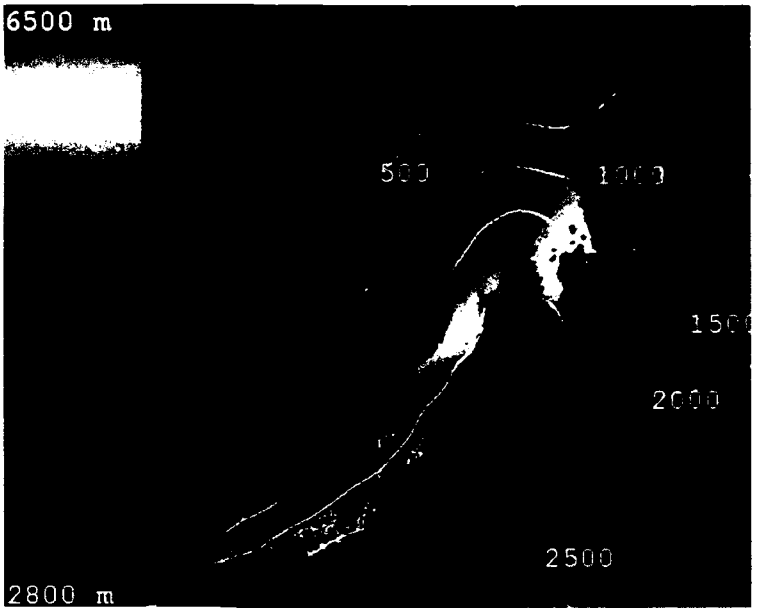

NRL-MRY has developed an icing product for marine aviation weather support. Potential icing threat areas are color-coded, with shades giving the maximum height of threat (see color bar on left). Yellow contours give the base of the threat in meters. This product is based on satellite microwave cloud liquid water, infrared imagery, and global model output. (T. Lee, Code 7531)

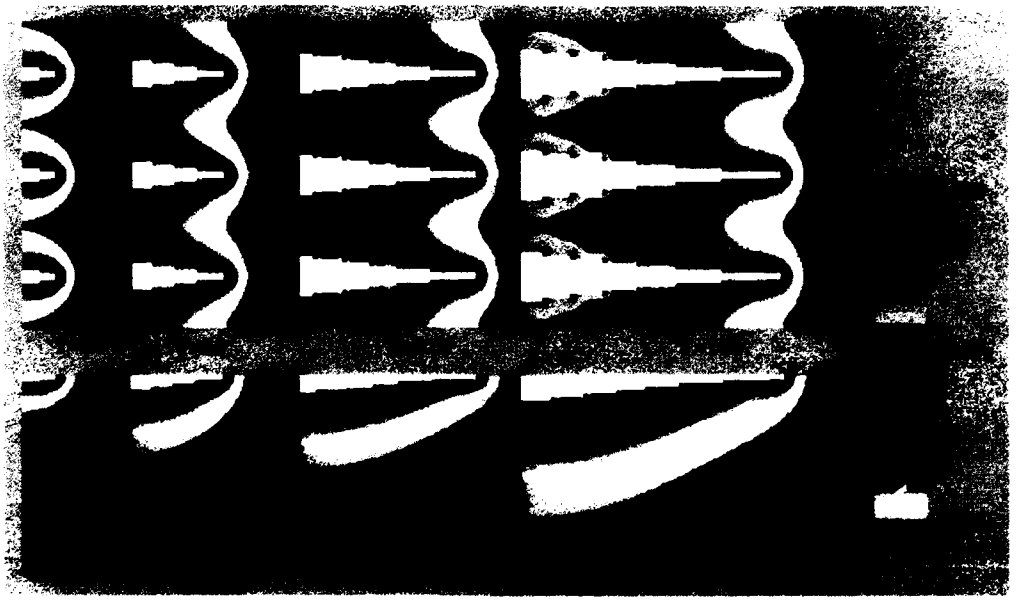

Evolution with time (T) of computer simulated solute concentration profiles surrounding precipitate plates growing by the ledge mechanism. The top frame corresponds to multiple precipitates spaced thirty ledge heights apart; the bottom frame corresponds to a single precipitate. (G. Spanos, R.A. Masumura, and R.A. Vandermeer, Code 6320)

Image produced from infrared measurements made by the Advanced Very High Resolution Radiometer on an operational NOAA meteorological satellite. These images provide maps of the ocean surface temperature at 0.5° precision and nominal 1 km resolution, 8 or more times a day. Measurements are used in a number of on-going research programs including fine-scale ocean dynamics, global ocean circulation, heat transport and global warming, environmental support for naval operations, operational support for fisheries management, and research in analysis visualization and exploitation of imagery data.
(A. Pressman, Code 7240)

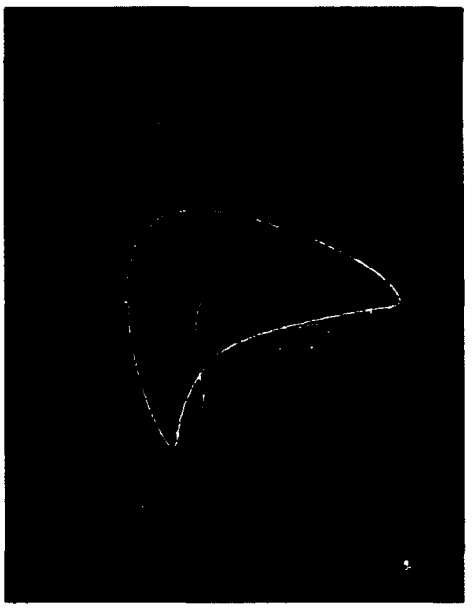

A Poincaré phase portrait for a four-junction array of Josephson junctions. The yellow filament is an out-of-phase attractor. Three orbits are shown spiraling into separate points on the filament.
(I. Schwartz and K. Tsang, Code 6700.3)

The probability of detecting a target from a spaceborne platform increases with grazing angle. This histogram shows the number of target sightings binned by grazing angle vs target latitude. Color is used to indicate the count for each bin. This histogram is used to produce the weighted positioning accuracy of the GPS constellation. (B. Sweeney and J. Michalowicz, Code 5621)

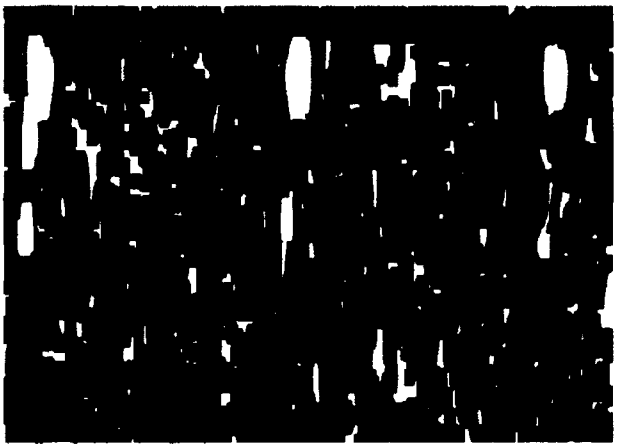

A plot of the *matched-field processing* output is used to locate a submerged source in a deep-ocean environment. The repetitive pattern displays the ambiguous nature of the underwater localization problem. (G. Smith, Code 7173)

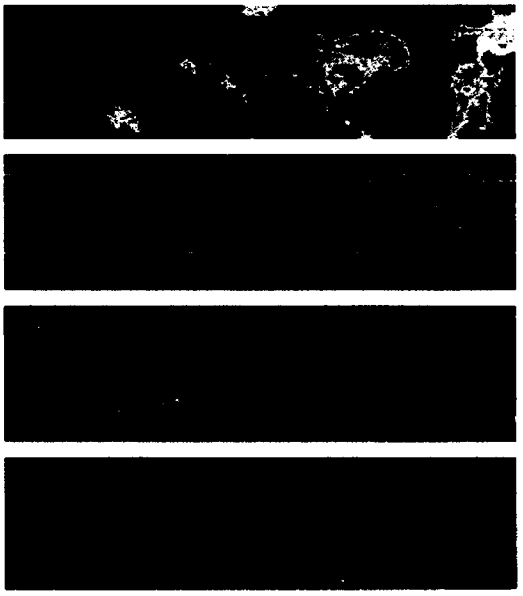

A new algorithm for the correction of image distortions and residual nonuniformity in a temporal sequence of images is illustrated here. The top figure shows a false color simulated IR image of the Earth's surface as viewed by a space-based scanner. Faint targets can be detected in a temporal sequence of such images using Frame Difference Signal Processing. The second image shows the residual detector nonuniformity in the difference of the temporal sequence. The third image shows the residual correlated noise that results from differencing without correcting the image distortions. The bottom image shows the difference image obtained using an algorithm that corrects the image distortion and removes nonuniformity from the differenced image. The red spot along with the dark blue spot to its left is the signature of a faint moving bomber-sized target, detectable using the new algorithm. (W.A. Shaffer, R.L. Lucke, and J.V. Michalowicz, Code 5621)

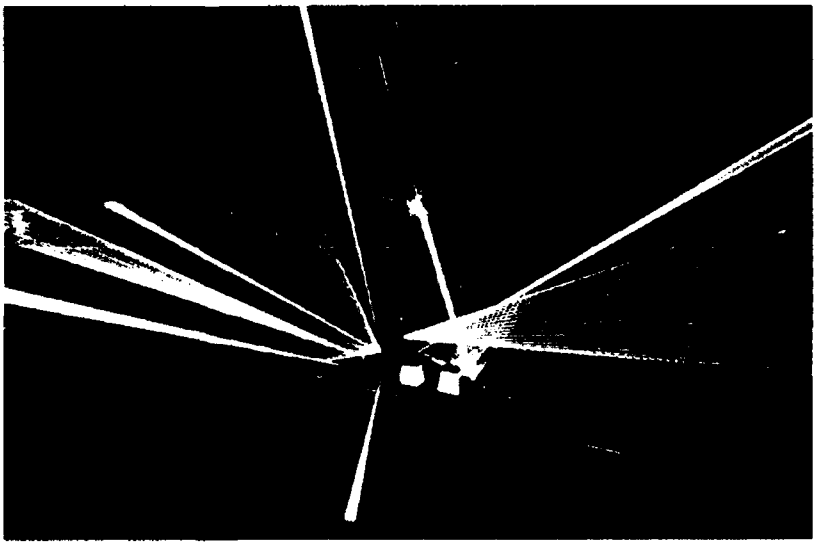

Electromagnetic emissions from a Burke (DDG-51) class destroyer during a simulated antiship cruise missile attack. The DDG-51 radars are shown with yellow beams; hostile missile homing radars are shown with red beams. (W.C. McIntyre, Code 5707)

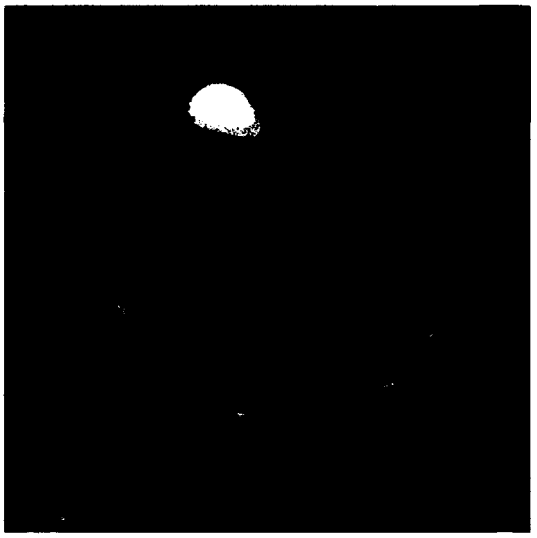

This image was generated by a low-frequency, acoustic pulse simulation running on a Thinking Machine CM-200. This simulation calculates interactions between the pulse and the ocean floor. This scene was created by the GeoData design team under the lead of Dr. Henry Dardy. (Code 5581)

Crystals of para-toluene sulfonate (PTS) diacetylenic lipid. Lipids are surfactants that in water form molecular bilayers, the building blocks for biological membranes. It has been difficult to establish the molecular order and morphology of such materials by X-ray diffraction because they do not easily crystallize. This PTS lipid is one of the few that has been crystallized, enabling NRL researchers to examine their structure by X-ray diffraction. The diacetylenes in the lipid are polymerizable, and the extensive conjugation of the polymer results in the bright colors seen here. The colors are due to regions of different crystalline order, which are reflected in variations in polymer conjugation. (B. Gaber, Code 6900)

Color-coded surface of density in a sub-Alfvenic plasma expansion. The expanding plasma shell *breaks-up* during the expansion and resembles a splashing drop of water. (J.D. Huba, Code 6780)

Featured Research at NRL

Opioid Peptides—X-ray Characterization of Two Potent Enkephalin Analogs

Judith L. Flippen-Anderson and Clifford George
The Laboratory for the Structure of Matter

INTRODUCTION

It has been known for some time that the key to understanding biological processes is knowledge of how chemical and biological reactions take place at the molecular level. X-ray diffraction is a powerful analytical method for completely characterizing molecular structures. Testimony to this fact is that data on almost 200,000 molecules are now available in several crystallographic databases. This number has increased dramatically over the past decade because of improvements in both data collection systems and computers, which have allowed researchers to fully exploit the mathematical methods that were developed at NRL to solve crystal structures. Since the early 1960s, NRL has been a leader in providing structural information in support of many different government research initiatives such as ONR, Army, and USDA programs on dense energetic materials, chemical vapor deposition and superconductivity, antimalarial agents, plant growth substances, pest control, and a variety of NIH programs to combat disease. This paper describes a current NRL project to work in concert with the National Institutes of Drug Abuse (NIDA) to develop new materials for use in the war on drugs.

THE PARADOX OF PAIN RELIEF

Opioids: Plants and Synthetics

Use of opium for pain relief and for pleasure is at least as old as the culture of classical Greece. In 1680, the English physician Thomas Sydenham credited opium with being the most universal and efficacious remedy known to man. It took centuries for the enchantment of the medical community to dim because of a growing awareness of opium's toxicity and addictiveness. In 1803, a young German pharmacist isolated an opium alkaloid he named morphine (for Morpheus, the Greek god of dreams), and by the middle of the 19th century, the use of pure morphine had supplanted the use of crude opium extracts. Once again, the toxicity and addictiveness of morphine only became clear after the drug had become a mainstay of clinical medicine.

It was the administration of such opiates to wounded soldiers during the Civil War that made opiate addiction a significant social problem in the United States. It also triggered an increase in research looking for nonaddictive opiates.

This noble goal has remained frustratingly elusive. Time and again the medical community has embraced a newly developed "nonaddictive" opiate, only to be disappointed when it was later proven not only to be addictive but often even more addictive than the drugs it was supposed to replace. For example, purified cocaine became commercially available in 1884, and while problems with it were evident almost from the beginning, popular opinion and leading medical experts depicted it as a remarkable, harmless stimulant. In fact, when Coca-Cola was introduced in 1886, it was marketed as a drink offering the advantages of coca but lacking the danger of alcohol. Cocaine was not removed from the drink until the year 1900. In 1898, one year before their introduction of aspirin, the Bayer company introduced a morphine derivative named heroin as a nonaddictive

analgesic. Much later, in the 1940s, meperidine (Demerol) was introduced, and it became the most popular opiate analgesic prescribed in American medical practice because it was thought to be nonaddictive. However, the growing number of Demerol addicts soon convinced the Bureau of Narcotics that the situation was otherwise, and it seemed that the analgesic effect of opiates was inextricably linked to their addictiveness. Today, the problems caused by addiction to these drugs have not abated, and drug addiction costs the United States over 70 billion dollars a year.

Research efforts to understand the mechanisms producing the analgesic and addictive properties of opiates contribute to two distinct goals. One is that new drugs may be produced with powerful analgesic properties but without addictive side effects. The second is that an understanding of the mechanisms of addiction may lead to drugs for the treatment of drug addiction.

Endorphins: The Body's Opiate

Although all of the materials described above were isolated or derived from plants, there are also substances that occur naturally in living animals that exhibit the pharmacological properties of morphine. These endogenous compounds, mostly opioid peptides, have been classified as endorphins. In 1975, two endorphins that exhibited this morphinelike factor were isolated from the brain of a pig. They were shown to consist of closely related pentapeptides and were named enkephalins from the Greek for "in the head." This finding, coupled with the characterization of the opiate receptor two years earlier, paved the way for extensive research using a molecular biology approach to study problems related to narcotic addiction. The goals were, and still are, to understand precisely how opiates act in the body and why they are addictive.

DRUG ACTION

Contemporary ideas of drug action are based on the assumption that the initial process is the formation of a reversible complex, or binding, between the drug itself (the ligand) and a cell component known as a receptor.

Receptors

Receptors are proteins, found in or on animal cells. Receptors have been divided into classes according to their particular location in the cell. Opioid receptors are among those found in cell membranes. Receptors perform two vital functions. The first is to recognize and discriminate among biologically active molecules. The second is to convey a signal to some appropriate effector (such as an enzyme) in such a way as to initiate a chain of biochemical reactions that ultimately leads to a characteristic physiologic or pharmacologic response. It is assumed that receptors evolved to interact with and mediate the effects of molecules endogenous (native) to the body such as hormones and neurotransmitters. However, as we have seen earlier, receptors also interact with many compounds that are found naturally in plants and synthetic compounds but are foreign to the body. A location at which these receptor-ligand interactions take place is known as an active site of the receptor.

Ligands

There are two types of ligands that interact with receptors. Agonists provoke a biological response when they interact with the receptor, and antagonists prevent a biological response by blocking the agonist's access to specific receptors.

Opioid narcotics are the ligands that bind to opioid receptor sites. They are optically active. That is, they exist in at least two optical isomers: mirror-images that are identical in chemical composition but, like left and right hands, cannot be superimposed in space. Usually only one of the two isomers can relieve pain, elicit euphoria, or produce any of the other actions associated with opiates. This behavior indicates that opiate actions are stereospecific and that the receptor can distinguish the "handedness" of an opiate molecule. Some parts of the opioid

molecule can be drastically altered with little or no change in pharmacologic activity while modifications to other parts of the molecule drastically alter its activity. It is even possible to use this type of molecular alteration to convert a compound from an agonist into an antagonist.

STRUCTURE ACTIVITY RELATIONSHIPS

To reach the elusive goal of finding nonaddictive analgesics, it is imperative to understand the relationship between structure and function. One approach to the problem is through molecular pharmacology, which considers molecules as fundamental functional units. It seeks to explain the pharmacological effects of biologically active compounds at the molecular level, that is, on the basis of molecular interactions and in terms of a molecule's structural and chemical properties. In a drug-receptor interaction, two properties are of special importance: the electronic charge distribution and the conformation, i.e., shape, of both molecules.

Both the ligands (the opioid peptides) and the receptor proteins are built up from basic building blocks called amino acids (Fig. 1). There are 20 commonly occurring natural amino acids differing from one another by the chemical composition of the "R" group. When amino acid residues link together via peptide bonds, they form polypeptides. Proteins are formed when polypeptides link together in the same way. The crossover between polypeptides and proteins can be anywhere between 35 and 50 residues depending on the biological behavior of the molecule.

The active receptor sites are thought to have a more or less rigid structure that cannot undergo large conformational changes. The ligands are much more flexible, and several factors can affect their activity. Structural factors affecting the performance of a drug are the stereochemistry of the drug itself, distances between certain atoms or groups within the molecule, the drug's electronic distribution, and overall configuration.

The forces that hold crystals together are the same forces that are responsible for ligand-receptor binding. In addition, stable patterns of aggregation and solvation present in solution

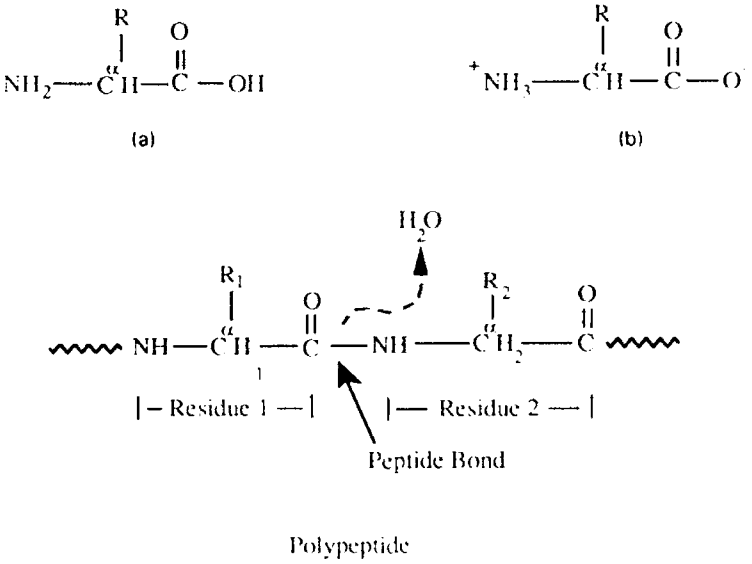

Fig. 1 Top: The general structure for an amino acid is shown in its (a) nonionized and (b) zwitterionic form. The amino group (NH_2), the carboxyl group (-COOH), a hydrogen atom (H), and a side chain (R group) are all attached to a carbon atom (C) known as the alpha (α) carbon. Bottom: A peptide bond is formed when the carboxyl group of one amino acid (residue 1) reacts with the amino group of a second amino acid (residue 2), with the elimination of a water molecule.

often persist in the crystalline form. Thus the structure of a bioactive compound in a crystal lattice can provide a model of the ligand as it exists in its natural setting.

STRUCTURE STUDIES ON ENKEPHALIN ANALOGS

We have recently begun a new program to study the structures of compounds in the enkephalin family of opioid peptides. These compounds bind at opiate receptor sites. However, soon after they were first isolated in 1975, it became apparent that many different responses were elicited by these opiate analgesics. This raised the question as to whether or not the responses might be mediated via different types of receptors. There are several different opioid peptides, each of which could interact with its own particular receptor, or they could act on multiple receptors. It is important to know how many opiate receptors exist and what their functions are. It is quite possible that different groups of receptors may possess functional specificity in that one group might be responsible for analgesia while others mediate addiction and other undesirable side effects. If so, it might be possible to synthesize molecules that have high affinity for the analgesic receptor, but low affinity for all others.

It is now known that there are at least three types of opiate receptors (μ, δ, and κ) and possibly a fourth (σ). The enkephalins, along with β-endorphin, are thought to be the main endogenous ligands for binding to the μ and δ receptors. The relative ease with which enkephalin analogs can be synthesized has led to the availability of a formidable number of them on which to perform binding studies, thus making it possible to define a set of structural criteria necessary for enkephalin-like activity (Fig. 2). Any change in the highlighted residues (Tyr^1, Gly^3, and Phe^4) results in loss of activity. Therefore, efforts to obtain highly bioactive analogs that are also single-site (μ or δ) specific has centered on modifying residues 2 (Gly) and 5 (Leu or Met) and on changing the length of the overall peptide.

The two compounds we will be discussing in this article, DTLET and DPDPE (Fig. 2), were both purposefully designed using the results of these studies. Both compounds are not only more active than the natural enkephalins but they also bind quite specifically to the δ receptor.

Getting Crystals

X-ray crystallography is the best analytical method available for fully characterizing the structures of the opioid ligands. However, most of the structural work done to date has been by solution methods (nuclear magnetic resonance, NMR, and optical rotatory dispersion, ORD) or by theoretical methods (molecular modeling and energy calculations). This is because it is quite difficult to grow uniform crystals of a quality sufficient for high resolution diffraction analysis. Therefore, a major part of our opioid program involves finding conditions under which these materials will produce the needed crystals. Empirical methods developed for protein crystallization are used most often. Large numbers of trials are often required varying conditions such as pH, temperature, precipitating agents, and concentration of both peptide and precipitating agents.

Structural Descriptors

Once crystals have been grown and data have been collected, the structure can be solved. It is then necessary to describe the results in a useful manner. This is done by having a common set of structural descriptors that are used and understood by all researchers studying a particular type of compound. For peptides, there are two main descriptors: torsion angles and hydrogen bonds.

Torsion angles, which define the relationship of any four contiguous atoms, are used to describe the general overall conformation of a peptide or protein (Fig. 3). In this way, using only three torsion angles per amino acid residue, it is possible to describe the overall backbone conformation (the - N - C^{α} - C' - chain) of even the largest proteins and enzymes.

Another common ground for comparing structures is hydrogen bonding (Fig. 3). A hydrogen bond is formed when a hydrogen atom

ENKEPHALIN Tyr-Gly-Gly-Phe-Leu (Met)

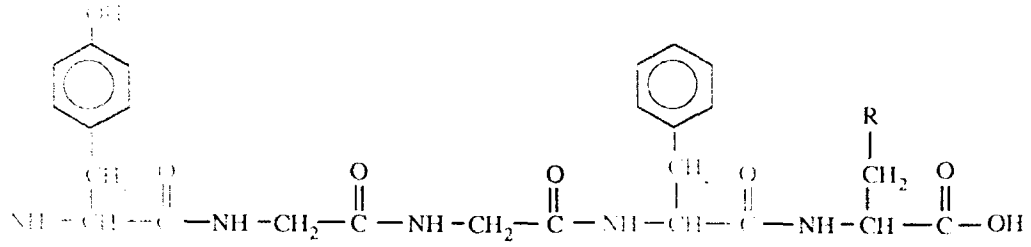

DTLET Tyr-D-Thr-Gly-Phe-Leu-Thr

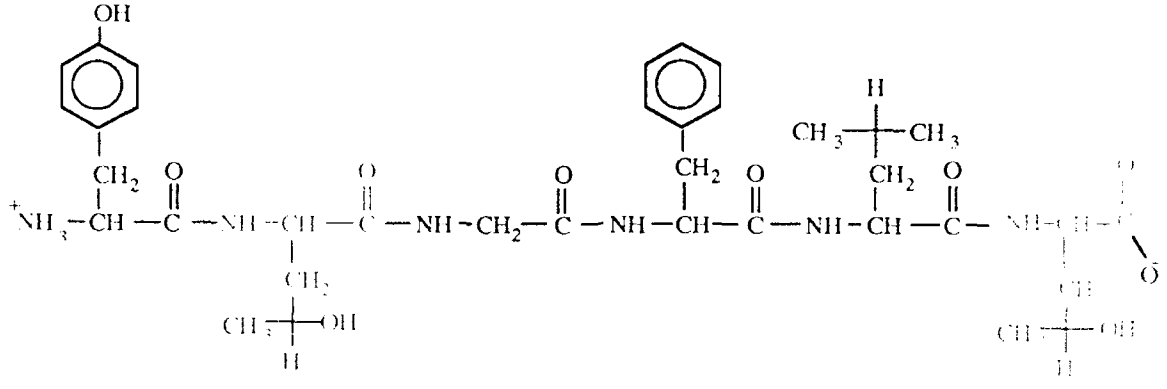

DPDPE Tyr-[D-Pen-Gly-Phe-D-Pen]

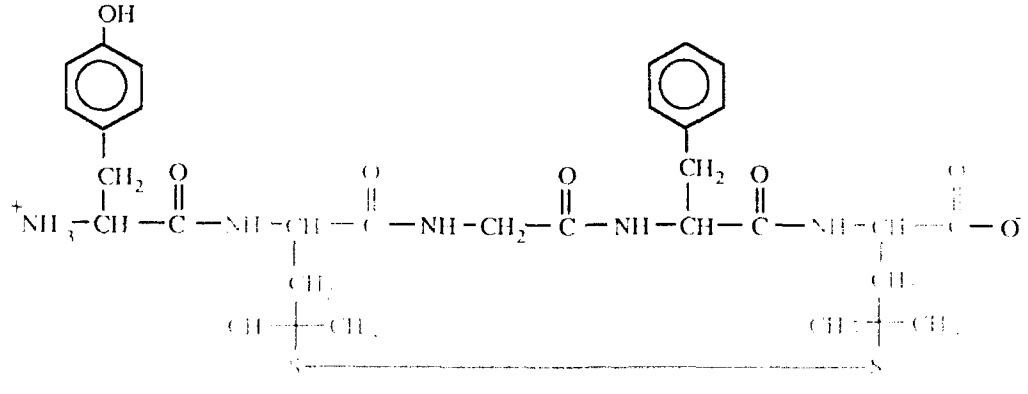

Fig. 2 — Top: Chemical structure of enkephalin. The structural elements necessary for activity are highlighted. For Leu-enkephalin, R = $CH(CH_3)_2$; for Met-enkephalin, R = CH_2SCH_3. Middle: Chemical structure of the linear hexapeptide deltakephalin (DTLET). Differences from Leu-enkephalin have been highlighted. Bottom: Chemical structure of the cyclic pentapeptide [D-Pen^2-D-Pen^5]enkephalin (DPDPE). Differences from Leu-enkephalin have been highlighted.

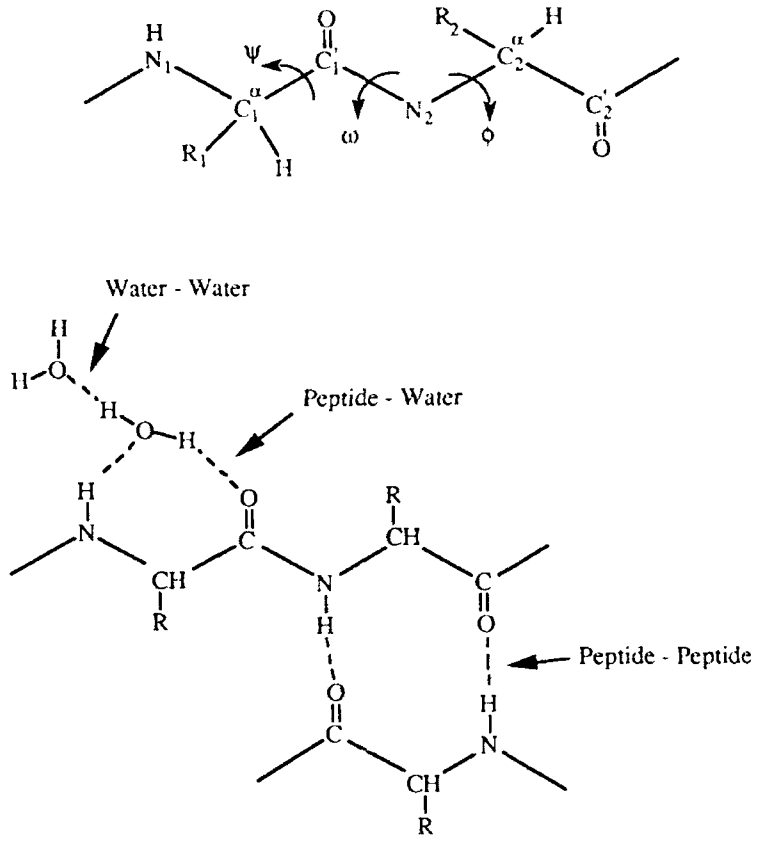

Fig. 3 — Top: The torsion angle of C^{α}-C′ bond is determined by calculating the amount of angular rotation necessary to cause atom N to eclipse atom N + 1. The "backbone" conformation of a peptide or protein can be described using three torsion angles called φ, ω, and Ψ, to define the conformation of each amino acid residue. Bottom: The three types of hydrogen bonding commonly found in peptides.

is linked to two or more electronegative atoms. One of the two bonds is usually a covalent bond, and it is stronger than the second bond, which is usually electrostatic. The weaker bond is known as the hydrogen bond. Peptides can form hydrogen bonds between atoms within the same peptide molecule (intramolecular) or between atoms in two neighboring peptide molecules (intermolecular). Other hydrogen bonds are formed between peptide molecules and solvent molecules (most often water) and between solvent molecules themselves. Hydrogen bonding plays a critical role in the way both peptide and protein molecules aggregate and interact in the body. They also contribute to the stability of drug-receptor complexes. Once both the torsion angles and the hydrogen bonding patterns are known, it is possible to completely describe the structure of the peptide. Torsion angles and hydrogen bonding information are both directly available from the results of an X-ray diffraction study.

In addition to a detailed picture of the molecule itself, an X-ray study provides information not available from any other analytical technique. It provides an electrostatic snapshot of how the molecules may interact not only with one another but also with their watery environments. There are two types of peptide side chains: hydrophobic (water-hating), which are nonpolar, having no atoms available to act as either hydrogen bond acceptors or donors, and hydrophilic (water-loving), having polar groups available to give or receive a proton in a hydrogen bond. The manner in which these side chains arrange themselves is thought to play a

role in determining the biological activity of a molecule.

There are two other structural descriptors that are used only to describe the results of an X-ray study. A crystal is a solid that contains a group of atoms or molecules that repeats regularly in all three dimensions. Therefore, to "solve" a crystal structure, it is necessary to locate only the molecule or molecules that form the basic repeating unit. This group of molecules is called the asymmetric (unique) unit. To complete the characterization of a crystal structure, it is necessary to describe the relationship of the molecules in the asymmetric unit to their nearest neighbors. This is known as the packing environment. Hydrogen bonds are integral parts of the packing environment.

DTLET — A Linear Hexapeptide Analog of Enkephalin

The backbone of a linear peptide is quite flexible. If each torsion angle in a polypeptide is considered to represent a degree of freedom, then it is easy to see that even a molecule as small as a pentapeptide can have thousands of theoretically possible conformations. In actuality, many of these conformations would be energetically unfavorable, mainly because of the repulsive forces existing between neighboring atoms. However, spectroscopic and theoretical calculations indicate that both folded (having U-shaped turns) and fully extended (sawtooth) enkephalin conformations would be consistent with energy minima.

To date, Met-enkephalin has only been observed in an extended conformation in the solid state. Crystal structure studies of Leu-enkephalin grown from different solvents have shown, however, that it adopts both a folded and extended conformation in the solid state. These studies have also identified the intra- and intermolecular hydrogen bonds that stabilize the respective conformations.

In 1983, the linear hexapeptide delta-kephalin (DTLET) was one of the first compounds designed as a pure δ-specific ligand (Fig. 2). The design process was successful in that, at that time, it was the most selective linear δ-agonist available. It differs from Leu-enkephalin (Fig. 2) in that a D-Thr residue has replaced the Gly^2 and a six residue, L-Thr, has been added. The D- and L- notation often found preceding the name of an amino acid refers to its optical activity (handedness). Most naturally occurring amino acids are L-isomers, and therefore usually only D- isomers are indicated in compound names.

The X-ray results (Fig. 4) showed that DTLET exists in a folded conformation. Figure 5 compares the conformation of DTLET to a folded conformer of native Leu-enkephalin and to two other synthetic analogs. Six types of folded conformations have been defined depending on where in the sequence the bends occur. Three of the four molecules exhibit the same type of folded conformation. One of the native compounds has two folds, both of which are of different types from that found in the others. The result of the double bend is that the molecule is more tightly "wound" in on itself bringing the two rings much closer together (5.0 Å) than they are in the three other molecules (9.6 - 11.3 Å).

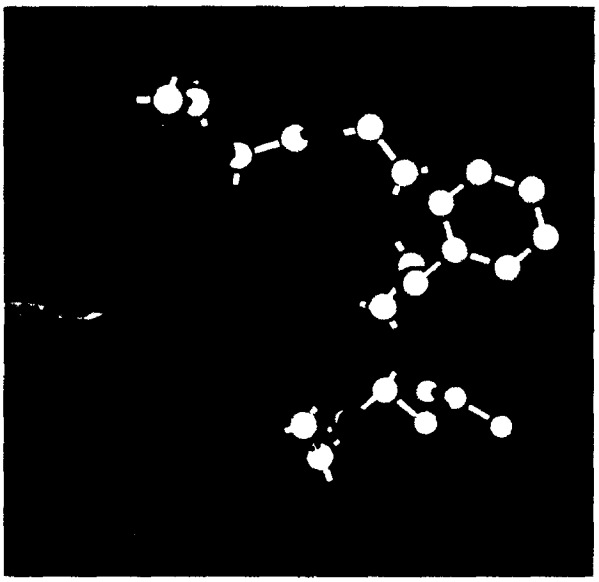

Fig. 4 — Conformation of DTLET as found in the crystal. Backbone carbon atoms are white, nitrogen atoms are green, and oxygen atoms are red. Hydrophobic side chain carbons are yellow, and hydrophilic side chain carbons are blue. The intramolecular β-bend hydrogen bond is also shown by the dashed line.

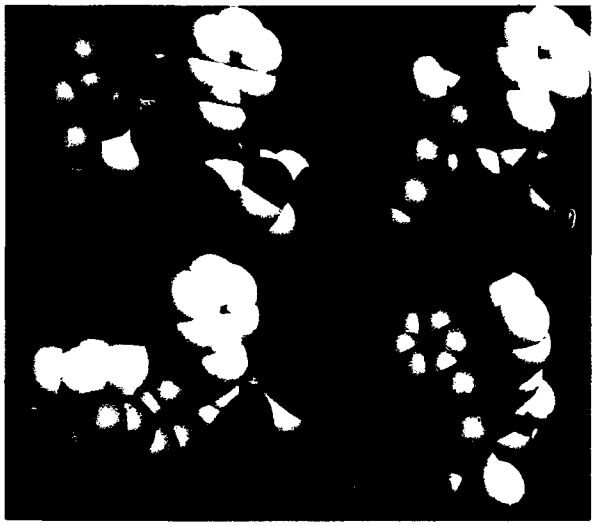

Fig. 5 Space filling diagram comparing the overall shape of DTLET (upper left) with that of three other related compounds. The compound with two β bends is shown in the lower right.

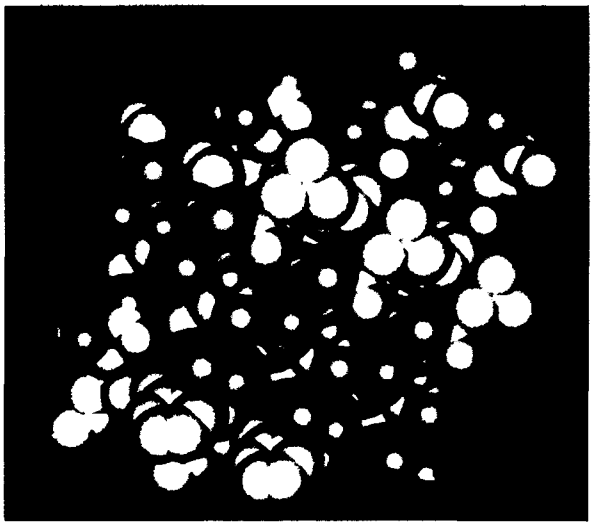

Fig. 6 Space filling diagram of DTLET showing the manner in which the side chains arrange themselves into hydrophobic and hydrophilic layers. In this figure, all the backbone atoms (C, N, and O) are white.

In DTLET, the hydrophobic side chains (Phe^4 and Leu^5) lie on the same side of the peptide backbone while the hydrophilic groups (Tyr^1, D-Thr^2, and Thr^6) all lie on the opposite side. When the molecules aggregate in three dimensions, this geometry creates alternating hydrophilic and hydrophobic layers with most of the included water molecules being in the hydrophilic layer (Fig. 6). In all enkephalin structures studied so far, both the hydrophilic Tyr^1 residue and the hydrophobic Phe^4 residue interact with surrounding solvent molecules. Since both of these residues are thought to be necessary for μ/δ opiate selectivity, it may well be that it is through this type of hydrogen bonding that the enkephalins interact with their opiate receptors.

DPDPE - A Cyclic Enkephalin Analog

As described above, the flexibility of linear enkephalins has been conclusively demonstrated by X-ray diffraction studies. In addition, spectroscopic studies have shown quite convincingly that in solution, enkephalins may exist in many different conformations. It is most likely that this conformational flexibility is the main reason for their lack of specificity towards the different opiate receptor classes, and therefore it is not possible to fully characterize receptor-ligand interactions by studying only the flexible opioids. Conformational flexibility can be reduced through incorporation of conformational restraints. Such analogs, because of their relatively rigid structure, are unlikely to undergo major conformational changes upon binding to the receptor, so they should be able to provide more meaningful information about receptor-ligand interactions. Also, they may offer improved receptor selectivity because analogs having a good affinity for one receptor type may no longer be able to undergo the conformational changes necessary to bind to other receptor sites. Several approaches have been tried to design conformationally restricted analogs. The most drastic of these has been the synthesis of cyclic enkephalin analogs.

At the same time that DTLET was being pursued, other scientists were using the principles of conformational restriction in conjunction with careful examination of structure-activity relationships to develop a series of receptor-selective cyclic peptide analogs of enkephalin. One of those compounds is [D-Pen^2-D-Pen^5]-enkephalin (DPDPE, Fig. 2), which contains a 14-membered ring formed by an S-S bridge between the two D-Pen residues. DPDPE was found to be even more δ receptor specific than DTLET. In fact, DPDPE has enough receptor selectivity to make it an excellent tool for

examining the physiological roles of δ receptors in peripheral and central nervous system tissue.

A considerable amount of effort has gone into trying to characterize its conformation. Several solution NMR and molecular mechanics studies have been reported. However, repeated attempts to obtain diffraction quality crystals were unsuccessful until crystals were grown recently at NRL. Once crystals were obtained, we were able to collect data and solve the crystal structure.

The crystal was found to contain three unique molecules of DPDPE and a great deal of water (Fig. 7). All three independent DPDPE molecules have nearly identical conformations with the exception of the orientation of the Tyr^1 side-chain (Fig. 8). This twist affects the distance between the centers of the aromatic rings and also has a significant effect on the manner in which this molecule interacts with surrounding water molecules.

Water accounts for approximately 17% by weight of this structure, which is a situation commonly found in proteins but is unusual in the smaller polypeptides. The three independent molecules of DPDPE and their associated water molecules aggregate in layers. Approximately half of the water in the crystal is tightly bound through hydrogen bonding to the DPDPE molecules. Additional hydrogen bonds link the layers into cylinders that physically trap the remaining water molecules in irregularly shaped channels (Figs. 9-11). Another unusual feature of this structure is that there are no peptide-peptide hydrogen bonds in the cylinders. The molecules are locked together solely by peptide-water and water-water hydrogen bonds. The amount of water in this structure and the way in which it interacts with the peptide molecules may well prove to be an important feature of its biological activity.

This work represents the first X-ray structure of a cyclic enkephalin analog. Many more structures must be found to provide truly definitive information on exactly which conformational features of these compounds are responsible for this biological activity.

ACKNOWLEDGMENTS

The color prints were prepared in the Connection Machine Facility. The authors appreciate this assistance.

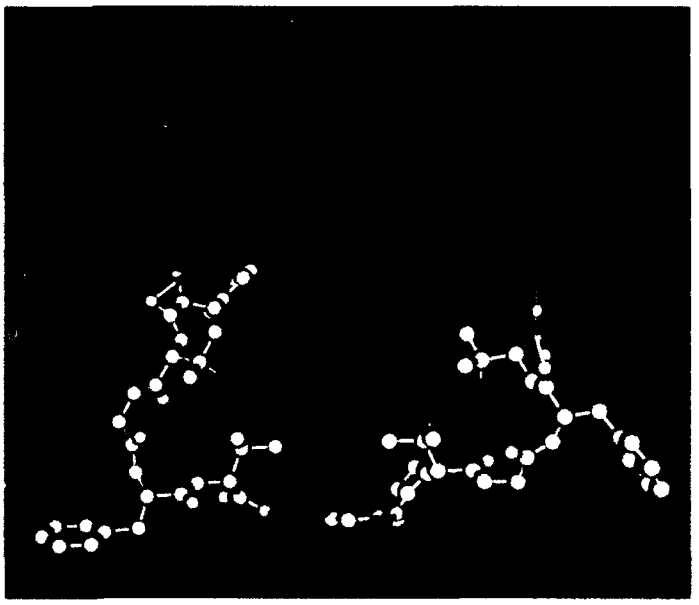

Fig. 7 — Asymmetric unit (only the full occupancy atoms are shown) of DPDPE, which when taken together outlines the solvent channel. The three independent DPDPE molecules are shown in red, yellow, and white with the S-S bridges in green. In this cluster, there are no peptide-peptide hydrogen bonds; all three molecules are interconnected by water molecules (colored cyan).

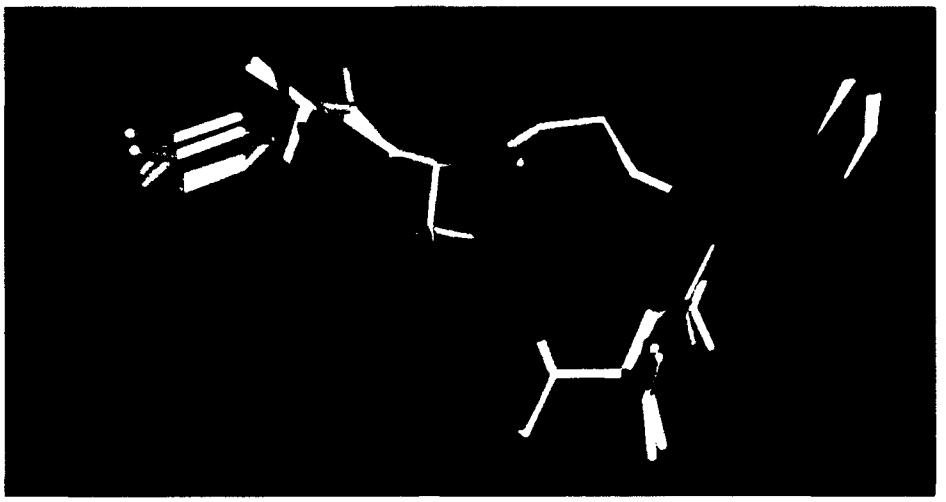

Fig. 8 – A least-squares fit of the three independent molecules of DPDPE

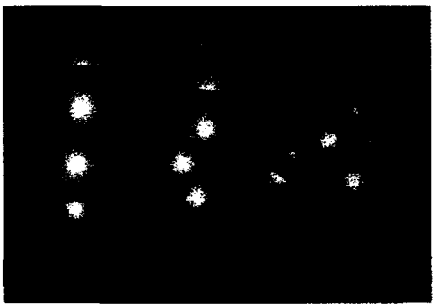

Fig. 9 The water channel found in DPDPE. There is one water molecule (magenta) that sits in a fully occupied position that is almost entirely surrounded by disordered water (green) giving the appearance of a ball, the surface of which is covered with the disordered water molecules. The dimensions of the channel are not uniform.

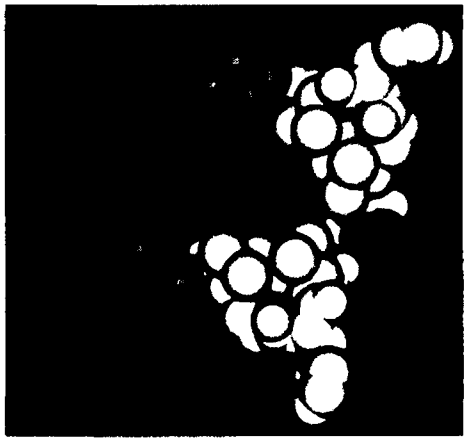

Fig. 10 A space filling illustration showing a "layer" of peptide molecules surrounding the solvent channel

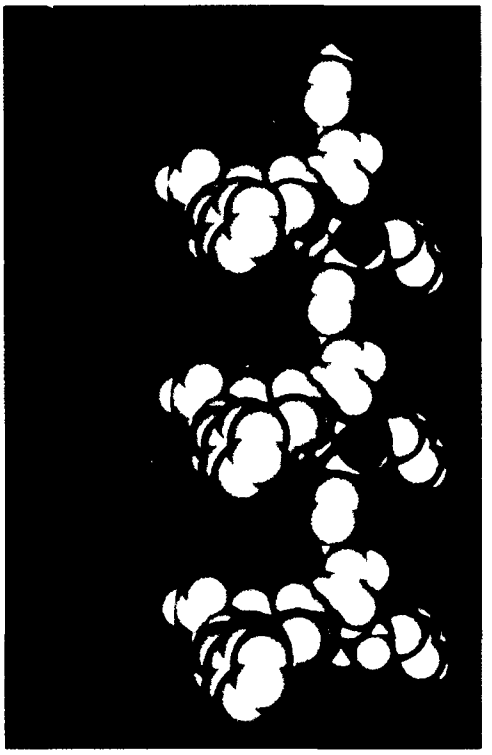

Fig. 11 Space filling illustration showing how the "layers" translate to aggregate into cylinders that trap the solvent channel into the crystal lattice

BIBLIOGRAPHY

A. Aubry, N. Birlirakis, M. Sakarellow-Daitsiotis, C. Sakarellow, and M. Marraud, "A Crystal Molecular Conformation of Leucine-Enkephalin Related to the Morphine Molecule," *Biopolymers* **28**, 27-40 (1989).

J.R. Cooper, F.E. Bloom, and R.H. Roth, *The Biochemical Basis of Neuropharmacology* (Oxford University Press, New York, 1982).

D.R.H. Gourly, "Receptors: A Review of Recent Progress," in *X-Ray Crystallography and Drug Action*, A.S. Horn and C.J. De Ranter, eds. (Clarendon Press, Oxford, 1984), pp. 95-112.

V.J. Hruby, "Design of Conformationally Constrained Cyclic Peptides with High Delta and Mu Opioid Receptor Specificities," NIDA Research Monograph 69, R.S. Rapaka, G. Barnett, and R.L. Hawks, eds., NIDA: Rockville, MD, 128-147, 1986.

I.L. Karle and J. Karle, "[Leu5]enkephalin: Four Cocrystallizing Conformers with Extended Backbones that Form an Antiparallel b-sheet," *Acta Cryst.* **B39**, 625-637 (1983).

D. Mastropaolo and A. Camerman, "Crystal Structure of Methionine-Enkephalin," *Biochemical and Biophysical Res. Comm.* **134**, 698-703 (1986).

D.F. Musto, "Opium, Cocaine and Marijuana in American History," *Scientific American* **265**, 40-47 (1991).

P.T. Prange and C. Pascard, "Opiaces Peptidiques: Structure et Conformation de Deux Fragments d'Enkephalines, Try-Gly-Gly-Phe et Gly-Gly-Phe-Leu," *Acta Cryst.* **B35**, 1812-1819 (1979).

Y. Shimohigashi, "Design Principles: Enkepalins with Predictable Mu/Delta Receptor Specificity," NIDA Research Monograph 69, R.S. Rapaka, G. Barnett, and R.L. Hawks, eds., NIDA: Rockville, MD, 65-100, 1986.

G.D. Smith and J.F. Griffin, "Conformation of [Leu5] Enkephalin from X-ray Diffraction: Features Important for Recognition at Opiate Receptor," *Science* **199**, 1214-1216 (1978).

S.H. Snyder, "Opiate Receptors and Internal Opiates," *Scientific American* **236**, 44-56 (1977).

J.J. Stezowski, E. Eckle, and S. Bajusaz, "A Crystal Structure Determination for Tyr-D-Nle-Gly-Phe-NleS: an Active Synthetic Enkephalin Analogue," *J. Chem. Soc. Chem. Comm.*, 681-682 (1985).

J. Zajac, G. Gacel, F. Petit, P. Dodey, P. Rossignol, and B.P. Roques, "Delta-kephalin, Try-D-Thr-Gly-Phe-Leu-Thr: A New Highly Potent and Fully Specific Agonist for Opiate δ-Receptors," *Biochemical and Biophysical Res. Comm.* **111**, 390-397 (1983).

THE AUTHORS

JUDITH L. FLIPPEN-ANDERSON graduated from Northeastern University in Boston, Massachusetts, with a B.A. degree in chemistry in 1963. She received an M.S. degree in physical chemistry from Arizona State University in Tempe, Arizona, in 1966. She came to NRL the same year and since that time has written or coauthored over 200 articles in structural chemistry covering such diverse areas as bioactive therapeutics, substances affecting the lives of plants and insects, dense energetic materials, and polypeptides. She is a coauthor on a patent involving an extremely potent plant growth promoter for which she received a Superior Service Award from the USDA. She has received several NRL publication awards and has served on several NRL computing committees. An active member of the crystallographic community, she is just completing her term as immediate past-president of the American Crystallographic Association. She has recently been elected Vice-Chairman of the U.S. National Committee of Crystallography. Current research activities center on structures of neuroactive peptides and other materials related to psychoactive drug abuse.

CLIFFORD F. GEORGE graduated from Washington and Jefferson College in Washington, Pennsylvania, with a B.A. degree in physics in 1963 and joined the Diffraction Branch of the Optics Division that same year. He received an M.S. degree in physics in 1971 and a Ph.D. degree in physics in 1978 from Catholic University, where his thesis concerned the structural analysis of thin solid films of amorphous silicon oxides by electron diffraction. Over the years, he has authored over 100 publications and professional society presentations in areas of electron and X-ray diffraction. His current areas of interest include energetic materials, neuroactive and therapeutic compounds, and organometallic precursors for ceramics, superconductors, and semiconductor device materials.

Ultrathin Magnetic Film Research at NRL

James J. Krebs
Materials Science and Technology Division

INTRODUCTION

Several years ago, scientists in the Materials Physics Branch recognized that recent advances in surface science and thin film preparation methods offered an unparalleled opportunity to produce high-quality, well-characterized, single crystal magnetic films suitable for probing the fundamental differences between very thin film and bulk behavior in a well-controlled fashion. At NRL, body centered cubic (bcc) Fe films were grown on GaAs substrates [1] and were used to study their surface anisotropy, microwave properties, thin film magnetization and its unusual phase transition behavior, as well as substrate-induced strain and crystalline perfection. In related follow-up work, German scientists produced similar Fe/GaAs samples and used Brillouin light scattering to study their properties. The thinnest Fe films examined in this work were about 18 Å thick, just at the upper limit of the ultrathin magnetic film regime, which we take to be films no more than 10 atomic monolayers (ML) thick.

During this period, a variety of research capabilities converged to spark an exciting advance in our basic understanding of the magnetism of ultrathin films. These developments include theoretical computational advances that allow one to calculate the electronic properties of ultrathin films accurately from first principles in a spin-unrestricted manner [2] and that predict marked property modifications in magnetic films only a few ML thick. The advance was also spurred by the commercial availability of molecular beam epitaxy (MBE) systems that have sufficient versatility to introduce specially designed, high-temperature effusion sources (as developed at NRL) for laying down transition metal films in ultrahigh vacuum (UHV) and that also have the ability to characterize the films in vacuum with a wide variety of crystallographic, chemical, electron spectroscopy, and thickness techniques. By using carefully chosen substrate materials and continuously monitoring film crystallinity during growth, one actually can produce single crystal magnetic films that are ultrathin and of high quality. This has led to an unusually fruitful and classic interplay between theoretical predictions for model systems, the experimental construction and testing of these and newly devised model systems, and both theoretical and experimental explanations of unexpected results.

Other factors that increased the level of interest in this area were the anticipation of achieving artificial man-made magnetic materials that exhibit true two-dimensional magnetic behavior, the ability to grow and stabilize normally unstable magnetic materials by use of nonequilibrium growth on suitable substrate templates, and the likelihood that some of the materials produced or effects discovered would have technological importance.

To illustrate some of NRL's contribution to this area, three material systems studied are described below. Several of these studies involved profitable collaborations with scientists from IFF-KFA Jülich, the National Institute of Standards and Technology, and from within NRL itself.

SINGLE ULTRATHIN LAYERS OF bcc Fe/Ag(001)

A fundamental problem of magnetism, the dimension at which long-range magnetic order occurs, is addressed in electronic and magnetic structure calculations carried out in the local density approximation [2]. These spin-resolved

band structure results indicate that epitaxial Fe monolayers on Ag should have an enhanced magnetic moment for 1 or 2 Fe ML. This is thought to arise from the decreased number of near-neighbor Fe atoms, their increased separation compared to that in a bulk Fe crystal, and the lack of overlap between electronic states of the neighboring Fe and Ag atoms near the Fermi level. A spin-resolved examination of these states by means of photoemission thus addresses the formation of and interplay between the magnetic and electronic character of the system in a fundamental way.

For the experimental study of magnetic crystals in the ultrathin regime, it is of paramount importance that the films be as atomically flat as possible with a layer-by-layer growth mode and that there be negligible interdiffusion between the film and substrate. Iron and Ag are mutually immiscible, and early studies elsewhere showed that the Fe/Ag interface is diffusion-free. In addition, a careful Auger electron spectroscopy and low-energy electron diffraction study in England proved that Fe grows on Ag(001) faces in a layer-by-layer mode for the first 3 ML. NRL scientists [3] showed that the layer-by-layer growth is bcc Fe since, if the bcc Fe(001) surface net is rotated by 45° with respect to the Ag(001) net, the atom positions match within 0.8%.

Spin-Polarized Photoemission Studies

In an NRL-Jülich collaboration [4], samples were prepared by epitaxially growing ultrathin films of Fe on approximately 150 Å of Ag(001). Using a synchrotron-produced photon beam chosen to have a photon energy to maximize the surface sensitivity of the experiment, the photoelectrons emitted from the sample were energy and spin-analyzed. The Fe thicknesses, ranging from 0.15 to 30 ML, were measured using a quartz crystal monitor, while surface cleanliness and the single crystal structure were verified with Auger spectroscopy and electron diffraction. Before the spin-polarized photoemission experiment was carried out, each sample was magnetically poled with a pulsed magnetic field.

The in-plane polarization found along the poled direction is shown in Fig. 1(a) for the 2.5 ML thick Fe film along with the corresponding electron energy distribution curve (EDC). In contrast to the predictions of an enhanced magnetic moment for 1 or 2 ML [2], *no* spin polarization or net in-plane ferromagnetic order is observed even though an exchange-split electronic structure is inferred from the EDC data. Nor was any spin polarization found for any thinner Fe film. On the other hand, the different EDCs found for different spin directions as shown in Fig. 1(b) clearly indicate an in-plane ferromagnetic order at 5.2 ML Fe. Thus by 5 ML, the Fe film has made a transition from a surface-dominated, two-dimensional behavior to a bulklike character.

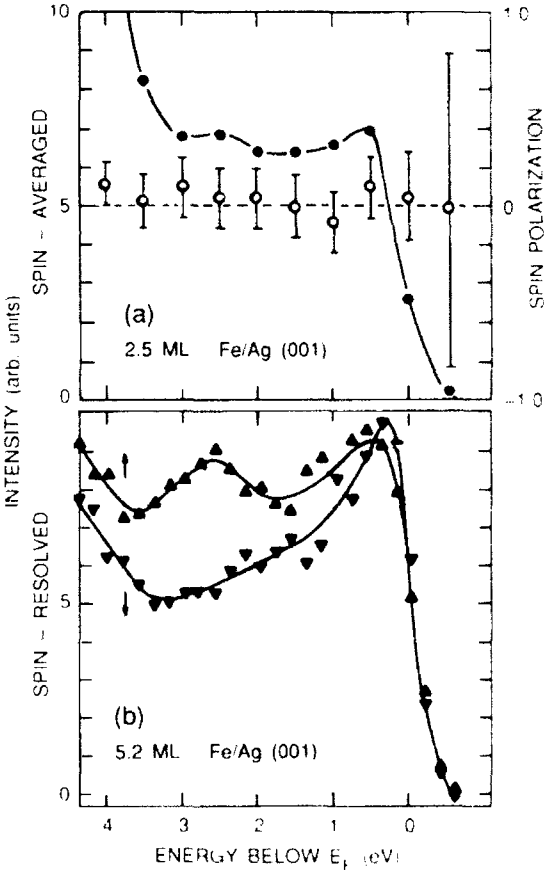

Fig. 1 (a) Spin averaged electron energy distribution curve (EDC) (closed circles) and spin polarization (open circles) for a 2.5 ML thick Fe film on Ag(001). (b) Spin resolved EDCs for a 5.2 ML Fe film majority spin (upward pointing triangles) minority spin (downward pointing triangles)

The striking absence of any net in-plane ferromagnetic order for Fe films up to 2.5 ML thick indicates that such films cannot be permanently magnetized in the plane at room temperature. NRL scientists suggested [4] that this could be caused either by a large magnetic anisotropy that requires the magnetization to point perpendicular to the film or by a magnetic ordering temperature that is below room temperature. A subsequent anisotropy calculation [5] for a free-standing Fe(001) monolayer at the Ag(001) lattice constant suggests that the easy magnetization axis should be perpendicular to the surface. One other possible explanation [4] of the lack of spin polarization is the existence of a fine pattern of magnetization domains in the area sampled by the photon beam. These NRL findings stimulated work on both ultrathin Fe/Ag(001) layers and on superlattices in several laboratories around the world.

Fe/Ag(001) SUPERLATTICES

The rationale behind growing [6] high-quality superlattice samples of Fe/Ag(001) containing ultrathin Fe^{57} layers is to address the behavior of the Fe magnetization in such films by conversion electron Mössbauer spectroscopy (CEMS). The existence of multiple, aligned ultrathin Fe layers increases the amount of material studied and permits one to acquire good data even on samples that have relaxation broadened CEMS spectra as is true for the Fe/Ag(001) system. Also, the total Fe moment becomes large enough to permit the sample magnetization to be studied directly as a function of magnetic field and temperature. Finally, X-ray diffraction can be (and was) used to examine the superlattice perfection.

Sample Preparation

At NRL, Fe/Ag superlattices were prepared using isotopically pure Fe^{57}. The thickness of the individual Fe layers (all the same in a given superlattice) ranged from 0.9 to 5.5 ML for different samples. The critically important Fe thicknesses were measured by X-ray fluorescence after growth, and the total Fe thickness lay between 50 and 100 Å in all cases. The chemical purity was established by Auger spectroscopy. The superlattices yield dramatic X-ray diffraction data that show well-defined superlattice satellite peaks in the neighborhood of the Fe(002) diffraction peak and indicate that the Fe/Ag interfaces are sharp and reproducible.

Mössbauer Results

The CEMS spectra of a 2.4 ML Fe superlattice and a thick Fe film at 15 K are shown in Fig. 2. For the thick film, the line intensity ratios are 3:4:1:1:4:3, exactly as expected when the Fe moments lie in the film plane. In the 2.4 ML sample, however, it is clear that the 2nd and 5th main lines are much weaker than in the thick film, indicating that the Fe moments are nearly perpendicular to the film. From the integrated intensities, one finds that there is either a uniform deviation of the moment direction of about 30° from perpendicular or that 80% of the moments are perpendicular to the film and the rest are in plane. In marked contrast, a 5.5 ML sample at 15 K gives intensity ratios that imply that most of the moments are in plane. Upon increasing the sample temperature to 300 K, the 5.5 ML spectra show that the moments are now completely in plane.

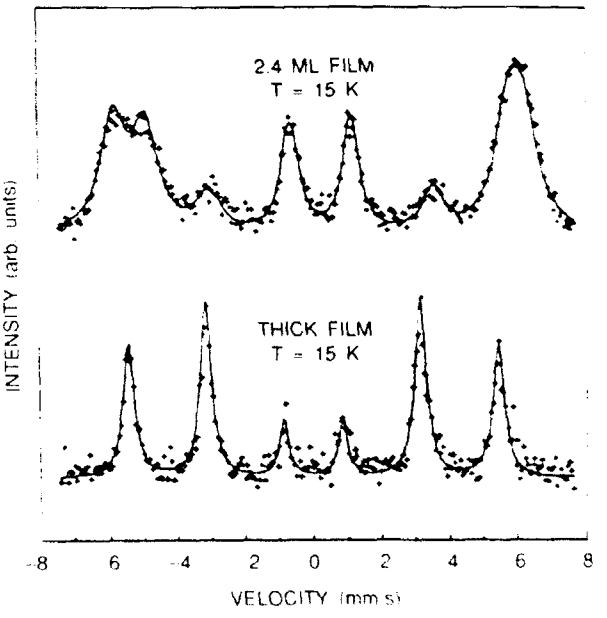

Fig. 2 Conversion electron Mossbauer spectra taken at 15 K for a thick Fe film (50 nm) compared to a superlattice film of 2.4 ML ^{57}Fe(001)/Ag(001)

Thus we see that at low temperatures, the preferred Fe moment direction is perpendicular to the plane for superlattices with Fe layers 2.4 ML or less thick, while it is in plane for those with layers 5.5 ML or more thick as the NRL workers suggested [4].

Nevertheless, the actual situation is more complicated than originally thought. For example, the 2.4 ML sample Mössbauer lines broaden above 50 K and completely collapse at room temperature, indicating that there is no net moment remaining at 300 K. One possible cause of such behavior is superparamagnetic relaxation. However, at all temperatures at which this film shows a hyperfine-split spectrum, there is a pronounced perpendicular orientation of the moments shown by the intensity ratios. This means that the relaxation is not that of three-dimensional superparamagnetic clusters but has a significant two-dimensional character.

Magnetization Measurements

SQUID (superconducting quantum interference device) measurements of the sample magnetization were carried out at NRL on the same samples as a function of temperature and magnetic field. Figure 3 shows the 10 K in-plane and perpendicular magnetization curves of the 1.8 ML sample. These data indicate two important features. First, it is much easier to saturate the magnetization when the field is applied perpendicular to the film than would be expected for a thick Fe film (indicated by the dashed line). In fact, in contrast to thicker Fe films, it is easier to saturate the film with a perpendicular H than with an in-plane field. Second, after the sample has been saturated with such a strong field, there is a remanent magnetization M_r that is a significant fraction of the saturation magnetization M_s. No such remanence is found after in-plane saturation.

From these and similar data on other samples, we conclude that, for Fe/Ag superlattices with Fe layers less than 2.4 ML thick, the preferred axis of magnetization is perpendicular to the film at 10 K in agreement with the Mössbauer results [7].

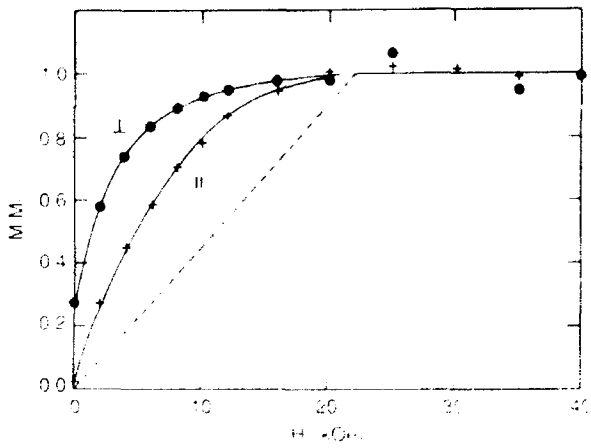

Fig. 3 — Relative magnetization vs applied magnetic field at 10 K for a (Fe/Ag) · 40 superlattice with the ^{57}Fe thickness 1.7 ML. Data were taken with the field parallel (∥) or perpendicular (⊥) to the film. The dashed curve shows the expected thick film curve for H perpendicular.

VERY THIN bcc Co(110)/GaAs(110) FILMS

The bcc form of Co is not a thermodynamically stable bulk phase. However, Prinz [8] was able to stabilize Co in this phase at NRL by growing very thin films on a GaAs(110) substrate, which closely matches twice the expected lattice constant of bcc Co. The films revert to the bulk phase during preparation if they are grown more than about 25 ML thick. The calculated band structure of bcc Co indicates that it is completely band saturated (the majority-spin d-band is completely full) and that it has a large exchange splitting . These aspects make bcc Co an ideal material in which to look for Stoner excitations as is shown below.

Stoner excitations are fundamental one-electron transitions in ferromagnetic metals in which the spin of a d-band electron is reversed with a consequent cost in energy. They can be studied by means of spin selective inelastic electron scattering from itinerant ferromagnets.

Spin-polarized electron energy loss spectroscopy (SPEELS) is a recent advance in spin-resolved methods for surface/thin film analysis that is proving useful for the observation of Stoner excitations. In this technique, conventional electron energy loss spectroscopy (EELS) is supplemented by using spin-polarized incident electrons and monitoring the dependence of the

EELS features on the spin direction of the electrons of the incident beam. Prior to the study summarized here [9], Stoner excitations had been sought in other ferromagnets (Fe, Ni), but complicating spin nonflip excitations and the lack of theoretical calculations of the Stoner transition density of states (DOS) made analysis difficult. Note that a large exchange splitting and a completely saturated band structure such as bcc Co possesses should make analysis of its Stoner spectra particularly clear.

The samples studied were grown by deposition from an electron beam heated Co source onto clean, well-ordered GaAs(110) substrates. Auger spectroscopy and electron diffraction were used to verify the surface cleanliness and crystallinity.

SPEELS Results

In the scattering geometry used for the SPEELS experiment on bcc Co, the spin-polarized incident electrons from an NBS-type electon source scatter off the Co surface, and the specularly reflected beam is energy analyzed. Prior to this measurement, each sample studied was magnetically poled along the easy in-plane axis, and subsequent measurements confirmed the films to be completely magnetized. When desired, the magnetization direction was reversed, and it was found that the spin asymmetry of the data reversed also. The use of such thin films (about 20 ML thick) eliminated any significant local magnetic field effects on the elecron polarization arising from the sample itself.

The analyzed SPEELS data are shown in Fig. 4(a). It is clear that the sharp loss features seen appear only in the spin-down (minority spin) spectrum. The spin-up spectrum shows a largely featureless background caused by spin-independent loss processes that also appear in the spin-down spectrum (dashed line).

The transition DOS can be calculated theoretically, and the details of this calculation are given in Ref. [9]. Using this calculation, the expected Stoner (solid line) and spin nonflip (dotted line) transition DOS are shown in Fig. 4(b). Comparison with the data shown in Fig. 4(a) allows one to assign the loss peak at

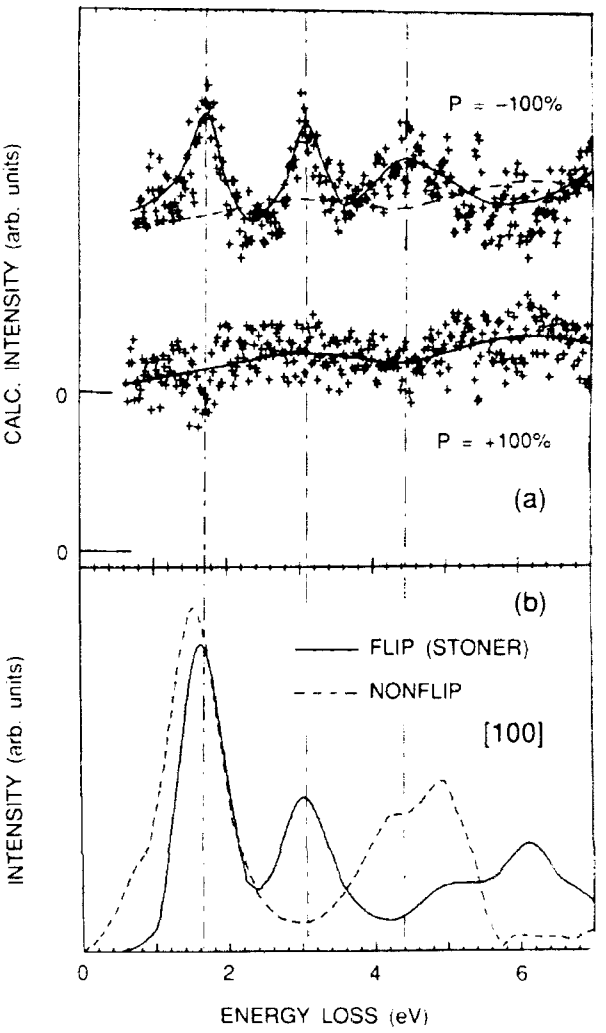

Fig. 4 — (a) Energy loss spectra for ±100% polarized electron beams incident on a film of bcc Co(001); (b) The calculated Stoner (solid line) and nonflip (dotted line) transition density of states for bcc Co(001) with the beam incident along the experimental direction

1.6 eV to the primary Stoner excitation although there is substantial spin nonflip contribution to this peak. The 250 eV incident energy used has a very small probing depth making SPEELS very surface sensitive. Yet the bulk band structure DOS calculations show excellent agreement with the experimental loss features. This suggests that transitions involving surface states do not contribute to the measured loss spectra. In fact, the experimental SPEELS spectra from surface-contaminated samples are only slightly different from those of uncontaminated samples.

These experiments demonstrate the importance of comparing measured SPEELS spectra

with calculated Stoner and spin nonflip DOS for proper identification of the loss mechanisms. The data represent the first observation of multiple features in SPEELS spectra and provide clear evidence for the identification of the Stoner excitations.

SUMMARY

In this article, we have described the program of experimental investigations being carried out by the Naval Research Laboratory group on ultrathin films of Fe grown on Ag(001), on Fe/Ag(001) superlattices containing ultrathin Fe layers, and on very thin Co(110) films grown on GaAs(110). The initial spin-resolved photoemission studies on ultrathin Fe(001) films, which found no in-plane magnetic moment for films 2.5 ML thick or less (when an enhanced moment was expected from theory) have spawned a surprisingly rich set of related theoretical and experimental follow-on studies. It is now a general observation that many ferromagnetic metal films a few ML thick have their magnetic moments normal to the surface at low temperatures, but, apparently because of relaxation effects, exhibit little or no static moment at room temperature. On the other hand, films more than 6 ML thick exhibit properties that are modified from those of thick layers in only minor ways. The initial suggestion, the theoretical support for it, and the confirmation that the ultrathin film magnetic anisotropy is sufficient to overcome the strong demagnetization anisotropy in these samples provides a classic case of worldwide cooperation and competition on a well-defined magnetic ultrathin film problem in a nearly ideal system. Similarly, the experimental results on a metastable phase of Co not found in nature have stimulated both theoretical and experimental work elsewhere on the growth and characterization of this and other metastable magnetic phases.

The vital importance of bringing a wide variety of surface characterization techniques to bear on the physical system used to probe ultrathin magnetic behavior is clearly shown in the Fe/Ag(001) case. These techniques are needed to validate the magnetic data, that is, to assure that one is actually studying the idealized ultrathin structure that was the goal of the sample preparation. This new field of ultrathin films places unusual burdens on the experimentalist and demands sophisticated, detailed experiments. Since there are only a few laboratories throughout the world capable of carrying out such studies, the essential cross-checking of results has generated a new international community of scientists devoted to a field that has come to be called "Surface Magnetism."

REFERENCES

1. G.A. Prinz and J.J. Krebs, *Appl. Phys. Lett.* **39**, 397 (1981).

2. Roy Richter, J.G. Gay, and John J. Smith, *J. Vac. Sci. Technol. A* **3**, 1498 (1985) and *Phys. Rev. Lett.* **54**, 2704 (1985).

3. B.T. Jonker and G.A. Prinz, *Surface Sci.* **172**, L568 (1986).

4. B.T. Jonker, K.-H. Walker, E. Kisker, G.A. Prinz, and C. Carbone, *Phys. Rev. Lett.* **57**, 142 (1986).

5. J. Gay and R. Richter, *Phys. Rev. Lett.* **56**, 2728 (1986).

6. N.C. Koon, B.T. Jonker, F.A. Volkening, J.J. Krebs, and G.A. Prinz, *Phys. Rev. Lett.* **59**, 2463 (1987).

7. J.J. Krebs, B.T. Jonker, and G.A. Prinz, *J. Appl. Phys.* **63**, 3467 (1988).

8. G.A. Prinz, *Phys. Rev. Lett.* **54**, 1051 (1985).

9. Y.U. Idzerda, D.M. Lind, D.A. Papaconstantopoulos, G.A. Prinz, B.T. Jonker, and J.J. Krebs, *Phys. Rev. Lett.* **61**, 1222 (1988) and *J. Appl. Phys.* **64**, 5921 (1988).

THE AUTHOR

JAMES J. KREBS received B.S. and Ph.D. degrees in physics from Saint Louis University in 1954 and 1959, respectively. He came to the Naval Research Laboratory in 1959 as a National Research Council postdoctoral associate in the Magnetism Branch. During his entire tenure at NRL, he has used a wide variety of spectroscopic techniques at radio, microwave, and optical frequencies to probe the behavior of magnetic insulators, III-V semiconductor materials, and magnetic films and multilayer samples via the magnetic ions and nuclei that they contain. Some of the topics investigated include electric field effects on and exchange coupling between transition metal ions, magneto-optical properties of magnetic alloys useful in ring laser gyroscopes, the unusual behavior of magnetic dopants in GaAs and InP microwave device substrate material, the modified properties of ultrathin magnetic films, and the technologically useful coupling and enhanced magnetoresistance in magnetic sandwich structures. During 1975-1976, he was a visiting fellow at Princeton University where he investigated the magneto-optical properties of transparent $RbNiF_3$ and related materials. He was elected a Fellow of the American Physical Society in 1983, based partly on his extensive investigations of semiconductors doped with transition metal ions. Since 1983 he has been a consultant for the Materials Physics Branch specializing in the properties of ultrathin magnetic films and superlattices.

Communicating with Chaos

Thomas L. Carroll and Louis M. Pecora
Materials Science and Technology Division

The study of chaos, a complex form of motion, is relatively new. It is only now that possible uses for chaos are beginning to emerge. We believe that many new technologies useful to the Navy will eventually emerge from this field. One possible application that we have been studying is the use of chaos as a broad band signal for communications.

Until recently, the study of classical mechanics proceeded in two different directions. On the one hand were deterministic mechanical systems, where one could write down all the laws of motion. Deterministic systems were believed to proceed in an orderly fashion, like clockwork; it was from these studies that the nineteenth century concept of God as a clockmaker arose. Small perturbations in the motion were possible, but it was believed that they would be damped out over time and have little effect.

On the other hand, statistical mechanics developed as the study of stochastic, or random, systems. No laws of motion existed, so these systems were not predictable. If one studied a large number of identical stochastic systems, one could find that their motion did fit certain statistical distributions. The study of statistical mechanics therefore involved the study of long time averages of the motion of a system or the average motion of many identical systems.

As early as the time of Newton, it was suspected that not all motion fit into these two neat classes. Newton had speculated that the deterministic motion of a planet in orbit might become highly irregular if it was perturbed by a third body, such as a comet. A foundation for the study of complex nonlinear dynamical systems was not laid until the late nineteenth century by the mathematician Poincaré. This work was not built on until the 1960s, when a more serious study of nonlinear dynamics and chaos began.

Communications depends on both deterministic and stochastic mechanics. Deterministic mechanical laws govern the behavior of such common devices as oscillators or filters. Stochastic mechanics is used in the study of noise and in random number generators for encryption or spread spectrum communications. The type of motion known as chaos has some of the properties of both of these types of motion. Chaos is a highly irregular, nonperiodic form of deterministic motion, which is extremely sensitive to initial conditions. In principle, one could calculate the future motion of a chaotic system, but a small error in specifying the initial conditions will grow exponentially with time. Since all measurement involves some error, it is practically impossible to predict the future motion of a chaotic system. The unique properties of chaos have not yet been exploited for any useful systems; most applied research has concentrated on suppressing chaos. We have been studying how to apply chaos to problems of interest to the Navy, such as communications. After a brief introduction to chaos, we will describe one possible application of chaos.

INTRODUCTION TO CHAOS

The description of chaos came about as a result of advances in the field of nonlinear dynamics [1]. A dynamical system is a system that changes over time in a way that may in principle be described by some set of rules, such as differential equations or recursion relations. A pendulum is an example of a dynamical system, as is an electrical oscillator. If one

knows the rules that govern a dynamical system, one may predict the future behavior of the system knowing only its starting point. For this reason, the type of dynamical systems that we describe here are known as deterministic.

The behavior of a dynamical system is typically described by plotting its trajectory in a phase space, where each direction corresponds to one dynamical variable. The systems we are concerned with are dissipative, so their motion in phase space will eventually settle down to a finite region known as an attractor. A system with periodic motion will follow a closed path in phase space. A system whose motion possesses incommensurate periods will move on the surface of a torus.

Complex motion is possible if one or more points in the phase space are unstable, so that motion in regions of phase space near these points diverges. Since all real systems are finite, this motion cannot diverge forever. It may be that the system variables reach some maximum possible value, such as a power supply voltage, and stay there. In other systems, some mechanism for folding the motion back in towards the unstable region may exist. In this type of attractor, trajectories repeatedly are stretched apart near the instability and folded back in. This repeated stretching and folding in phase space produces the complex motion known as chaos. The stretching and folding also cause the motion to depend sensitively on the initial conditions, making prediction a practical impossibility.

The rate of this stretching is described by the Lyapunov exponents. One may measure what happens to small perturbations to the trajectory in phase space. The average change in a perturbation is measured over the entire attractor. The natural logs of the components of the average change vector are the Lyapunov exponents. A positive exponent means that perturbations are increasing along some direction, a negative exponent means that perturbations are decreasing, while a zero exponent means that perturbations are staying the same size. A chaotic attractor has at least one Lyapunov exponent greater than zero, while the largest exponent for a periodic attractor is zero.

CHAOTIC SYNCHRONIZATION

Since chaos looks like noise, most applied work on chaos has been directed toward eliminating it. We saw these noiselike properties as useful. One might think of a chaotic system as a noise source that, because of its deterministic nature, may be easily characterized. It occurred to us that if we could produce a chaotic signal at one location and reproduce an identical chaotic signal at a remote location, then we could encode information onto the original chaotic signal and decode it using the reproduced signal. Because of their great sensitivity to initial conditions, isolated chaotic systems not only will not synchronize with each other, but their outputs will not even be correlated with each other. It is necessary to send information from one chaotic system to the other in order to synchronize them.

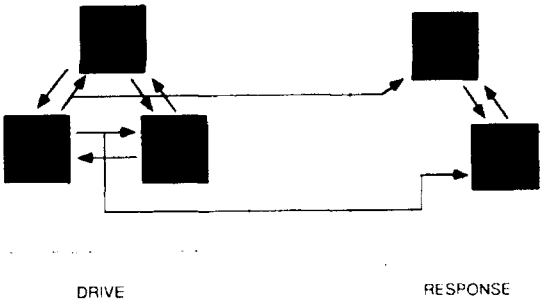

Fig. 1 – Block diagram of synchronizing chaotic systems. The response system is a duplicate of part of the drive system. The response system is driven by the signal or signals that come from the missing part of the system.

Our approach was to view a chaotic system as a group of interconnected subsystems. We could then reproduce one of the subsystems and drive it with whatever chaotic signals it originally saw from the full chaotic system [2]. Figure 1 is a schematic of this arrangement. We call the full chaotic system the drive system, and we call the driven subsystem the response system. The output of the response system depends on its Lyapunov exponents. If all the Lyapunov exponents of the driven response

system are less than zero, then the response system will follow the drive signal, so that a particular signal in the response system is synchronized with the corresponding chaotic signal in the drive system. Because the response system is stable, this method is not sensitive to small amounts of noise or mismatch in the drive and response systems. The range of initial conditions over which this synchronization occurs varies from system to system and depends mainly on the presence of other basins of attraction in the system.

We may demonstrate this synchronization with a numerical experiment. We use the Lorenz equations, which are well known in the field of nonlinear dynamics:

$$\frac{dx}{dt} = \sigma(y - x)$$

$$\frac{dy}{dt} = -xz + rx - y$$

$$\frac{dz}{dt} = xy - bz.$$

When $\sigma = 10.0$, $r = 60.0$ and $b = 8/3$, these equations produce chaos. We used a numerical integration routine on a workstation to integrate these equations. We chose a subsystem consisting of the x and z equations and drove them with the y variable from the full chaotic system. Figure 2 shows how the z variable in the response system converged to the z variable in the drive system within a few cycles of the drive.

CASCADING SYNCHRONIZED CHAOTIC SYSTEMS

We may actually choose other response systems for the Lorenz equations above. The y and z equations together also form a stable subsystem that may be used as a response system when driven by the x variable. Since there are two possible response systems, we may also cascade these response systems as shown in Fig. 3. One may think of the cascaded response systems as a black box where a chaotic signal from the drive signal goes in and a chaotic signal comes out. If the response systems are synchronized to the drive system, the output chaotic signal matches the input signal. If we change a parameter in the drive system, then the output chaotic signal does not match the input chaotic signal. In this way, we may send information using the chaotic signal as a carrier.

We wanted to show that this chaotic synchronization worked in real systems, so we built the simple chaotic circuit shown in Fig. 4 [3]. This circuit becomes chaotic through a period doubling cascade as shown in Fig. 5(a-d), which shows that a series of attractors seen as resistor R12 is decreased. Figure 6 shows the power spectrum of the voltage measured at the x_1 point in the circuit. This power spectrum is broad band with a few prominent frequency peaks. More complex chaotic systems can have power spectra that resemble colored noise.

Designing even a simple chaotic circuit such as this was a challenge. There are no general laws that determine when a given system will be chaotic. We could merely use our intuition and experiment to find chaotic circuits. We also had to find a chaotic circuit that could be divided into at least two response subsystems. There is no general method for designing a circuit so that it has stable subsystems. We were able to come up with a few guidelines that work in simple cases, but again much intuition was necessary.

The hardest problem to solve was matching the response subsystems to the full circuit. Matching the circuits required finding nonlinear elements whose behavior matched to within 1 or 2% over a wide range. Typical semiconductor devices by themselves never come close to these figures. Some manufacturers produce chips that perform analog multiplication, but these still were not reproducible enough. We finally solved the problem of producing reproducible nonlinearities by using an arrangement from analog computer technology known as a diode function generator. In this type of circuit, diodes are used to switch different linear characteristics on or off to produce a piecewise linear approximation to any function. The boxes in Fig. 4 labeled g1 and g2 contain diode function generators.

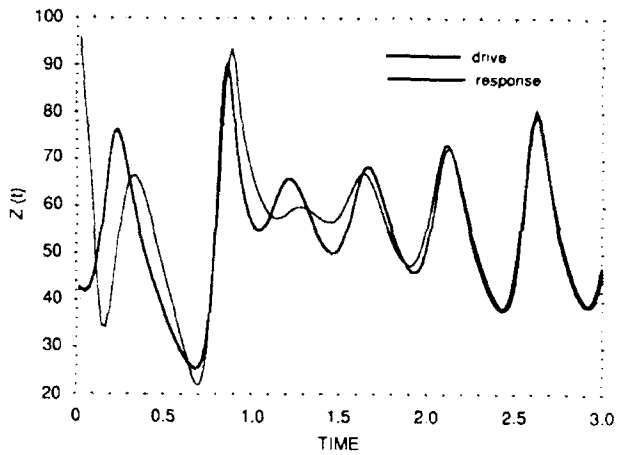

Fig. 2 — Time series from the computer simulation of the Lorenz equations showing how the response system converges to the drive system

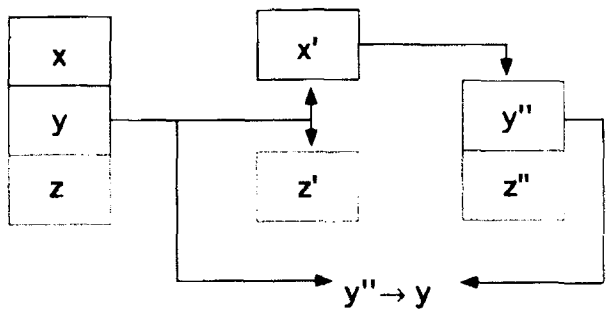

Fig. 3 — Block diagram of cascading the synchronized chaotic Lorenz equations

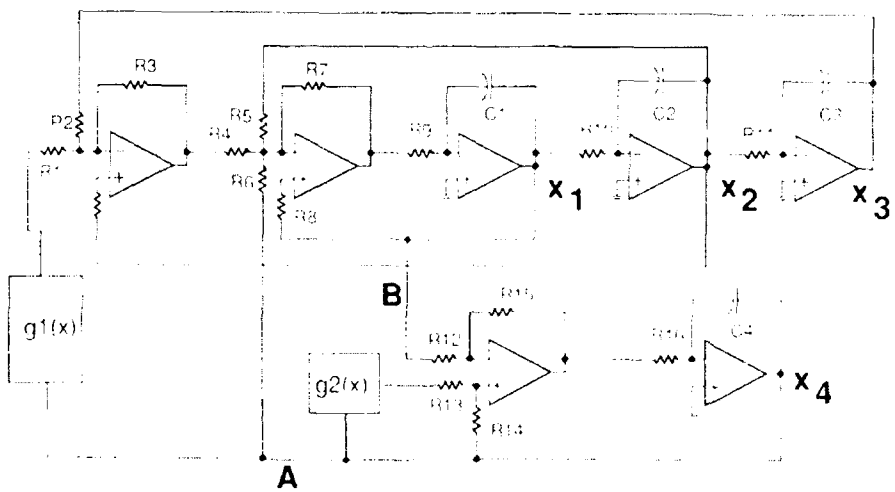

Fig. 4 — Schematic of a circuit used to study the cascading of synchronized chaotic systems. Voltages were sampled at the points labeled x_1, x_2, x_3.

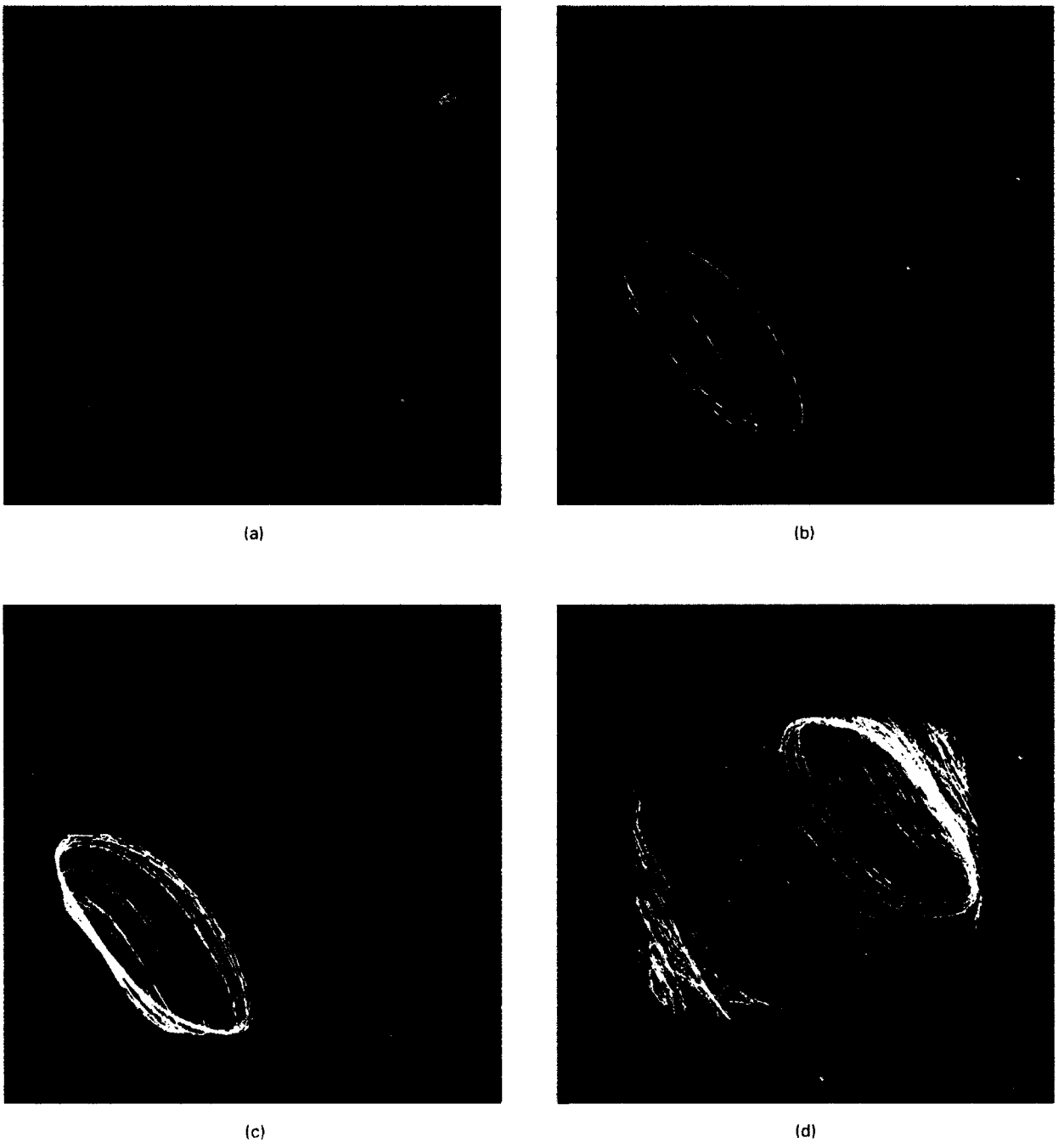

(a) (b)

(c) (d)

Fig. 5 — A series of attractors seen in the circuit as resistor R12 is decreased

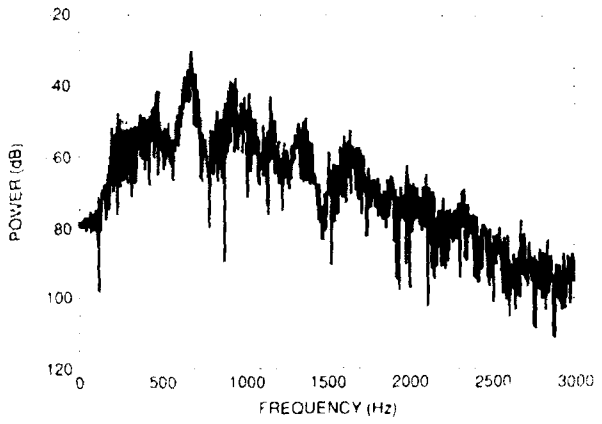

Fig. 6 — Power spectrum of the x_1 signal from the circuit when the circuit is in the chaotic attractor seen in Fig. 5(d)

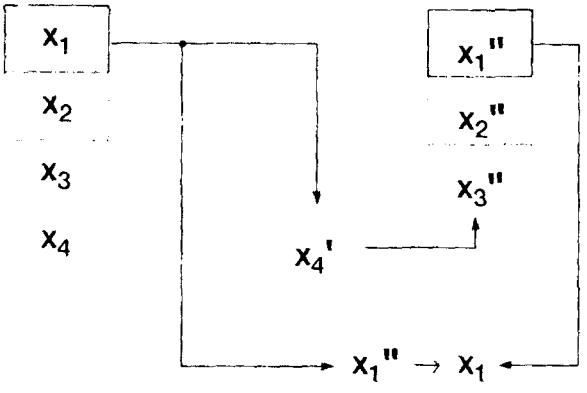

Fig. 7 — Block diagram of cascading the synchronized chaotic circuit

This circuit could be divided into two subsystems, one containing the x_4 variable and the other containing the x_1, x_2, x_3 variables. Figure 7 shows schematically how the circuits were cascaded, with the full system driving the x_4 subsystem, which then drove the x_1, x_2, x_3 subsystems. With this arrangement, the x_1 signal used as an input and the x_1 output match to within about 2%.

APPLYING CHAOTIC SYNCHRONIZATION

We have tried several methods for sending information with our chaotic carrier signal. The simplest method involves using a single noncascaded response system. In this arrangement, the drive signal is used to synchronize the response system to the drive system. In the Lorenz system, for example, the x-z subsystem would be driven by the y signal. Information would then be added to another of the chaotic signals, such as the z signal. This signal would also be transmitted to the response system. The synchronized z signal produced by the response system could then be subtracted from the transmitted $z+$ information signal to yield the information. We have successfully demonstrated this method in a circuit.

This approach is simple, but it does require that the user send two signals. A more elegant approach is to use our cascaded synchronized chaotic systems to send information with only one signal. We have tried two simple methods: one that is analogous to the amplitude modulation that is already in use, and another that resembles phase modulation. We applied these ideas to both numerical experiments and the circuit described above. In this space we will describe only the circuit results.

In our amplitude modulation experiment, we used an analog multiplier chip to multiply the output of the drive system by $1 + 0.1 \sin(\omega t)$. We used a modulation frequency ω of 6 Hz, which was about 1% of the most prominent frequency (700 Hz) in the power spectrum of the chaos. The effect of the modulation was easily detected by taking the difference between the modulated driving signal and the output of the response circuit. There was a limit to the fastest modulation signal that could be used. The rate at which the response system converged to a drive signal was determined by the least negative of the Lyapunov exponents, which was about $-600\ s^{-1}$ for this system. If a modulation signal of 70 Hz was used, the response circuit could not follow the drive signal as well.

An alternate method for sending a signal on a chaotic carrier with the cascaded synchronized chaotic circuits was to modulate a parameter in the drive circuit. We put an analog multiplier chip in front of one of the operational amplifiers in our chaotic circuit and used a potentiometer to set the multiplication factor. Changing this multiplication factor would change the output of the drive circuit, so that the input to and the output from the response circuit no longer matched. Using this difference, one could calculate the difference between the multiplication

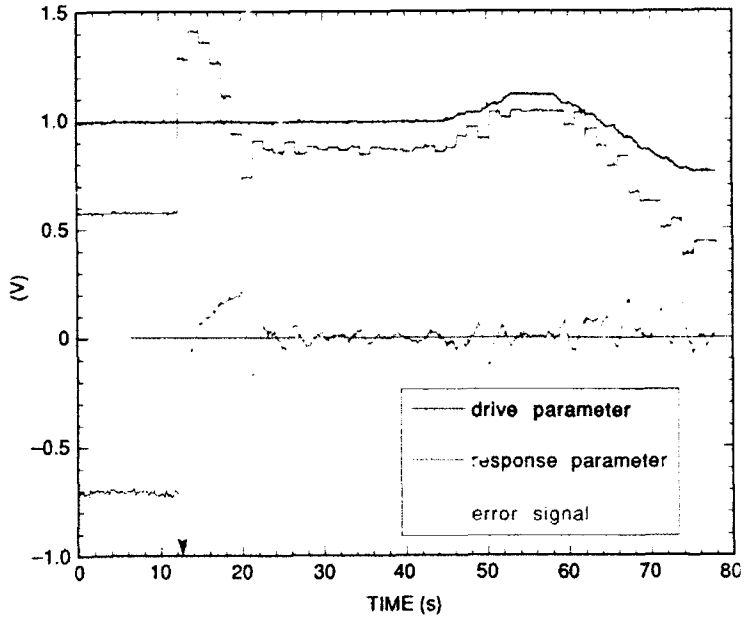

Fig. 8 — Results of using a chaotic carrier from the circuit to send the value of a parameter to a cascaded response circuit

factor in the drive circuit and the multiplication factor applied to a multiplier in the corresponding part of the response circuit. The multiplication factor in the response circuit could then be corrected to track the multiplication factor in the drive circuit. Used in this fashion, the cascaded circuits resembled the chaotic version of a phase locked loop.

Extracting the parameter difference from the difference between two chaotic signals was not as straightforward as the same procedure for two periodic signals, where one could compare frequency or phase. A chaotic signal does not have a single frequency or a phase. In this case, there is a quantity resembling an average phase for the chaotic signal that can be used. When all circuits are synchronized, if we strobe the output of the response system when the drive signal crosses zero, the result will be zero. If the drive and response are not synchronized, then the output of the response will not be zero when the drive crosses zero. The average of the output signal at this zero crossing varies approximately linearly for small parameter differences. An analog integrator circuit is used to create this average from the output of a sample and hold circuit. This average is then used with an analog control circuit to correct the value of the multiplication factor in the response circuit.

Figure 8 shows that this technique works in a real circuit. This figure shows the value of the multiplying factor in the drive circuit and in the response circuit. At $t = 12$ s, the control is turned on. The multiplication factor in the response circuit is immediately affected and soon settles to a value near the multiplication factor for the response circuit. The response does not match the drive more closely because these parameters are set with analog multiplier chips, which do not match very well but were convenient to use for this experiment. The response multiplication factor is able to track changes in the drive multiplication factor, as is shown in the figure.

CONCLUSIONS

These simple experiments merely serve as proof that these concepts work. These examples may not correspond to the way that these principles would actually be used, but that is not important. The important part of this work is that it starts engineers, physicists, and mathematicians thinking differently about using chaotic

systems. The idea that chaotic systems may be taken apart and recombined to form new, useful systems is completely new. So is the idea of driving a system with a chaotic signal. There are many variations on these ideas that we have not discussed.

In our experiments, we also have the luxury of no noise. Chaotic signals are transmitted by wires. In a real communications system, the chaotic signals would be broadcast through a noisy background. Separating a nonperiodic signal from noise is not an easy task. There are several new software algorithms being developed that might work adequately with our system to allow us to detect chaotic signals in a noisy background.

SUMMARY

We have shown how one may take apart and reconnect chaotic systems so that one may drive one system with another, which then synchronizes to the drive. We have used these techniques to create chaotic versions of AM or FM radios, where the periodic carrier is replaced with a chaotic carrier. These ideas may have applications in encryption or in spread spectrum communications, technologies that are important both to the Navy and to civilian industries.

REFERENCES

1. P. Berge, Y. Pomeau, and C. Vidal, *Order within Chaos* (Wiley, New York, 1984).

2. L.M. Pecora and T.L. Carroll, "Driving Systems with Chaotic Signals," *Phys. Rev.* **A44**, 2374-2383 (1991).

3. T.L. Carroll and L.M. Pecora, "A Circuit for Studying the Synchronization of Chaotic Systems," *Int. J. Bifurcations and Chaos*, Vol. 2, pp. 659-667, September 1992.

THE AUTHORS

THOMAS L. CARROLL received degrees in physics from Carleton College (B.S., 1981) and the University of Illinois at Urbana-Champaign (M.S., 1983; Ph.D., 1987), where he did spectroscopic studies of molecules under high pressure. He came to NRL in 1987 as an Office of Naval Technology postdoctoral fellow and became a permanent NRL employee in 1991. His initial research at NRL concerned nonlinear dynamics and chaos in ferromagnetic resonance experiments in yttrium iron garnet. Since that time, his research has focused on new applications for chaos and building analog electronic circuits or computer models to test these circuits. He has published approximately 30 papers and has applied for four patents.

LOUIS M. PECORA received his B.S. degree in physics from Wilkes College in 1969. After two years of graduate work at Purdue University and a year as a foreman in the Hazleton Weaving Company, he enrolled in the Syracuse University Solid State Science program from which he received a Ph.D. in 1977. His dissertation topics included the effects of adsorbed gases on the magnetic properties of fine iron particles and correlations between metallic properties and atomic electronic states in transition metals. Following an NRC postdoctoral fellowship at NRL in 1977, he took a permanent position in 1979 and continued the positron work into areas of reconstruction of momentum densities using novel tomographic techniques in collaboration with the international group at the University of Geneva. In the mid-1980s, Dr. Pecora moved into the field of nonlinear dynamics in solid state systems. Early work led to the discovery and characterization of chaotic transients in spin-wave behavior in yttrium iron garnets. More recent work has focused on the applications of chaotic behavior, especially the effects of driving systems with chaotic signals. This has resulted in the discovery of synchronization of chaotic systems and pseudoperiodic driving of nonlinear systems. Dr. Pecora has published over 50 scientific papers and has applied for four patents for the applications of chaos.

Trans-Oceanic Acoustic Propagation and Global Warming

B. Edward McDonald, William A. Kuperman, and Michael D. Collins
Acoustics Division

Kevin D. Heaney
Planning Systems, Inc.

INTRODUCTION

Can the world's oceans be used to monitor global warming? NRL is conducting theoretical/numerical investigations into the physics of ocean basin-scale acoustic transmissions to help answer this provocative question. If the coupled atmosphere/ocean system is warming at rates estimated from known greenhouse gas increases, sound travel times across major ocean basins may provide one of the most stable and accessible measures of major trends in global average temperature [1].

Acoustic Thermometry

The oceans contain a significant fraction of the ecosphere's heat content. It has been estimated that the oceans have absorbed about half of the heat content involved in temperature trends averaged over the past century. Measurements of sound propagation times across major ocean basins can provide temperature information averaged over large ocean volumes containing heat stored or lost during atmospheric temperature changes. The use of sound to measure temperature changes is referred to as acoustic thermometry. The Defense Advanced Research Projects Agency (DARPA) has recently initiated a multiyear program for Acoustic Thermometry of Ocean Climate (ATOC).

The sound speed of ocean water depends upon temperature, salinity, and pressure. Its most sensitive dependence is upon temperature, increasing on the order of 0.3%/° C warming. The measured atmospheric warming rate averaged over the past century is approximately 0.02° C/yr [2]. From this rate, modelers estimate a present warming rate 1 km below the ocean surface of roughly 0.005° C/yr [1]. Since measured sound transit times across the longest known ocean acoustic paths are roughly 10,000 s, the estimated present warming rate of the deep ocean should decrease the transit time by slightly more than 0.1 s/yr, a rate within the range of present measurement technology. Transit time measurements over a multiyear program may reveal whether the ocean is indeed warming at rates that might be of societal concern.

The Heard Island Feasibility Test

In January 1991, an ocean experiment of unparalleled interest and international cooperation was conducted from the vicinity of Heard Island in the Indian Ocean (Fig. 1). The Heard Island Feasibility Test (HIFT) was proposed and executed by Munk and colleagues [1] to establish whether sound from nonexplosive sources can be detected across major ocean basins and to provide a testbed for signal transmission algorithms. The location was chosen for its access to high-quality acoustic paths to both coasts of North America and other potential listening stations (some of which are illustrated in Fig. 1). A vertical array of ten sources operating near a center frequency of 57 Hz and generating approximately 100 kW total acoustic power was deployed near a mean depth of 175 m. A total of 18 installations consisting of oceanographic ships and/or hydrophone stations were donated by nine countries to listen for the signal in all major ocean basins except the Arctic. Cooperation with the experiment was

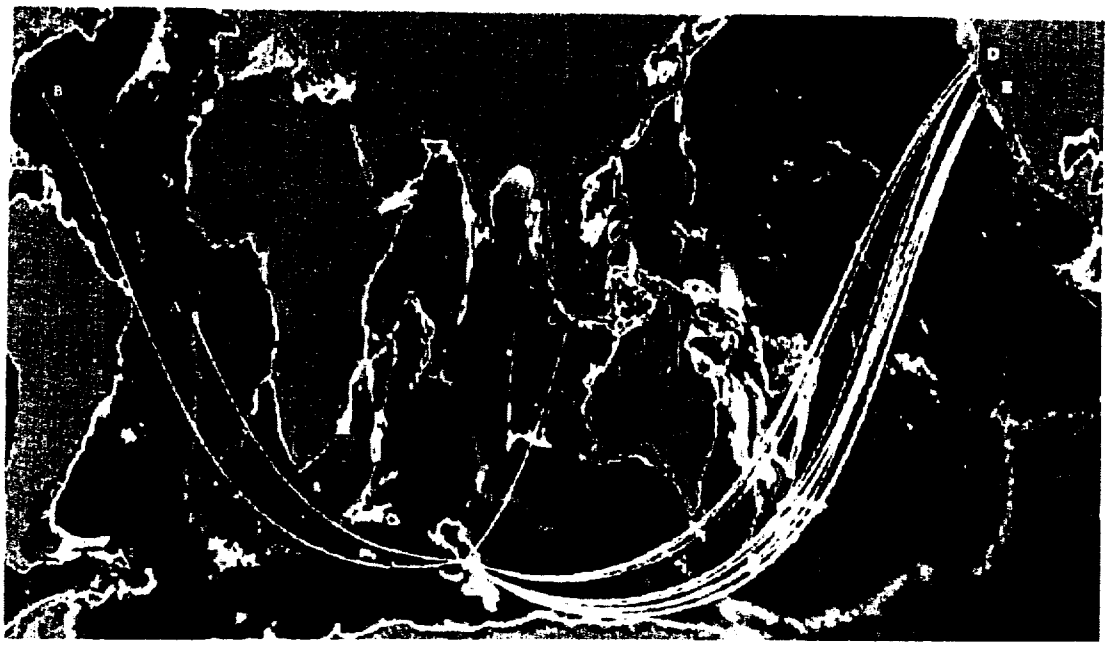

Fig. 1 — Calculated propagation paths from Heard Island to receivers at Ascension (A), Bermuda (B), Christmas (C), Oregon (D), and California (E). Each acoustic normal mode may in principle follow a different path: mode 1 is white, 2 is magenta, 3 is yellow, and 4 is red. Color scale for ocean depth: red is 0-200 m, yellow covers 1-2 km, and black is 6 km or more.

voluntary and without international organizational structure. Receptions of good to excellent quality were obtained at most stations. Adequacy of source levels was established, and timing accuracy had been established in earlier experiments as 0.001 s for a 1000 km path.

Why the Ocean?

The deep ocean has been known for decades to be a truly remarkable waveguide for long distance propagation of sound. The deep ocean sound speed as a function of depth typically reaches a minimum at a depth of roughly 1 km (Fig. 2). Proceeding down from the surface, the sound speed first decreases because of decreasing temperature. At great depth, temperature and composition parameters are roughly constant. The sound speed then begins to increase gradually downward because of increasing hydrostatic pressure. The roughly horizontal layer near the sound speed minimum is referred to as the ocean sound channel; the locus of the minimum is known as the axis of the sound channel. Snell's law for acoustic propagation in the deep ocean states that rays representing a propagating wave bend toward water of lower sound speed. A consequence of the existence of a vertical minimum in sound speed is that low grazing angle rays oscillate about the sound channel axis. Over long distances, they trace out approximately sinusoidal curves with wavelengths of order 50 km. Rays that oscillate about the axis without touching the surface or bottom are considered "trapped" in the sound channel.

Ray descriptions of wave propagation represent a high frequency approximation. To obtain a more accurate description of ocean acoustics at frequencies below roughly several hundred Hz, one deals with the continuous wave field of acoustic pressure oscillations. As with many cases of small amplitude oscillations in physics, it is helpful to resolve the acoustic pressure field into normal modes. Figure 2 shows the normal mode representation of trapped acoustic waves in the sound channel. These modes propagate horizontally in the sound channel, free of strongly dissipative interaction with the ocean surface or bottom. At low frequencies (e.g., 30-100 Hz), volume attenuation processes such as viscosity or molecular relaxation fall in the

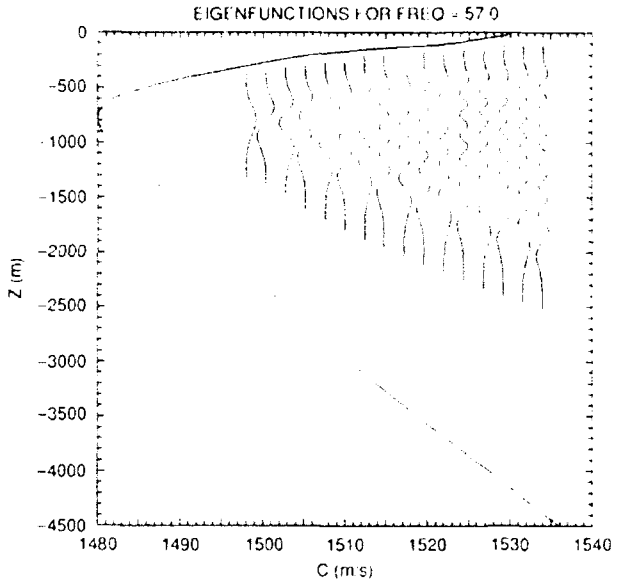

Fig. 2 — Normal modes of acoustic oscillation typical of the deep ocean. The sound speed profile $c(z)$ (left curve) was taken near Ascension Island in the South Atlantic (A in Fig. 1).

range of 10^{-4} to 10^{-3} dB/km. Signals in this frequency range have been received halfway around the world from their source, their amplitudes gradually decreasing as the inverse square root of distance (i.e., cylindrical rather than spherical spreading caused by the vertical constriction of the ocean waveguide).

Why not make measurements directly in the atmosphere? Atmospheric temperature records have been kept for over a century [2], but they are subject to major oscillations from weather systems and seasonal variation. Indeed, one has to average over decades just to begin assessment of a trend. Is acoustic thermometry over a large volume of atmosphere feasible? The atmosphere contains an acoustic waveguide caused by a vertical minimum in sound speed occurring in the stratosphere, and it exhibits an increase of sound speed with temperature comparable to that of the ocean. The atmosphere, however, is far too active, lossy, and plagued with natural and manmade noise to permit global scale sound transmission experiments to obtain volume-average temperature trends.

ACOUSTIC PROPAGATION PATHS

Two issues remain unanswered in the conceptual task of using ocean thermometry to monitor global warming: ambient variability and multipath in the received signal. The NRL work addresses the second. If two or more paths exist to the receiver because of reflection or refraction, establishment of travel times may be impeded by signal interference among the different paths. Understanding of detailed propagation paths may help in the choice of acoustic array location and/or interpretation of receptions.

The Perth-to-Bermuda Benchmark

An example of NRL's use of theoretical/numerical models to interpret experimental results is the 1960 acoustic propagation from a set of TNT charges detonated in the ocean near Perth, Australia. The experiment sought to detect the detonations with a set of hydrophones in the ocean near Bermuda, within 200 km of the antipode of the source location. The conceptual model used to locate the source and receiver was that of acoustic rays following great circles on a spherical Earth surface. All great circles through a given point meet exactly halfway around the globe. The convergence of rays on the antipode implies signal intensification; the signal should be of locally maximum amplitude near the antipode and hopefully detectable. Assuming sound propagation along great circles, there appeared to be an open water path between source and receiver (Fig. 3).

The experiment was an apparent success. Approximately 13,000 s after the detonation of

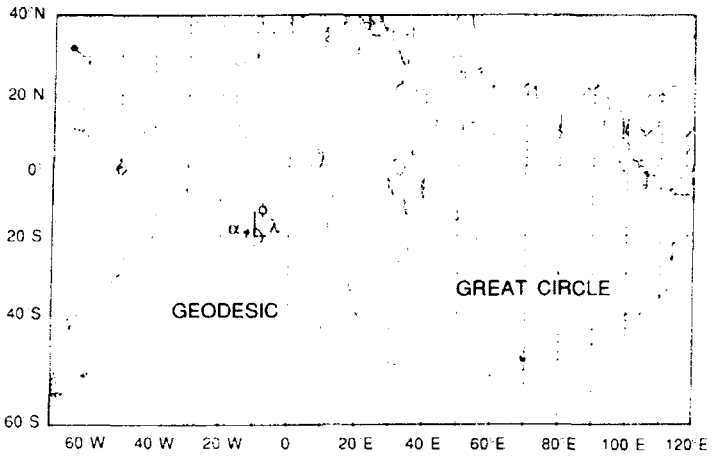

Fig. 3 — The great circle path from Perth to Bermuda compared to the geodesic (shortest distance path) on an ellipsoidal Earth as distorted by rotation. The large departures between great circle and geodesic result from the end points being very nearly antipodal.

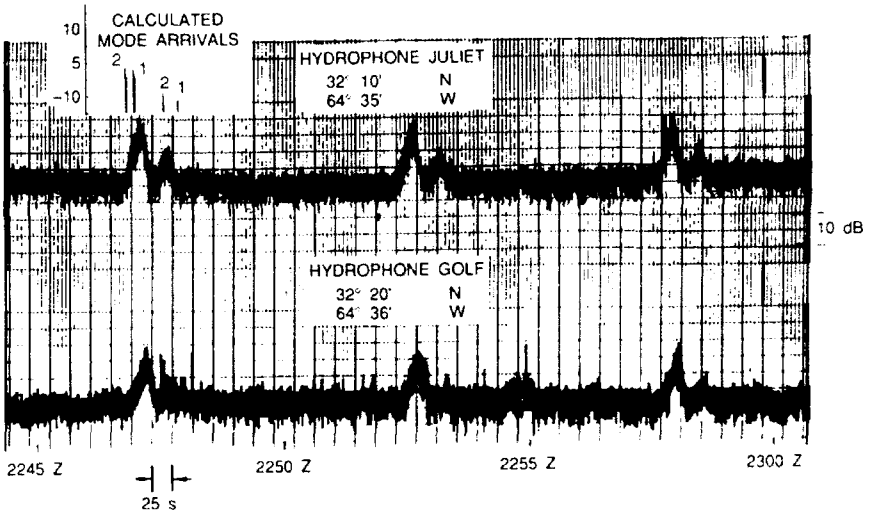

Fig. 4 — Strip chart from the 1960 Perth-Bermuda transmission. Approximately 13,000 s after the detonation of each 300-lb TNT charge, a pair of arrivals separated by approximately 30 s was recorded near Bermuda. The inset in the upper left gives the mode arrivals as calculated from the NRL adiabatic mode model.

each TNT charge near Perth, a pair of arrivals separated by approximately 30 s was recorded on the Bermuda receivers (Fig. 4). The double arrival structure had not been anticipated, but was conjectured to have resulted from an unidentified multipath. It was realized some years later that two important effects had been ignored in analyzing the 1960 experiment: (1) the distortion of the Earth's shape caused by rotation, and (2) the horizontal gradient in the ocean's acoustic index of refraction caused by the pole-to-equator temperature gradient. The importance of the Earth's nonsphericity can be seen in Fig. 3, which compares the great circle path from Perth to Bermuda to the corresponding geodesic on the ellipsoid that most closely represents the Earth as distorted by rotation (no refractive effects are included in Fig. 3). The geodesic path is considerably to the south of the great circle, but is apparently a clear water

path. The attempt to correct for the refractive effect, however, was not greeted with apparent success.

In 1988, a refractive correction was computed [3] for the Perth-Bermuda path using the assumption that sound trapped in the sound channel propagates at the vertical minimum sound speed of the channel. This assumption allows a three-dimensional sound speed field c to be replaced with the two-dimensional field c_{min}, the minimum of c over depth. The 1988 work further simplified the calculation by assuming that c_{min} depends on latitude only, approximating the average north-south refractive gradient. The eigenrays (which connect source and receiver and satisfy a differential form of Snell's law in the intervening medium) calculated from these assumptions were displaced to the north and beached on the east coast of Africa, leaving the Bermuda receiver deep in a shadow zone. Considerable interest was stirred in explaining why the 1960 experiment worked. A global scale acoustic model should be able to explain Perth-Bermuda if it is to address comparable future experiments with success.

THE NRL EFFORT

The current NRL project in global acoustic propagation began in 1990 with an attempt to understand the negative result in the 1988 refraction calculation. It consists of two numerical/theoretical modeling areas: (a) adiabatic mode calculations for determination of acoustic normal modes, horizontal propagation paths of the modes, and times of flight and (b) newly emerging developments in parabolic equation (PE) methods for integrating outgoing wave fields in two dimensions—depth and range.

Adiabatic Normal Modes

We have used adiabatic mode theory to calculate horizontal phase speeds c_n ($n = 1, 2, \ldots$ being the mode number) as a function of latitude and longitude from existing ocean databases. From c_n and Snell's law, we find the horizontal path taken by mode n. The three-dimensional acoustic wave field may be represented as a sum over normal modes each possessing two-dimensional (horizontal) propagation characteristics. Adiabatic normal mode theory assumes that the ocean waveguide varies so slowly in the horizontal that energy in mode n at any given location remains totally in mode n as the signal propagates through the waveguide. Calculation of the vertical normal modes yields the horizontal phase speed for each mode, including dependencies on ocean and bathymetric parameters. In general, modal phase speeds increase toward shallow water. A result of this dependency in light of Snell's law is that sound rays tend to veer away from bathymetric features and toward deeper water.

Upon numerical integration of the horizontal ray equations derivable from adiabatic normal mode theory [4], we found that each of the first several modes possesses multiple eigenray solutions for the Perth-to-Bermuda path. Figure 5 illustrates the five eigenrays found for mode 1 and six for mode 2. Northern and southern eigenray bundles (denoted A and B) result from blockage of the intervening region by Kerguellen Banks (near 70° E longitude). Micromultipath within bundles A and B results from grazing bathymetric reflections in regions denoted by rectangles. Integration of group travel times along the modal propagation paths yielded good agreement (Fig. 4) with the experimental data, including the double arrivals.

Even though the experimental data are 30 years old, the NRL work since 1990 has produced the following unexpected but quantitatively sound interpretation of the Perth-Bermuda results: The first of each double arrival is a signal along the shorter and faster path A, with the second being along the longer and slower path B. (By faster, we mean that the average sound speed is higher. This is a result of the waters along path A being warmer than those along path B.) The pulse widths at the receivers are consistent with the calculated levels of dispersion in the ocean waveguide along the propagation paths.

The PE Method

The PE method, which accounts for coupling of energy between modes, involves approximating the full wave equation with a

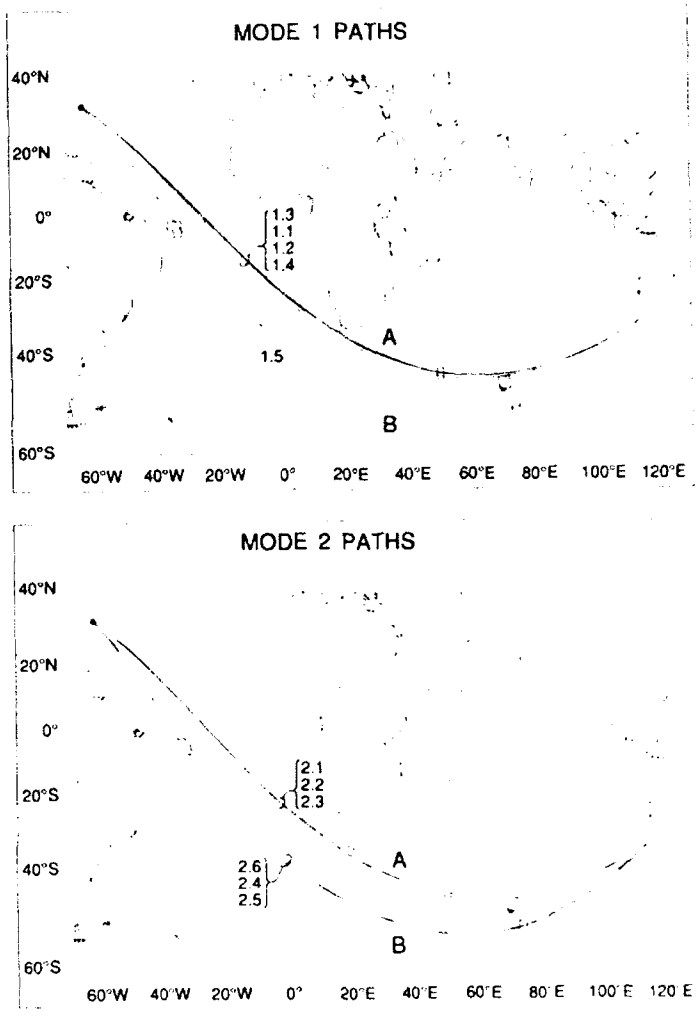

Fig. 5 -- Modal eigenrays for the Perth-Bermuda experiment as calculated by the NRL model

one-way wave equation that may be solved efficiently. The PE method is accurate because its assumptions about how sound propagates are generally applicable to the ocean: energy is mostly outgoing, and the speed of sound varies gradually in the horizontal directions. Until recently, PE solutions were obtained with the following two-step procedure: (1) apply a Padé approximation (which is more accurate than a Taylor series) to derive a one-way wave equation and (2) apply standard numerical techniques to solve the one-way wave equation.

It is possible to combine these steps so that the robustness of the Padé approximation is exploited to reduce both asymptotic and numerical errors [5]. A PE model based on this approach is about two orders of magnitude faster than contemporary PE models with similar capability. Once the horizontal propagation paths are determined, this PE model is used to solve for the outgoing wave field in the two-dimensional space defined by depth and horizontal range along the propagation path. Since the new PE model permits very large steps in the range integration, it is practical to consider all of the major HIFT propagation paths.

THE HEARD ISLAND RESULTS

Several features of the 1991 HIFT data are in excellent agreement with expectations. Many of the listening stations received clear signals;

most arrival angles were in close agreement with the NRL model's calculated eigenrays [6]. Launch angles for the eigenrays (inferred experimentally from Doppler shifts at the receivers) were also in general agreement with eigenray calculations. At Christmas Island, the received signal contained a Doppler shift that was used to infer source motion along the line of sight. The source ship's motion recorded via satellite agreed with the Doppler-inferred position within 10 m over the course of one hour's transmissions.

There were, however, some surprises. Some of these remain unresolved, but some have found interpretation via the NRL model. A vertical array off California detected approximately eight modes surviving the nearly 18,000 km flight from Heard Island. It had been expected that bathymetric interaction near New Zealand would strip off modes higher than the first few, since shallow coastal seafloors absorb energy preferentially from high modes.

Another surprise was the complexity of the signal received at Christmas Island. The propagation path from Heard to Christmas was primarily south-to-north, so that the signal spent minimal time in the dispersive conditions near the Antarctic Circumpolar Convergence. A synthesized 0.1-s pulse transmitted from Heard had spread to over 5-s width in 5,500 km propagation to Christmas. Despite the phase stability implied by the accuracy of the received Doppler shift, the signal amplitude structure within the 5-s pulse width changed markedly during transmissions repeated at 45-s intervals.

The NRL Predictions

Figure 1 shows modal propagation paths from Heard Island to major receiving stations, as computed by the NRL adiabatic mode model. For most of the paths, results for travel time and signal bearing at the receiver agreed with experimental data. The paths through the Tasman Sea (between Australia and New Zealand), however, were apparently blocked or subject to strong absorption. A Japanese team near Samoa failed to receive signals along this path. As determined from signal travel time and bearing at the receiver, a hydrophone installation off the coast of Oregon received the signals passing south of New Zealand, but the ones through the Tasman Sea were not detected.

Figure 6 gives the NRL model interpretation of the signals received at a vertical array off San Diego. Figure 6(a), gives the propagation path for mode 1. In Fig. 6(b) we give a depth-range PE calculation of the sound intensity along the mode 1 path. The calculation is initialized near Heard with a point source at 175 m depth. In Fig. 6(b), one sees evidence of bottom loss from Heard to the southernmost point (B) of the ray path and then on the shoulders (C) of the New Zealand plateau. Many modes are present at zero range as a result of point source excitation. One sees rather modest exchange of energy between modes until just before the New Zealand plateau (C). Just before the shallowest water along the path, Fig. 6(c) reveals that modes higher than about 9 suddenly disappear. Figure 6(b) at this point indicates the sudden presence of deeply penetrating sound in the bottom, i.e., mode dumping. Past the New Zealand plateau, there is only modest modal redistribution. When the ray reaches California, the first eight modes are well populated. This result is consistent with the vertical array's unexpected reception of roughly eight modes off California. The NRL model attributes the origin of these modes to bathymetric interaction south of New Zealand.

One of the HIFT exercises demonstrated "pulse compression" by transmitting different frequency components of a short pulse in different time windows. The frequency components were later combined in a common time window during signal processing. The simulated wavetrain consisted of five cycles of a 57 Hz sine wave, for a total pulse length of approximately 0.09 s.

The various frequency components of the pulse were transmitted with coded phase shifts for identification purposes. After propagating a distance of 5,500 km (Heard to Christmas Island), the signal components were recorded and later superimposed numerically. The synthesized pulse revealed unexpected multiple arrivals with an envelope of width approximately 5 s (Fig. 7). On the Heard-Ascension Island leg (9000 km, result not shown here), the pulse

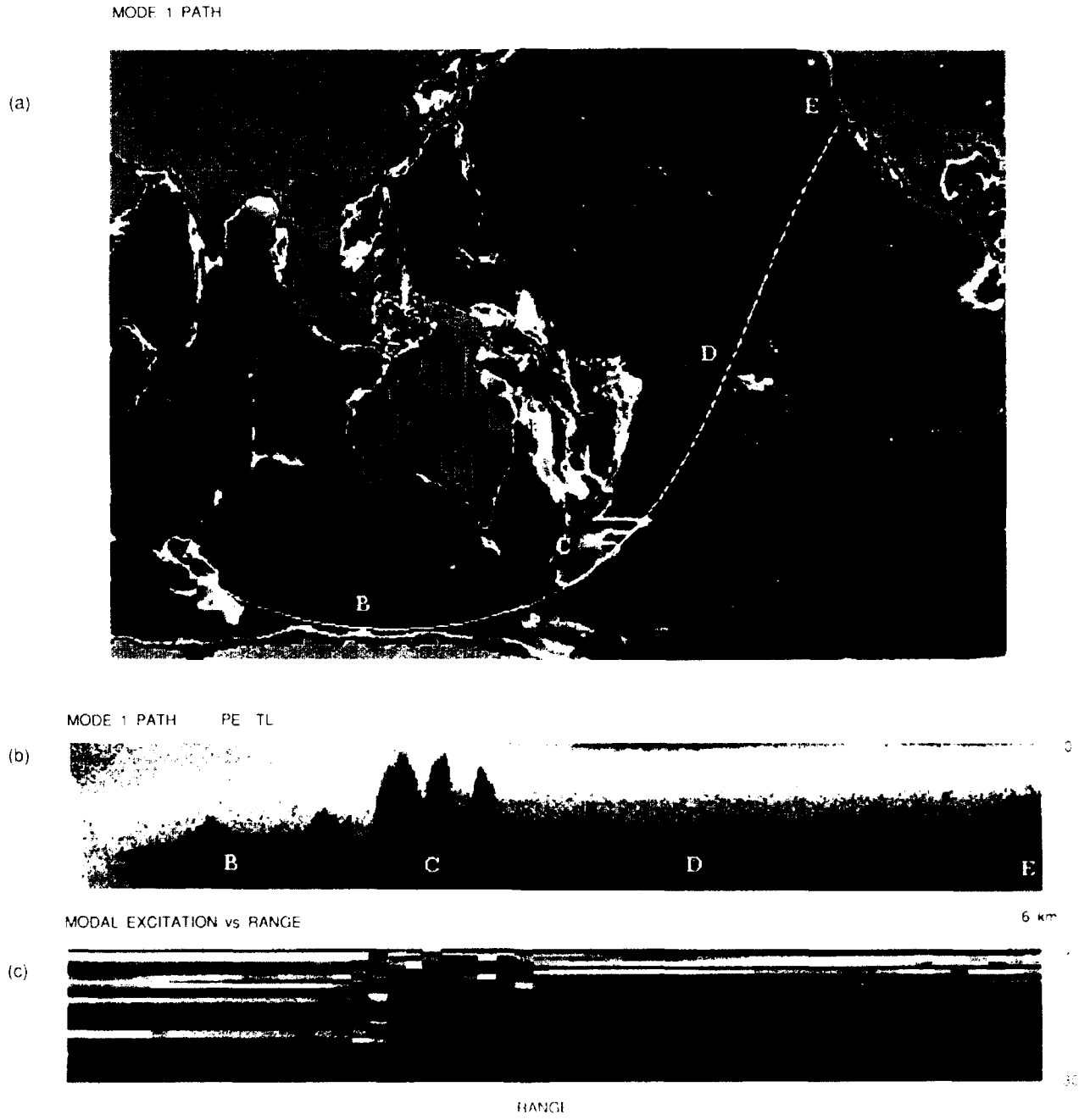

Fig. 6 Depth-range PE calculation from Heard Island to the array off San Diego for a point source at 175 m depth. (a) The ray path used is that for mode 1 at 57 Hz, (b) acoustic intensity and bathymetry along the ray, and (c) modal excitation levels along the path for modes 1 to 30. The vertical extent of Fig. 6(c) is divided into 30 strips for modes 1 to 30. The *maximum mode amplitude* at any given range is represented by red and the minimum by black.

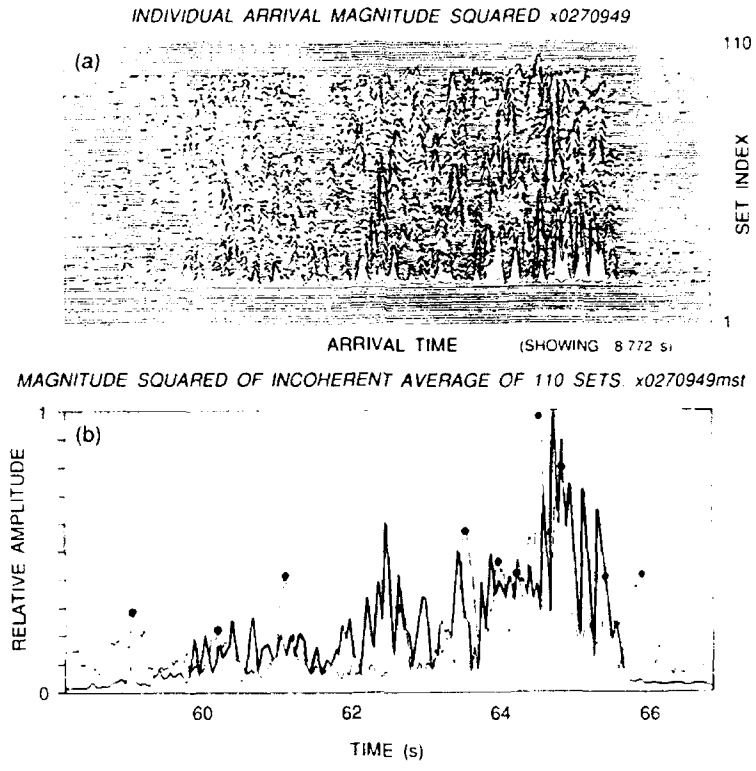

Fig. 7 — (a) Pulse-compressed transmissions as received at Christmas Island, 27 January 1991. The transmissions were repeated at 45-s intervals; and (b) solid line is average intensity for (a). Dashed line with dots denoting maxima: NRL Heard-to-Christmas Island pulse calculation. (Figure courtesy of K. Metzger, University of Michigan.)

width had spread to roughly 7 s. Different transmissions of the same pulse along the same path resulted in different microstructure in the reconstructed pulse, but the length of the synthesized pulse train was fairly consistent from transmission to transmission.

In Fig. 7, we give model calculations and experimental results for time domain pulse transmission from Heard to Christmas Island. Our numerical Heard-to-Christmas pulse transmission was carried out using mode theory with coupling terms to account for the exchange of energy between modes during interaction with bathymetry. We are in the process of repeating the pulse transmission calculation with the PE for comparison. The calculation illustrated in Fig. 7 excited 30 vertical modes appropriate to point source excitation at 175 m depth. For each mode, coupled mode calculations were performed for 21 equally spaced frequencies between 52 and 62 Hz. Resulting modal phase speeds were interpolated to a fine set of 512 frequencies and used to synthesize a pulse consisting of five cycles of a 57 Hz sine wave. All integrations were carried out on the 57 Hz mode 1 path. Although this compromises the separate identity of modal paths, it should be a good approximation. Fermat's principle states that along eigenrays, the path integrated phases are stationary with respect to ray displacement.

While microstructure in the results shown in Fig. 7 differs considerably from that of the experiment, the temporal spread and shape of the pulse envelope is fairly reasonable. One should not even hope for detailed agreement with observed microstructure since it changed with each pulse transmission. The approximate agreement in wavetrain envelope indicates that our calculated modes are subject to approximately the right levels of dispersion (i.e., differences in group velocity). In any event, our calculation appears to capture complex arrival structures not anticipated by experimentalists for this path.

SUMMARY

The NRL global-scale acoustic propagation models are being used in support of an experimental effort to monitor global warming. These models have yielded new interpretations of global-scale ocean acoustic propagation data, suggesting that horizontal multipath must be taken into account when designing global-scale acoustic networks and analyzing data. The NRL models are currently being used to analyze the results of the Heard Island Feasibility Test. The capability represented by the NRL models will contribute to a multiyear DARPA program, Acoustic Thermometry of the Ocean Climate (ATOC). The goals of ATOC are to monitor temperature trends in the deep ocean as one means of detecting global warming.

REFERENCES

1. A.B. Baggeroer and W. Munk, "The Heard Island Feasibility Test," *Physics Today* **45**(9), 22 (1992).

2. J. Hansen and S. Lebedeff, "Global Trends of Measured Surface Air Temperature," *J. Geophys. Res.* **92**, 13,345 (1988).

3. W.H. Munk, W.C. O'Reilly, and J.L. Reid, "Australia-Bermuda Sound Transmission Experiment (1960) Revisited," *J. Phys. Oceano.* **18**, 1876 (1988).

4. K.D. Heaney, W.A. Kuperman, and B.E. McDonald, "Perth-Bermuda Sound Propagation (1960): Adiabatic Mode Interpretation," *J. Acoust. Soc. Am.* **90**, 2586 (1991).

5. M.D. Collins, "A Split-Step Padé Solution for the Parabolic Equation Method," *J. Acoust. Soc. Am.*, to appear April 1993.

6. B.E. McDonald, M.D. Collins, W.A. Kuperman, and K.D. Heaney, "Comparison of Data and Model Predictions for Heard Island Acoustic Transmissions," *J. Acoust. Soc. Am.*, in prep. (1992).

THE AUTHORS

B. EDWARD McDONALD received degrees in physics from Utah State University (B.A., 1966) and Princeton (M.S., 1968; Ph.D., 1970) after which he joined the NRL Plasma Physics Division in 1970. He has published in the fields of solar physics, fluid dynamics, plasma physics, numerical analysis, oceanography, and ocean acoustics. From 1970 to 1980 he carried out numerical investigations of ionospheric plasma processes related to high altitude nuclear weapons effects and to naturally occurring plasma turbulence affecting satellite communication. From 1980 to 1990 he worked for the Naval Ocean R&D Activity/Naval Oceanographic and Atmospheric Research Laboratory developing theory and numerical solution techniques for fluid dynamics and nonlinear acoustics. He joined the NRL Acoustics Division in 1990. Since that time he has developed theory and computer models for prediction and interpretation of ocean experiments in the following areas: sonar echoes from the sea surface under wind conditions, underwater acoustic propagation across major ocean basins, and acoustic thermometry of the ocean climate. The latter area is an ongoing effort to use acoustic properties of the oceans to monitor global warming trends. McDonald holds NRL Publication Awards (1975 and 1980), a number of performance awards, Division and Directorate Best Product Awards (1989), and is a Fellow of the Acoustical Society of America.

WILLIAM A. KUPERMAN received degrees in physics from Polytechnic Institute of Brooklyn (B.S., 1965), the University of Chicago (M.S., 1966) and the University of Maryland (Ph.D., 1972). He joined the NRL Acoustics Division in 1967. Beginning in 1976, he spent five years at the SACLANT Undersea Research Centre in La Spezia, Italy, where he founded the Environmental Modeling Group. He returned to head the Numerical Modeling Division at what is now the Stennis Space Center. In 1985 he returned to Washington, DC, and became the Senior Scientist of the Acoustics Division. He has done theoretical and experimental research and has, over the years, spent about one year at sea. He has conducted research and published papers on linear and nonlinear propagation, scattering, ambient noise, geophysical inverse theory, signal processing, and nonlinear optimization using simulated annealing. Among his present activities, he is the senior scientist of a multicountry, multiship set of experiments to be conducted in the Tasman Sea investigating the use of the ocean environment to enhance signal processing. Dr. Kuperman was elected a Fellow of the Acoustical Society of America in 1980 and is an associate editor of the *Journal of the Acoustical Society of America*.

MICHAEL D. COLLINS received degrees in mathematics from Massachusetts Institute of Technology (B.S., 1982), Stanford University (M.S., 1986), and Northwestern University (Ph.D., 1988). Dr. Collins was a Volkswagen mechanic prior to being hired in 1985 by the Naval Ocean Research and Development Activity (now NRL-Stennis Space Center). Dr. Collins joined NRL in 1989 shortly after completing his thesis, which involved asymptotic and numerical methods for sound propagation and scattering in the ocean. His research at NRL involves modeling the propagation and scattering of acoustic and elastic waves, developing methods for solving signal processing and inverse problems, designing and performing at-sea experiments, and analyzing data. Problems he has investigated include localization of a source in a medium with unknown properties, time-domain beamforming by parameter optimization, inversion for ocean-bottom properties, and global-scale sound propagation in the ocean. Dr. Collins is a member of the Society for Industrial and Applied Mathematics (SIAM) and was among the youngest to be named a Fellow of the Acoustical Society of America (ASA) in 1990. From NRL, he received a Special Act Award in 1991 and an Alan Berman Research Publication Award in 1991, 1992, and 1993. He has been selected to receive the R. Bruce Lindsay Award from the ASA in 1993.

KEVIN D. HEANEY received degrees in physics from the University of California at Santa Barbara (B.S., 1987) and the University of Maryland (1990). While at the University of Maryland, he qualified for the Ph.D. program. His research was in the area of magnetic reconnection in solar and space plasma physics. He worked at Mission Research Corporation in Santa Barbara, California, and Newington, Virginia, during his undergraduate and graduate education. He did computational work in optical pattern recognition and electromagnetic particle simulations. After receiving his M.S. degree, Mr. Heaney joined Planning Systems, Incorporated as an on-site contractor at NRL in 1990. Since that time he has done analysis and computer simulation in the areas of acoustical oceanography, underwater acoustic propagation, scattering, nonlinear acoustics, and signal processing. Mr. Heaney developed the adiabatic normal-mode propagation code (RAYTRACE) used in the accompanying article. RAYTRACE is now being used by oceanographers and physicists at Scripps Institute of Oceanography at UCSD, CSIRO in Hobart, Tasmania, and SAIC in McLean, Virginia. Mr. Heaney's work has provided theoretical support for the Heard Island Feasibility Test and the upcoming ATOC experiments. His current research is in the area of broadband propagation through complex ocean environments and other aspects of acoustic tomography.

Acoustics

Electroacoustic Transducer Transient Suppression

J.C. Piquette
Underwater Sound Reference Detachment

A fundamental physical property of vibrating systems is that they tend to oscillate at their natural resonance frequency (or frequencies) when disturbed. For example, when a guitar string is plucked in an arbitrary manner, the frequencies of the sounds produced are multiples of the fundamental vibrational frequency of the string, and these frequencies are simply related to the length of the string. Another example is that of a bell, which tends to radiate sounds that are strongly related to the size, shape, and material of the bell but are only weakly related to the manner of excitation.

One consequence of the tendency of a vibrating system to radiate at its natural frequency regardless of how it is excited is that transient radiation tends to appear shortly after the initiation (or cessation) of an excitation. The total duration of this transient radiation is also a natural characteristic of the oscillating system, and little can be done to change this duration—short of changing the system in some fundamental way.

Underwater acoustic projectors, which may be components of a sonar system or which may be an integral part of an acoustical experiment, are oscillating systems that exhibit natural frequencies of oscillation. When such projectors are driven with an arbitrarily shaped driving voltage waveform, they tend to radiate at their natural frequency. When the frequency of excitation is far from the natural frequency, the transient portion of the radiated waveform is a combination of the drive frequency and the natural frequency. When the frequency of excitation is close to the natural frequency, the transient portion of the radiated waveform exhibits an exponential rise toward steady state. If the duration of the transient portion of the radiation is sufficiently great, undesired echoes from the boundaries of the test facility may arrive at the acoustic detector prior to the arrival of the desired steady-state radiation in any given test of interest. (In order to simulate environmental conditions of temperature and pressure found at great ocean depths, such test facilities must generally be of rather limited size.) Hence, such transient radiation can preclude the performance of accurate transducer calibration tests, as well as reflection and/or scattering tests, that may be needed to evaluate a passive acoustical material. Since the results of such tests are essential to the reliable design of sonar systems, when the tests cannot be accurately conducted, acoustic systems can be more difficult and costly to design, and the resulting system might be unreliable.

The Transient-Suppressing Drive: A transducer is ordinarily driven with a voltage waveform that is a segmented, or gated, sine wave. Figure 1 shows the resulting radiation when such a gated-sine drive is applied to an F56 transducer—a standard transducer of piezoelectric spherical shell design. The transient radiation is clearly visible in the form of an initial buildup of the radiation at drive initiation and in the persistance of the radiation after drive cessation.

Figure 2 shows an equivalent circuit for the F56 transducer. By theoretically assuming a perfect segmented sine wave at the circuit output (which appears across the radiation-load circuit elements L_w and R_w) and "calculating backward" through the circuit to the arbitrary waveform generator, a preformed voltage drive can be deduced [1,2]. Figure 3 shows this drive. When the drive of Fig. 3 is applied to the F56, the pressure waveform shown in Fig. 4 is produced. As can be seen by comparing Fig. 4 with Fig. 1, both the turn-on and turn-off transients have been significantly suppressed.

Demonstration and Impact: The method has been demonstrated to successfully suppress transient radiation from numerous electroacoustic transducer types. These types include piezoelectric spheres, moving coils, Helmholtz resonators, flexural disks, and tonpilzs. The method has also been demonstrated to successfully suppress transient radiation from several transducer arrays, including a square array of

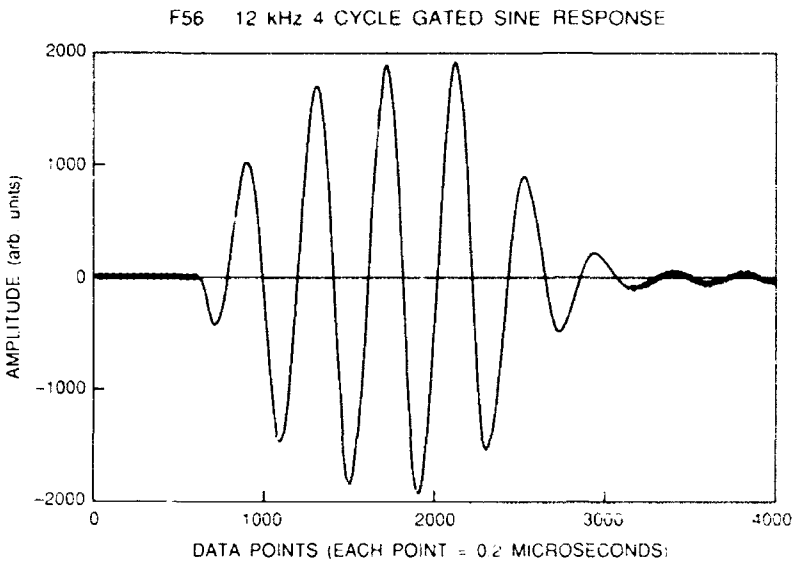

Fig. 1 — The pressure waveform radiated from an F56 transducer when driven with a four cycle gated sine driving voltage waveform. The resonance frequency of the F56 is approximately 12 kHz.

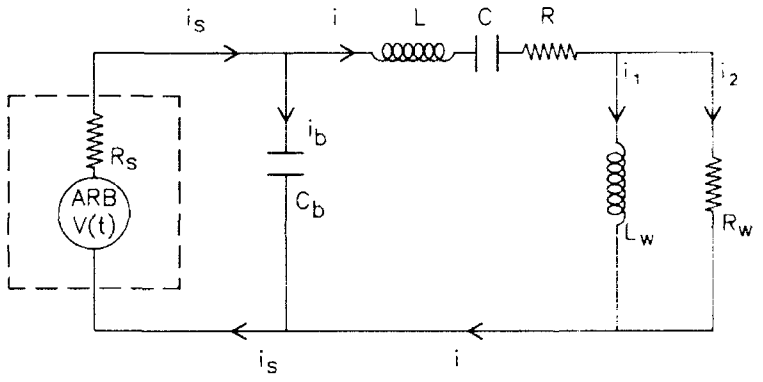

Fig. 2 — A transducer equivalent circuit useful in designing the transient-suppressing drive. The notation ARB denotes an arbitrary waveform generator that produces the driving voltage waveform $V(t)$. The circuit output, which is assumed to be a scaled replica of the radiated pressure waveform, appears across the parallel elements L_w and R_w.

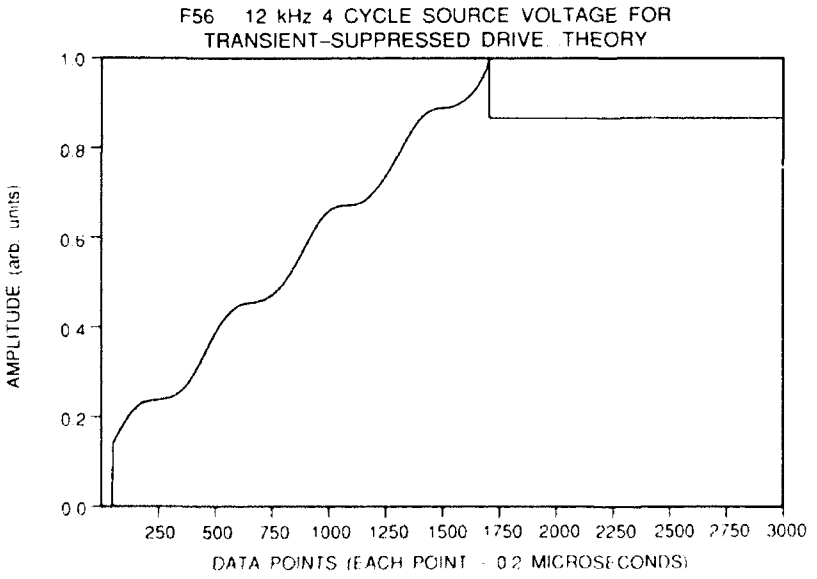

Fig. 3 — The transient-suppressing, driving voltage waveform $V(t)$ that must be produced by the arbitrary waveform generator of Fig. 2 to cause the F56 to radiate a four-cycle segmented sine wave. The waveform is deduced by assuming theoretically that a perfect four-cycle segmented sine appears across the output elements of Fig. 2 and then "calculating backward" through the circuit to the arbitrary waveform generator.

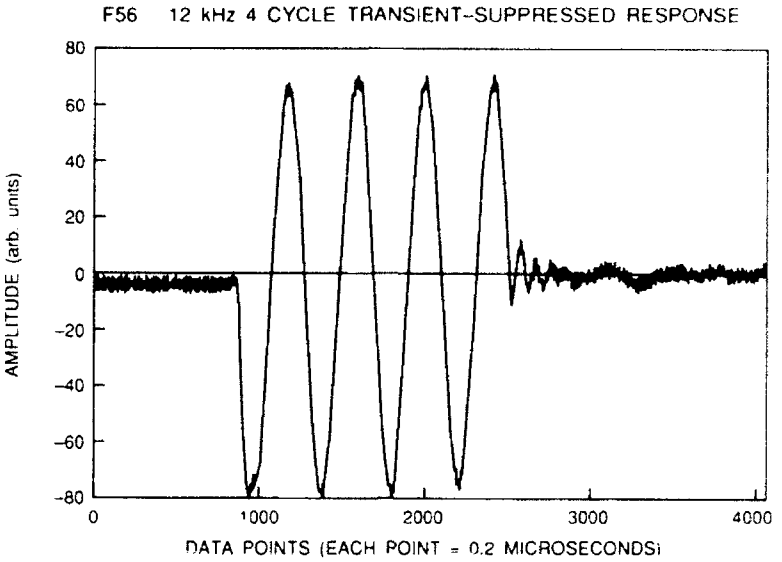

Fig. 4 — The pressure waveform radiated by the F56 when the voltage waveform of Fig. 3 is applied

piezoelectric tubes, a line array of piezoelectric cylinders, and a dual circular array containing piezoelectric disks and squares. Moreover, the method has been successfully used to carry out a scattering experiment that otherwise would have been precluded by the effects of radiation transients. The method permits calibration and reflection/scattering measurements to be conducted in existing test facilities at much lower frequencies than previously possible and thus has the potential to revolutionize the ways in which such measurements are conducted.

[Sponsored by ONT]

References

1. J.C. Piquette, "Method for Electroacoustic Transducer Transient Suppression. I. Theory," *J Acoust. Soc. Am.* **92**, 1203-1213 (1992).

2. J.C. Piquette, "Method for Electroacoustic Transducer Transient Suppression. II. Experiment," *J. Acoust. Soc. Am.* **92**, 1214-1221 (1992). ■

BiKR — A Range-Dependent, Normal-Mode Reverberation Model for Bistatic Geometries

S.N. Wolf, D.M. Fromm, and B.J. Orchard
Acoustics Division

Introduction: An active sonar system operates by transmitting an acoustic signal and detecting the echo from a target of interest. Reverberation, or echoes from the ocean boundaries and volume, acts as a source of noise that interferes with the echo detection. The Navy has an ongoing requirement for computerized models that project the performance of existing and candidate system designs in various ocean environments. In the shallow, continental-shelf oceans the characteristics of low-frequency echoes and reverberation that influence the performance of sonar transmitting and receiving arrays will be determined by waveguide propagation effects, much as optical signals transmitted in thin optical fibers are influenced by the diameter and material characteristics of the glass. Under guided-wave conditions, the acoustic signal and reverberation are conveniently

described by acoustic normal mode theory, which represents the signal as a collection of individually propagating normal modes. The characteristics of the acoustic normal modes, such as speed of propagation, are controlled by the ocean environmental features, such as water depth, the ocean bottom material, and the ocean sound speed structure of the water and bottom. As a result, the characteristics of the acoustic normal modes change as they propagate in a range-dependent environment. Since most shallow oceans are near land masses, water depth and other ocean environmental parameters can change considerably, even over short distances. Thus the Navy needs to quantify not only the influence of a depth-dependent ocean on sonar performance, but also that of a range- and azimuth-variable ocean environment.

Computer Model: NRL is developing a normal-mode computer model of acoustic reverberation that is suitable for use with bistatic sonar systems (which have source and receiver separated) as well as monostatic sonar systems (which have source and receiver at the same location) in a range-dependent environment. At present, the model accounts only for ocean-bottom reverberation; extensions to include ocean surface and volume scattering are in progress. This model was prepared by combining a previously developed range-dependent acoustic propagation code, WRAP [1] with the numerical area-integration used in BiRASP [2], a deep-water reverberation model. The area-integration is necessary because the ocean bottom is a continuously distributed scatterer, which results in a temporally continuous reverberation field. The calculation of the reverberation time dependence is made complex in the case of a range-dependent environment because the sound field's speed depends on mode order and position and by the condition that, for bistatic sonars, the sound travels along different paths from the source to the scatterer and from the scatterer to the receiver. In developing the computer code, we considered that the model would be used for two purposes.

The first purpose is assessment of sonar system designs in "realistic" areas having different types of environmental complexity. To support this application, the tedious specification of the environment was automated to allow convenient use of digital bathymetric databases. In applications of this type the model is run repeatedly for different system configurations, and a large number of range- and azimuth-dependent results are produced. We have also developed automated techniques for assessing system performance for a large number of computer runs.

The second, and more "scientific" purpose that the model serves is to develop intuition and physical understanding of the interplay between acoustic propagation in a range-dependent environment and the resulting characteristics of the reverberation field. In carrying out this application, simpler range-dependent environments are used so that the results are not obscured by complex environmental structures. For these studies, we require a different type of model output, such as the mode-order dependence of the ocean bottom scattering strength or reverberation field as a function of water depth, range, or some other parameter of interest. In constructing the computer code, these component results were made readily accessible, to enable examination of the reverberation field from a variety of viewpoints. An example of the "scientific" output is given below.

Sample Calculation: Reverberation level was calculated as a function of azimuth and time for a simple, wedge-shaped ocean. To show the dependence of reverberation on acoustic mode order, the calculation was performed for various choices of mode order in the insonifying (acoustic source) field. The level (color) is shown in Fig. 5 as a function of apparent scattering position for an idealized receiver having an angular resolution of 0.5 degrees. Water depth increases from 0 m (bottom) to 200 m (top) in the figure, which represents a 100 km by 100 km area. The source and receiver are configured bistatically near the center of the figure. A total of 35 mode orders were used in the calculation. Figure 5(a) shows the reverberation due to the lowest five mode orders; the field due to the next five mode orders are shown in Fig. 5(b), etc. Figure 5(f) presents the sum over all 35 modes. At short range, reverberation intensity is higher for the

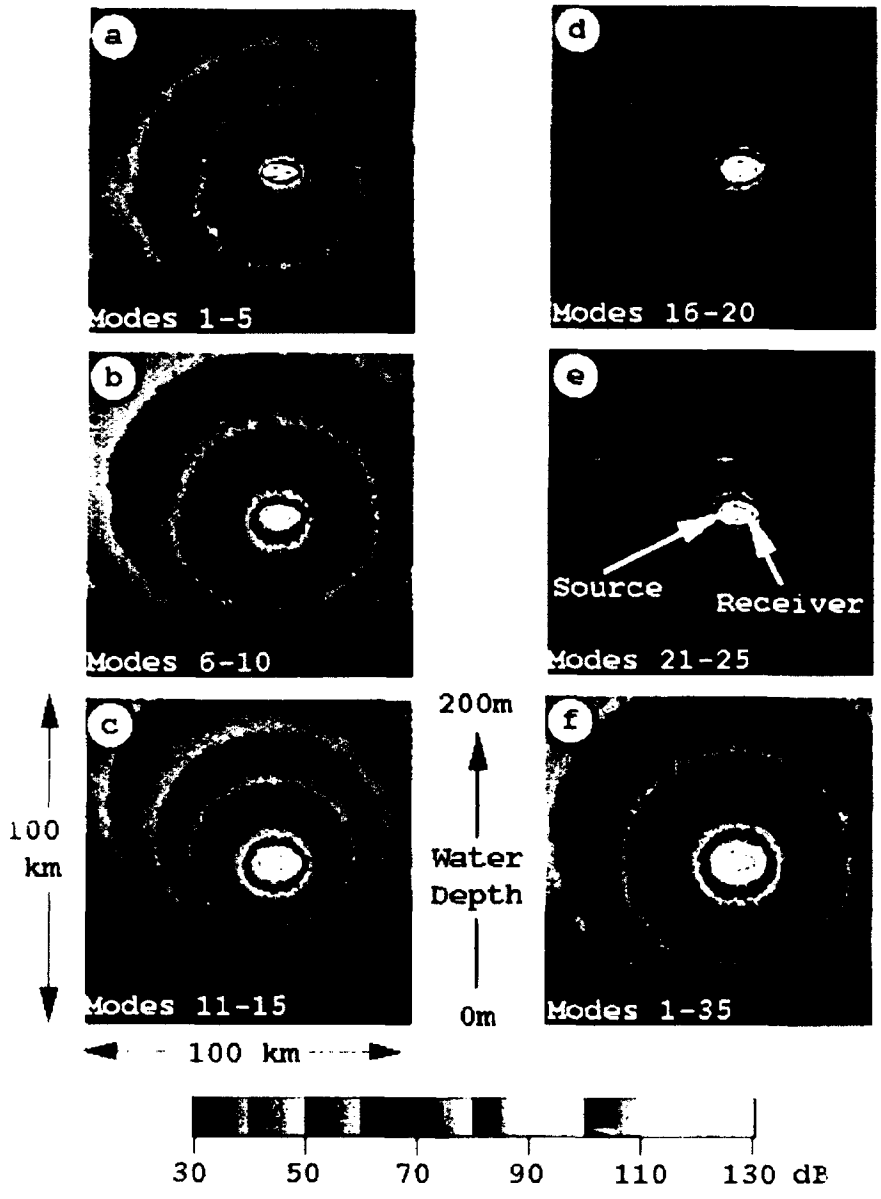

Fig. 5 Bottom reverberation for various partial sums over the propagating source modes are shown in plan view with respect to the receiver. The source mode orders used are indicated in the lower left corner of each plot. Each displayed area is 100 by 100 km, with depth going from 0 m at the bottom to 200 m at the top. The source and receiver are at depth 12.5 and 65 m, respectively, and are located over the 100-m depth contour with the source 10 km to the left of the receiver. The reverberation intensity is represented by color according to the scale at the bottom. Each color corresponds to a change of 10 dB, and variations of individual color brightness indicate changes with the 10 dB interval. The calculation does not include the direct path; the high intensity (i.e., yellow and white) region between the source and receiver is due to strong forward scattering. The reverberation time series were mapped into apparent range with respect to the receiver using 1500 m/s as the assumed sound speed.

higher order modes than for the lower order modes; this mode-order dependence is due to the stronger scattering of the high order modes by the ocean bottom. As range from the source increases, higher order modes in the incident field are attenuated and contribute less to the reverberation field. We find in each illustration that the reverberation depends on azimuth, with the reverberation from the upslope higher than from the downslope direction at the same range. This directional effect is due to a change in the strength of interaction of each mode order with the ocean bottom as the water depth decreases.

Summary: We have developed a bistatic, normal-mode, range-dependent acoustic reverberation that model provides the detailed information required to help explain the behavior of a reverberation field. Currently, the model addresses only bottom scattering. Surface and volume scattering will be incorporated in the near future.

[Sponsored by ONT]

References

1. W.A. Kuperman, M.B. Porter, J.S. Perkins, and R.B. Evans, "Rapid Computation of Acoustic Fields in Three-Dimensional Ocean Environments," *J. Acoust. Soc. Am.* **89**(1), 125-133 (1991).

2. L. Bruce Palmer and David Meloy Fromm, "The Range-Dependent Active System Performance Prediction Model (RASP)," NRL Report 9383, 1992. (A report documenting the bistatic version is in preparation.) ■

Predicting Acoustic Signal Distortion in Shallow Water

R.L. Field and J.H. Leclere
Acoustics Division

As acoustic signals propagate in the ocean their temporal and spectral character varies as a function of space and time. This is especially true of short-duration signals propagating in shallow-water environments where the signal may encounter numerous boundary interactions with significant loss due to absorption. The change in temporal and spectral character of the signal as a function of space and time can be completely characterized by the broadband ocean impulse response (OIR) function.

The ability to predict the effects of shallow-water environments over a broad frequency band will provide a basis for the rational design of emerging Navy systems operating in shallow water. Realistic simulations of the OIR will allow the environmental acoustic limits on detection, localization, and classification of acoustic signals to be determined.

Ocean Impulse Response Simulations and Measurements: To predict the broadband OIR, NRL developed the time-domain parabolic equation (TDPE) model and performed sea experiments to measure the ocean response [1,2]. The measurements were obtained over a 25-150 Hz bandwidth in a bottom-limited ocean of 915 m depth.

Figure 6 is a comparison between the impulse responses modeled by TDPE and those measured at a range of 12,900 m. The depth axis corresponds to the aperture of the vertical hydrophone array used in the experiment. The source depth is 96 m. The normalized TDPE waveforms are shown in Fig. 6(a). The signals received at each hydrophone were correlated with the measured source waveform and normalized; these are shown in Fig. 6(b). Because the pulse is propagating from left to right, the time axis is labeled from right to left. The brackets labeled 1-4 at the top refer to the number of bottom bounces each group has undergone. Each group represents a number of unresolved arrivals. The bracket at the bottom, labeled 0, is the remanent of the direct and surface-reflected paths. Taking a horizontal slice of these contours at a particular depth results in the time waveform of the OIR.

Figures 7(a), 7(b), and 7(c) show the time waveforms of the source (after correlation), the model OIR, and the measured OIR, respectively, at the 250-m depth. (The time axis is now labeled from left to right.) The brackets label the order of the bottom-interacting groups

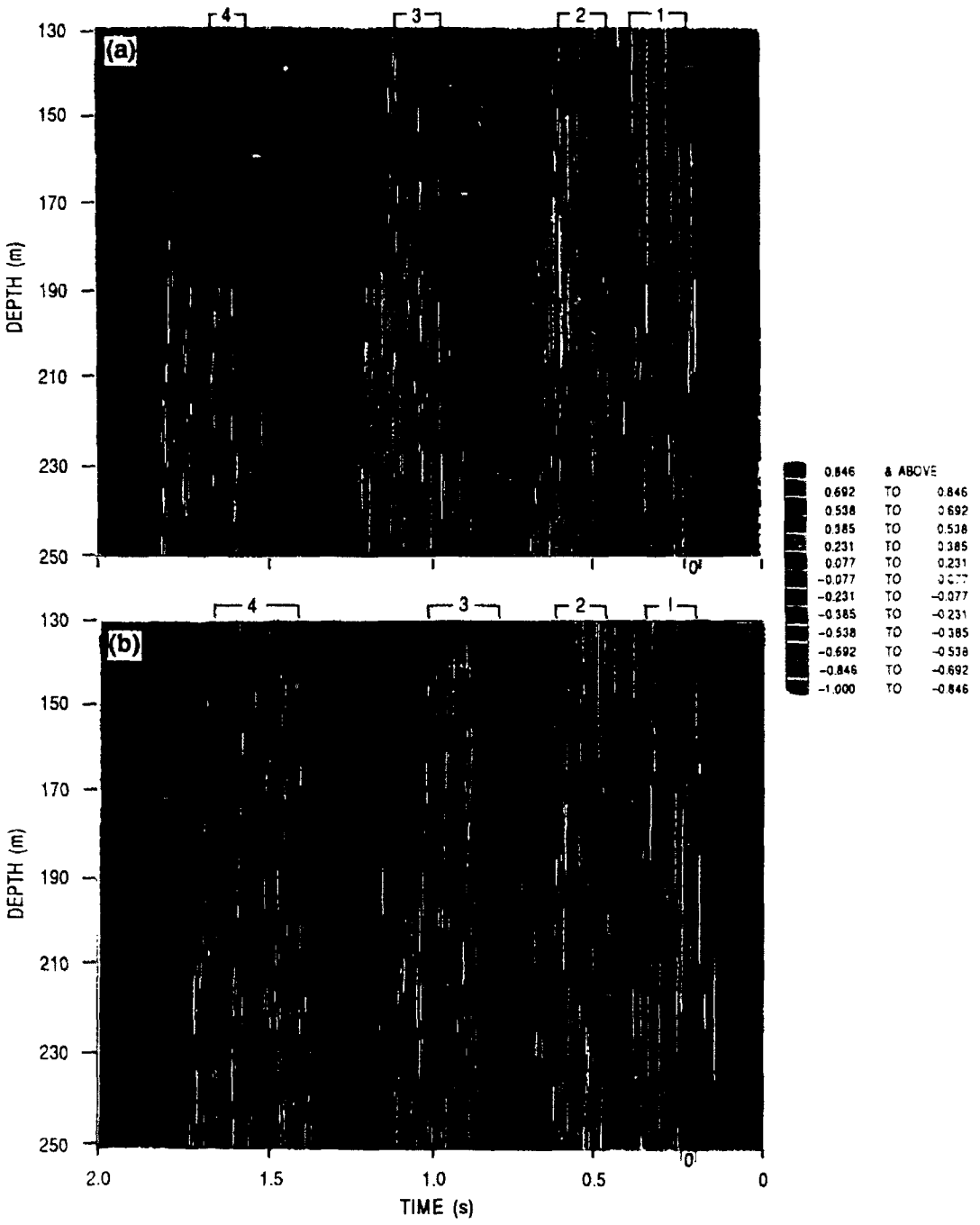

Fig. 6 — Comparison of modeled and measured bandlimited impulse responses at the 12,900-m range. (a) Contours of TDPE impulse responses; (b) contours of measured impulse responses.

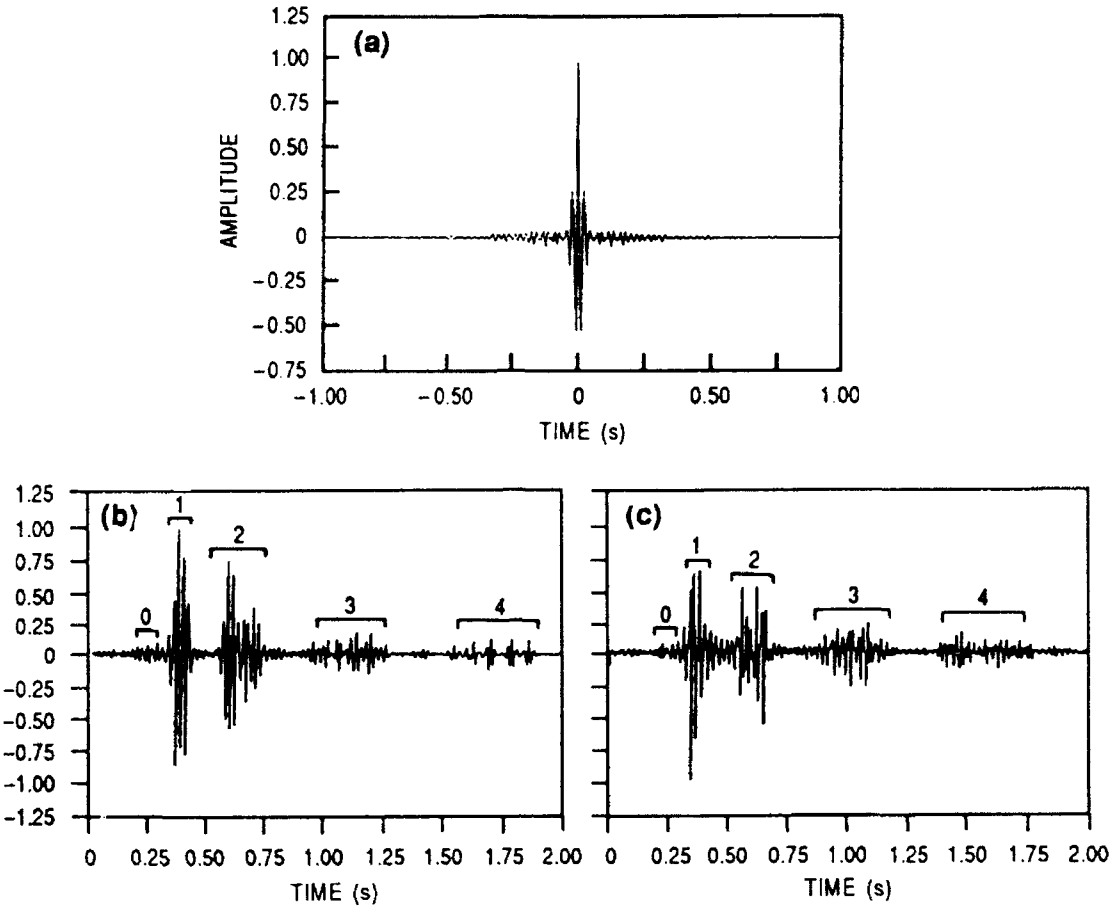

Fig. 7 — Impulse response waveforms at 12,900-m range, 250-m receiver depth. (a) Correlated source; (b) TDPE response; (c) measured.

referred to above. Figures 6 and 7 show that the TDPE model computes OIRs that are consistent with the experimentally measured responses. The next section evaluates the model more quantitatively.

Simulated and Measured Signal Distortion: The normalized correlation coefficient (NCC) between the source and received waveforms is used as a measure of waveform distortion. The NCC is defined as

$$\gamma_{s,r} = \frac{|R_{s,r}(z,\tau_{\max})|}{\sqrt{R_{s,s}(z,0)\ R_{r,r}(z,0)}}.$$

The numerator is the absolute value of the correlation between source and received waveforms at depth z. The correlation is evaluated at the time value $\tau_{\max}$, where the function is a maximum. The denominator is the square root of the product of the autocorrelations of the source and received waveforms at depth z. With the absolute value in the numerator

$$0 \leq \gamma_{s,r} \leq 1.$$

If the NCC is computed for all possible receiver locations over a 15-km range, then signal distortion can be mapped to the range/depth plane. Figure 8(a) displays this mapping over a portion of the experimental track. Figure 8(a) is the signal distortion predicted by the TDPE model for the source pulse shown in Fig. 7(a). The yellow regions, where the NCC is close to 1, are depths and ranges

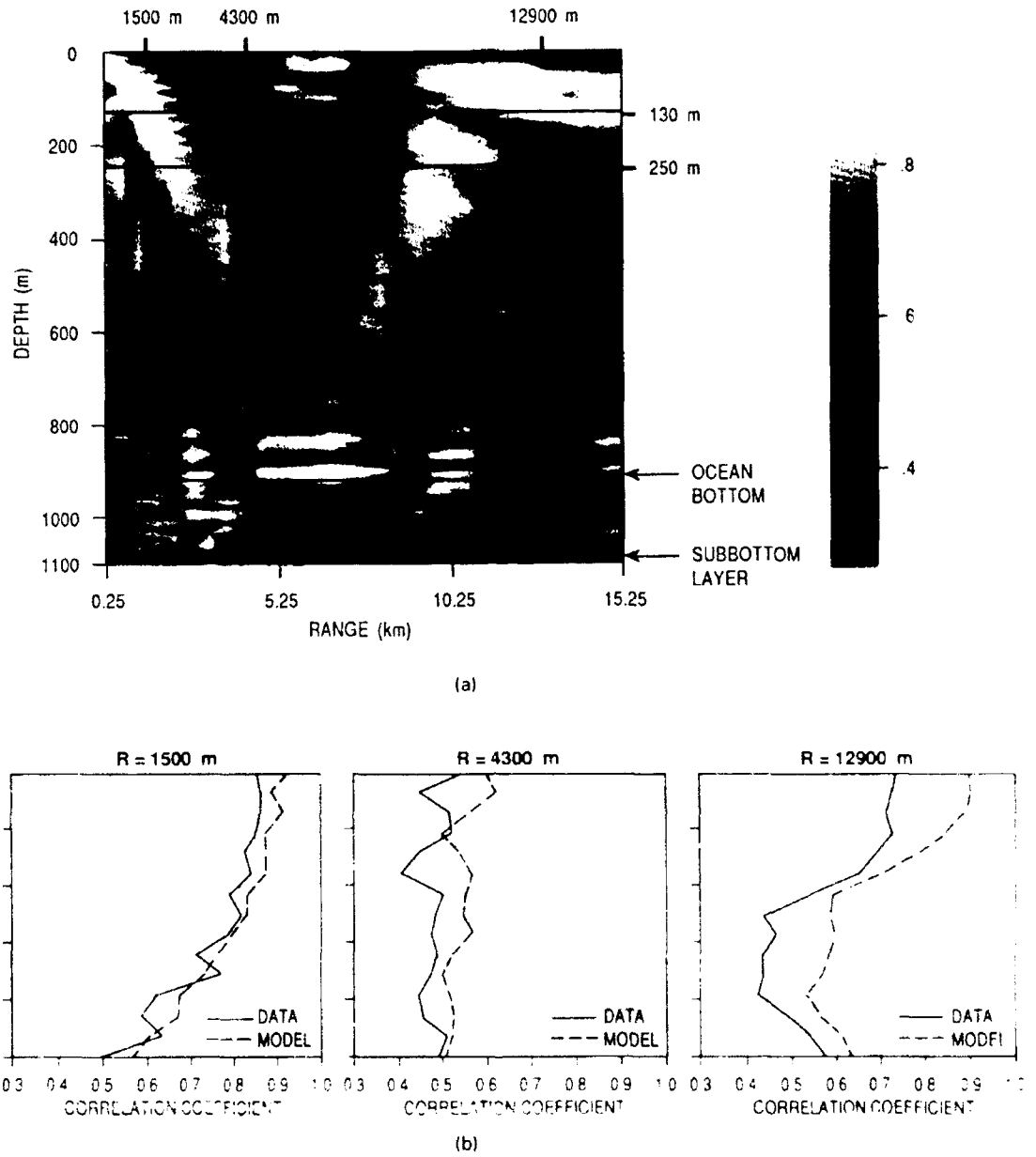

Fig. 8 — Normalized correlation coefficients as a measure of signal distortion. (a) Coefficients computed by TDPE at all possible receiver locations; (b) comparison of measured vs model coefficients at three experimental ranges.

where there is little distortion. The dark blue areas are regions of high distortion. Such a mapping can be used to determine how the ocean distorts an acoustic signal as it propagates. The horizontal lines at the 130 and 250 m depths, and the three bars at the top represent the aperture of the vertical array and three ranges, respectively, where the acoustic measurements were taken. Figure 8(b) displays the comparison between the correlation coefficients predicted by TDPE, with the correlation coefficients estimated from the data as a function of depth at the three ranges. The figure shows that the TDPE model accurately predicts signal distortion in a complex environment. From accurate simulations of the OIR, any signal feature can be mapped in this way, thus providing a basis for "matched field feature selection" and optimum receiver placement for signal classification.

[Sponsored by ONR]

References

1. M.D. Collins, "The Time-Domain Solution of the Wide-Angle Parabolic Equation Including the Effects of Sediment Dispersion," *J. Acoust. Soc. Am.* **84**, 2114-2125 (1988).

2. R.L. Field and J.H. Leclere, "Measurements of Bottom-Limited Ocean Impulse Responses and Comparisons with the Time-Domain Parabolic Equation," *J. Acoust. Soc. Am.* (to be published, 1993). ■

Chemical/ Biochemical Research

Development of Polyurethane/Epoxy Based Interpenetrating Polymer Networks for Damping Applications

R.N. Capps and C.S. Coughlin
Underwater Sound Reference Detachment

In selecting polymeric materials for broadband damping applications, it is desirable to have polymers with a high loss modulus or loss tangent in shear or extension, covering a wide temperature and frequency range in the glass-rubber relaxation [1]. In general, pure homopolymers have relatively narrow glass-rubber transition regions, limiting their use in these applications.

Interpenetrating polymer networks (IPNs) are materials composed of two or more crosslinked polymers, permanently intertwined. Even though the two polymers might normally be immiscible as a simple blend, they can be crosslinked in place before fully phase separating, if the kinetics of both components of the IPN-forming reaction are similar. Depending upon the degree of microscale phase separation, such IPNs may exhibit very broad transitions in their dynamic mechanical spectra. It is this broad transition region that makes IPNs useful as damping materials [2].

Synthesis and Characterization: Several series of polyurethane/epoxy IPNs have been prepared for possible use as broadband damping materials. The polyurethane component contained a poly(caprolactone) soft segment and a carbodiimide modified hard segment, for oxidative and hydrolitic stability. This was chain-extended with either trimethylolpropane or butanediol. The epoxy component was a standard bisphenol-A resin (Epon 828) cured with either a BCl_3-amine complex or BF_3-etherate. All IPNs, as well as separate polyurethane and epoxy components, were characterized by dynamic mechanical spectroscopy (DMS), differential scanning calorimetry (DSC), Fourier transform infrared (FTIR) spectroscopy, and dielectric spectroscopy. Modal analysis was performed on uncoated and coated metal plates using a shock chord, impact hammer, and spectrum analyzer to evaluate extensional damping of the IPNs.

All IPNs showed single glass transitions in both DMS and DSC curves, indicating that they were true single-phase IPNs. This is shown for some BCl_3 cured materials in Fig. 1. The glass transition temperature (Tg) is shifted upward and broadened as the epoxy content is increased. IPNs prepared with BF_3 showed similar behavior but exhibited less dependence of transition temperature on epoxy content.

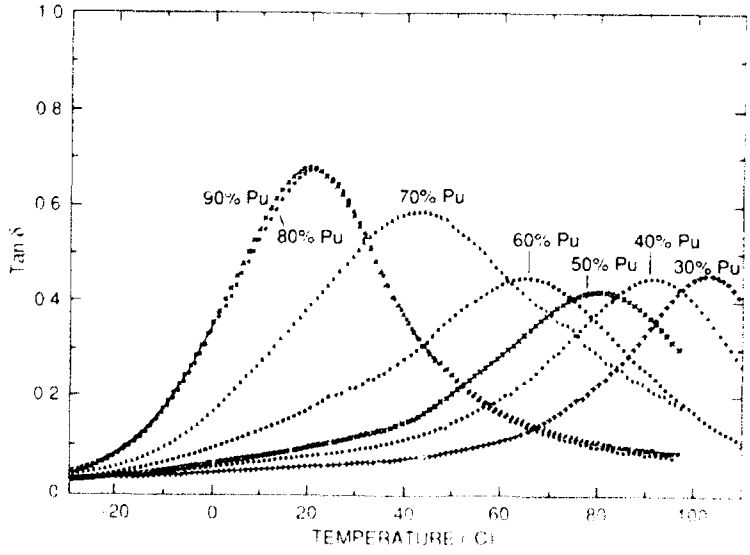

Fig. 1 Loss tangent vs temperature at 10 Hz for series of polyurethane/epoxy IPNs using BCl_3 amine complex as epoxy catalyst

Although the BF_3 cured materials exhibited high dynamic mechanical losses and good plate damping behavior, the dielectric measurements showed high dielectric losses as a function of temperature (Fig. 2), indicating ionic conductivity due to unreacted epoxy. This was confirmed by FTIR spectra of IPN samples extracted with methanol. Higher levels of BF_3 in IPNs resulted in very short gel times, with higher glass transitions and some still unincorporated epoxy. All of this indicated that the unreacted epoxy component was plasticizing the IPN, lowering the glass transition temperature and increasing the loss. BCl_3 is a more suitable curative, but the results obtained with the BF_3-etherate indicated that the use of more suitable types of plasticizers should be effective in these systems. This is currently under investigation. We are also investigating the use of a more flexible epoxy component, using the BCl_3 curative. This gives an IPN with a higher loss and lower glass transition, as compared to use of the standard bisphenol-A resin.

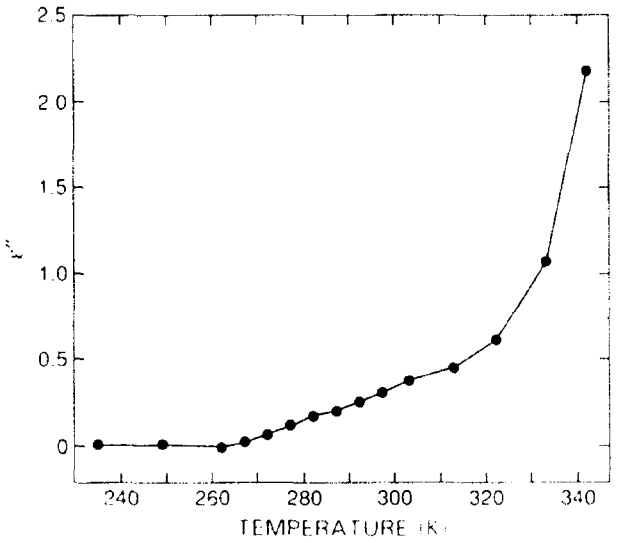

Fig. 2 – Dielectric loss vs temperature at 1000 Hz for 50/50 wt. % polyurethane/epoxy IPN using BF_3-etherate as epoxy catalyst

Conclusion: Several series of IPNs were prepared and characterized. IPNs prepared with BCl_3-amine as the epoxy curative showed no, or very small, scale phase separation. BF_3-etherate-cured IPNs showed good damping, but the epoxy component was not fully incorporated and could be leached out. Ongoing work is focusing on BCl_3-amine systems incorporating a polyurethane with a lower hard segment content, a more flexible epoxy component, and use of plasticizers to increase damping and lower the Tg.

[Sponsored by ONT]

References

1. R.D. Corsaro and L.H. Sperling, eds., *Sound and Vibration Damping with Polymers*, A.C.S. Symposium series #424 (American Chemical Society, Washington, DC, 1990).

2. R.Y. Ting, R.N. Capps, and D. Klempner, "Acoustical Properties of Some Interpenetrating Network Polymers: Urethane-Epoxy Networks," op cit, pp. 366-381. ■

Ultrafast Photochemical Processes

A.P. Baronavski and J.K. Rice
Chemistry Division

Femtosecond (10^{-15} s) laser sources have opened up a new temporal regime for scientific study. Due to the mass differences between electrons and nuclei, molecules can effectively be "frozen" in a particular internuclear configuration, while the electronic state evolves in time. We now have the ability to study processes such as photodissociation, isomerization, photoionization, charge transfer, and liquid-phase solvation in real time. Previously, the dynamics of these processes could only be inferred from the products of the reactions; now they can be observed as they take place. After a brief description of our femtosecond laser pump-probe apparatus, we will discuss two areas of research in which this level of temporal information is important: the initial charge-transfer step in photosynthesis and the photodetachment and subsequent solvation of an electron in aqueous solutions.

Experimental Apparatus: Figure 3 shows our system, which is built around a colliding-pulse-modelocked (CPM) dye laser. This laser is capable of producing 50-femtosecond pulses at a repetition rate of 90 MHz, a central wavelength of 620 nm, and a bandwidth of 8 nm. However, because the energy per pulse is only 100 picojoules, we use an amplifier system that boosts the energy to ~15 microjoules per pulse at a repetition rate of 6 kHz. The pulses are temporally broadened to 150 femtoseconds by the dispersion of the amplifying medium; that is, red components of the pulse precede blue components. By propagating the beam through two prisms, we can equalize the group velocities of the spectral components and recompress the pulse to 60 femtoseconds. The beam then passes through a thin frequency doubling crystal, which converts ~20% of the energy into ultraviolet light at 310 nm. This becomes the excitation or pump beam in our experiments. The remainder of the 620 nm light is tightly focused into a flow cell containing water. High-order nonlinear processes result in spectral broadening of the pulse into a white light continuum, with wavelengths from 300 to 1300 nm. This continuum has the same temporal characteristics as the laser. We use a filter to select a particular wavelength as our probe pulse. The pump and probe pulses are synchronized by a variable optical delay line that allows us to vary the arrival of the probe pulse (−2 to 100 picoseconds) relative to the pump pulse. We observe signals with a photomultiplier tube as either a decrease (absorption) or increase (bleaching) in the probe beam intensity.

Photosystem II Reaction Centers: The primary processes involved in photosynthesis have been an intense area of study for a number of years. However, it is only with the advent of ultrafast sources that we possess the temporal resolution necessary to unravel these complex reactions. The first reaction to occur following light absorption is believed to be charge separation. Energy absorbed by chlorophyll antennae generates an exciton that migrates to the photosynthetic reaction center. This results in electronic excitation of a chlorophyll dimer and subsequent electron transfer. Previous studies on reaction center cores (where direct excitation of the chlorophyll dimer is possible) indicate that this initial electron transfer occurs in 3 to 21 picoseconds, but these studies were limited by the temporal resolution of the apparatus.

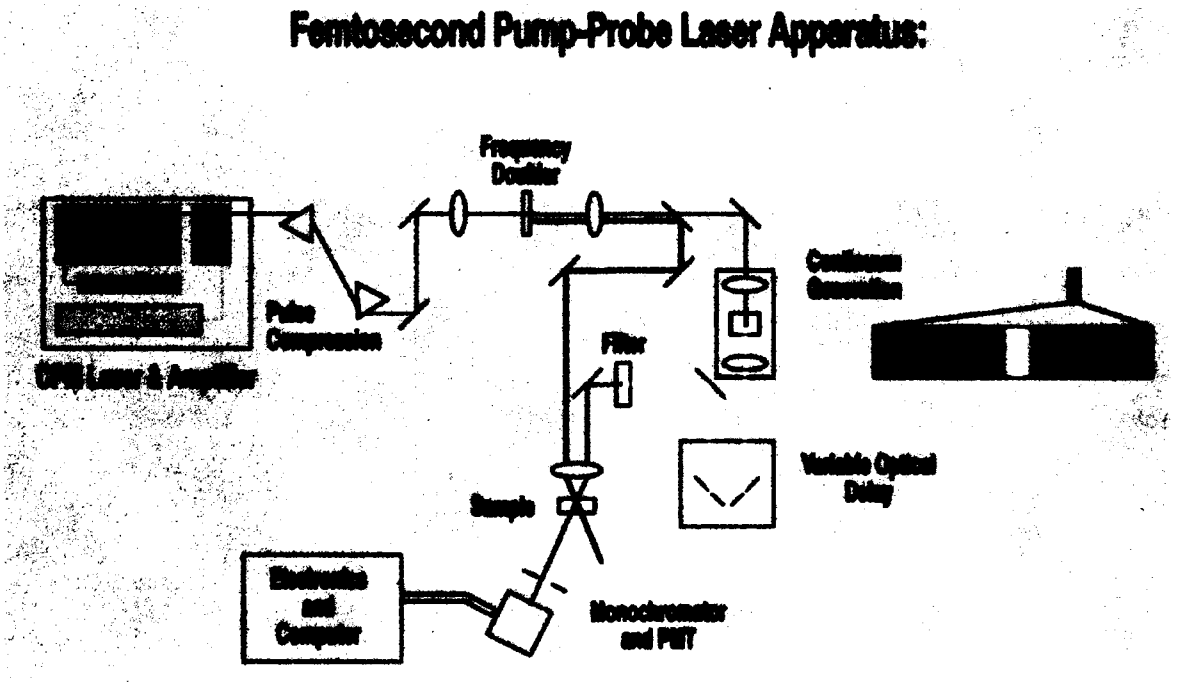

Fig. 3 — Experimental apparatus used for ultrafast photochemical studies

We have performed similar experiments in an effort to observe dynamical processes that may occur on the subpicosecond timescale. We use reaction centers extracted from spinach at concentrations of ~100 micrograms/ml. Excitation occurs at 310 nm, and we use a 10-nm portion of the continuum centered around 672 nm, corresponding to the maximum absorption of the chlorophyll moiety as the probe. In this experiment, signals are observed as an increase in probe intensity. Under equilibrium conditions, the intensity of the probe pulse is reduced due to absorption by chlorophyll. However, when excitation occurs, a large excited state chlorophyll population is created, decreasing the ground state population and causing an increase in probe intensity. At each delay time, as many as 3000 laser shots are averaged to increase the signal/noise. Figure 4 shows a typical scan. The very fast initial decay (~150 femtoseconds) is thought to be due to intramolecular vibrational relaxation, while the longer recovery (~13 picoseconds) is likely due to a combination of processes, one of which is charge transfer. At the present time, we are unable to separate these processes, but by probing at different wavelengths, we may be able to isolate some of them for further study.

Photodetachment Studies: Another process that has generated much interest is the generation and solvation of electrons in aqueous solutions. In our studies, iodide anions are used as a source of electrons. The $(I^-)_{aq}$ species has a characteristic electronic state known as a charge-transfer-to-solvent (CTTS) state, which absorbs at 215 nm. Excitation to this state ultimately results in the formation of an electron and neutral iodine atom. Our goal is to observe the temporal evolution of both this state and the electrons formed from it from the time of its initial excitation to the formation of the fully solvated electron. In order to excite this state, we focus the pump and probe beams on the sample. Two photons from the pump beam are simultaneously absorbed, resulting in efficient excitation of the CTTS state. By using appropriate wavelengths from the continuum, we can

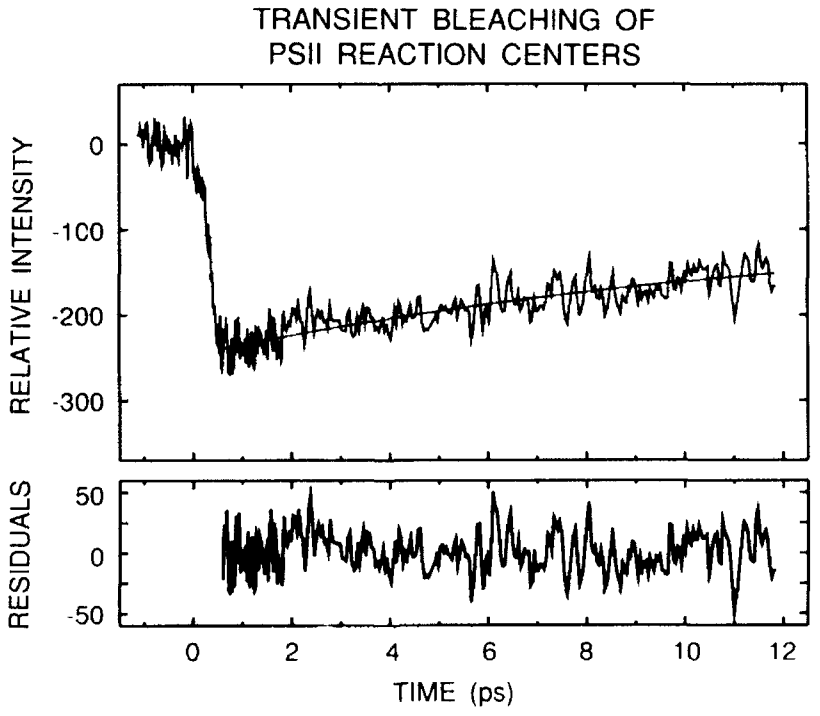

Fig. 4 Temporal profiles from the excitation of Photosystem II reaction centers at 310 nm, probed at 672 nm. Larger negative values correspond to increasing intensity. The red solid line is a single exponential fit to the recovery time and corresponds to 13 picoseconds.

independently probe (1) absorption by the CTTS state itself; (2) absorption by the electron as it first leaves the CTTS state (known as the "wet" electron); and (3) absorption by the fully solvated electron. Since these three species absorb in different spectral regions, we can probe them individually. Figure 5 shows the absorption spectrum of the CTTS state. This state lives for only ~120 femtoseconds before forming a neutral iodine atom and an electron. This is the shortest lived state that has been observed. By looking in other spectral regions, we can also observe the formation and decay of the intermediate, "wet" electron. Its lifetime is ~240 femtoseconds before it becomes fully solvated. These experiments provide the entire history of the electron generated by photodetachment, from formation to full solvation.

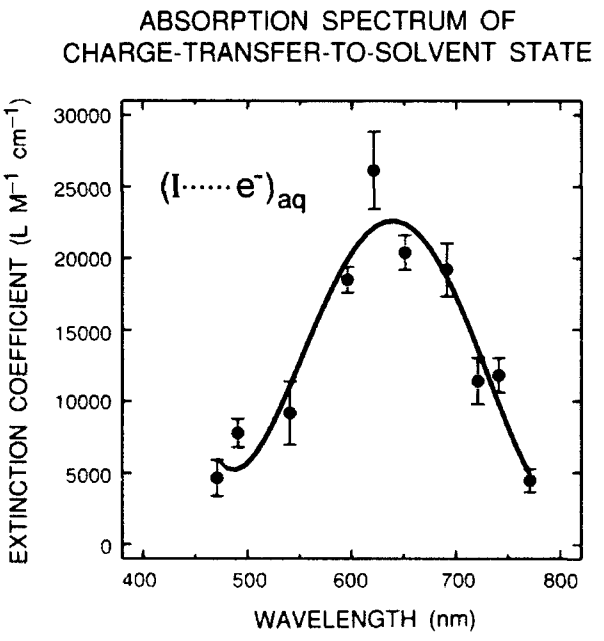

Fig. 5 – Transient absorption spectrum of the $(I^-)_{aq}$ CTTS state. This state has a lifetime of 120 femtoseconds. The solid line is a regression through the experimental data and is meant only as a guide.

We are also studying several other systems, particularly photodissociative systems, in which we hope to take "snapshots" of a molecule as it dissociates. By using ultrafast laser sources, we have already observed processes, which only a few years ago, were thought to be unobservable.

[Sponsored by ONR] ■

Chemical Adhesion Across Composite Interfaces

A.W. Snow and J.P. Armistead
Chemistry Division

A composite of stiff reinforcing fibers embedded in a tough matrix is mechanically superior to a continuous uniphase material. This occurs because stress does not concentrate at a small number of bulk material flaws but is distributed over a very large interfacial area by the ductile matrix, and macroscopic deformation is prevented by the fiber reinforcement. As such, fiber-reinforced organic matrix composite materials are achieving wider application as vessel component parts for present and future space, supersonic, and submarine operations. The current limitation of many of these materials is the ability to transfer stress across the fiber-resin interface. Upgrading the interface will result in performance enhancement not only of composite materials currently in use but also of advanced composites currently under development. To understand structural aspects that contribute to interfacial stress transfer, components must be identified and their contribution quantified.

Isolating Structures: For the technologically very important case of carbon fiber organic matrix composites, adhesive chemical interactions across the interface are a major contributor to this stress transfer. Of these interactions, hydrogen bonding is the most significant. This interaction with two classes of matrix resins is schematically illustrated in Fig. 6. Carbon fiber surfaces, as a result of an oxidative treatment during processing, are characterized by oxygen containing functional groups (phenol, quinoid, carboxylic acid) that are acidic in nature. The resin structures are crosslinked macromolecular networks with functional groups characteristic of the polymeric linkage. For the epoxy resin, these groups are tertiary amine (basic), hydroxyl (amphoteric) and ether (weakly basic); for the cyanate resin, they are triazine (basic) and ether (weakly basic). Hydrogen bonding is illustrated as a proton sharing between the fiber (donor) and

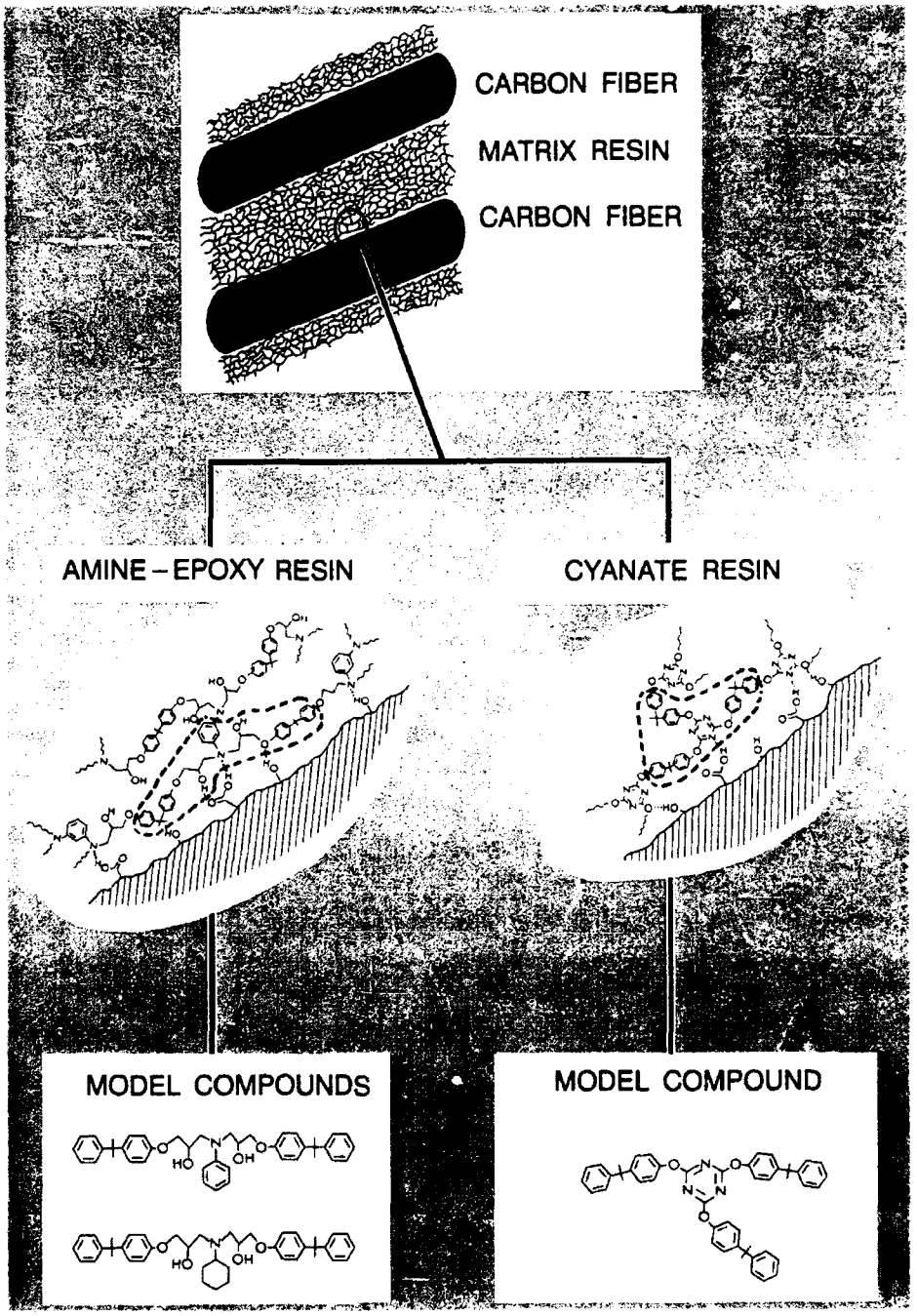

Fig. 6 – Composite interface illustrating hydrogen bonded chemical interactions between functional groups of the resin and the carbon fiber surface. The encircled resin chemical structure corresponds to that mimicked by the model compound. There are two amine-epoxy resins – one derived from an aromatic diamine (shown) and the other derived from an aliphatic diamine (not shown, but identical to the aromatic amine-epoxy except that the ring attached to the nitrogen is saturated, causing this resin's basicity to be much stronger).

resin (acceptor). To properly quantify the strength of the hydrogen bonding, it is necessary to isolate an appropriate segment of the resin structure and rank the strength of its hydrogen bond relative to other resins. An appropriate segment of the resin structure is a model compound that mimics the polymer repeat unit.

Determining Attractive Forces: The strength of hydrogen bonding is related to the magnitude of the equilibrium constant for hydrogen bond complex formation. This constant is measured for a complex of the resin model compound with a reference hydrogen bond donor or acceptor compound at high dilution in a nonhydrogen bonding solvent. The constant is then converted to a universal index or scale of hydrogen bonding acceptor strength (β-scale) or hydrogen bond donor strength (α-scale) depending on the role of the reference compound [1]. These α- and β-scale values serve as parameters to characterize the hydrogen bonding of the corresponding resin. The α- and β-scale experimental values corresponding to the resins in Fig. 6 are presented in Table 1.

Measuring Adhesion: As a measure of fiber-to-resin interfacial adhesion, a tensile test on a single fiber composite is performed as illustrated in Fig. 7. When this composite is strained, a shear stress is transferred from the resin through the interface to induce a tensile stress on the fiber. The fiber fractures when the tensile strength of the fiber is exceeded. Continued strain results in further fiber fracture until a critical fragment length is reached where the fragment's cylindrical interface area is no longer sufficient to transfer stress in excess of the fiber strength. Bright birefringent patterns develop around the fiber fragments as the test is performed (Fig. 7). The fiber critical length is measured and used to calculate an interfacial shear strength from a force balance between the shear strength over the fragment surface area equated to the fiber tensile strength over its cross-sectional area. This interfacial shear strength is used as an index of adhesion. Table 1 presents the corresponding results. For this series of fiber-resin combinations, the interfacial adhesion correlates with the resin β-scale

Table 1 — Comparative Epoxy and Cyanate Resin Hydrogen Bond Donor (α-scale) and Acceptor (β-scale) Strengths and Resin to AS4 Carbon Fiber Interfacial Shear Strength (τ)

Resin	Acidity (α-scale)	Basicity (β-scale)	τ (MPa)
Epoxy (aromatic Amine)	1.02	0.43	46
Cyanate	0.00	0.48	59
Epoxy (aliphatic amine)	0.88	0.51	59

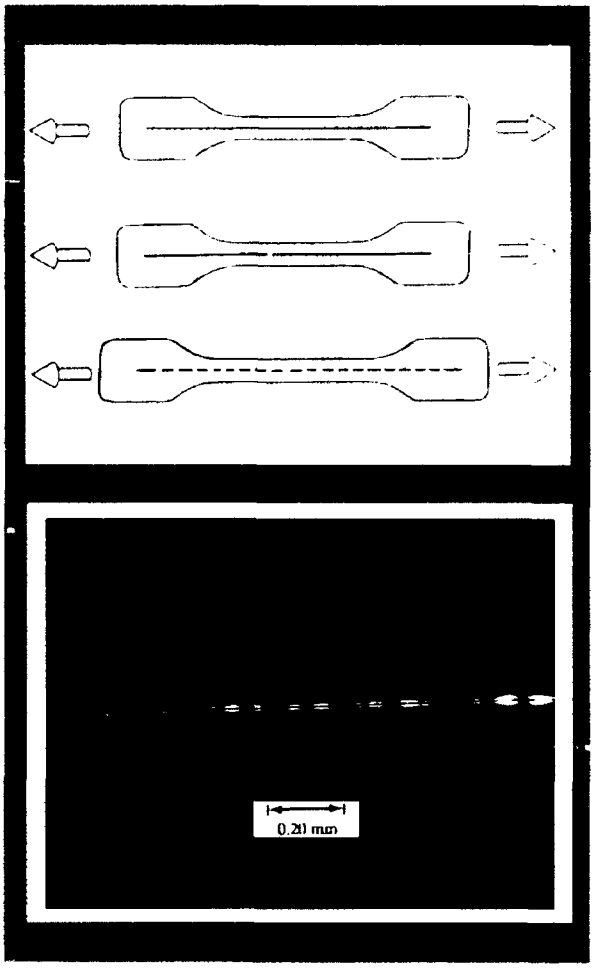

Fig. 7 — A single fiber composite test specimen illustrating strain induced fracture of the fiber and subsequent fragmentation. This shows the birefringence that develops around the fiber fragments during the test.

values. This is consistent with the acidic character of the carbon fiber surface. This correlation appears to approach a threshold at high levels of adhesion and is an indication of an over simplification of contributing factors to interface stress transfer. Other factors include interfacial stresses from resin cure shrinkage, stresses from differential thermal expansion between fiber and matrix, and effects from elastic and plastic deformations at the interface. Relating adhesion to these factors represents the opportunities for interdisciplinary research in this field.

[Sponsored by ONR]

Reference

1. M.J. Kamlet and R.W. Taft, *J. Am. Chem. Soc.* **98**, 377 (1976). ■

Nanocapillarity in Fullerene Tubules

J.Q. Broughton and M.R. Pederson
Condensed Matter and Radiation Sciences Division

The recent discovery of fullerene tubules [1,2] prepared by arc-discharge evaporation suggests that under more carefully controlled conditions, tubules of specific diameter and topology may be attainable. The tubules are believed to comprise unsaturated hexagonal hydrocarbon rings similar to those found in graphite. The π-electrons are expected to be highly polarizable along the tube axis, implying that such tubules will interact strongly with electrostatic and magnetic fields. Given their longitudinal cavity, these systems will be natural container compounds. In addition to charged and dipolar species, Van der Waal's molecules will migrate easily into their interior. These ideas are being explored by first-principles electronic structure (LDA) and molecular dynamics (MD) calculations [3,4]. Their ramifications are important.

LDA Calculations: Local Density Approximation calculations were performed on a fullerene tubule comprising a 120-atom cylindrical carbon cage with 24 hydrogens passivating the mouth (Fig. 8). The resulting tubule has a length of 12.8 Å and a radius of 3.9 Å. To study the interaction of dipolar molecules, two symmetrically placed hydrogen fluoride (HF) molecules (oriented with fluorines nearest) were allowed to traverse the longitudinal axis. The center of the tube is taken as origin. Figure 9 compares the bare interaction (i.e., HF - FH) with that when the tubule is present. Apart from a dip at short range (a correlation energy

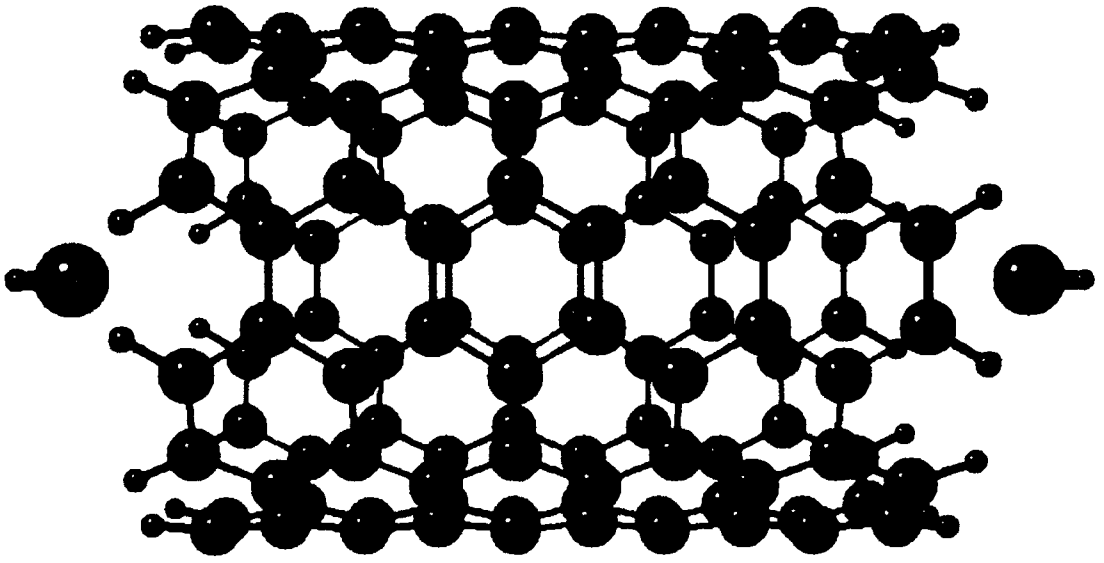

Fig. 8 – Graphene tubule used in the LDA calculations. Two HF molecules are constrained to move along the axis of symmetry.

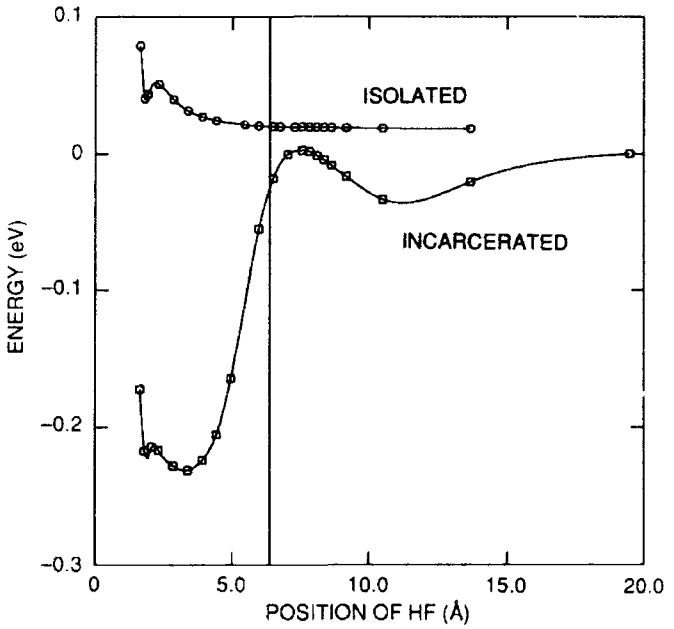

Fig. 9 — Binding energy, $E[C_{120}H_{24}(HF)_2]$-$E[C_{120}H_{24}]$-$E[(HF)_2]$, as a function of the HF position according to LDA

effect), the bare interaction is repulsive, as expected, at all distances. The interaction in the presence of the tubule is very different. Outside the tube mouth, at long range, the attractive r^{-6} dipole induced-dipole interaction dominates as a result of the polarizability of the tube π-electrons. Near the mouth but still outside, an "up-hill" region is caused by overlap of the tubule and HF closed-shell orbitals. But inside, the full effect of polarization dominates once again, and the molecules are incarcerated with an energy of 0.1 eV/molecule (i.e., 1200 K). The repulsive region near the mouth will diminish for tubules of larger radius but so also will the incarceration energy. Model Hamiltonians (with which to perform simulations) to describe the interaction of larger systems with external magnetic and electrostatic fields are being developed.

MD Simulations: The π-electrons of the tubule will interact via Van der Waals forces with simple nonpolar liquids. Graphitic sheets are held together this way. Simulations on tubules (of length 100 Å and radius 4-10 Å), approaching the surface of liquid inert-gases (comprising approximately 20,000 atoms), show that the liquid atoms are sucked into the tubule. The liquid wets the inside and outside of the tube, but the precise structure inside depends on the tube radius. Figure 10 shows an example of a 4 Å tube dipped into liquid Ne at 25 K; the liquid is rising to the mouth of the tube. Correlation functions of neon atoms inside the tube show that they form a helical structure. How fluid flows through such systems (nanopathways for lubricants in future nanoengines) and whether such macroscopic ideas as conductance are valid on these length scales is the subject for further research.

Conclusions: Tubules are clearly container compounds. They act as "molecular straws" capable of withdrawing molecules from the vapor or fluid phases by interactions akin to wetting and capillarity. Tubules may also lower reactive activation barriers between entrapped polar intermediates. Furthermore, the winding topology of a tube determines insulating or metallic behavior; hence the degree of screening from outside fields may be tailored. Also, different mouth passivators may lead to selective

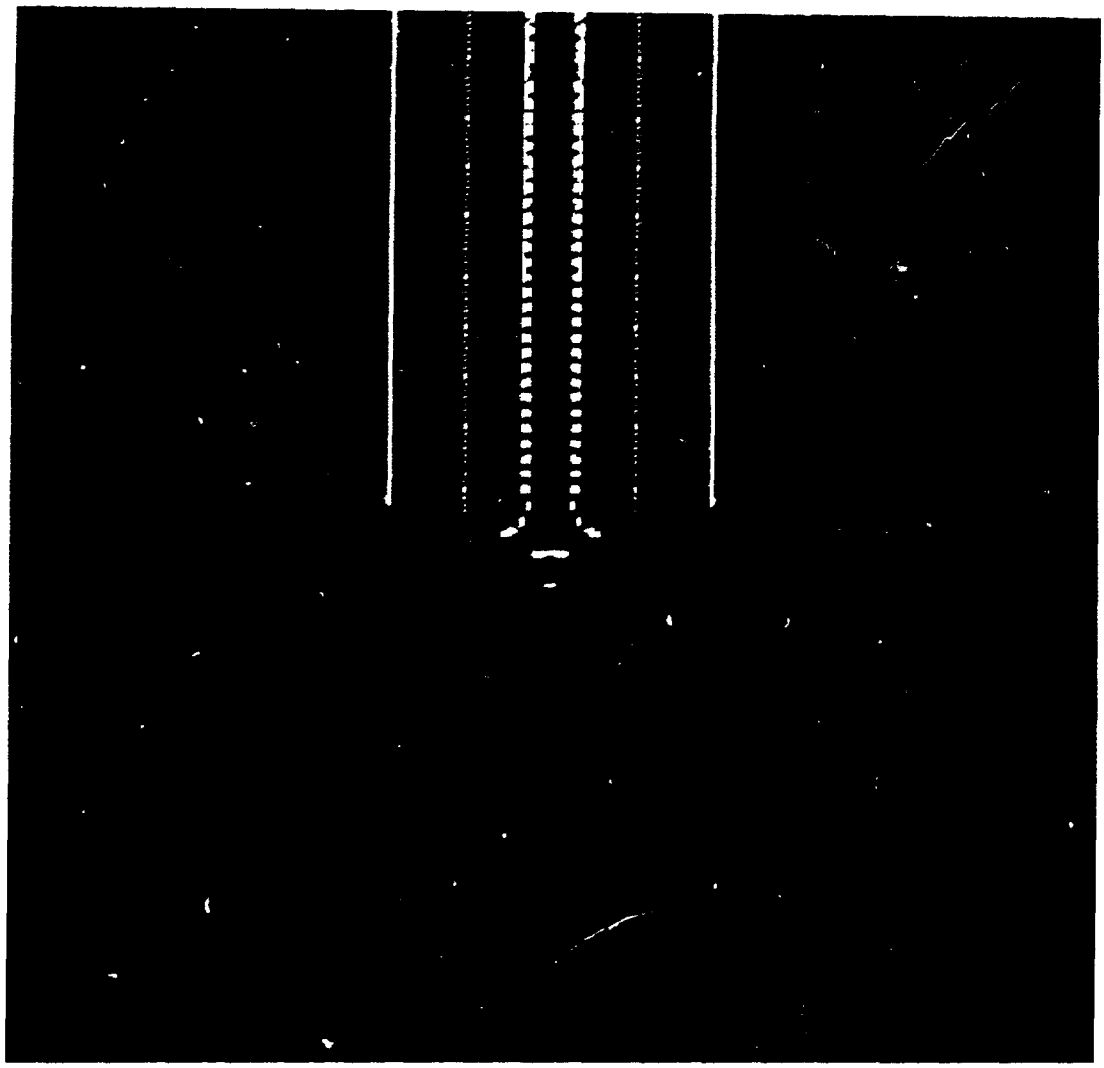

Fig. 10 — Atom density in a (cylindrically averaged) longitudinal plane through the neon/tubule system. Red (blue) color implies high (low) density; yellow is intermediate.

molecular incarceration. Applications such as nanoscale solenoids and piezoelectric devices are being pursued.

[Sponsored by ONR]

References

1. S. Wang and P.R. Busek, "Packing of C60 Molecules and Related Fullerenes in Crystals: A Direct View," *Chem. Phys. Lett.* **182**, 1-4 (1991).

2. S. Iijima, "Helical Mictrotubules of Graphitic Carbon," *Nature* **354**, 56-58 (1991).

3. M.R. Pederson and J.Q. Broughton, "Nanocapillarity in Fullerene Tubules," *Phys. Rev. Lett.* **69**, 2689-2692 (1992).

4. "Simulated Fullerene Tubules Act as Straws," *Science News* **142**, 327 (1992) (E. Pennisi, reporter). ■

Neuronal Patterning

D.A. Stenger
Center for Bio/Molecular Science and Engineering

The mammalian central nervous system is composed of an exquisitely well-ordered cellular communication network. The modulation of precisely arranged synapses between different neurons is one of the most aggressively studied subjects in modern science. However, attempts to study the detailed interactions between small groups of mammalian neurons is complicated by an unknown degree of connectivity in intact brain tissues. Furthermore, dissociated neurons from mammalian tissues develop randomly in culture, extending neurites in random directions.

A new method was recently developed at NRL for submicron resolution patterning of self-assembled monolayers (SAMs) using deep ultraviolet lithography [1]. Figure 11 shows a schematic description of the fabrication process. In particular, this research involves: (1) the design and fabrication of metallized masks for photolithographic definition of substrates suitable for patterning cultured neurons, (2) optimizing cell culture parameters, (3) determining which cell-adhesive materials, line widths, lengths, and geometries are most suitable for the interaction between two or more neurons.

We have used this approach to define substrate patterns for the selective adhesion and outgrowth of tumor-derived neuroblastoma cells [2] and dissociated mammalian neurons [3]. In the latter case, we have focused on patterning

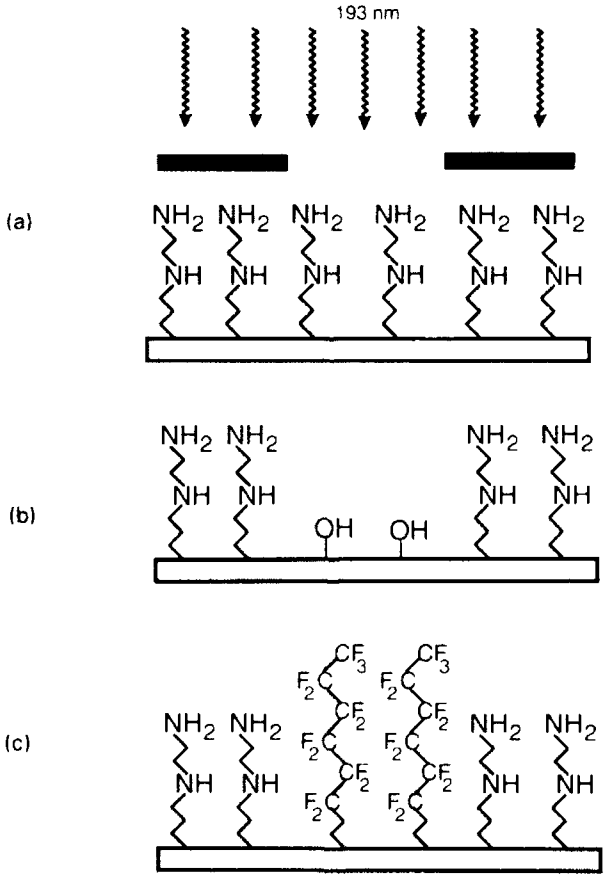

Fig. 11 — Schematic for production of patterned SAMs for selective neuronal cell adhesion. SAMs prepared from a cell-adhesive ethylenediamine (EDA) aminosilane on silica surfaces are photocleaved by patterned deep UV radiation (a,b). The exposed regions are refunctionalized (c) with a perfluorinated alkylsilane (13F) which forms hydrophobic Teflon-like surfaces that inhibit cell adhesion.

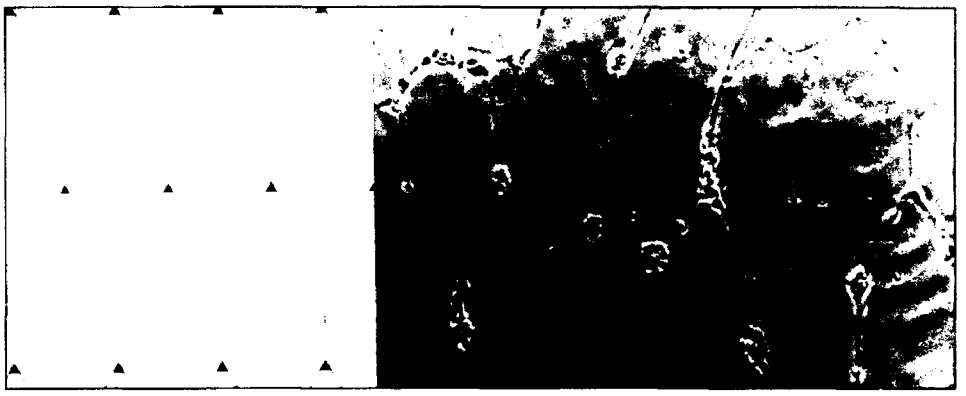

Fig 12 – (Left panel) – First generation lithographic mask for neuronal patterning. The dark features of the mask represent chromium used to block UV irradiation while the rest of the mask is quartz, allowing photolithographic definition of triangle-shaped EDA regions (triangle sides range from 5 to 20 μm) that are large enough to promote adhesion when the cells were initially plated. Narrow lines (widths range from 0.5 to 5.0 μm) in the mask allow definition of EDA channels that are not wide enough to promote cell adhesion during plating, but provide pathways for the exploratory growth cones of the developing neurons (right panel). (Published with the permission of the *Journal of the American Chemical Society*.)

the geometric interactions of pyramidal neurons isolated from the embryonic rat hippocampus, which have well characterized mechanisms of synaptic plasticity. Figure 12 (left panel) shows that a photolithographic mask was designed specifically for this purpose and fabricated at the NRL Nanofabrication Facility. Figure 12 (right panel) shows the resultant pattern of hippocampal neurons that develops on EDA/13F patterns defined by this mask at 48 hours after plating. In general, neuron adhesion occurs only at the triangular nodes and line intersects. Neurite processes are almost exclusively directed along the EDA pathways.

Currently, we are developing second generation masks to allow more refined neuronal geometries and testing their physiological properties. In addition, patterned neuroblastoma cells that are sensitive to a wide variety of neurotoxins are being integrated with microelectrode arrays for potential use as chemical/biological warfare detection devices.

[Sponsored by ONR]

References

1. J.M. Calvert, J.H. Georger, M.C. Peckerar, P.E. Pehrsson, J.M. Schnur, and P.E. Schoen, "Deep UV Photochemistry and Patterning of Self-assembled Monolayer Films," *J. Thin Solid Films* **359**, 210/211, 359-363 (1992).

2. C.S. Dulcey, J.H. Georger, Jr., V. Krauthamer, D.A. Stenger, T.L. Fare, and J.M. Calvert, "Deep UV Photochemistry of Chemisorbed Monolayers: Patterned Coplanar Molecular Assemblies," *J. Science* **551**, 252 (1991).

3. D.A. Stenger, J.H. Georger, C.S. Dulcey, J.J. Hickman, A.S. Rudolph, T.B. Nielsen, S.M. McCort, and J.M. Calvert, *J. Am. Chem. Soc.* **114**, 8435-8442 (1992). ■

Electronics and Electromagnetics

CRUISE_Missiles Electronic Warfare Simulation

A.J. Goldberg and R.J. Futato
Tactical Electronic Warfare Division

For over a decade, the Advanced Techniques Branch of the Tactical Electronic Warfare Division (TEWD) has evolved progressively sophisticated digital electronic warfare (EW) simulation models to support the study and design of improved countermeasures for defending ships against antiship cruise missiles (ASCMs). Recent breakthroughs in NRL modeling technology by TEWD and the Radar Division, sponsored by NAVSEA and the 6.2 EW Block, have allowed the latest of these models, *CRUISE_Missiles*, to be augmented with a pedigreed inventory of modern ship representations (notably DD-963, CG-47, and DDG-51) that create true spatially extended signatures directly traceable to ship architecture. The coupling of these models with the powerful numerical algorithms optimized for supercomputing within *CRUISE_Missiles* permits accurate simulation of the complex envelope signal processing of fundamentally important ship/EW interactions on a pulse-by-pulse basis at model update rates approaching the actual pulse repetition frequency (PRF) of the missile radar. This unique modeling achievement has proven of benefit not only to EW designers and tacticians but also to ship architects and ASCM developers as well.

ASCM Cellular Viewpoint: The motivation behind the development of these detailed ship models comes from the manner by which advanced ASCM radar-guided threat seekers resolve their quarry. A radar-guided ASCM typically uses a seeker with a narrow pencil-beam antenna combined with range gating to create a compact three-dimensional cell in space (see Fig. 1). The azimuth and elevation dimensions and orientation of the cell are formed by the seeker antenna pattern (and range to target), while the range extent and location is formed by the combination of transmit pulse, receiver response, and range gate. The focus of the seeker at any instant is the contents of this cell, and the ASCM tends to disregard targets, real or simulated, that lie outside of it. The cell therefore establishes a mechanism for resolving individual targets.

For much of the terminal end-game, range is the dimension of highest resolution, so that seeker target resolving power is essentially parameterized by the radar pulse width. Long pulse seekers with relatively low resolution

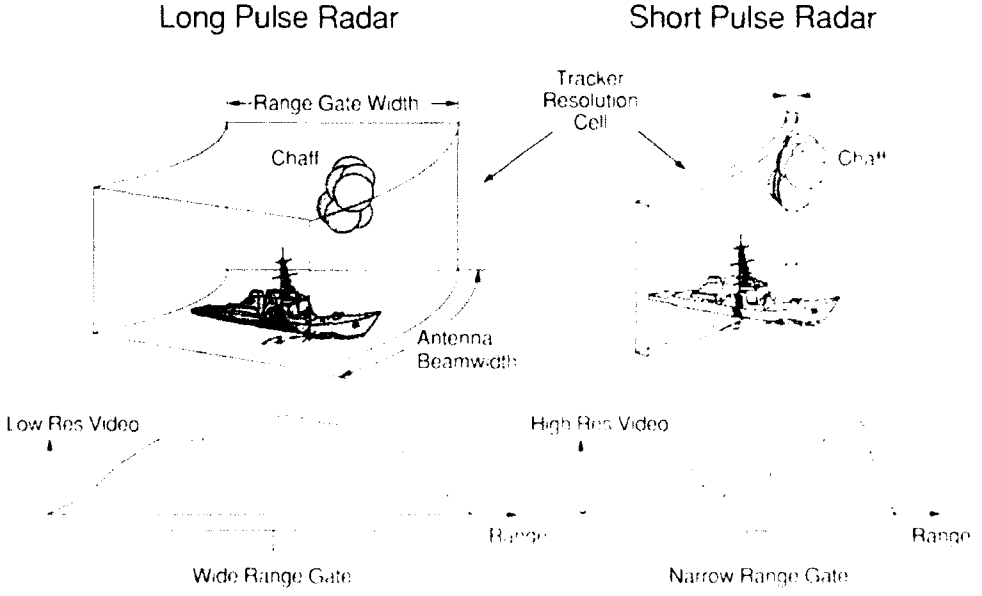

Fig. 1 Long and short pulse radar cellular resolution of ship and chaff countermeasure targets

(Fig. 1, left diagram) sense the ship target in aggregate, and the ship can therefore be characterized to these seekers on a pulse-by-pulse basis by a single quantity such as radar cross section (RCS). Conversely, short-pulse, high-resolution seekers resolve detailed features of the ship structure (Fig. 1, right diagram), which cannot be captured by a single RCS characterization alone. Since EW typically involves creating disturbances that compete with true targets within the radar resolution cell, the proper assessment of the EW/target competition outcome requires the simulation of the true spatially extended character of the ship signature.

While it is the narrow range extent of the resolution cells within short-pulse seekers that creates the need for a spatially extended target signature model, it is the finite size of these cells that also bounds the complexity required of the model and permits the use of a discretized target representation in place of the real, continuously distributed target. Within *CRUISE_Missiles*, the discretized target model takes the form of individual point scatterers populated around the ship platform at a density that exceeds the range resolving power of the seeker. All *CRUISE_Missiles* ship representations are sufficient for use with the shortest pulse seekers of interest, yet produce consistent results for long pulse seekers as well.

Unique modeling technologies are used within *CRUISE_Missiles* to represent and process the radar returns computed by the target models. The radar returns are passed to software models of the threat radar hardware as sampled complex envelopes carrying both amplitude and phase information. It is again the finiteness of the threat resolution that provides the basis for the rigorous approximation of the wide bandwidth continuous time signal processing hardware within the digital software models.

Spatially Extended Ship Representation: The *CRUISE_Missiles* ship model carries the strength of a rigorous physical representation tied to actual ship architecture. The signature representation consists of a collection of point scatterers located on a moving coordinate frame (see Fig. 2). The ship coordinate frame is updated by ship motion models that are obtained from the developer (Naval Surface Warfare Center, Carderock Division). Dominant scatterers have reflectivity patterns corresponding to physical primitives—spheres, plates, dihedrals, trihedrals, or cylinders—and contribute substantially to the ship signature. These scatterers usually correspond to actual counterparts on the real ship. The remainder of the signature is formed by a multitude or cloud of smaller contributors, and these are represented in the model by a carefully constructed discretized RCS distribution.

The basis for the ship representation is a unique highly detailed ship RCS prediction model called Radar Target Signature (RTS) developed by NRL's Radar Division. Briefly, the RTS model starts witha geometric description the ship derived from ship drawings and/or field measurements. RTS analyzes this

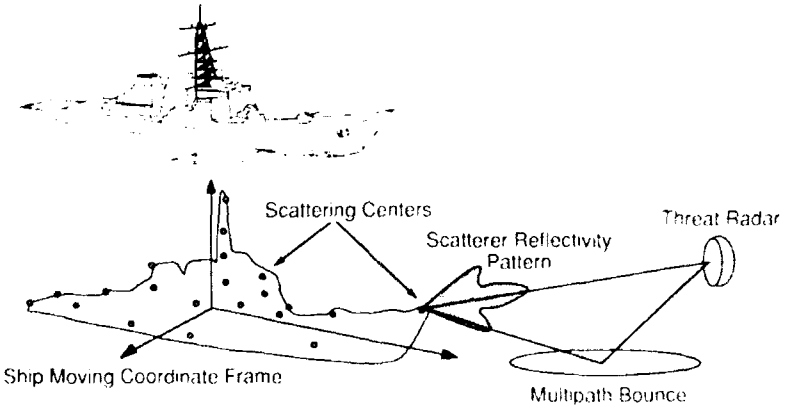

Fig. 2 *CRUISE Missiles* ship representation

database to identify multiple bounce sequences, and then uses first-principles electromagnetic calculations to compute the RCS for individual primitives. RTS emphasizes detail at the expense of run time, and has been subjected to extensive validation by the Navy. Typical RTS ship representations comprise over 200,000 primitives, and can require 15 to 30 minutes for the calculation of RCS at a single geometry. The *CRUISE_Missiles* simulation, on the other hand, demands update rates on the order of milliseconds, and thereby requires a modeling strategy that accelerates the RTS calculation by 5 to 6 orders of magnitude.

TEWD has achieved this speed-up by a sequence of adaptations. The RTS model provides more than simply total RCS predictions. It provides an ordered ranking of contributors that is used to rigorously bound a simplified approximation of dominant scatterers and a basis for characterizing the distributed background or cloud. Further, RTS provides a comprehensive database of scatterer types and locations, and mono- and bistatic pattern formulas for each primitive. This information is essential to producing a representation that both rigorously approximates the RTS calculation and is capable of being integrated with dynamic ship motion and sea multipath calculations. The resulting *CRUISE_Missiles* representations typically involve 1000 scatterers, of which one third are visible at any one aspect angle. The scatterer calculations are then organized for rapid computation using a combination of table look-up and vectorization amenable to supercomputing architectures. The resulting ship signatures can be processed by the radar signal chain and represented as complex video at pulse-by-pulse rates approaching the PRF of the actual ASCM seeker. Figure 3 shows a so-called hour-glass

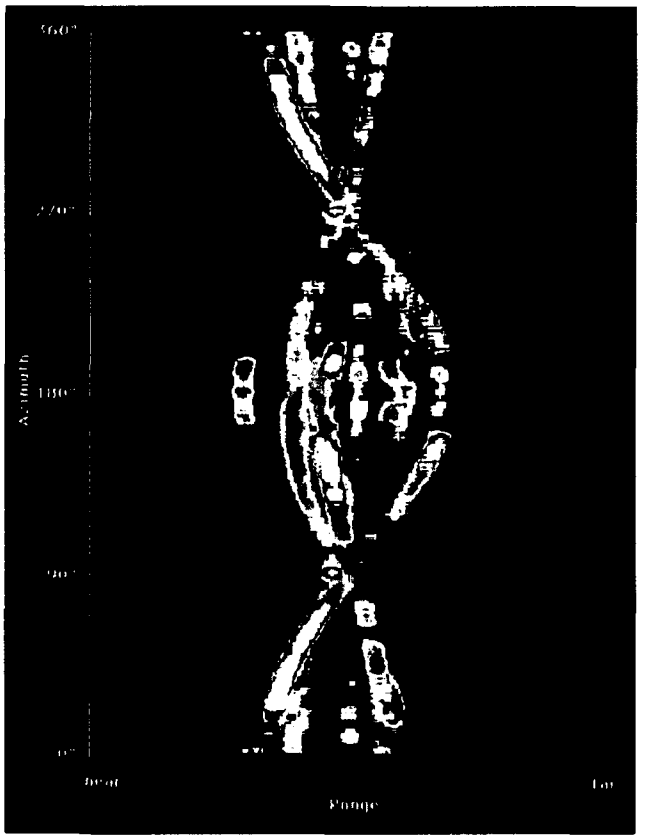

Fig. 3 — Hour-glass visualization of simulated ship signature pro-files as a function of range and azimuth. Here the different colors represent a graduation of RCS values, with white being the highest and black the lowest. In this figure, the radar range resolution is 20 feet.

representation of the *CRUISE_Missiles* ship model video profiles over a full 360-degree range of aspect angles, emphasizing the aspect dependence and spatial extent of the ship representation.

Applications: These ship models, combined with the *CRUISE_Missiles* model's detailed radar simulation framework, enable several major research pursuits of great importance to the Navy. Because the scatterer distribution directly traces back to the physical ship architecture, *CRUISE_Missiles* play a unique role in determining the EW effectiveness benefit of ship modifications. With accurate spatially extended representations of actual ships, simulations carried to missile impact provide highly confident estimates of hit-point statistics for use in the assessment of ship survivability. Simulated ship signatures may serve as candidates for use in advanced spoofing countermeasures, and the inclusion of ship motion and sea multipath allows these effects to be considered as well. Because these models involve all-digital technologies, the benefits also extend beyond current ship platforms to notional ship designs that are still on the drawing board.

Acknowledgments: The authors wish to recognize and thank Gerald Friedman, Robert Gover, Huck Mok, Sheldon Wolk, and Naba Barkakati of the TEWD and Radar Division team headed by Harold Toothman who (along with the authors) were directly responsible for creating this new modeling capability, and to NAVSEA and the 6.2 EW Block sponsors for their support.

[Sponsored by NAVSEA] ■

Flying Radar Target (FLYRT) Technology Development

K.G. Ailinger, H.E. Chaplin,
K.G. Limparis, and S.K. Tayman
Tactical Electronic Warfare Division

The Flying Radar Target (FLYRT) is an active RF decoy capable of being launched from the shipboard MK 36 launcher. The air vehicle is boosted from the launcher by a solid fuel rocket motor. Preloaded tail surfaces for stability deploy as the round leaves the barrel. Following motor burnout, and prior to apogee, the motor is separated and drops away. At apogee, the electric motor is turned on, the wing and antennas are commanded to deploy and the round is transformed into an autonomous flying decoy capable of several minutes flight duration. Figure 4 shows the deployment scenario. The key technology areas include achieving efficient aerodynamics within strict packaging constraints; developing lightweight yet rugged deployment mechanisms, lightweight avionics, autopilot, sensors, and electric propulsion; and achieving the required RF antenna isolation for successful payload operation. In each of these areas, NRL has adapted or developed state-of-the-art technologies including: advanced low Reynolds number aerodynamics, fiber-optic gyros, samarium cobalt electric motors, silver-zinc battery packs, composite materials, and antenna isolation measurement and coupling reduction techniques.

Efficient Aerodynamics Within Strict Packaging: Limited in size by the packaging volume of the launch container and in speed by the mission requirement to fly at ship-like speeds, the FLYRT operates in the low Reynolds number flight regime, where drag increases and lift decreases due to viscous effects. The FLYRT features a constant chord wing and the Wortmann FX63-137 low Reynolds number airfoil. Hinged outer wing panels double the wing area by increasing the span and therefore the aspect ratio, reducing the induced drag (i.e., the drag caused by lift). Since the drag of the fuselage is a small percentage of the overall vehicle drag, the need for large internal packaging volume defines the very unconventional shape of the FLYRT fuselage.

Mechanisms: The wing deployment mechanism is designed for simplicity and reliability and uses aerodynamics rather than mechanical systems to operate. When stowed, the wing is held in place by an over-center locked bell-crank, which is released using a servo actuator.

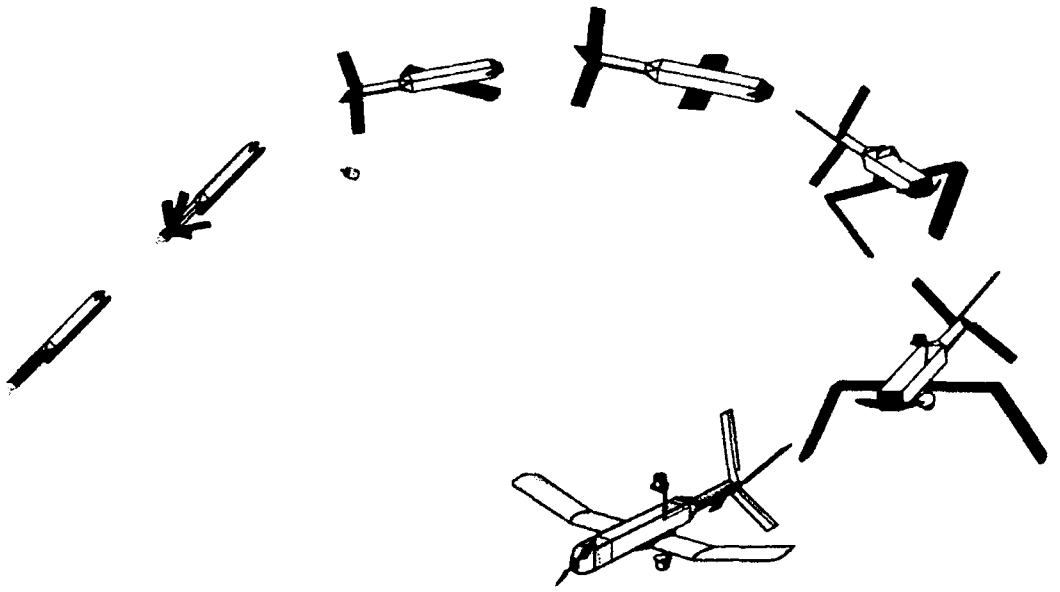

Fig. 4 — Deployment scenario

As the wing rotates into position, the pin holding the outer tips is released and the lift generated by the tip panels provides the necessary aerodynamic moment to "fly" the outer wing panels into position. This mechanism was verified using three 2/3 size, lightweight gliders. The first glider demonstrated the fully deployed wing (see Fig. 5), the second demonstrated the outer tip deployment, and the third the full wing pivot and outer tip deployment. This low-cost testing verified the simple deployment mechanism and reduced program risk.

Avionics: FLYRT uses a three-axis fiber-optic gyro (FOG) to provide highly accurate angular rate data to the avionics computer. The patent pending NRL FOG design uses a low-cost open loop gyro, and electronically closes the loop to provide linear output at high rates. This design eliminates optical closed-loop components, only requires low-cost telecommunications grade fiber, and has a simple electronics package. The FLYRT FOG covers a wide dynamic range (25 deg/hr to $\pm$200 deg/s) and maintains accuracy over a temperature span of 20° C. The design includes onboard A/D converters that are read by the avionics computer 50 times per second and integrated to provide vehicle attitude information. A miniature, single board, commercially available computer (2.75" $\times$ 4.0" $\times$ 0.5") is used for the FOG data integration task, along with the remaining navigation and autopilot functions.

Fig. 5 — Fixed wing glider deployment

Electric Propulsion: The FLYRT is a battery-powered vehicle with a high performance dc electric motor driving an NRL-designed propeller through a reduction gear drive. Electric propulsion was chosen because

of its reliability and simplicity, especially important for an operational decoy that may be dormant for years before being activated. The platform for the folding propeller was designed using an in-house minimum induced-loss propeller design computer code. A full-scale propeller, 2 feet in diameter, was tested in NRL's low-speed wind tunnel and found to be 77% efficient. High-strength samarium cobalt magnets and silver graphite brushes make possible a 1.5 pound, 1.5 horsepower dc electric motor. A silver-zinc battery pack provides the power for a 12 minute flight. Aerodynamic hub fairings were designed to reduce the torque due to the drag of the large hub and blade pivot pin.

Isolation: FLYRT requires a very high isolation antenna configuration. Development of this configuration is complicated by the close proximity of the antennas, a complex vehicle shape, and the requirement of minimal impact on the vehicle. Efforts to develop this high isolation antenna configuration are concentrated in three major areas: (1) measurements techniques; (2) antenna design; and (3) development and placement of radar absorbing material (RAM) and radar absorbing structures (RAS). The isolation measurement system uses remote mixers set in an anechoic chamber and time domain software to diagnose the isolation problems (see Fig. 6). Extremely sensitive measurements can be made in a short time and the data directly highlights the problem areas. Special material with gradually decreasing conductivity provides low antenna backlobes (energy radiated in undesired directions) while maintaining excellent antenna radiation patterns. RAM and RAS were used to achieve a combination of absorption and scattering in a direction away from the antennas to reduce the isolation problems. These components in conjunction with composite fabrication techniques create an extremely high isolation antenna pair on a small vehicle.

[Sponsored by OPNAV] ■

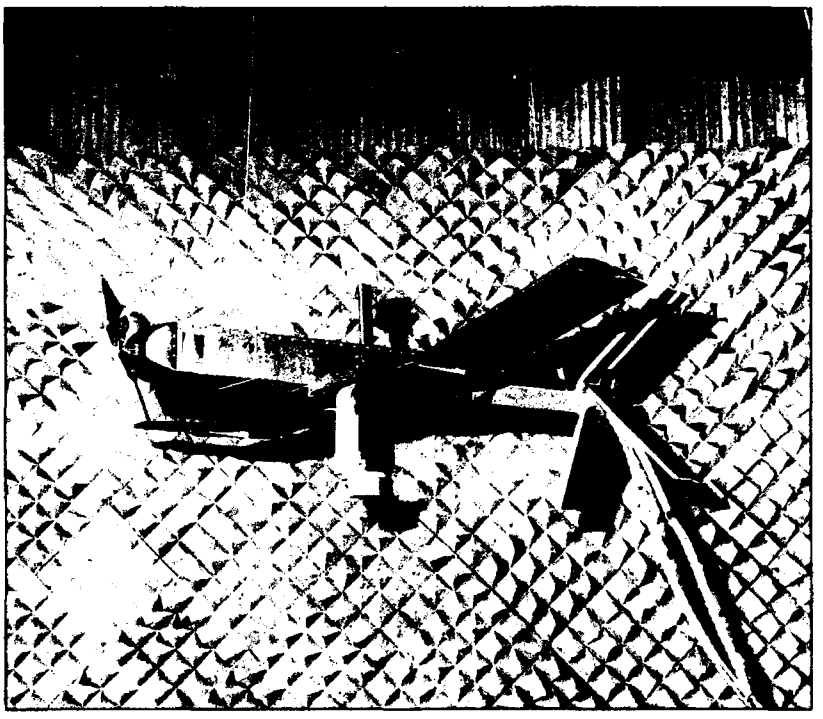

Fig. 6 – Isolation test model

Airborne Electromagnetic Hydrographic Techniques

E.C. Mozley, T.N. Kooney, and D.E. Fraley
Marine Geosciences Division

The importance of maintaining accurate information on water depths and sediment distributions in coastal regions is becoming increasingly important as large groups of the global population concentrate in these areas. Both commercial and defense segments of society require accurate and timely bathymetry in this dynamic environment. The traditional measurement techniques that have been used to monitor the evolution of these rapidly changing coastal zones are slow and expensive. As a result, charts of many parts of the world are grossly outdated. To lessen this problem, airborne lidar mapping systems have been developed and are currently being used. However, the performance of these systems is degraded by the numerous existent environmental conditions such as water clarity, water surface roughness, and bottom vegetation. To circumvent these problems, airborne electromagnetic (AEM) methods have been developed for measuring water depths and sediment conductivity from helicopter platforms. The first generation of digitally controlled AEM systems have been evaluated and found to provide accurate water depths and water conductivities from the shore to depths in excess of 20 m.

Measurement Fundamentals: The AEM bathymetry technique is based on the use of the physical phenomenon of electromagnetic induction in the seawater and seafloor sediments. When an electromagnetic transmitter is used above water overlying a saturated sedimentary sequence, the time varying primary fields will induce eddy currents within the water column that will in turn diffuse through water into the sediments at a rate defined by electrical conductivity of the media. The secondary fields, which are generated by the diffusive eddy currents that first move through the highly conductive water and then through the more resistive sediments, provide a frequency response that reflects both the depth and conductivity of the water as well as the conductivity of the sediments. The water conductivity is a function of water temperature and salinity, and the conductivity of the saturated sediments is related to both water conductivity and sediment porosity and permeability.

The AEM technique was developed in Canada during the 1950s as a mineral prospecting tool. Over the years, the technology evolved into sophisticated multifrequency systems capable of mapping sedimentary cover. These mapping systems required a large number of analog circuit elements that resulted in complex and poorly calibrated systems with very high drift rates. These system traits caused a high degree of uncertainty in the interpretation of the data. As a solution, the Navy developed a program to design and fabricate an advanced, digitally controlled, wide band AEM system. The system's characteristics are summarized in Ref. 1.

Field Results: The AEM hydrographic system was used over the St. Mary's river in the vicinity of Kings Bay, Georgia, entrance channel as shown in Fig. 7 to chart water depths and map variations in seafloor sediments. The survey provided a set of high quality data that overlapped a region covered by two high density acoustic surveys. In addition, in situ water temperature and conductivity measurements were obtained over the tidal cycle and along the surveyed channel.

The interpretation of the AEM data indicated that the inferred water conductivities agreed with in situ measurements to an accuracy of 0.1 Siemens/meter (S/m). The root mean square difference between the water depths that were provided by the AEM measurements and a suite of acoustic fathometer data was less than 0.6 m over an 11 km^2 subregion. A summary of the survey data and processing procedures are provided in Ref. 2. Figure 8 shows a map of the AEM water depths over the entire surveyed region. The seafloor conductivities were spatially coherent and provided a realistic range in values as Fig. 9 shows. These values correspond to a variation of bottom material ranging from a clean, well consolidated sand to a poorly consolidated clay or silt. Thus, the technique

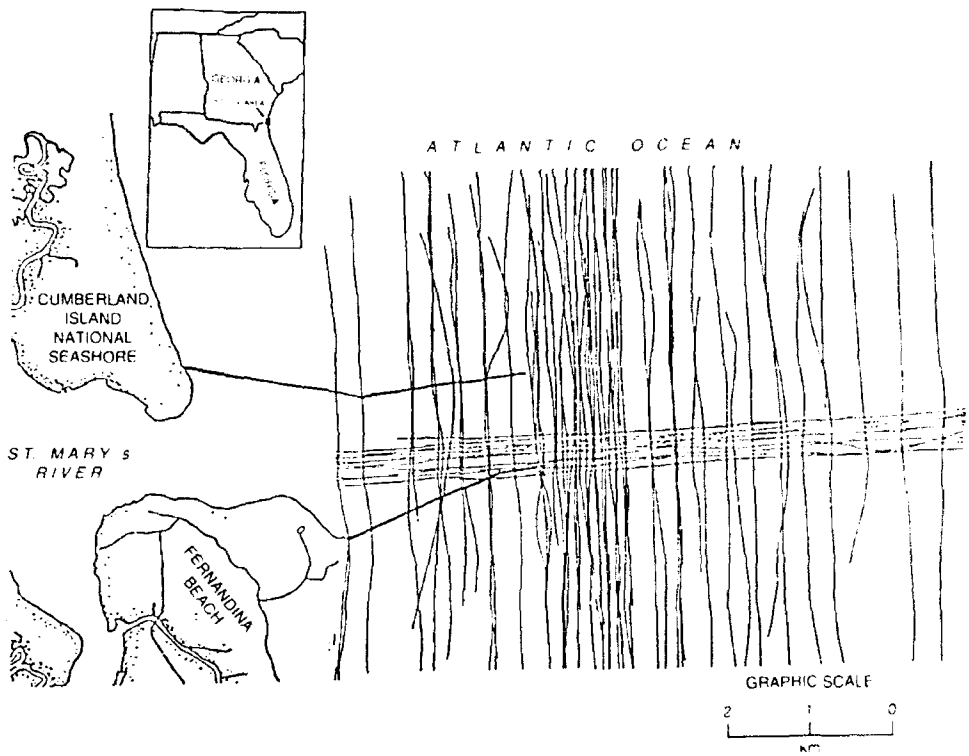

Fig. 7 – Map of the location where AEM flight lines were distributed and data were collected at a rate of 30 samples per second

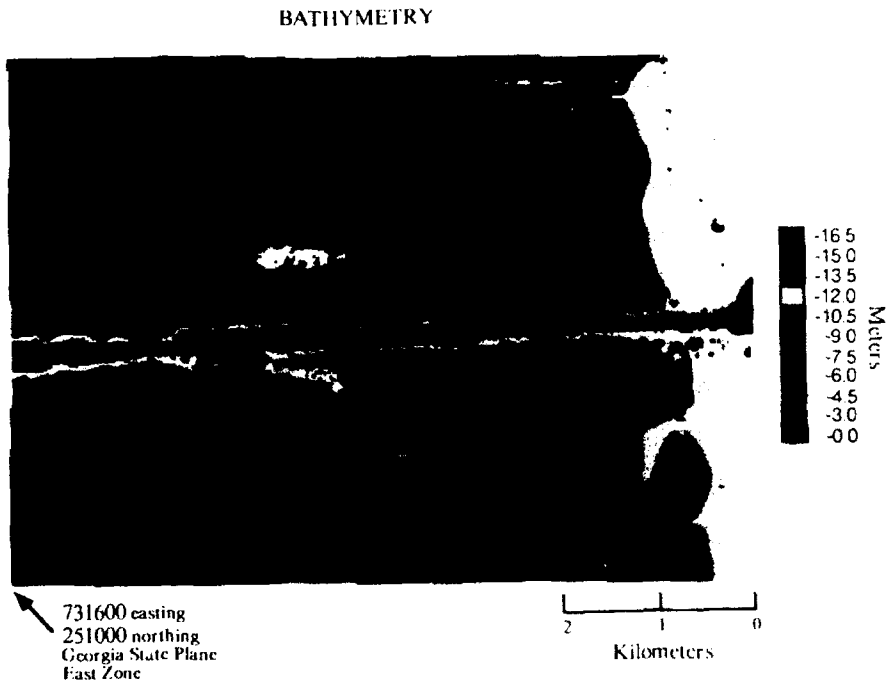

Fig. 8 – The distribution of water depths in the survey area are shown as color coded regions that are defined on the right side of the figure. The heavy black lines on the left side of the map represent the stone jetties that protect the river entrance.

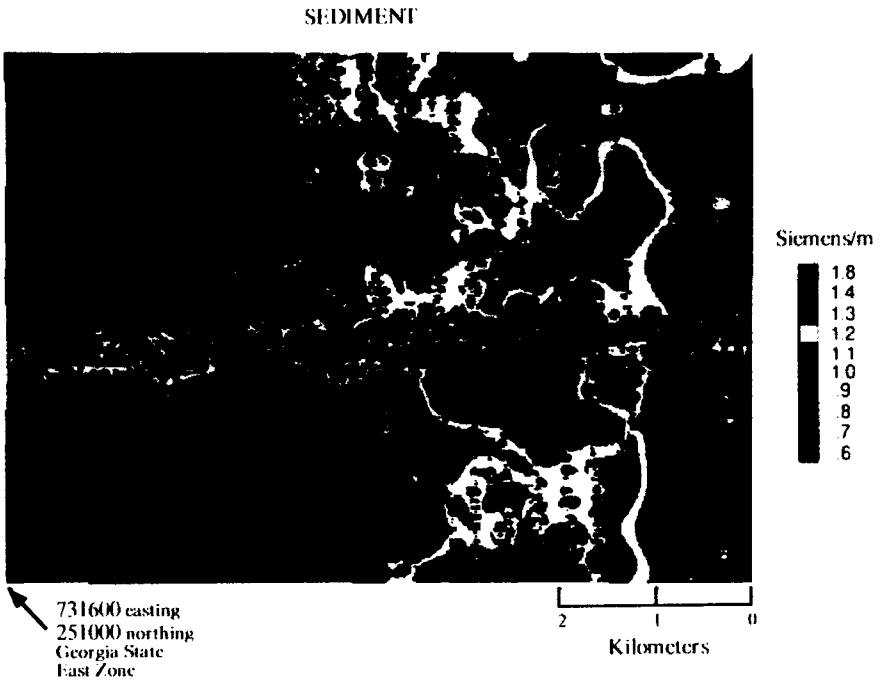

Fig. 9 — The sediment conductivity variations are displayed according to the color coded map. The values vary over 300% moving from the beach on the left side of the map to the seaward side.

proved to be an important tool to remotely measure multiple oceanographic and geotechnical parameters.

Acknowledgements: The AEM Kings Bay survey was funded by CNO (OP-096) through program element 603704N under the management of the Tactical Oceanographic Warfare Support Office, NRL-SSC, Mississippi (Kenneth Ferer). LT David Dyman provided a significant contribution in the field and during the data processing phase of the effort. The instrumentation was fabricated by Geophex, Ltd., Raleigh, North Carolina, and modified by Right By Design, Markham, Ontario, Canada.

[Sponsored by CNO]

References

1. Edward C. Mozley, Timothy Kooney, and David Byman, "Advanced Airborne Electromagnetic Hydrography," *Proc. MTS '91*, **II**, 883-889 (Nov. 10-14, 1991).

2. Edward C. Mozley, Timothy N. Kooney, D.A. Byman, and D.E. Fraley, "Airborne Electromagnetic Hydrographic Survey Technology," *Proc. of the Society of Exploration Geophysicists Sixty-First Int. Mtg*, **I**, 468-471 (Nov. 10-14, 1991). ■

The High Temperature Superconductivity Space Experiment (HTSSE)

A.R. Peltzer, C.L. Lichtenberg, and G.E. Price
Space Systems Development Department

The High Temperature Superconductivity Space Experiment (HTSSE) program was initiated by NRL in 1988. The HTSSE program is being developed and managed by NRL. The overall goal is to demonstrate the potential advantages of high-temperature superconductor (HTS) electronic components subsystems in space. The first phase of the program is HTSSE-I, which will prove that passive HTS microwave devices have the ability to survive

and operate in the space environment. There are 15 passive HTS devices that have been space qualified and integrated within a cryogenic payload. A microwave measurement subsystem and digital subsystem are used for extracting the performance of the HTS devices on orbit. The HTSSE-I subsystems have been successfully integrated onto a DoD spacecraft as an experimental payload. The experimental payload was designed, developed, built, and space-qualified by NRL.

HTSSE-I Devices: State-of-the-art electronic components are required for improving military and civil satellites. The existing satellite systems have limited channel capacity and link performance. Increase in electrical performance and decrease in weight and power are the benefits of using HTS materials. HTSSE-I will demonstrate passive microwave circuit devices including: thin-film ring and linear resonators, coated-bulk cavity resonator, thin-film band-pass and low-pass filters, HTS/dielectric resonator band-pass filter, branchline coupler, and miniaturized patch antenna.

Device contractors were funded to fabricate two prototype devices and five optimized flight devices for delivery to NRL. NASA/Jet Propulsion Laboratory, Lockheed-Sanders, and University of Wuppertal supplied the devices to NRL at no charge. The devices provided by each supplier were subjected to the rigors of space qualification. The testing, performed at NRL, involved cryogenic thermal cycling, electrical characterization, random vibration, pyrotechnic shock, and irradiation. Each of the HTSSE-I devices that passed the qualification testing showed improved performance over equivalent normal-metal devices. Figure 10 shows measured responses of two flight devices.

HTSSE-I Space Hardware: HTSSE-I will collect data on the HTS devices in the space environment and will demonstrate high reliability, potentially long life, and active cryogenic support system. The development of cryocooler technology and cold package integration are crucial for successful implementation of HTS technology in spacecraft. The HTSSE-I comprises 15 HTS microwave experiments and

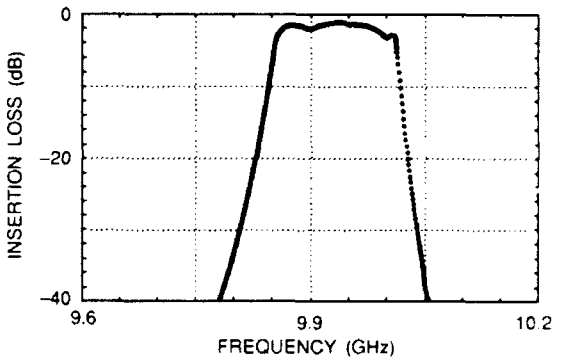

Fig. 10(a) — Measured insertion loss for Westinghouse band-pass filter at 78 K collected during satellite thermal-vacuum testing using the completed HTSSE-I space system, $IL_{min} \approx 1.3$ dB

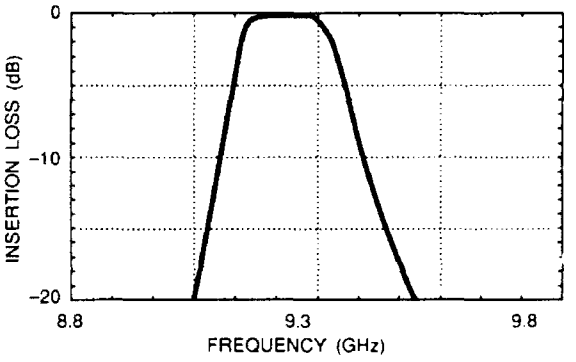

Fig. 10(b) — Measured insertion loss for Space Systems/Loral band-pass filter at 78 K collected during satellite thermal-vacuum testing using the completed HTSSE-I space system, $IL_{min} \approx 0.2$ dB

four normal-metal reference devices mounted on a cryogenic bus. HTSSE-I is an unclassified secondary payload on board a classified DoD satellite that will be placed in a relatively high-radiation orbit. A total dose of greater than 1 Mrad (Si) is expected over the six-month mission HTSSE-I time. Six dosimeters on board HTSSE-I will provide cumulative dose information.

HTSSE-I contains three major subsystems: the cryogenic cold bus package and cryocooler, RF measurement instrumentation, and control electronics. Figure 11 shows a detailed block diagram of HTSSE-I depicting individual electronic subassemblies located on the electronics deck and major components on the experiment deck/cold bus.

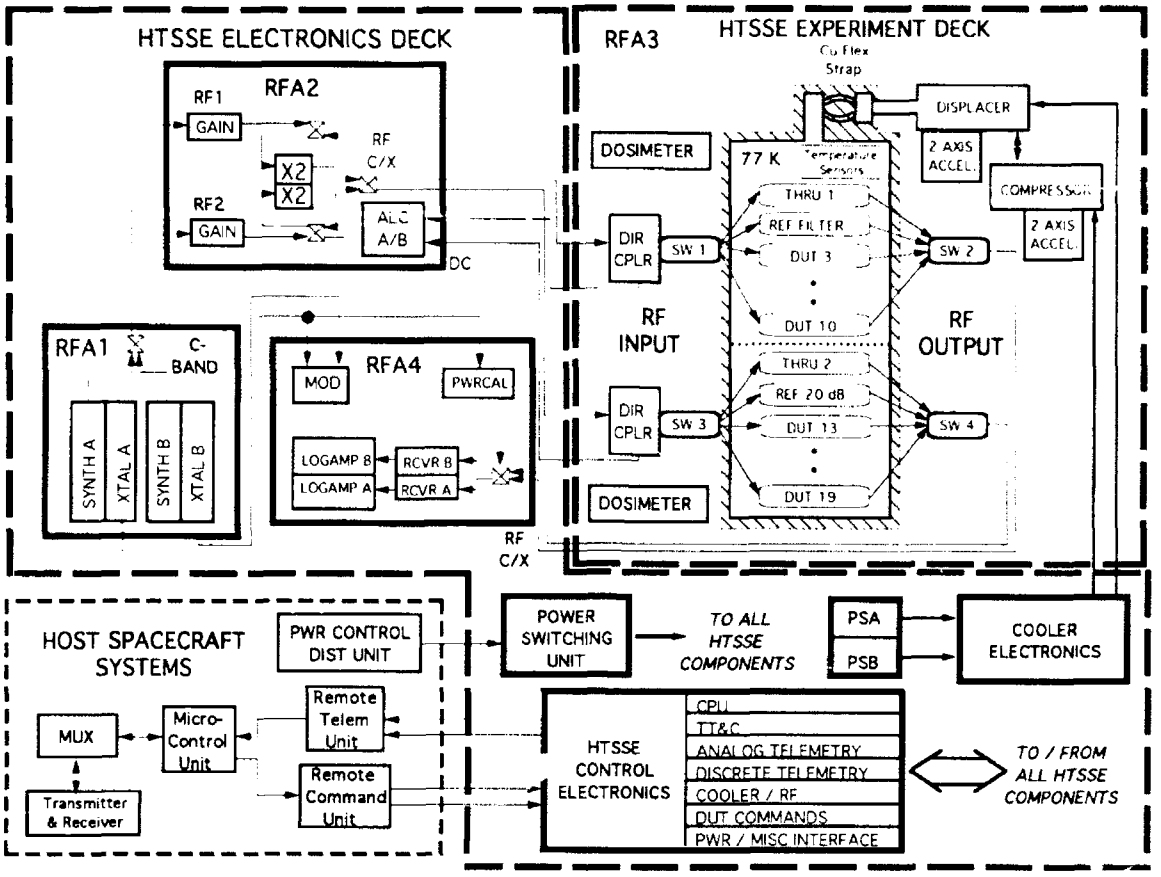

Fig. 11 — HTSSE-I detailed functional block diagram

Cryogenic Cold Bus Package and Cryocooler: The HTS and reference devices are located on a cylindrical cryogenic cold bus. This bus is structurally secured by six, low-thermal conductivity, glass-fiber epoxy composite tension straps. The cold bus is radiatively isolated from the surrounding ambient spacecraft temperature by a 40-layer double-aluminized Mylar blanket with the layers separated by silk mesh. Thirty-eight coaxial cables provide RF transmission between the HTS devices on the cryogenic bus and ambient RF distribution switches. Low thermal loss 21-mil (0.053 mm) outside diameter stainless steel coaxial cable is used. Each cable has an estimated thermal loss of 2 to 3 mW. The cryopackage has a total measured thermal loss of about 400 mW in the warmest estimated environment on orbit. The cryocooling is supplied by a mechanical, split-Stirling-cycle cryocooler developed by the Oxford University and built by British Aerospace. The cryocooler is conductively linked to the cryogenic bus by a flexible copper strap. The maximum cooling capacity of the cryocooler is approximately 650 mW at 75 K, which is required to maintain the cold bus at 77 K.

Microwave Measurement Subsystem: The microwave measurement subsystem functions as a scalar network analyzer (SNA) that measures insertion loss (decibel of magnitude of S_{21}) of a device under test (DUT). The system delivers over 50 dB of normalized dynamic range across C-band or X-band for each device. A C-band continuous-wave test signal is generated in RFA1 by a digitally controlled frequency synthesizer spanning 4.25 GHz to 5.25 GHz in 5 KHz increments. The synthesizer is phase-locked to an internal lowdrift 10 MHz crystal reference. The C-band signal is then gained controlled, amplified, and refiltered in RFA2. A frequency doubler circuit is activated in RFA2 when X-band testing is selected. Directional detector assemblies are used to control incident

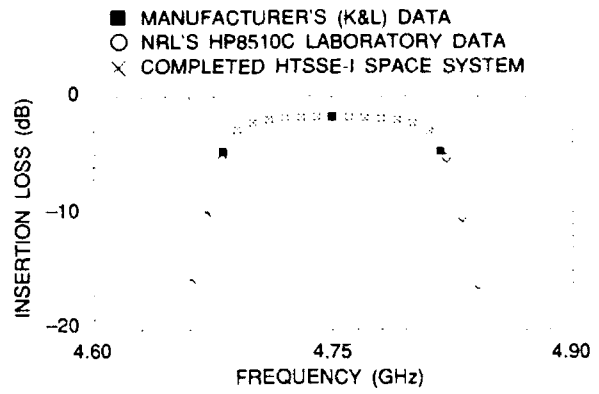

Fig. 12(a) — Overlay of normal-metal reference filter insertion loss data illustrates measurement consistency among test equipment, and it verifies HTSSE-I space hardware system accuracy at 20-26° C (cryogenic performance is comparable)

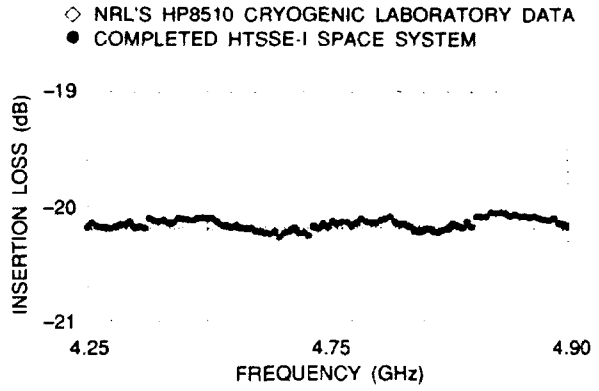

Fig. 12(b) — Overlay of 20 dB reference attenuator (at 77 K) insertion loss data demonstrates high system accuracy of HTSSE-I space hardware

power at each device to 0 dBm. Two THRU paths are used for frequency response normalization. A normal-metal band-pass filter and 20 dB attenuator are used for room temperature system verification. Figure 12 shows the system performance. The microwave measurement system has amplitude precision to better than 0.1 dB and accuracy on the order of ± 0.15 dB.

Control Electronics: The HTSSE-I digital subsystem performs command and control signal processing and data collection for all HTSSE-I subsystems. This subsystem consists of HTSSE-I Control Electronics (HCE), Power Switching Unit (PSU), and all wiring harnesses. The PSU contains 28 V relay power distribution circuits. The HCE contains payload command and telemetry circuitry. The HCE collects and processes all analog and digital telemetry and science data from all payload subsystems by using a dedicated microcontroller. Ground station operators send commands to the HCE via the host satellite's Command Receiver and Remote Command Unit (RCU). All HTSSE-I telemetry data is formatted into three channels of 16-bit serial words, which are relayed to the ground station through host satellite's Remote Telemetry Unit (RTU) and Telemetry Transmitter.

On Orbit Operations: Design planning for HTSSE-I anticipates a minimum operation of six months on orbit. Detailed baseline performance characterization curves for each DUT will be taken and downlinked. This data will be compared with the data taken during the prelaunch payload integration phase to determine if any DUT changed during launch. Each DUT will then be routinely tested once each week and its performance data downlinked. Comparison of the data from week to week will provide indications of any degradation in the performance of the individual DUTs.

Acknowledgments: Sponsorship and funding for HTSSE are provided by the U.S. Navy's Space and Naval Warfare Systems Command (SPAWAR). The authors give thanks to Tom Kawecki, Bill Mevers, Mark Johnson, and Marty Nisenoff for their effort in providing material for this paper. Special appreciation is also given to the managers, engineers, and technicians whose dedicated support throughout the project produced the results reported in this paper.

[Sponsored by SPAWAR] ■

Energetic Particles, Plasmas, and Beams

Beyond the Horizon Radar Technique

E.E. Maine, Jr.
Radar Division

In many situations involving radar, the utility of the sensor is limited by the line-of-sight constraints imposed by nature. If we can overcome these constraints to a degree, then the effectiveness of the sensor can be improved. Just as aerial reconnaissance was used to improve the optical field of view to more efficiently collect troop movement information, radar from an airborne platform enjoys a greatly enhanced field of view. This technique is used to advantage in border surveillance by carrying entire radar systems to high altitudes aboard tethered aerostats. The disadvantage of such an approach is that the aerostats must be very large to provide the necessary payload capacity. This article describes an approach to achieving performance increases from a surface-based radar without dramatically altering the nature of the radar system by merely adapting the aerostat approach to the radar antenna. The radar electronics remains on the Earth's surface, significantly reducing the weight requirements, and thus the size of the lifting device.

The Concept: This concept was devised approximately three years ago. Figure 1 depicts its possible use in the naval environment. An RF mirror carried by an aerostat or other lifting devices is used to redirect the radar energy from a surface-based antenna. The radar energy is directed to the mirror by a parabolic antenna. The mirror is secured to a gimballed mount driven by a control system such that the redirected beam illuminates the radar horizon. The mirror is flown at an altitude of approximately 150 m, giving the radar antenna an effective height equal to the mirror altitude. Since the distance to the radar horizon increases as the antenna altitude increases, the horizon is extended.

Hardware: In the last three years, NRL built and tested a developmental version of the concept. The mechanical and electromechanical design was performed by the Radar Division Mechanical Engineering Staff with fabrication by the NRL Engineering Services Division. Radar Division personnel also designed and fabricated the microprocessor-based control system. The control system is driven from a personal computer on the ground and a microprocessor-based system aboard the aerostat. The ground system defines the spot on the horizon to which the radar beam is directed at any given moment, calculates the angles of the mirror positioning system necessary to achieve that pointing, and communicates that information to the microprocessor-based system on the aerostat via a fiber-optic transmission line. The system aboard the aerostat reads reference gyroscopes for orientation information, passes that information to the ground system, reads the current position of the mirror, and drives the mirror until the required position is reached.

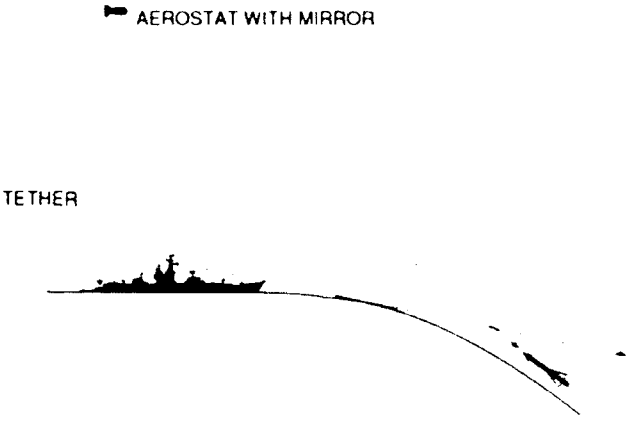

Fig. 1 — The concept shows the line-of-sight difference between a surface-based and an airborne antenna to detect objects beyond the radar horizon

Experiment: The coupling to the radar system in this exercise consisted of data exchange to first enable the mirror control computer to be able to read the azimuth and elevation positions of the radar antenna as it tracked the aerostat, and second to provide azimuth position registration to the radar for the display. Other than the tracking of the aerostat with the antenna mount, the radar system was operated in a normal mode. If the concept were being applied to a system that lacked a circular antenna of the appropriate size, an auxiliary antenna would be used to illuminate the mirror.

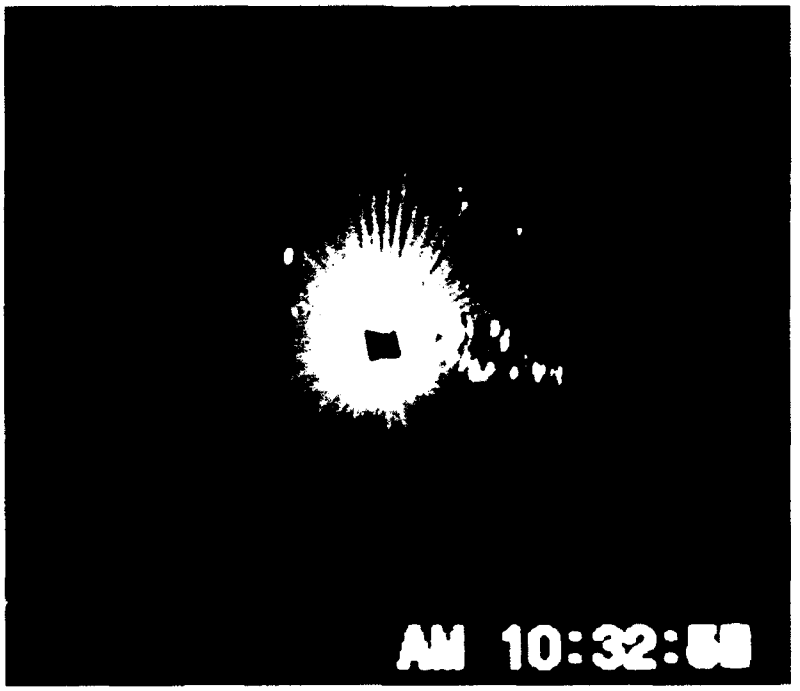

Fig. 2 -- A photograph of the radar display centered at CBD using the normal antenna. The antenna has obstacles in most directions, severely limiting the field of view.

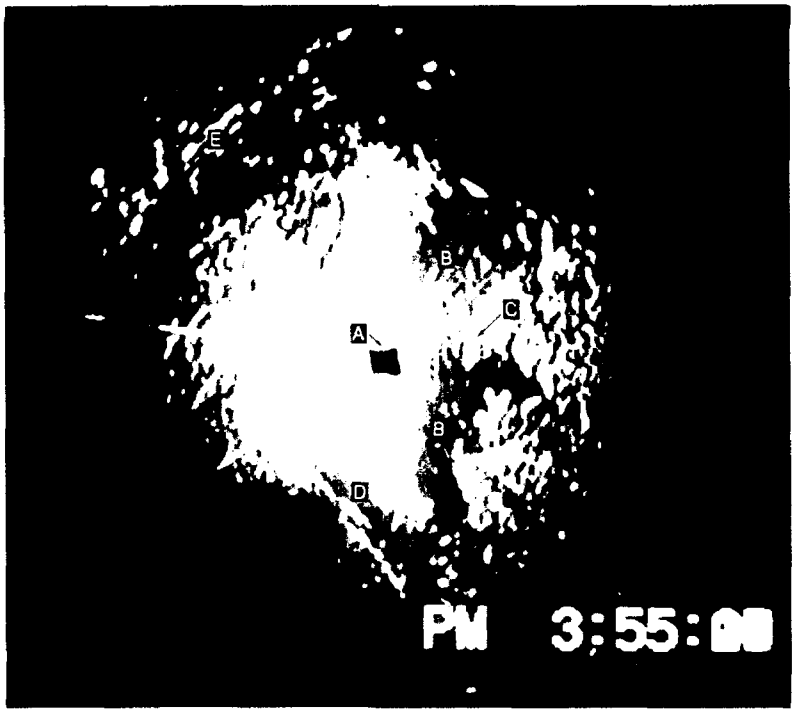

Fig. 3 A photograph of the radar display centered at CBD (A) using the extended antenna. The maximum range extent on the display is 40 nmi. Prominent features of the surrounding terrain such as the Chesapeake Bay (B), Tilghman Island (C), and the Patuxent River (D) are clearly identifiable. The returns in the upper left of the display (E) are from the Washington Baltimore corridor.

Results: The mirror antenna was initially tested aboard an aerostat during May 1992 at NRL's Chesapeake Bay Detachment (CBD). Figure 2 is a photograph of the radar display taken while the radar was operating with the normal antenna. Figure 3 is the same display while using the mirror to extend the radar horizon. The difference is most dramatic in this case since the radar was located primarily for ease in operating with the aerostat and had a clear line of sight to only a small sector of the surrounding terrain. This was accomplished with an airborne payload of only 178 pounds. A more extensive test is planned for 1993.

[Sponsored by ONT] ■

Polarimetric Radar Studies of Laboratory Sea Spikes

M.A. Sletten and D.B. Trizna
Radar Division

J. Wu
University of Delaware

"Sea spikes" is the name given to the large, transient radar echoes often seen by radar operators observing the ocean surface at near grazing incident angles. These targetlike echoes are a phenomena which, until recently, have managed to evade proper analysis due in part to a lack of suitable instrumentation with which to investigate them scientifically. Conventional radars that can track small targets in space and time are prohibitively expensive. Recently, an inexpensive, ultra-wideband, polarimetric radar based on a time-domain reflectometer (TDR) has been developed that is ideally suited to this task. This instrumentation radar can track the polarimetric properties of small-scale water features in space and time and, thereby, can provide a unique means of inferring the temporal evolution of the deterministic scattering features responsible for sea spikes. Results of laboratory experiments using this instrument are provocative and indicate that two scattering mechanisms may be involved.

System Description: Figure 4 shows a block diagram of the system and its associated signal processing. The system is a polarimetric extension of a radar used in earlier wave tank experiments [1]. The fast rise-time TDR voltage step is passed through a microwave amplifier to generate short (5-10 cm) X-band (3-4 cm wavelength) microwave pulses. Using PIN diode switches, the pulses are switched between the vertical (V) and horizontal (H) inputs of a dual-polarized, wideband antenna. A similar antenna/switch/amplifier chain is used in the receive channel to allow the collection of the four RF waveforms received when the system cycles through the four possible antenna polarization combinations (referred to as VV, HH, VH, and HV). Four milliseconds are required to collect each waveform, resulting in a 16 ms update rate. The system is polarimetric in that the magnitude and phase relationships between the four waveforms are detected. The polarization scattering matrix for the target as a function of frequency can then be obtained by calibrating the fast Fourier transforms (FFTs) of the sampled waveforms. This calibration includes an adjustment of the phase of the FFTs to remove any distortion introduced by target motion.

Experimental Results: Results of recent experiments using this system provide new insights regarding the sea spike scattering process. Experiments designed to investigate the polarimetric properties of sea spikes generated by small breaking waves were performed at the University of Delaware wave tank facility. Figure 5 illustrates the dramatic RF bandwidth difference observed in the VV and HH echoes received from the same wave system. The figure inset shows the corresponding VV and HH time-sampled waveforms. The narrow VV bandwidth corresponds to a relatively broad waveform, while the wideband HH signal is much more localized in space, indicating that different scattering mechanisms may be at work. Further evidence that distinct mechanisms may dominate the two polarizations is found in the time history of the phase difference between the VV and HH echoes. This phase difference often progresses in a regular manner, suggesting that the dominant VV and HH scatterers are

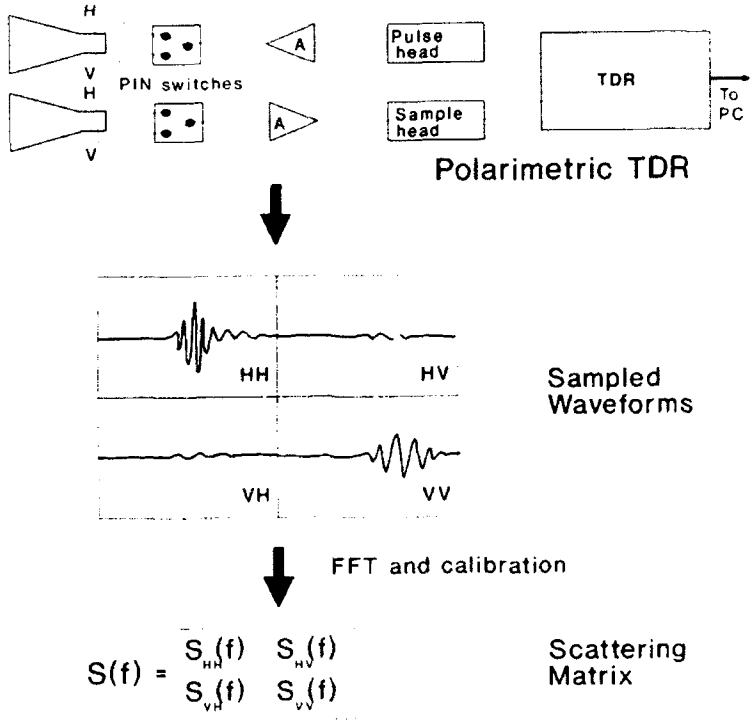

Fig. 4 — Schematic diagram of the polarimetric TDR radar and its associated signal processing

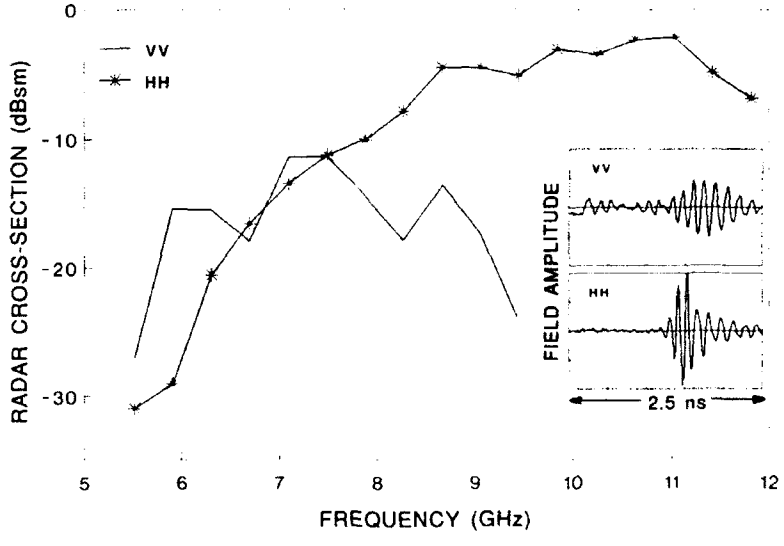

Fig. 5 — VV and HH radar cross sections vs RF frequency for a small breaking wave generated in a wave tank. Measured waveforms shown in the inset.

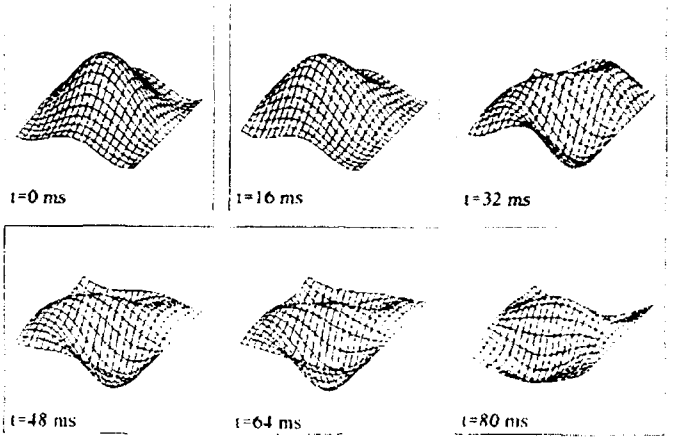

Fig. 6 — Co-pol response at 7 GHz of a wave tank sea spike at 16 ms intervals

distinct and moving at different velocities. Figure 6 illustrates the polarimetric properties of a particular sea spike by using "polarization response" surfaces [2]. This figure shows the response as a function of time, where the steady progression of the phase difference from 0 to 180° manifests itself as a twist in the polarization response curves relative to the symmetric form assumed when the difference is 180°, seen here in the 80 ms frame.

The ability of the TDR system to track the ultra-wideband, polarimetric properties of small-scale features on the water surface makes it an ideal tool in the study of scattering mechanisms found over the ocean surface. Further analysis and experimentation should clarify the number and type of scattering mechanisms involved.

[Sponsored by ONR]

References

1. D.B. Trizna, J.P. Hansen, P. Hwang, and J. Wu, "Laboratory Studies of Radar Sea Spikes at Low Grazing Angles," *J. Geophys. Res.* **96**(C7) (1991).

2. J.J. van Zyl, H.A. Zebker, and C. Elachi, "Imaging Radar Polarization Signatures: Theory and Observation," *Radio Sci.* **22**(4) (1987). ■

A Plasma Mirror for Microwaves

A.E. Robson, W.A. Manheimer, and R.A. Meger
Plasma Physics Division

Radars that use metal antennas are limited in the speed with which they can be redirected because of the inertia of the reflectors. While this is not a serious disadvantage for many applications, such as the rotating surveillance radars that are a familiar feature of ships and airports, there are military applications that require more rapid redirection (*agility*) than is possible with movable metal reflectors. For these purposes, electronically steered phased-array antennas have been developed, the most celebrated example of which is the *Aegis* system. Although undeniably effective, phased-array antennas are complicated and costly because of the large number of elements involved, and there are problems in applying this concept to high-frequency radars. We are investigating the possibility that extremely agile plasma mirrors could be used to steer a beam of high-frequency microwaves, thus combining the simplicity of a mechanically directed radar with the electronic steering capability of a phased array.

Plasma Mirrors: An ionized gas (*plasma*) reflects electromagnetic radiation whose frequency n is less than a characteristic frequency

(the *plasma frequency*) $n_p : 10^4\ n_e^{1/2}$ where n_e is the plasma electron density. Thus 10 GHz (X-band) microwaves can be reflected by a density of about 10^{12} electrons per centimeter, which is easily produced by passing a few amperes of current through a low-pressure gas. When the current stops flowing, the plasma density decreases rapidly as the electrons and ions recombine. A plasma mirror could thus be formed in one orientation, extinguished by recombination, and then reformed in another orientation. This would allow a radar to be redirected on a timescale determined by the time that it takes for the plasma to be created and to decay.

Demonstration: To demonstrate the principle, we have produced a plane sheet of partially-ionized plasma, about 15 cm square and 1 cm thick, by means of a pulsed, hollow-cathode glow discharge in air at a pressure of 150 mTorr. The cross section of the sheet is defined by the dimensions of the cathode, and the plasma is confined by an axial magnetic field of 150 gauss. Ten GHz microwaves from a low-power source were directed at 45° to the sheet, and the transmitted and reflected signals were detected by appropriately placed horns (Fig. 7). When the discharge was excited with an 80-ms, 6-Å pulse of current, the transmitted signal was cut off and a reflected signal appeared (Fig. 8). From the rise and fall of these signals we infer that the plasma mirror was created in about 20 ms and extinguished on the same timescale. This suggests that it could form the basis of an extremely agile radar system. By rotating the cathode we could measure the reflected power as a function of angle (Fig. 9). The circles were obtained by reflection from the plasma mirror, and the points connected by the solid line were obtained by reflection from an equivalent metal plate. The close correspondence out to the 5 dB point shows that the plasma mirror is as effective as a metal mirror in reflecting microwaves.

In a practical radar, the repositioning of the plasma sheet would be accomplished electronically (for example, by energizing a selected linear array of emitting points in a two dimensional matrix cathode, and/or by changing the direction of the magnetic field). Furthermore, mirrors of different shapes could be formed by shaping the cathode and the magnetic field.

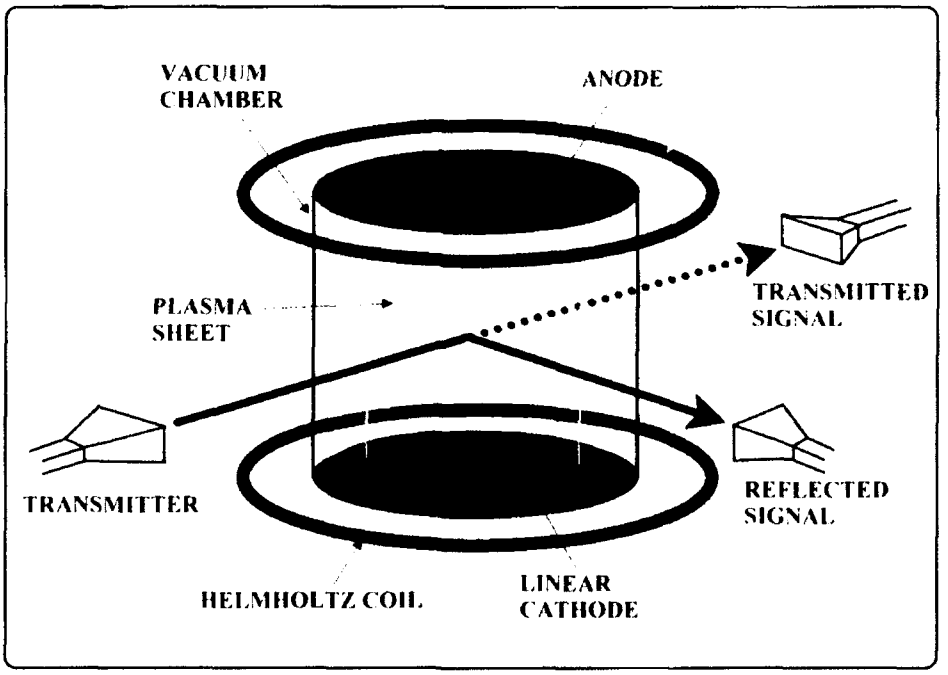

Fig. 7 — Layout of plasma mirror experiment

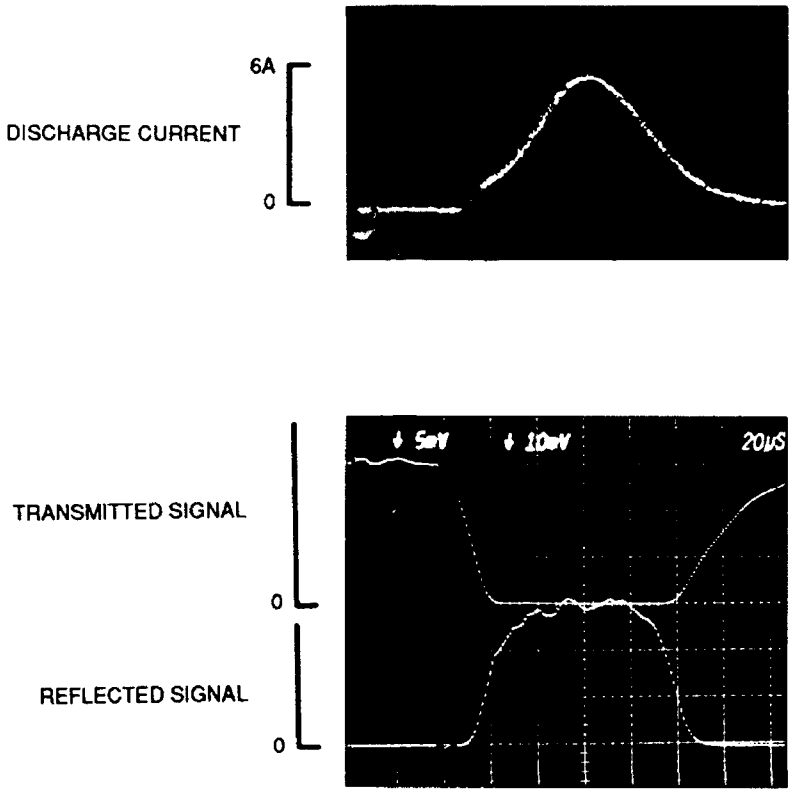

Fig. 8 — Plasma current pulse and transmitted and reflected microwave signals

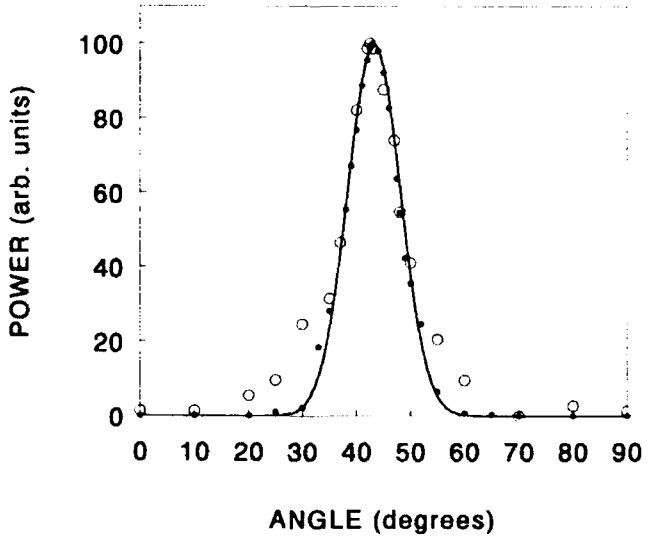

Fig. 9 — Signal into fixed horn as reflecting sheet is rotated. Hollow circles: plasma mirror; points and solid line: metal reflector.

Finally, by increasing the density of the plasma, agile mirrors could be used at millimeter wavelengths.

[Sponsored by ONR]

References

1. W.A. Manheimer, "Plasma Reflectors for Electronic Beam Steering in Radar Systems," *IEEE Trans. Plasma Sci.* **PS19**, 1228-1234 (1991).

2. A.E. Robson, R.L. Morgan, and R.A. Meger, "Demonstration of a Plasma Mirror for Microwaves," to appear, *IEEE Trans. Plasma Sci.* **PS21**(6) (Dec. 1992). ■

Satellite Laser Ranging for Platform Position Determination and Ephemeris Verification

G.C. Gilbreath, J.E. Pirrozoli, T.W. Murphy, W.L. Lippincott, and W.C. Collins
Space Systems Development Department

This year, NRL's first satellite laser ranging (SLR) capability was established by the Naval Center for Space Technology for spaceborne platform position verification, ephemeris validation, and other applications. The direct detection system was designed, integrated, and operated by NRL. The system is installed at the Air Force Optical Tracking Facility in Malabar, Florida. The NRL system in combination with the bistatic optical acquisition and tracking capability proffered by the Air Force facility comprise joint services effort with unique capability [1].

Direct Detection Laser Ranging: In a direct detection system, a time-tagged start pulse is directed toward the target. The return pulse is also time-tagged and the difference between the two is used to compute the position in radial range. The result is corrected for atmospheric distortion and other losses. The key to accuracy obtained by using this method is the Laser Ranging Cross Section (LRCS) of the target. Some satellites are equipped with optical retroreflectors that can enhance the return by making it more robust against system and environmental losses, and thereby enabling more accurate radial range estimation. The basic components of the NRL system are: laser transmitter, receiver subsystem, optics, and tracking and acquisition telescopes.

Transmitter: The optical transmitter in the system is a doubled Nd-YAG laser that radiates at 532 nm at 300 mJ per pulse into a 250 ps pulsewidth at 10 Hz. These parameters translate into an output of 1.2 GW per pulse. The beam is directed through, and the divergence is varied by computer control from 140 μrad to 70 μrad. This feature is useful for initial platform acquisition when the largest divergence is used and for increasing the amount of intensity, or power per unit area, on the target when a specific satellite is acquired. The laser is almost twice as powerful as most satellite laser ranging optical transmitters operational today.

Receiver: The receiver subsystem is composed of a photomultiplier tube (PMT) with gain enhanced by a micro-channel plate. Gains on the order of 10^6 at room temperature are readily achievable with this device. In addition, constant fraction discriminators are used to correct nonlinearities in the return pulse. Wideband amplifiers and a time gate on the PMT are configured to increase the signal-to-noise. A 4 GHz wideband oscilloscope is configured into the system, which will enable determination of point-of-reflection from targets that do not have optical retroreflectors on board to provide enhanced returns. This wideband oscilloscope is an important attribute in the system as it will enable more accurate range-finding of targets with small LRCSs.

Tracking and Acquisition: A unique feature of the NRL system is the bistatic acquisition mode proffered by the telescope site and the self-tracking done from the ranging telescope, once the target is acquired. Specifically, the target is optically acquired with a 48" telescope when it is sunlit, however the tracking

station is in the dark. Once acquired, a smaller 24″ telescope is trained on the satellite and the laser transmits along the optic axis of this smaller telescope. The return pulse is intercepted along the same path, making the SLR system monostatic. Optics are configured in the receiver optical bench to enable tracking of the 24″ telescope by using the return pulses. Consequently, antenna pointing accuracy can be improved considerably by increasing probability of intercept, thus probability of signal returns. This feature is very important when tracking and lasing on unenhanced satellites, when the system is operating in a photon-counting mode. Figure 10 illustrates the bistatic acquisition system using the monostatic NRL SLR configuration. The Air Force optical tracking facility site at Malabar is shown in Fig. 11.

Results: The increased power, wideband signal processing capability, bistatic optical acquisition, and self-tracking off the return signal once a platform is acquired, combine to make the NRL SLR system unique. These advantages combine to enable identification of points-of-reflection from unenhanced targets, thereby, potentially locating such platforms to within meters rather than kilometers.

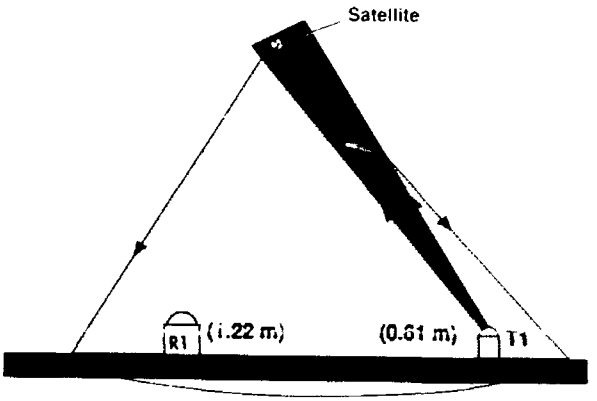

Fig. 10 – Diagram of bistatic acquisition of satellite with monostatic laser transmit and receive by slaved telescope, T1

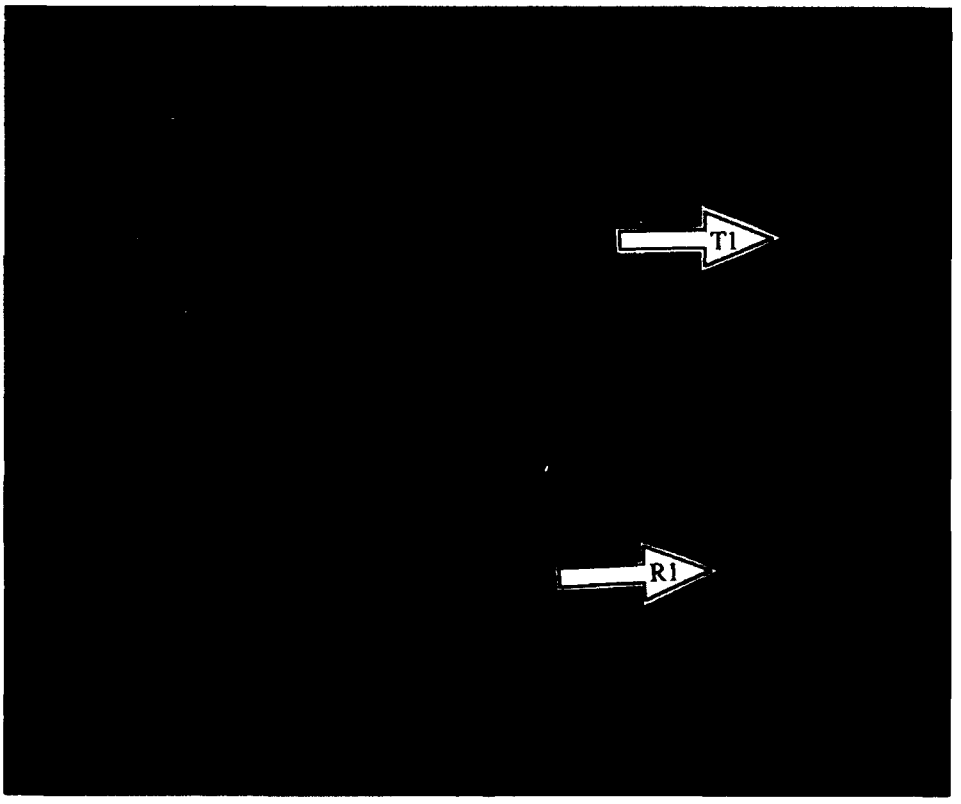

Fig. 11 – Site view of the Air Force Optical Tracking Facility at Malabar, Florida, where the NRL Satellite Laser Ranging capability acquisition and tracking is achieved by using the 48″ telescope, R1, and SLR transmit/receive is done by using the 24″ telescope, T1.

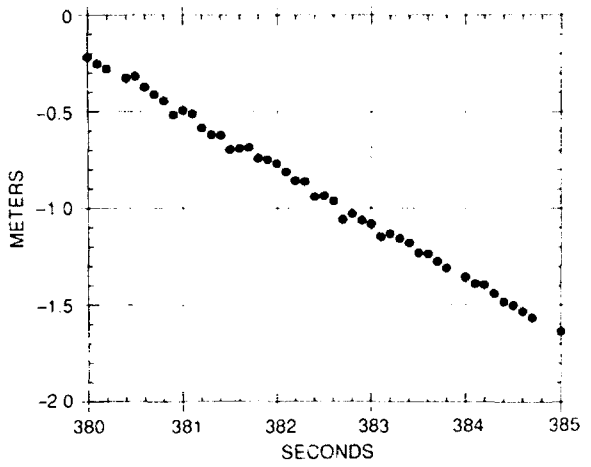

Fig. 12 — NRL satellite laser ranging returns from NASA satellite, LAGEOS. Slope is caused by the offset between observed and predicted values.

The system was calibrated against LAGEOS, a satellite consisting of many optical retroreflectors that orbits at ~6000 km. The satellite's radial range uncorrected for atmospheric effects was determined to within 8 mm rms by the system. Figure 12 shows a graph illustrating these data. The slope is caused by a shift between the predicted range and the observed value.

In addition, the system demonstrated viability in the photon counting regime. Photon returns were achieved from an unenhanced target at ~1700 km using the system, enabling uncorrected radial range estimates of the position of the satellite to be estimated within meters.

Potential applications in LIDAR also exist for the system. Photon returns off reflections from clouds at varying heights were examined as a preliminary investigation to rocket plume illumination.

Acknowledgment: The authors would like to acknowledge Stefanie Peterson for her dedication and effort in the development of the data acquisition and control software for the system.

Reference

1. G.C. Gilbreath and H. Newby, "Ground-Based Laser Ranging for Satellite Location," *8th Int'l. Proc. on Laser Ranging Instrumentation* (May 1992). ■

Information Technology and Communication

Tripod Operators for Efficient Object Recognition

F.J. Pipitone
Information Technology Division

Progress in the development of advanced robotic systems has been limited by the difficulty of providing them with adequate perception of their surroundings. In particular, the rapid recognition of previously seen objects based on their surface shape is required in such applications as automatic target recognition, robot navigation, automatic assembly and inspection, and object retrieval. This problem has been studied using numerous approaches. Early approaches used intensity images exclusively, but the difficulty of inferring surface shape from the intertwined effects of illumination, surface pigmentation, and surface shape has led increasingly to the use of range images. A range image is a 2-D array of depth measurements of a scene; essentially a dense sampling of points in 3-D space that lie on visible surfaces. They are obtained from *rangefinders*, instruments based either on time-of-flight (e.g., LIDAR) or triangulation (e.g., stereo). This article describes a mathematical construct that greatly facilitates the recognition and location of objects in a range image.

Tripod Operators: The tripod operator is a class of feature extraction operators for range images [1]. It consists of three points in 3-D space fixed at the vertices of an equilateral triangle and a procedure for placing several curves, called probe curves, in the coordinate system of the triangle. The arc lengths along these curves at which intersection with the surface occurs are regarded as a feature vector. This vector is completely invariant under rigid motions. That is, it depends on where the three tripod points are placed on the surface of an object, but not on the location of the object with respect to the rangefinder. A tripod operator can be regarded as a way to select N point samples of a surface, producing a feature vector with $N-3$ components. This vector contains all the shape information in the N points, since one can use it to reconstruct their relative positions, but it contains no other information. Figure 1 shows a particular kind of order 3 tripod operator (6 points) on a synthetic object. The rangefinder is at the purple spot. The tripod points lie at the vertices of the purple triangle. The outer three points swing along circular probe curves described by swinging the outer three triangles about the purple "hinges" to form feature measurements, which are proportional to hinge angles.

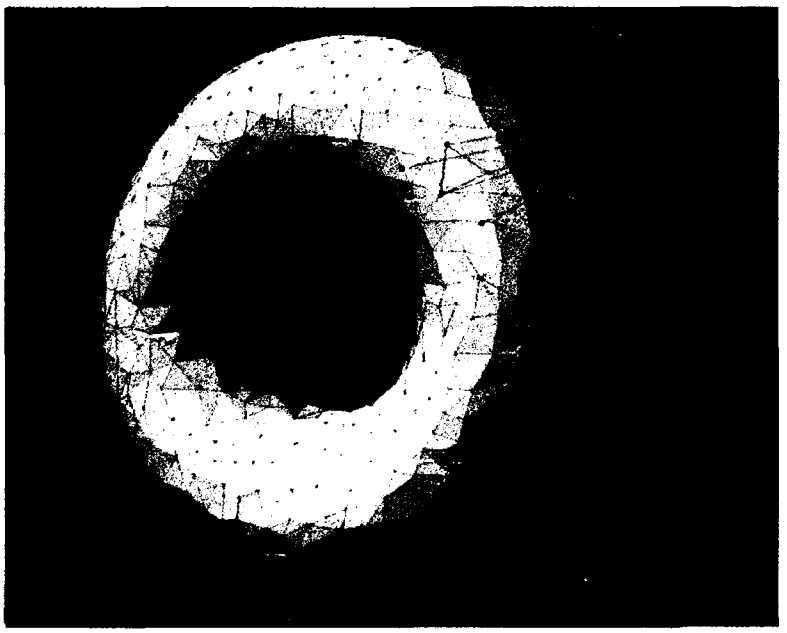

Fig. 1 — A synthetic object (triangle-tiled torus) showing a single placement of an order 3 tripod operator

Processing Objects: To enable rapid recognition, each object of interest is processed prior to recognition by placing tripod operators at many random locations on several range images of the object. The resulting feature vectors are then stored in such a way that they can be quickly indexed by their values. The *pose* of the object (a 6-vector) with respect to the tripod may be stored along with its name. Since the tripod can be moved on a surface in only three degrees of freedom and each tripod placement yields a single feature vector, only a 3-D manifold of points in feature space is generated, at most, for an object. In practice, a few thousand placements often yields a dense sampling of feature space for one object.

Recognition: When a new range image is presented for recognition, tripod operators are placed at a number of random locations. For each placement, the prestored data immediately provides hypotheses in the form of the names of objects that have similar prestored feature vectors and (optionally) their poses with respect to the tripod. Multiple operator placements can be treated statistically to provide estimated probabilities of hypotheses. Pose information can be ignored, or used to further disambiguate recognition, since only hypotheses agreeing on where an object is can be accepted.

Experiments have shown that tripod operators of low order (e.g., 4-D feature space, 7 points) allow very fast and accurate recognition, even with considerable image noise, for a wide variety of surface shapes, in the case of isolated objects. Work is underway to use pose information to interpret cluttered scenes.

[Sponsored by ONR and ONT]

Reference

1. F. Pipitone and W. Adams, "Tripod Operators for Recognizing Objects in Range Images: Rapid Rejection of Library Objects," *Proc. IEEE International Conf. on Robotics and Automation*, Nice, France, May 1992, pp. 1596-1601. ■

Direct Manipulation in the Modern Cockpit: A "Workstation" with Multiple, Concurrent Tasks

J.A. Ballas, C.L. Heitmeyer, and M.A. Pérez
Information Technology Division

The rapid evolution of user interfaces is occurring not only in office systems but also in modern cockpits, which are computer-based and include advanced graphical displays [1]. Many office applications use direct manipulation interfaces (e.g., Motif, Openlook, Macintosh, and Windows), which are easy to learn and can reduce user errors. A question of interest is whether a direct manipulation interface would be effective in mission-critical applications, such as aircraft cockpits [2]. Fundamental differences between office applications and modern cockpits may limit the use of direct manipulation in the cockpit. One critical difference is that modern cockpits often include sophisticated automation, such as the ability to fly on automatic pilot. The automation is sometimes intermittent, moving the pilot in and out of tasks. We were specifically interested in whether direct manipulation could smooth the transition from automated to manual mode.

Approach: To address this issue, we investigated a theory formulated by Hutchins, Hollan, and Norman that proposes two factors—low distance and direct engagement—to account for the advantages of direct manipulation interfaces [3]. According to Hutchins et al., the first factor is the "information processing distance between the user's intentions and the facilities provided by the machine." The key to the second factor is interreferential I/O, which permits "an input expression to incorporate or make use of a previous output expression." Although other researchers have investigated direct manipulation, none has determined the importance of each factor for user performance.

Our hypothesis was that a direct manipulation interface would smooth the transition from automated to manual mode and thus reduce the initial deficit in performance that occurs when a

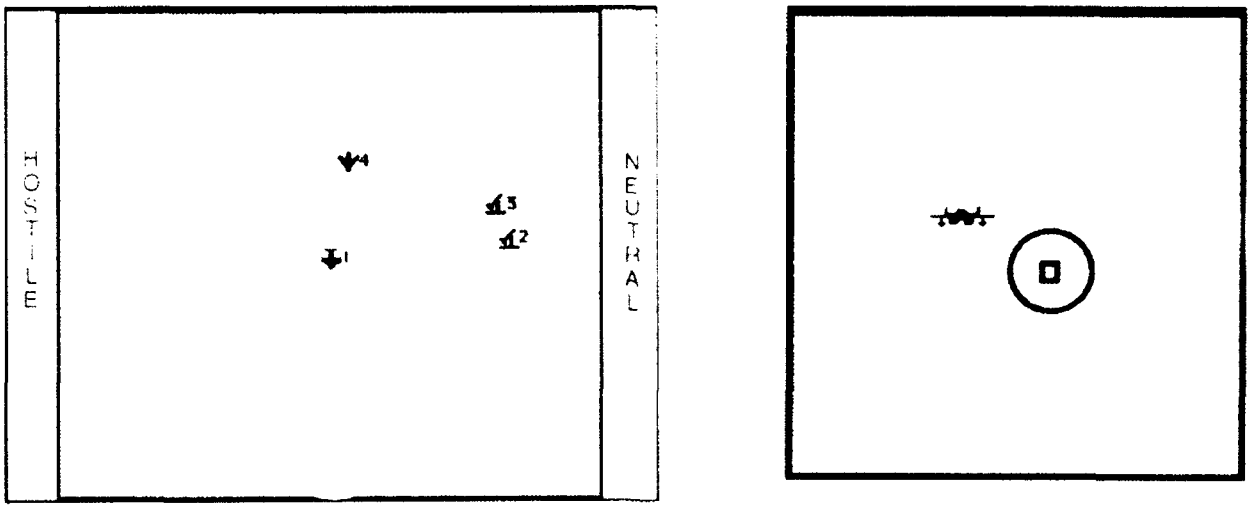

Tactical assessment

Display: graphical / tabular
Input: touchscreen / keypad
User involvement: intermittent

Tracking

Difficulty: two levels
Input: joystick
User Involvement: continuous

Automation Logic

Tracking task difficulty: L = low; H = high	L	H	L	H	L	H	L	...
Tactical Mode: M = manual; A = automatic	M	A	M	A	M	A	M	...

Fig. 2 — Details of the two tasks simulated in the experiment

person resumes a task. We tested this hypothesis by designing interfaces and testing them in an experiment in which two pilot tasks were simulated: a tactical assessment task and a pursuit tracking task (Fig. 2). Tactical assessment, a critical task in a combat aircraft, has become more challenging with the capabilities of modern aircraft. Subjects had two types of tactical decisions: a confirm decision that acknowledges the target classification recommended by the computer system, or a classification decision whereby the subject assigns a classification to the target based upon its behavior.

Tactical Interfaces: We designed and built four tactical interfaces (Fig. 3) to represent and evaluate the two theoretical factors. The *direct manipulation interface* (Fig. 3(a)) has direct engagement and low semantic distance. This interface simulates a radar display with continuously moving symbols representing the targets. A touchscreen overlays the display. To confirm or classify a target, the subject picks a target symbol on the display and selects one of two strips, labeled HOSTILE and NEUTRAL, located on either side of the display. The *command language interface* (Fig. 3(d)) has indirect engagement and high semantic distance. The tactical assessment window is partitioned into a top portion, which displays a table of target names and attributes, and a bottom portion, which is for subject input and error feedback. Each entry in the table describes a single target, providing the target's name (an integer), the target's class, and continuously updated data about the target. The table is decluttered: i.e., it only presents the critical attribute for the given target class. The subject uses a keypad to invoke a confirm or classify operation. The third and the fourth interfaces (*tabular-touch screen and*

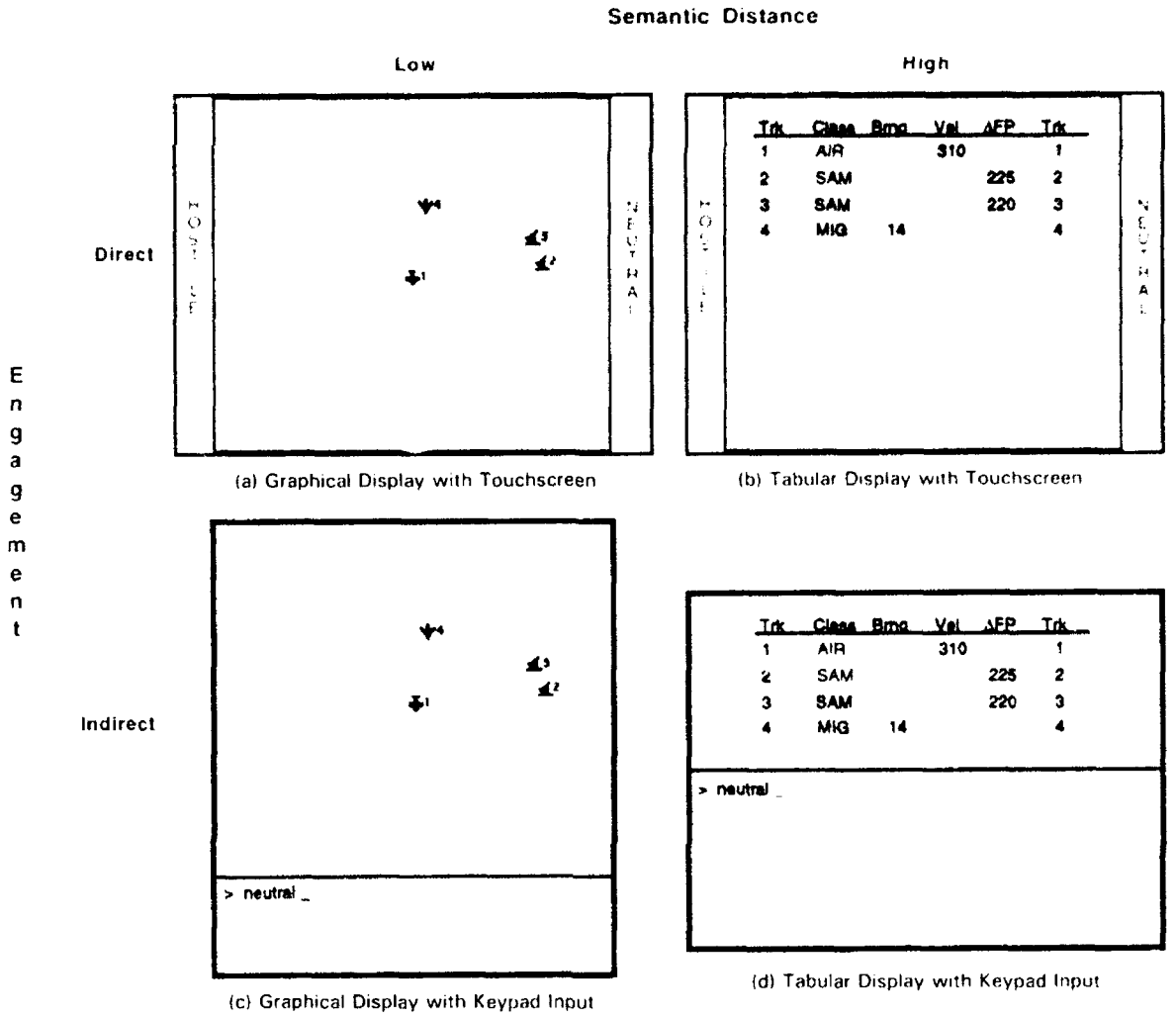

Fig. 3 — Four interfaces for the tactical assessment task, combining levels of semantic distance and engagement

graphical-keypad, Figs. 3(b) and 3(c)) are hybrid combinations of the two levels of semantic distance and engagement.

To establish a setting for intermittent automation, the difficulty of the tracking task was varied (Fig. 2). When the difficulty of the tracking task was low, the subject performed both the tracking task and the tactical assessment task. When the difficulty of tracking increased, the tactical assessment task was automated, and the subject performed only the tracking task. When the difficulty of tracking returned to a low level, the subject resumed the tactical assessment task. Our key measure of interface effectiveness was how well the subjects did when they resumed the tactical assessment task. An increase in response time on the first response after manual mode was resumed is an indicator of initial performance deficit.

Results: We assessed performance deficit by comparing user performance on the first and the seventh response and found that initial performance deficit was least with the direct manipulation interface. The deficit depends on how long a person has been out of the task. If a person has not performed tactical assessment for a short time (about 40 s), then performance suffers only with the command language interface (Fig. 4). When the tactical assessment task is automated and a person is out of the task for about 2 min., then performance deficit is

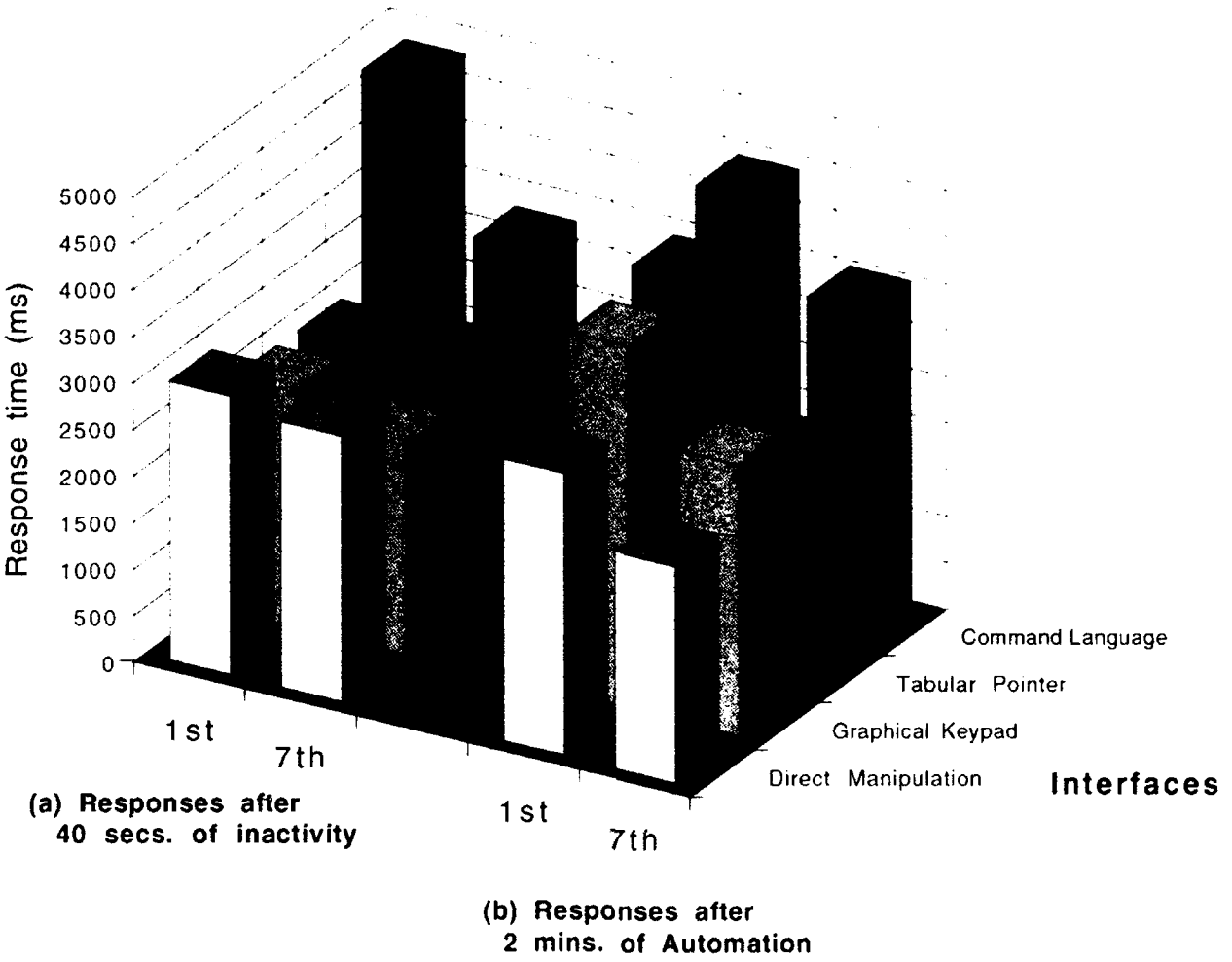

Fig. 4 — Interface effect on response time immediately following (i.e., the first response) a brief period of inactivity and following a period of automation, compared to response time later (i.e., the seventh response)

present in the two hybrid interfaces as well. Using the command language interface, performance had not improved by the seventh response.

However, the direct manipulation interface was not optimal in all situations. We hypothesized and found that in unaided classification decisions, automation deficit was greater with the tabular displays, i.e., command language and tabular-touchscreen. However, we found that in decisions confirming an algorithm's classification, the deficit was greater with the graphical displays, i.e., direct manipulation and graphical-keypad. In these decision, the user had to accept a classification by the system, and the tabular presentation of the recommendation supported quicker performance initially. An interesting intratask effect of engagement (keypad versus touchscreen) was found when the performance on the tracking task was examined. Those using the keypad for the tactical assessment task had better tracking in the initial phase of resuming the tactical assessment task than those using the touchscreen.

Conclusion: Our general conclusion is that increases in the cognitive complexity of an interface adversely affects the resumption of its use after a period of automation. Our results have implications for the theory of direct manipulation as well as for the design of interfaces in systems where users are performing two or more tasks concurrently. Although the predictions we made were generally supported, the theory has limitations. It does not address hybrid interfaces nor the special conditions when

direct manipulation may not be best. Further, the theory needs to be extended to address decision complexity and multiple levels of representation for different requirements. We found that semantic distance and direct engagement are difficult terms to define operationally and to evaluate. Although our results were found in a cockpit application, extension to other systems is appropriate, particularly systems in which the user is intermittently moving from one task to another.

[Sponsored by ONT and ONR]

References

1. E.L. Wiener, "Beyond the sterile cockpit," *Human Factor* **27**, 75-90 (1985).

2. J.A. Ballas, C.L. Heitmeyer, and M.A. Pérez, "Direct Manipulation and Intermittent Automation in Advanced Cockpits," Technical Report NRL/FR/5534-92-9375, July 21, 1992.

3. E. Hutchins, J.D. Hollan, and D.A. Norman, "Direct Manipulation Interfaces," in *User Centered System Design*, D.A. Norman and S.W. Draper, eds. (Erlbaum Associates, Hillsdale, NJ, 1986), pp. 87-124.

Risk Assessment and Directed Energy Weapons

A.I. Namenson and T.J. Wieting
Condensed Matter Radiation Sciences Division

N. Seeman
SFA, Inc.

Risk assessment refers to quantifying our confidence that an endeavor will succeed. We determine a probability of success from experimental data but because of measurement uncertainties, we must also associate a confidence ($< 100\%$) with our probability. For example, we might seek a 90% confidence that by using a directed energy weapon (DEW), there is at least a 99% chance of upsetting and defeating an attacking missile. There are generally so many unknowns (e.g., missile type and engagement geometry), it is surprising that data seem to follow a simple "lognormal" probability law.

Lognormal Distribution: When many random factors are multiplied together the lognormal distribution results. The logarithm of the product is normally distributed because it is the sum of many random logarithms. For example, the splitting of rocks so the size is divided many times by random ratios would result in particle sizes that are lognormally distributed [1]. An example of a more complex phenomenon (a recent study at the National Institutes of Health) is a lognormal distribution for the doses of enzymes required to break down peptide molecules [2]. This latter phenomenon resembles the problem in this article: What is the stress (dose, intensity or kinetic energy) required to upset a complex system?

Displaying Lognormal Data: Lognormal data are displayed on special graph paper as explained by the three plots in Fig. 5. Building on this explanation, Fig. 6 shows a sample lognormal plot of the populations of the 50 states

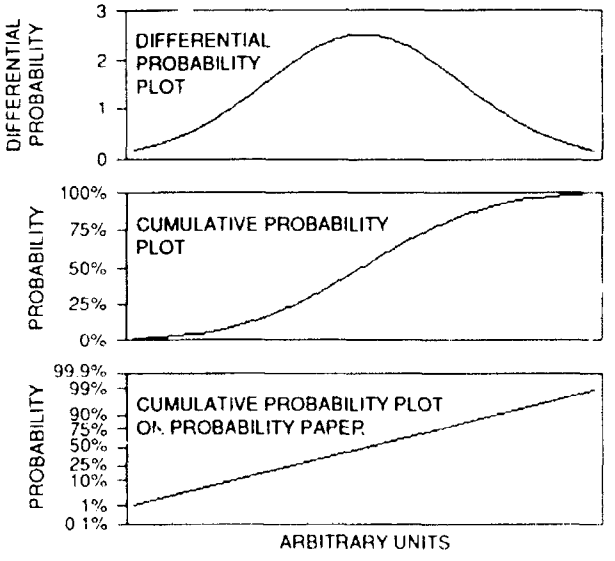

Fig. 5 – Lognormal probability paper. The x-axis in all three plots is a logarithm scale. The top curve is the bell shaped normal distribution, the middle curve is its integral, and the bottom curve is a remapping of the middle curve with the y-axis distorted to make the curve a straight line.

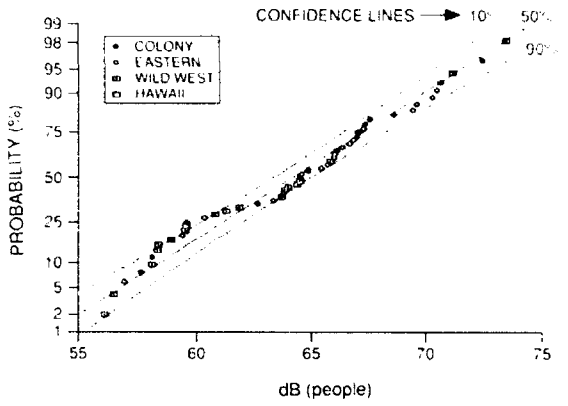

Fig. 6 — Lognormal plot of the United States, plus the District of Columbia. Populations are expressed in decibels (10 times the logarithm to base 10). Different symbols are used for states in different regions. No systematics appear.

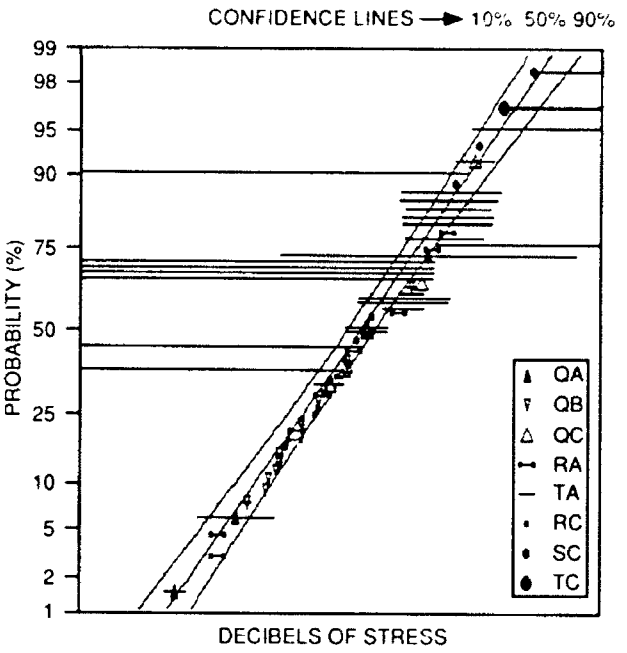

Fig. 7 — Stress-to-upset on lognormal paper. Each symbol indicates a different missile or change in method of stress that would make the missile appear as a different type. The lines indicate where the stress was bounded between two limits (a step-stress measurement). Lines extending all the way to the right indicate that no upper bound was determined. Lines extending all the way to the left indicate that no lower bound was determined.

of the United States, plus the District of Columbia. The states are ranked by population, with the least populous state (Alaska) as first and the most populous (California) as last (51st). A "probability" is then assigned to each state that equals its rank, divided by $N + 1$ where N is the sample size. Thus, for our sample size of 51, Alaska has a probability of 1/52, New York (the next most populous state), 50/52 and California, 51/52. The probabilities are plotted against logarithms of population, and if the data is lognormally distributed, the points will roughly follow a straight line. Our experience has been that the human eye is an adequate detector of discrepancies from the lognormal distribution. It is evident that U.S. state populations are distributed lognormally. The confidence lines on the graph (derived from rather complex mathematics) indicate the confidence and probability that some new state will have less than a given population. For example, Fig. 6 shows that the District of Columbia, the only proposed new state, would be a typical state. It is interesting that all readily available censuses of other populations exhibited the same lognormal property as the U.S. Indeed, the two censuses recorded for the tribes of Israel in the biblical Book of Numbers show this property. Our techniques were applied to these last two censuses not to assess risk but to check if the recorded data were reasonable. They are.

Measurements: NRL measurements of radiation stresses to upset for missiles are plotted on lognormal paper in Fig. 7. The exact nature of the stress is not relevant to the conclusions. The horizontal scale is in arbitrary units. The interesting fact is that the data fit a simple lognormal distribution. To corroborate this finding, we looked at studies done elsewhere on radiation stress to damage (as opposed to upset) on a wide range of systems and also saw lognormal behavior. Recently, a panel of national experts assembled at NRL and made theoretical estimates of stress to upset for missiles. The investigators had no thought at the time of whether any statistical rule would emerge concerning their predictions. However, their estimates produced textbook cases of lognormal distributions.

Although many in the research community find our results reasonable, there is no hard theory of why the lognormal distribution works

so well. The data are sufficiently in accord with a lognormal distribution that we can make statistical estimates of upset phenomena in missiles with up to 90% confidence and up to 95% probability. We continue to look for exceptions to our results. As in the case of populations, deliberate human intervention (e.g., hardening of systems to radiation stress) could distort the lognormal distribution. But knowing how missile systems normally behave, such distortions could be characterized and identified as a distinct class.

[Sponsored by SPAWAR and ONT]

References

1. J. Aichison and J.A.C. Brown, *The Lognormal Distribution* (Cambridge at the University Press, 1957), p. 5, Introduction and p. 100, Ch. 10.

2. S. Kozlowski, private communication. ■

Fig. 8 – Digital moving map display

The U.S. Navy's Compressed Aeronautical Chart Database

M.C. Lohrenz
Marine Geosciences Division

The implementation of digital moving map systems (DMS) aboard tactical naval aircraft has resulted in a dramatic shift from the use of paper charts to digital chart products for naval mission planning and navigation. A DMS computer stores all of the digital maps that are required for a particular mission and displays up-to-date threats, intelligence, or other information as pilot-selected overlays to the base chart. An effective DMS provides pilots with precise, hands-off route selection and navigation information (Fig. 8). The DMS that is currently used on AV-8B Harriers and F/A-18 Hornets was originally designed for night-attack air missions, since the system provides valuable positional information when visual flight navigation is limited. In direct support of these navigation and mission planning systems, the Naval Research Laboratory-Stennis Space Center (NRL-SSC) is developing the Compressed Aeronautical Chart (CAC) database [1].

CAC Overview: CAC is a global, seamless database of scanned aeronautical charts at six different scales (ranging from 1:50,000 to 1:2,000,000). CAC data are derived from the Defense Mapping Agency (DMA) ARC (equal Arc-second Raster Chart) Digitized Raster Graphics (ADRG) database, which is a collection of charts that have been scanned into red, green, and blue pixel components. NRL-SSC digitally compresses ADRG by 48:1 to generate CAC, which is mastered onto Compact Disk-Read Only Memory (CD-ROM). NRL-SSC has been processing CAC since April 1990, and DMA distributes CAC to the navigation community as a standard product. The following sections briefly describe the steps that are involved in processing ADRG into CAC, including a map projection transformation and two compression phases, and relevant research efforts.

Projection Transformation: CAC is stored as a seamless, global database such that the transition from one source chart to another is transparent to the pilot. The data are stored in discrete 50.8-mm (2 in.) square segments of source chart that cover the entire globe (Fig. 9). The model is known as the Tessellated Spheroid (TS) and was originally developed by Honeywell, Inc. In TS, each segment of CAC data is projected onto the DMS display in an equirectangular projection. Transformation from the DMA ARC system to TS is accomplished with a neighborhood averaging function that effectively reduces the image resolution from 10 pixels per mm (the resolution at which ADRG data has been scanned) to approximately 5 pixels per mm and results in a 4:1 data compression. This reduction in resolution is required for compatibility with aircraft displays.

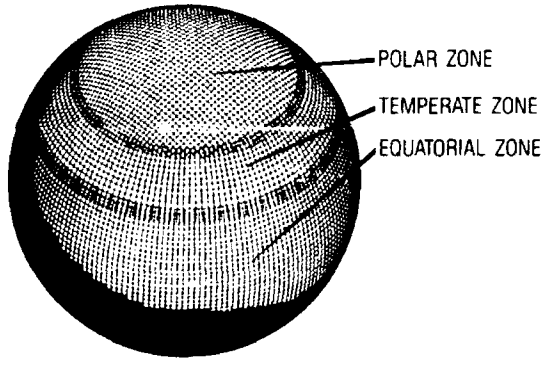

Fig. 9 – Tessellated spheroid model

Color Compression: Each ADRG pixel is 24 bits long: 8 bits each of red, green, and blue (RGB) intensities. Thus, more than 16 million (2^{24}) possible colors may exist in the ADRG database. The Navy DMS system can display only 256 (2^8) colors: 16 colors are reserved for graphic overlays, and 240 are used to display the chart images. Consequently, data storage requirements are reduced from 24 bits per pixel (bpp) to 8 bpp. Following the transformation from ARC to TS, ADRG data undergo a 3:1 color compression in which each 24-bit pixel is replaced by a similar 8-bit color. Color compression is achieved by subjecting the image data to a color vector quantization process that selects the closest match from 240 8-bit colors in a predefined palette to represent each input pixel [3]. A decompression color table is also generated to convert each 8-bit code back to its original (or close to original) RGB value for DMS display. Because the number of possible colors that can be used to represent each pixel has been reduced from 16 million to 240, this compression is not lossless. However, any observable loss of information is usually perceived as a normalization of the map colors and does not sacrifice image integrity.

Spatial Compression: A second compression is performed to further reduce data storage requirements. This is referred to as "spatial" compression, during which each nonoverlapping set of 2 × 2 pixels in the color-compressed image is replaced by a 1-byte codeword. Because each color-compressed pixel is 1 byte (8 bits) long, this represents a 4:1 compression. The method by which a fixed set of best-fitting codewords is chosen to represent all of the image's 4-pixel patterns is based on color vector quantization [3]. Spatial compression is not lossless but, as in color compression, the loss of information is not significant for DMS applications.

Research Efforts: The original ADRG ⇒ CAC compression algorithms were developed by Honeywell, Inc., and Honeywell maintains proprietary rights for that software. Consequently, the source code for those algorithms is not available to the Navy, and the software can never be ported to any computer other than that for which it was developed (a VAX/VMS system). Over the past two years, NRL-SSC has developed a comparable compression method that would be distributable and installable on any government computer system. This year, NRL-SSC mastered a prototype CD-ROM, which contains CAC data that were compressed with this new software, and distributed it to more than 20 government agencies for evaluation. Although the evaluation is not complete, preliminary results indicate that the NRL-SSC compression method is comparable or superior to the original in producing quality chart images. NRL-SSC introduced a "clean-up" stage

to the color compression that reduces the degree of scanner noise and produces a sharper image, particularly in large areas of similar color (such as oceans and desert areas). As a result, text features in those areas are easier to read. Furthermore, NRL-SSC is developing additional color tables that will allow users on limited-color systems (e.g., 16-color PCs) to display CAC data with reasonably good color quality.

Significance to the Navy: The Oceanographer of the Navy recently proclaimed that CAC is the standard aeronautical chart database supporting naval air navigation. F/A-18 and AV-8B aircraft are in the process of replacing all of their paper and filmstrip charts with CAC data. Many of these aircraft relied on CAC for mission planning and navigation during Operation Desert Storm, and the Navy's F/A-18 program office reported that the integration of CAC with their DMS contributed significantly to the success of F/A-18 pilots during that conflict. In addition to the U.S. Navy, several foreign countries, including Kuwait, Finland, Switzerland, and Australia, have recently purchased DMS-equipped F/A-18s and plan to use the NRL-SSC CAC database.

[Sponsored by NASC]

References

1. M.C. Lohrenz and J.E. Ryan, "The Navy Standard Compressed Aeronautical Chart Database," NOARL Report 8, NRL-SSC, July 1990.

2. Defense Mapping Agency, "Product Specifications for ARC Digitized Raster Graphics (ADRG)," First edition, DMA Systems Center/West Group, St. Louis, Missouri, April 1989.

3. M.C. Lohrenz, P.B. Wischow, H. Rosche, M.E. Trenchard, and L.M. Riedlinger, "The Compressed Aeronautical Chart Database: Support of Naval Aircraft Digital Moving Map Systems," *Proceedings of IEEE PLANS '90 Conference*, Las Vegas, March 1990. ■

Materials Science and Technology

Development of New Concepts for Fatigue Crack Thresholds

K. Sadananda
Materials Science and Technology Division

A.K. Vasudevan
Office of Naval Research

It is well known that there is a threshold stress intensity amplitude ΔK_{th}, below which a fatigue crack cannot grow. The knowledge of the threshold values is important for safe design of structural components. The values, however, depend on many variables, including material properties, microstructure, residual stresses, temperature, load ratio, load history, and environment. During the past twenty years, the dependence of fatigue crack threshold on most of the above variables has been explained by using a crack closure concept. There are over 1500 papers and several symposia published on crack closure aspects during the past twenty years. It is one of the most widely used, yet least understood concepts.

Role of Crack Closure: In the absence of crack closure, the crack tip driving force is related to the applied stress amplitude ΔK_{ap}, given by the difference between maximum (K_{max}) and minimum (K_{min}) stress intensities. When crack closure is present, the driving force is decreased to an effective amplitude ΔK_{eff} given by $K_{max} - K_{cl}$, where K_{cl} is the stress intensity at which crack closure occurs. Major support for closure concept came from observations that fatigue crack growth rates da/dN got compressed to a narrow band when the data for different load ratios R, ($R = K_{min}/K_{max}$), were represented in terms of ΔK_{eff}, instead of in terms of ΔK_{ap}. This contributed to many problems for a structural designer, since threshold values and crack growth rates, because of closure, do not depend on applied driving forces but on effective driving forces. For a structure, closure levels are impossible to determine or predict a priori, since they are system and application specific.

To resolve this problem, we have critically reexamined crack closure concepts and sources believed to contribute to crack closure using concepts from dislocation theory. Crack tip plasticity, oxidation, or corrosion products inside the crack, and asperites arising from tortuous crack path are believed to be major sources for crack closure. Our analysis [1] shows the following: (a) plasticity does not contribute to crack closure, since crack opening displacements are always greater than crack closure displacements; (b) complete crack closure occurs only when crack is filled fully with oxide or corrosion products, and such a situation has never been observed; (c) asperities occur randomly, and hence, asperity-induced closure cannot explain deterministic behavior of ΔK_{th} dependence on load ratio R; (d) partial crack closure can occur locally by asperities, but their effects on crack tip stress fields are very nominal. Thus closure, in all cases, is either nonexistent or insignificant to affect fatigue crack growth.

New Concepts of Fatigue Thresholds: Since closure is no longer a factor, we have reanalyzed fatigue threshold data [2] of many materials published in the literature and arrived at the following conclusions: (1) to fully define fatigue, two independent parameters are required, and hence, fatigue is a two-parametric problem; (2) most of the confusion in the literature including crack closure is from attempts to analyze fatigue crack growth data in terms of a single variable ΔK; (3) because of two parameters there are two thresholds rather than one, a critical cyclic stress intensity amplitude ΔK^*_{th} and a critical maximum stress intensity amplitude K^*_{max}; (4) both need to be satisfied simultaneously for crack growth to occur; (5) ΔK_{th} as well as K_{max} dependence on load ratio R can be fully explained without invoking crack closure by the requirement that both need to be satisfied simultaneously. In the limited R regimes, one or the other parameter varies to meet the critical value of the other (see Fig. 1(a)); (6) at low R ratios, fatigue is K_{max} controlled in the sense that ΔK_{th} increases with decreasing R to ensure that the critical K^*_{max} is met. Similarly at high

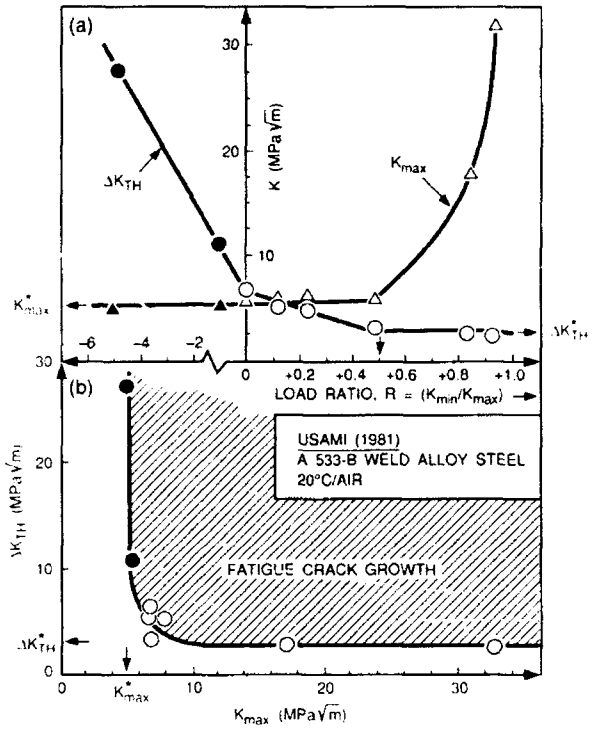

Fig. 1 — (a) There are two critical thresholds—one in terms of cyclic amplitude ΔK^*_{th} dominant at high R values and one in terms of peak stress K^*_{max} dominant at low R values; (b) the two critical values define the fatigue threshold map outlining regions where fatigue crack growth occurs and where it does not, thus defining safe regions for design [2].

R ratios, fatigue is ΔK controlled, and K_{max} increases to ensure critical ΔK^*_{th}; (7) both parameters can be determined by plotting ΔK_{th} versus K_{max} (as shown in Fig. 1(b)). This plot provides interrelation between the two parameters defining regimes where cyclic loads are damaging (above the curve) and where there are not (below the curve). Understanding these regimes is important for safe design; (8) physically, ΔK^*_{th} provides the minimum cyclic amplitude required to establish a characteristic fatigue damage and K^*_{max} provides the critical stress required to break open the crack tip bonds in the fatigue damaged region. Figure 1(b) provides a typical plot showing interdependence of the two to ensure fatigue crack growth; and (9) microstructure, slip character, crack tip environment, etc. affect each of the two parameters. For example, with increasing aggressiveness of the crack tip environment (oxygen, hydrogen, or water vapor) the role of K^*_{max} becomes increasingly important, since these affect more the crack tip bonds than the fatigue damage zone ahead of the crack tip.

Implications: The implication of the above concepts are far reaching. Fatigue crack growth behavior is now shown to be related to measurable and deterministic variables, and therefore is predictable rather than related to any extrinsic factors such as crack closure, which is not predictable. Fatigue crack growth rate data need to be represented in terms of three-dimensional plots involving da/dN vs ΔK and K_{max} instead of ΔK alone. Many of the fatigue crack growth phenomenon that have been attributed to crack closure require reexamination in the light of the above concepts. These new concepts will have a profound impact in terms of fundamental understanding of the kinetics of fatigue crack growth and its application to life prediction of structural components.

[Sponsored by ONR]

References

1. A.K. Vasudevan, K. Sadananda, and N. Louat, "Reconsideration of Fatigue Crack Closure," *Scripta Metallurgica et Materialia* **27**(12), 1673 (1992).

2. A.K. Vasudevan, K. Sadananda, and N. Louat, "Two Critical Stress Intensities for Threshold Fatigue Crack Propagation," *Scripta Metallurgica et Materialia* **28**(1), 1993 (in press). ■

Utilization of Empty Space to Enhance Material Properties

M.A. Imam, V. Provenzano, and K. Sadananda
Materials Science and Technology Division

Introduction: It is an article of faith among material scientists that the presence of voids in materials is deleterious to mechanical properties. Accordingly, it is with caution,

even with the rider that certain conditions are met, that one broaches the notion that the presence of such imperfections can be beneficial. These conditions relate to shape, size, and distribution of voids. For a void of given volume, the larger the ratio of its length to thickness, the more detrimental to mechanical properties. However, for circumstances where voids are small and uniformly distributed and they are spherical or nearly so in shape, the strength of material increases by impeding the motion of dislocation. The increase in strength of the composite is combined with high damping as well as low density.

Production: The production process entails the melting of a powdered metal in the presence of an insoluble gas at high pressure, forming a dispersion of gas-filled voids; releasing pressure prior to solidification permits the voids to expand to an equilibrium size under zero external stress. This procedure eliminates any stress concentrations associated with voids. Figure 2 is an example of a scanning electron fractograph of a copper specimen showing voids.

Fig. 2 – SEM fractograph showing voids

Basic Properties:

- The composites can achieve strengths which meet or exceed those obtainable from the strongest materials currently in service, while offering a substantial reduction in density.
- The incremental strength due to voids can be maintained without significant degradation at high temperatures. The voids themselves can change only by Ostwald ripening but can be prevented by choosing the contained gas to be insoluble in the matrix material. Weakening mechanisms, like grain boundary sliding at high temperatures, cannot occur since accompanying boundary migration is prevented by the presence of the voids.
- Voids will interact strongly with propagating cracks, either by blunting the cracks or by slowing the propagation rate. The net result is a significant increase in fracture toughness over the matrix material.
- The intensity of forced, resonant vibrations is smaller than in the monolithic matrix because voids act as inert inhomogeneities that strongly scatter low-frequency excitations (i.e., those with wavelength greater than the average spacing of voids).

Applications: Because of their high strength-to-weight ratio, high temperature strength retention, and high damping capability, the materials are specifically suited for:

- transorbital aircraft and critical orbital devices, where the advantages are the enhanced strength at high temperatures and resistance to vibrations caused by impact or sudden configurational change;
- radiation-absorbing coatings for use on submarine and aerospace devices; and
- components or coatings for the transport industry, where there is a reduction in weight with no strength or toughness penalty. With the added capacity for sound absorption, void-metal composites will improve the competitive position of the domestic automobile industry.

Acknowledgments: The authors acknowledge Dr. N.P. Louat and Dr. M.S. Duesbery of Fairfax Materials Research, Alexandria, Virginia, for their helpful discussions.

[Sponsored by ONR] ■

The Mechanism of Visible Photoluminescence in Porous Silicon

S.M. Prokes and O.J. Glembocki
Electronics Science and Technology Division

The importance of visible photoluminescence (PL) in silicon was first reported by Canham [1]. Because the porous silicon light-emitting structures can be fabricated by using a relatively simple and inexpensive etching technique that can easily be integrated into existing silicon technology, the mechanism responsible for this effect must be understood.

The visible light emission in this material is surprising since bulk crystalline silicon has an indirect gap at 1.1 eV at room temperature; this results in a very inefficient PL in the infrared. One mechanism suggested to explain the visible luminescence assumes that the porous silicon structures are in nanometer-scale dimensions, leading to a quantum size effect in the silicon band structure. However, recent results obtained at NRL suggest a mechanism that does not depend on confinement effects but relates to surface/interface chemistry.

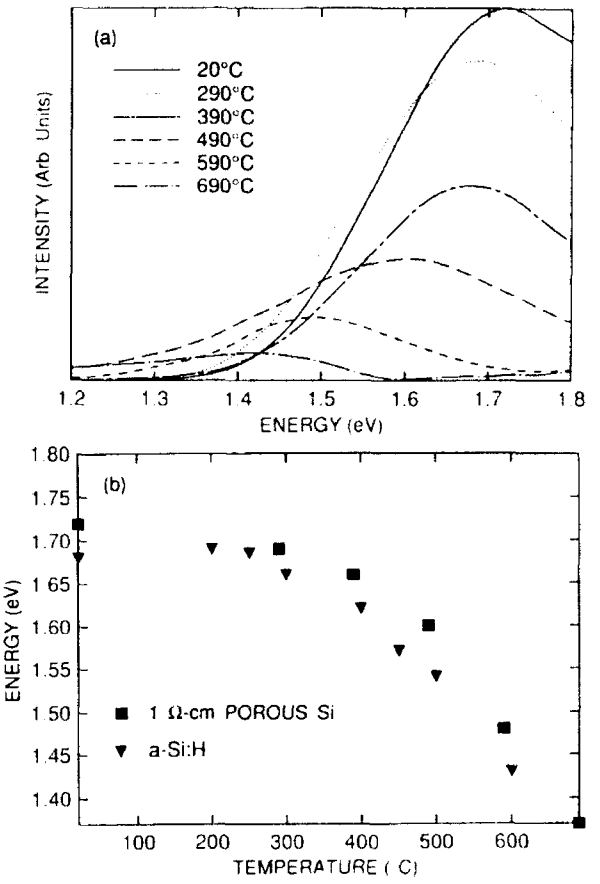

Fig. 3 — (a) Plot of photoluminescence as a function of anneals and (b) shift of PL energy for porous silicon and *a*-Si:H as a function of annealing

Thermal Behavior: One of the first indications suggesting an alternate PL model involves the PL redshift and the disappearance with heating of porous silicon (Fig. 3(a)). This PL redshift and disappearance coincides with the desorption of SiH_x complexes [2]; the PL can be recovered by reintroducing these complexes onto the surface by hydrofluoric acid (HF) dipping. Furthermore, the redshift of the PL tracks identically with the shrinking of the optical bandgap in amorphous hydrogenated silicon with hydrogen desorption (Fig. 3(b)). This suggests that hydrogen may play a direct role in the luminescence process, and does not simply act as surface passivation.

Particle Size: The red luminescence in porous silicon occurs at an energy close to 1.7 eV (Fig. 3(a)). For the quantum confinement model, this requires particle sizes in the 2.8 nm range, shifting to higher energy with decreasing particle size. This, however, is not true for 0.1 Ω-cm *p*-type and *n*-type red luminescing samples. These have been reported to have porosities as low as 10%, resulting in particle sizes on the 100 nm scale [3]. To examine the PL change with the collapse of the 0.1 Ω-cm porous silicon structure, samples were annealed at high temperature in ultrahigh vacuum. Figure 4 shows the resulting structures. It is quite obvious that the material in Fig. 4(c) is markedly different from the initial structure (Fig. 4(a)). Significant coarsening has led to a new structure having spherical particles of sizes on the order of 150 nm. No luminescence is visible for the porous silicon above roughly 690°C, and no SiH_x complexes exist above this temperature. The structure in Fig. 4(c), however, exhibits PL at the same energy as shown in Fig. 3(a) when dipped for 1 s in HF. Since the porous silicon has been collapsed and much larger structures

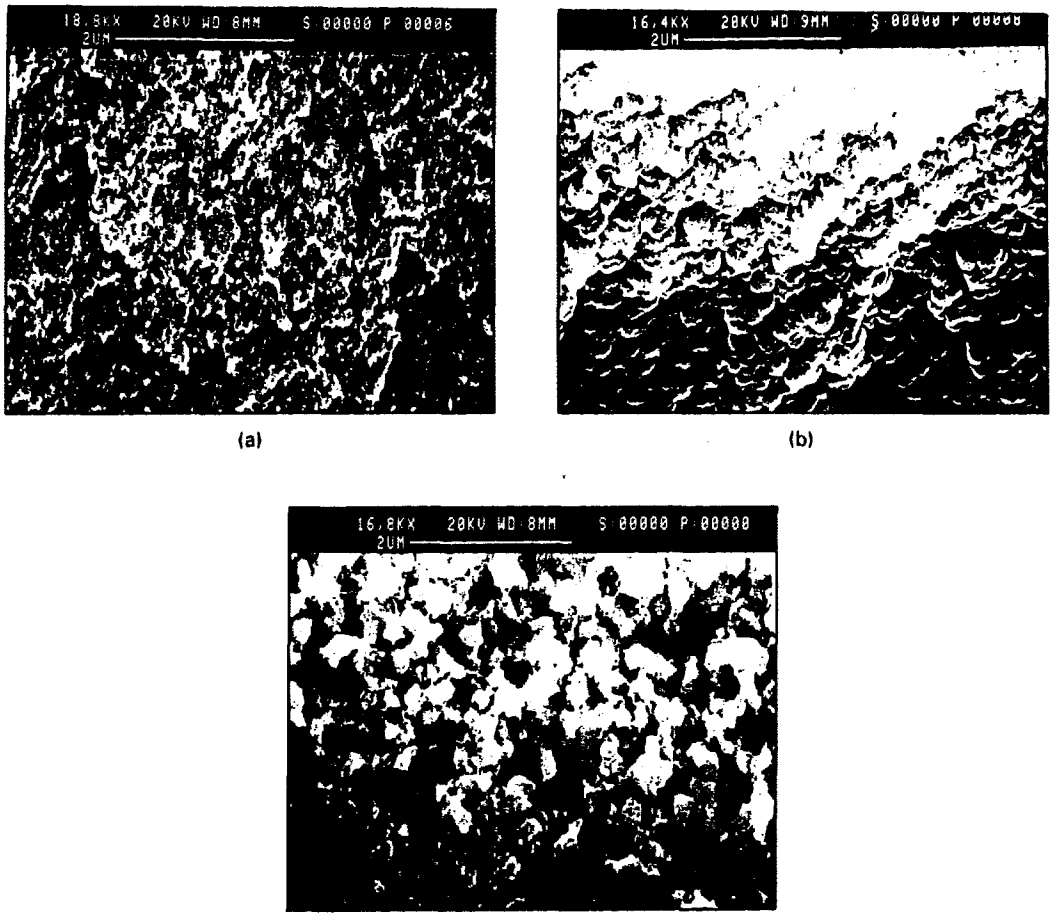

(a) (b)

(c)

Fig. 4 — Scanning electron micrographs of porous silicon (a) unannealed, (b) at 900°C for 1 min, and (c) annealed at 1200°C for 1 min

have been formed that did not change with the HF dip, it is clear that the red PL cannot originate from confinement effects, but may be related to hydrides and surface chemistry.

Finally, a controlled low-temperature oxidation/HF stripping has also been performed (Fig. 5). Because the oxidation process/HF stripping should result in a particle size decrease for each successive cycle, a continuous blueshift of the PL is expected for the confinement case. In fact, the PL should shift to roughly 3.4 eV after the fourth cycle, based on an estimate of the oxide thickness grown in each cycle. The fact that the PL cycles repeatably between two energies with SiH_x creation and desorption again suggests a hydrogen-related luminescence process.

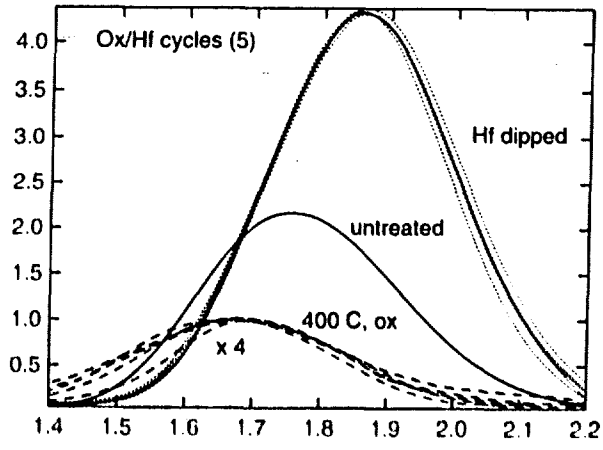

Fig. 5 — Photoluminescence peaks for 1 Ω·cm porous silicon as a function of heating and HF cycling; for as etched sample (----), oxidized for 1 min at 400°C (- -), and dipped in 25% HF for 1 s (• • • • •)

Various porous silicon structures of differing particle sizes exhibit red PL with electrochemical etching, and a mechanism applicable to all must be considered. Thus, a surface/interface-type luminescence mechanism clearly cannot be ignored. Before this issue can be settled, however, it will be necessary to examine more consistently the PL and particle size changes, and the effect of other elements (such as oxygen) on the interfacial characteristics and the photoluminescence properties of this system.

[Sponsored by ONR]

References

1. L.T. Canham, "Silicon Quantum Wire Array Fabrication by Electrochemical and Chemical Dissolution of Wafers," *Appl. Phys. Lett.* **57**, 1046 (1990).

2. S.M. Prokes, O.J. Glembocki, V.M. Bermudez, R. Kaplan, L.E. Friedersdorf, and P.C. Searson, "SiH_x Excitation: An Alternate Model for Porous Silicon Photoluminescence," *Phys. Rev.* **B45**, 13788 (1992).

3. J.M. Macauley, F.M. Ross, P.C. Searson, S.K. Sputz, R. People, and L.E. Friedersdorf, "Microstructural Characterization of Photoluminescent Porous Silicon," *Mat. Res. Soc. Symp. Proc.* **256**, 47 (1992). ■

Superconductivity of Layered Superconductors: An Interlayer Coupling Model

A.K. Rajagopal
Electronics Science and Technology Division

During the past six years, a large number of high T_c superconducting materials have been synthesized with transition temperatures (T_c) in the 30 to 125 K range. Of main concern here are the layered cuprates. These discoveries have given rise to speculations about the mechanisms of such high T_c phenomena in cuprates—ranging from a suitable generalization of the Bardeen-Cooper-Schrieffer (BCS) pairing theory to include electronic exchange mechanisms in strongly correlated systems to radically new theories based on strong correlation effects in two-dimensional Cu-O layers. Radical approaches to the problem are needed because the normal state properties do not fit the conventional Fermi liquid picture in which the usual pairing theory of the low-T_c superconductor is based. Moreover, the conventionally attractive phonon-exchange mechanism cannot lead to transition temperatures above 50 K. Also, these systems have low electron densities (with their Fermi energies an order of magnitude smaller) and highly anisotropic coherence lengths (about three orders of magnitude smaller in Cu-O planes than in the low T_c systems). The coherence length in the direction perpendicular to the planes is about a third of that in the plane. The cuprates are all type-II superconductors with very high in-plane upper-critical magnetic fields (approximately two orders of magnitude larger than for the usual systems). There is no consensus as to which of the theories can explain all the observed properties of these cuprates. We describe below an interlayer coupling model to understand superconductivity in these systems.

The structural characteristics of the various cuprate superconductors (Table 1) show five possible geometrical configurations of Cu-O complexes in the unit cell: Cu-O chain denoted by C; Cu-O plane denoted by P; and half octahedron of $Cu\text{-}O_4$ pointing up (P_u) and pointing down (P_d); and full $Cu\text{-}O_4$ octahedron (0). They also occur in staggered configurations. Table 1 clearly shows a correlation between the values of T_c and these configurations. These complexes are often well separated within each of the unit cells. It appears essential that any theory of these fascinating systems incorporate these "layered" structures to account for the unusual anisotropic physical properties. We [1] have developed a generalized pairing theory for layered materials without actually specifying the nature of possible exchange mechanisms (electronic charge fluctuations, ionic excitations, etc.). Also, the theory is formulated to avoid

Table 1 — Calculation of T_c

Compounds	No. of CuO_2 layers per unit cell	Intralayer Coupling Const.	Interlayer Coupling Const.	Interlayer Coupling Const. (staggered)	T_c (calculated)	T_c (experimental)
		Unit Cell Cu-O Complex Configuration				
Tl_1 - compounds		0.33	0.48	—		
$Tl_1Ba_2Ca_0Cu_1O_5$	1	0			15*	13-15
$Tl_1Ba_2Ca_1Cu_2O_7$	2	P_d - P_u			91*	91
$Tl_1Ba_2Ca_2Cu_3O_9$	3	P_d - P - P_u			116*	116
$Tl_1Ba_2Ca_3Cu_4O_{11}$	4	P_d - P - P - P_u			126	122
$Tl_1Ba_2Ca_4Cu_5O_{13}$	5	P_d - P - P - P - P_u			132	117
	...				...	...
	∞				143.5	?
Tl_2 - compounds (staggered config.)		0.33	0.48	0.41		
$Tl_2Ba_2Ca_0Cu_1O_6$	2	0 - $(0)_s$			80*	80
$Tl_2Ba_2Ca_1Cu_2O_8$	4	$(P_d\text{-}P_u)$ - $(P_d\text{-}P_u)_s$			120	110
$Tl_2Ba_2Ca_2Cu_3O_{10}$	6	$(P_d\text{-}P\text{-}P_u)$ - $(P_d\text{-}P\text{-}P_u)_s$			131	127
	...				...	...
	∞				143.5	?
Bi_2 - compounds (staggered config.)		0.26	0.48	0.12		
$Bi_2Ba_2Ca_0Cu_1O_6$	2	0 - $(0)_s$			22*	22
$Bi_2Ba_2Ca_1Cu_2O_8$	4	$(P_d\text{-}P_u)$ - $(P_d\text{-}P_u)_s$			89	85
$Bi_2Ba_2Ca_2Cu_3O_{10}$	6	$(P_d\text{-}P\text{-}P_u)$ - $(P_d\text{-}P\text{-}P_u)_s$			110	110
	...				..	...
	∞				136.5	?
$La_{2-x}Sr_xCuO_4$ (staggered config.)		0.37	—	0.12		
	2	0 - $(0)_s$			40*	40
$YBa_2Cu_3O_{7-x}$		0.30 (av)	0.36	—		
	3	P_d - C - P_u			90*	90
$YBa_2Cu_4O_8$		0.27 (av)	0.29	—		
	4	P_d - C - C - P_u			80*	80

*Parameters fitted with experiment

the Fermi-liquid form of the normal state properties. In this way, we have presented a field-theoretic framework in which an effective dynamic interaction may lead to a phase-coherent state of the electron pair condensate. We also introduce the so called "layer-representation" for describing the single electron states of these systems: a delocalized two-dimensional Bloch picture in the plane of the layers and a one-dimensional localized Wannier picture in the direction perpendicular to the layers for the electron motion. In this way, the anisotropic system properties are built into the theory from the beginning. Moreover, this layer representation naturally leads to intralayer and interlayer couplings within the same unit cell and between cells as well, among the electrons in the system, irrespective of the nature of the effective interaction. This theory leads to the following model.

To gain more insight into this general framework, we have proposed a highly simplified phenomenological model for the interaction and the single-particle properties. Assuming *intralayer intracell couplings to be attractive and* strong, and interlayer coupling among nearest layers (taking care to distinguish the coupling in the staggered configuration), we have been able to reconcile the variations in the transition temperature (see Table 1) across the various systems with only a few parameters. This leads us to conclude that the presence of interlayer couplings tend to enhance the transition temperature (T_c) in general. The anisotropy in the order parameter is found to be due to intercell coupling. This conclusion is borne out most dramatically in the superconducting properties of PrBCO-YBCO superlattice systems where PrBCO is structurally the same as YBCO but is not superconducting [2]; here the intercell, interlayer pairing plays an all-important role. Another feature of this simplified model is the prediction that a saturation of T_c occurs as the number of Cu-O complexes increases.

To conclude, we have developed a general theory of layered superconductors in which the pairing theory of superconductivity includes both the single-particle as well as two-particle properties arising from the appropriate layer representation of the system. The theory is sufficiently general to incorporate magnetic field effects in these systems, and these are currently being studied. The various anisotropic system properties mentioned earlier may be understood in terms of intercell, intra- and interlayer couplings. This theory is also applicable to low T_c systems such as Ge-Nb.

Acknowledgments: This work is a collaborative effort of the author with Professors S.S. Jha of TIFR, Bombay, and S.D. Mahanti of MSU, East Lansing.

(Sponsored by ONR)

References

1. A.K. Rajagopal and S.S. Jha, "Generalized Pairing Theory of Superconductivity in Layered Crystals," *Physica* **C174**, 161-179 (1991).

2. A.K. Rajagopal and S.S. Jha, "Structure of Intralayer and Interlayer Interactions, the Anisotropy of Order Parameters, and the Transition Temperature in Layered Superconductors," to appear, *Phys. Rev.* **B47** (1993).

3. A.K. Rajagopal and S.D. Mahanti, "High T_c Superconductivity of $YBa_2Cu_3O_7$/$PrBa_2Cu_3O_7$ Superlattices: An Interlayer-Coupling Model," *Phys. Rev.* **B44**, 10210-10214 (1991). ■

Numerical Simulating, Computing, and Modeling

A High Fidelity Network Simulator for SDI

E.L. Althouse, D.N. McGregor,
R.R. Nair, and S.G. Batsell
Information Technology Division

A High Fidelity Network Simulator (HiFiNS) was developed to analyze the communication system performance for the proposed Strategic Defense Initiative (SDI) architecture. This architecture includes both the National Missile Defense First Site System (NMD FSS) and the Global Protection Against Limited Strikes (GPALS) strategic defense system. Such a simulation is necessary to verify that the envisioned strategic defense communication system will provide timely, secure, and reliable communications for surveillance, command and control, and weapons delivery to adequately perform its mission. The basic simulator is flexible enough to handle both ground- and space-based communication networks for SDI and is generally extensible to other large scale network applications.

SDI Network Application: The physical architecture under consideration for the NMD FSS consists primarily of a ground-based network connecting Grand Forks, North Dakota, and Colorado Springs, Colorado, as well as a satellite relay net between the two sites. As the NMD architecture evolves over time into GPALS, there will be additional ground sites, space-based surveillance components called Brilliant Eyes (BE), and possibly space-based interceptors called Brilliant Pebbles (BP). Figure 1 represents a generic version of the NMD FSS architecture without specifying the details and connectivity of the components at each of the two sites. For example, the Grand Forks site will include a Ground Based Radar (GBR) for tracking approaching missiles, a total of 100 Ground Based Interceptors (GBIs) spread over several remote launch bases, several Ground Entry Points (GEPs) that will control access to the GBIs as well as GEPs that control access to the space relay platform. The Grand Forks site will comprise several subnetworks connected by terrestrial T-3 landlines; connectivity within a subnetwork will be via a local area net using Fiber Distributed Data Interface (FDDI) technology. Connectivity from Grand Forks to Colorado Springs will incorporate both satellite relay and terrestrial T-1 landlines.

Simulation of the SDI communication network represents quite a challenging and complex problem. Approximately 150 platforms comprising the NMD FSS have to be modeled in conjunction with certain rules for their connectivity. In addition, several types of communication traffic (sensor tracking, command and control, health and status, weapons targeting, etc.) must be sent according to different levels of precedence and timeliness in conjunction with some battle management philosophy. Finally, a threat model must be incorporated into the network that would represent the approaching missiles as a function of time. This threat model then acts as a stimulus for SDI message generation. Figure 1 shows a sample scenario where a single intercontinental ballistic missile (ICBM) is launched towards the U.S. resulting in several reentry vehicles (RVs) each targeting a particular location. Under the NMD FSS architecture, the GBR will track these approaching RVs and pass the information throughout the network so that appropriate battle management decisions can be made to allow an appropriate number of GBIs to attack the incoming RVs. With larger threats, the overall complexity will increase and there will clearly be a premium on effectively launching an appropriate number of GBIs out of the available resource pool. As the NMD system matures into GPALS additional space assets will exist for both the sensing (BEs) and shooting (BPs) of RVs at a much faster rate than will be possible under the NMD FSS architecture. These additional assets will allow for intercepts to occur on a global scale as well as during the boost and post-boost phases of ICBM launches rather than only during the terminal phase. It is expected that hundreds to thousands of platforms will need to be modeled for GPALS using HiFiNS. Past efforts [1] at NRL have resulted in the development of a large-scale network simulator that models up to 5000 platforms.

HiFiNS Overview: HiFiNS is a nonreal-time discrete-event simulator [2] that is intended

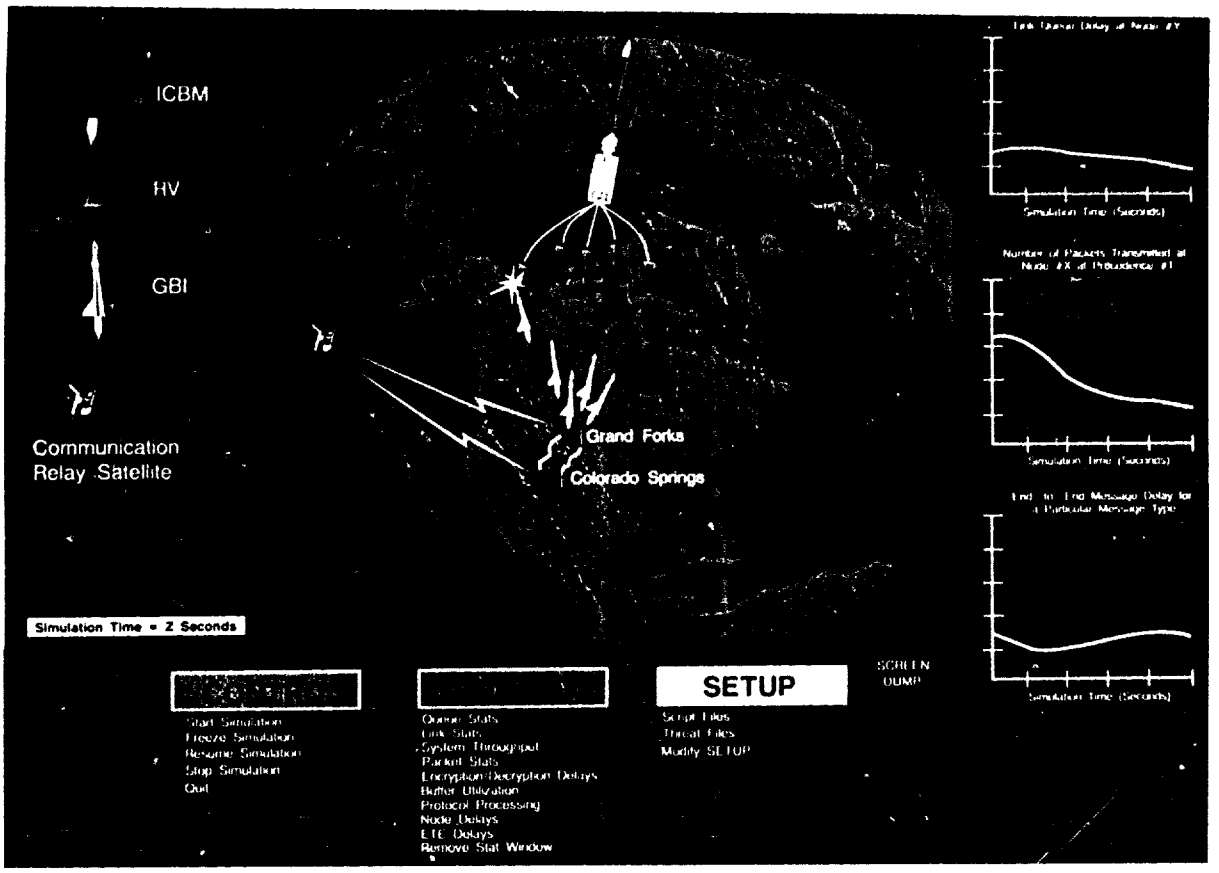

Fig. 1 SDI NMD FSS architecture and HiFiNS graphical display

to analyze the NMD and GPALS communication network, including terrestrial, space, and space-to-ground links. The simulation models the entire SDI network topology, sensor surveillance, message generation, communication links, networking protocols and algorithms, threat-object missile trajectories, interceptor trajectories, element response, battle management approaches, and environmental perturbations. It is a design tool that can be used to assess and evaluate overall communication network performance and examine the system effects of architectural design changes and excursions to terrestrial and space-based node configurations, connectivities, networking algorithms, battle management philosophy, and so forth.

HiFiNS can be functionally decomposed into the following components as shown in Fig. 2: (1) a discrete-event, message-passing simulator; (2) an environment that controls the quality of the communications links via packet error infliction from the effects of noise and multiple nuclear weapons detonations; (3) a threat-driven scenario that projects the threat and computes the probable response of the sensor system; (4) an element response module that represents the host-level message response to messages delivered to or sourced by a GBR, GBI (both the service site and the inflight vehicle), GEP, etc.; (5) an operational message set to represent peacetime and wartime communications; (6) a network management station that provides the human-in-control function for network management; (7) node-level functions such as network protocols, queuing, congestion control, and routing algorithms; and (8) a graphical user interface (GUI) that provides control of the simulation and display of the results.

HiFiNS will be made available to the SDI user community through a series of Builds, each

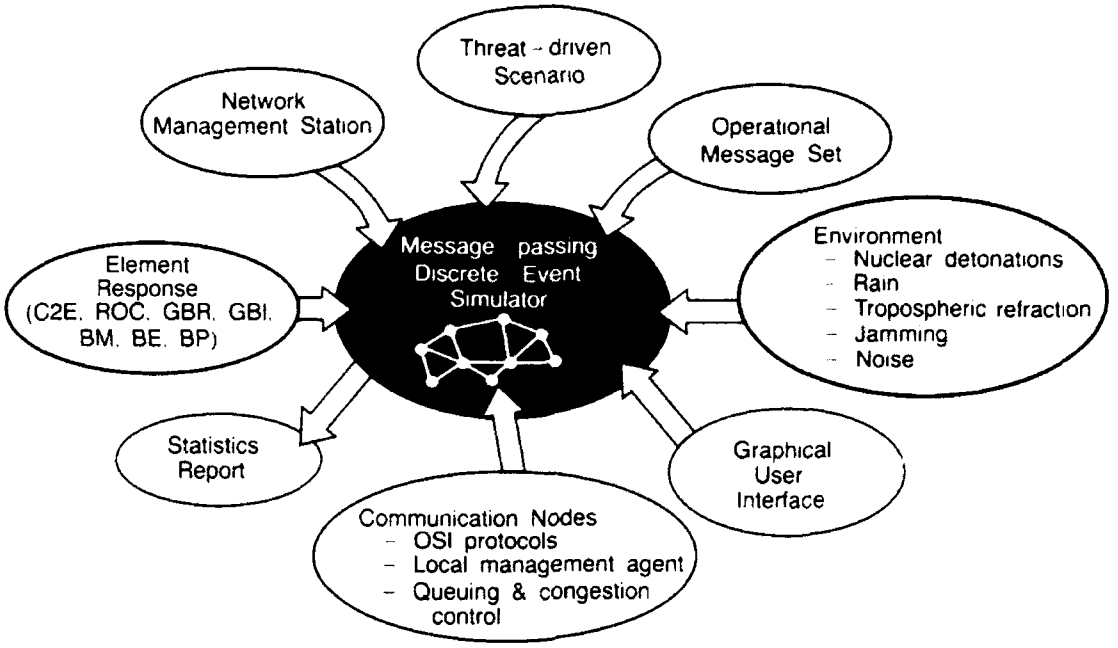

Fig. 2 — HiFiNS components

offering incremental improvements. The first Build was intended to be developed as a rapid prototype that would provide an early demonstration of the NMD FSS functional capability. It includes the Colorado Springs and Grand Forks sites consisting of several terrestrial and satellite relay subnetworks that connect the GBR, GBI farms, and GEPs. The software was essentially completed in September 1992. After a short period of testing and performance checkout, HiFiNS Build 1 became operational in January 1993. The second Build will provide a higher fidelity representation of the larger NMD architecture and is scheduled for completion in October 1994. The third Build will represent the full GPALS architecture as well as include major improvements in simulator fidelity and performance capabilities.

Simulation Results: HiFiNS is hosted at NRL on a cluster of high-performance RISC computer workstations and a capability is planned for eventual remote user access within the SDIO community via the National Test Bed network. A GUI has been developed to provide user control of HiFiNS via the menus shown at the bottom of Fig. 1. The *Control Menu* allows the user to start, freeze, resume, and stop the simulation at his discretion. The *Statistics Menu* allows the user to examine and collect numerous communications-related statistical parameters on a node, link, or end-to-end basis as a function of simulation time, which is also displayed. A maximum of three different statistical parameters can be shown as graphs during the simulation using the GUI; each of these graphs can be deleted and new graphs can be displayed since the GUI allows for interactive user operation with the simulation. Some examples are shown in Fig. 1 for illustration. Although the emphasis is on communications-related performance, the output files also capture related events, such as connectivity changes, link and node failures, interceptor launches, intercept events, kill success, etc., so that association between battle and communication events is preserved. Sufficient detail is captured to allow graphical replay of the entire simulation. Communications-related measures of effectiveness include end-to-end message delays, queuing delays, link utilization, throughput, packets transmitted and received, encryption delays, buffer utilization, message discard statistics (caused by congestion control processes), lost message instances, etc., as a function of simulation time. These data are provided separately for each of the 31 types of

messages (each with one of three possible levels of precedence) in the complete operational message set. The *Set Up Menu* allows the user to run HiFiNS in either its normal interactive mode or to use script files for message generation. When HiFiNS is run without basing the network message traffic on deterministic scripts, it then allows significant battle events, such as RV intercepts and associated probability of kill, to be influenced by communication network delays and relative closing geometry of the RV and interceptor. Therefore, the outcome of HiFiNS simulations is nondeterministic in this case. In addition to the built-in causal relationship between battle-management and communication-related simulation events, HiFiNS permits user-imposed changes to the simulation during runtime via the GUI; for example, nodes and links may be disabled for system robustness studies.

Summary: This simulator is being used as an analytic tool for SDIO to examine the effectiveness of the NMD FSS and GPALS designs. Our approach is to perform sensitivity tradeoffs of the physical architecture and the networking algorithms that control its operation. Simulations of the NMD FSS architecture began in January 1993 using HiFiNS. Our fundamental goal is to provide those system tradeoffs that will allow for the development of a robust SDI baseline architecture. However, the simulator structure is flexible and can easily be extended to other large-scale complex networks.

[Sponsored by SDIO]

References

1. D.N. McGregor, R.R. Nair, and E.L. Althouse, "A Communication Network Simulator for the SDI Brilliant Pebbles Architecture," *Proceedings of the 1991 Military Communications Conference*, McLean, Virginia, November 4-7, 1991, pp. 503-507.

2. E.L. Althouse, S.G. Batsell, and D.N. McGregor, "High Fidelity Communication Network Simulator for SDIO," *Proceedings of the Armed Forces Communications and Electronics Association on Modeling and Simulation in Today's Defense Environment*, Annapolis, Maryland, October 14-15, 1992, Panel 4. ■

Optimal Resource Allocation Using Genetic Algorithms

K.E. Grant
Tactical Electronic Warfare Division

A stationary target in a hostile environment is equipped with defensive resources. An arbitrary number of threats arrive, each with the goal of hitting the target, during a finite period of time. The success of a defensive resource in countering an attack is probabilistic. The problem of allocating defensive resources to maximize the probability of target survival is considered in this paper. Genetic algorithms, their application as a heuristic device to find the optimal allocation scheme, and simulation results are discussed. Genetic algorithms use procedures that allow for rapid convergence to a recommended allocation scheme in time-critical engagements as compared to common optimization and exhaustive search procedures that are time consuming.

Terminal Defense Scenario: During a hostile engagement, the defensive target initiates a set of consecutive actions. The initial defensive response is threat detection and identification. The threats are then prioritized according to their danger to the target. At this time, rule-based methods are used to generate a schedule of events to counter the attack and prevent the threats from hitting the target. A schedule is a finite, discrete-time indexed list of decision instants with associated events. A single optimal schedule cannot always be determined via rule-based methods. A schedule optimizer was developed to which a set of feasible schedules may be handed off and from which an optimal schedule is quickly returned. After the optimized schedule has been initiated, an effectiveness assessment, using an updated threat status, is performed to decide whether the threats were countered or, if not, whether the threats should

be reprioritized. A new set of rule-based schedules may be generated with assistance from the schedule optimizer and the process is repeated. Figure 3 depicts a typical threat engagement scenario highlighting the participation of optimal resource allocation.

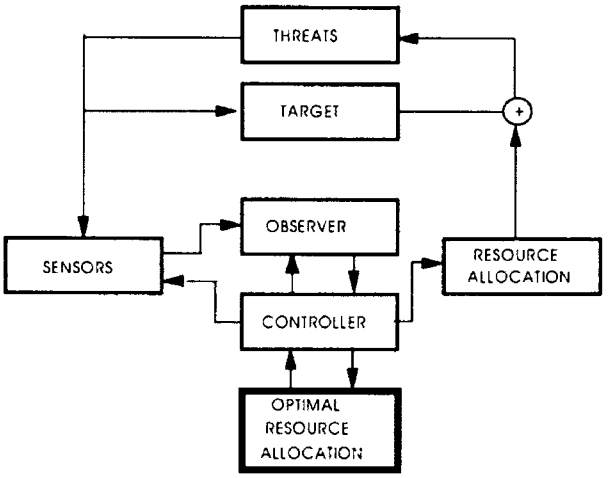

Fig. 3 — Intuitive representation of a typical threat engagement scenario, highlighting the participation of optimal resource allocation

Genetic Algorithms in Optimization: Genetic algorithms are heuristic search algorithms for optimization based on the mechanics of natural selection and natural genetics. The schedules are encrypted into strings, which may be manipulated by the genetic algorithms to exploit similarities in performance. Multiple resources are represented via substrings. Genetic algorithms search from a population of points, not a single point, which increases the probability of locating the global maxima. Genetic algorithms also use a cost function, in this case the probability of target survival, for a probabilistic transition rule. The probability of target survival against multiple threats is calculated with a multidimensional cost function.

The mechanics of a simple genetic algorithm, described in Ref. 1, include reproduction, crossover, and mutation. Reproduction is the process in which individual strings are copied according their cost function P_s. Crossover is the process in which two new strings are generated by randomly swapping substrings. Mutation is the occasional (with low probability) random alteration of a string position's value; the mutation operator protects against loss of possibly useful genetic material. At each iteration in the genetic algorithm, the cost function P_s has to be determined only for each string in the population. This dramatically reduces the number of times P_s must be calculated, as opposed to the number required for an exhaustive search. Genetic algorithms provide an acceptable compromise between lengthy search procedures and performance.

Given both a random and weighted initial population of 10 schedules, each with 12 decision instants that uniformly describe a 60 second time interval, genetic algorithms were applied to 10 scenarios, with one or two attackers arriving at various angles and times, to determine an optimal schedule. Genetic algorithms determined the optimal schedule 81% of the time on average. The optimal schedule was verified via an exhaustive search. Little difference was noted between schedules estimated from random or weighted initial populations. Initial estimates result in semioptimal schedules that continue to improve with time. In general, genetic algorithms were found to perform well when applied to optimal resource allocation. Valid and near optimal schedules were promptly determined for time-critical threat engagements.

[Sponsored by NRL]

Reference

1. D.E. Goldberg, *Genetic Algorithms in Search, Optimization and Machine Learning* (Addison-Wesley Publishing Company, New York, 1989). ■

Numerical Simulation of Bubble-Free Surface Interaction

M.H. Emery and J.P. Boris
Laboratory for Computational Physics and Fluid Dynamics

The interaction of air bubbles with themselves and with the ocean surface is a problem of vital concern to the Navy because of the role

that this interaction plays in the generation and longevity of ship wakes and in turbulent two-phase flows. Bubbles are generated by breaking waves at the bow of a ship, at the shear layer along the length of the ship, and by cavitation inception on the propeller surface as air is entrained with the water. These bubbles interact dynamically with surfactants (surface active materials) and the free surface of the ocean to produce wakes that may be visible for long distances. The numerical simulation of bubble dynamics and the interaction of the bubbles with the free surface is complicated by the need to accurately and efficiently calculate the sharp interface between the air and the water as convection and turbulence cause the interface to break and reconnect. Recent advances in the evolution of interface-capturing techniques has led to the development of a three-dimensional (3-D) bubble dynamics model, which satisfies the criteria of accuracy and efficiency and models the dynamics of the interaction of bubbles with complex free-surfaces as the topology of the air-water interface continuously changes.

Model: The basic algorithm for the 3-D bubble dynamics code is the parallelized, fully compressible flux-corrected-transport (FCT) technique developed for efficient, high resolution, fluid dynamic convection, coupled with a new interface-capturing technique, which keeps arbitrarily complex and merging interfaces sharp. The numerical complexity arises from two sources; (1) the need to treat flows that have relatively low speed and thus are essentially incompressible, and (2) the need for a simple, yet accurate, means to treat the convoluted, time-dependent interface between air (with a density of 1.2×10^{-3} gm/cm^3) and water (with a density of 1 gm/cm^3). The cell-averaged densities of air and water are integrated forward in time using the FCT algorithm to solve the respective mass conservation equations. This algorithm now includes a velocity-dependent antidiffusion steepener that limits the diffusion between the two media and maintains the sharp interface while retaining accuracy. The total cell-averaged density (the sum of the air and water densities) also satisfies the mass and momentum conservation equations. The momentum conservation equation incorporates the force densities arising from gravity and gradients of the pressure. The pressure is determined from separate equations of state for air and water in terms of their respective sound speeds and the *actual* densities of air and water. The *actual* densities of the air and water phases are defined in terms of the cell-averaged densities and f, the fraction of a cell volume (no matter how distributed) that has water in it and $(1 - f)$, the fractional cell volume of air. What is needed is an efficient and accurate determination of f. Recognizing that in a mixed cell, the pressures of the two species are equal, leads to a quadratic equation for f in terms of the cell-averaged densities, the ratio of the sound speeds, and the initial density of the water. This provides a robust, parallel, accurate, easy-to-use, 3-D computational model that can be used to simulate the interaction of air bubbles with the ocean surface, air entrained in water, and even sprays of water droplets in air.

Numerical Results: Here we present the results from a calculation simulating the evolution of a 3-D underwater explosion bubble as it broaches the free surface. The bubble has an initial over pressure of 7 atm, is 2.2 m in diameter, and is 3.5 m below the surface of the water. The bubble is on the axis of a cylindrical tank that has a radius of 4 m. The computational mesh is $80 \times 100 \times 80$ grid cells. The air pressure above the water surface is 1 atm. The bottom, side, and top (above the air) surfaces of the container are "hard walls." The bubble undergoes a rapid pulsation and, because of its great buoyancy, begins to migrate upward. At the moment of maximum expansion, the bubble is almost a perfect sphere, with deviations due to the growth of a Rayleigh-Taylor instability. After a slight contraction and as it begins to rise, the sphere is distorted (Fig. 4). This is caused by the difference in hydrostatic pressure between the top and bottom of the explosion bubble. The bottom of the bubble is pushed inward faster than the top and a kidneylike shape is formed. Figure 5 illustrates a cutaway view of the bubble at this time. The two interfaces can actually impinge upon one another forming a water jet up through the

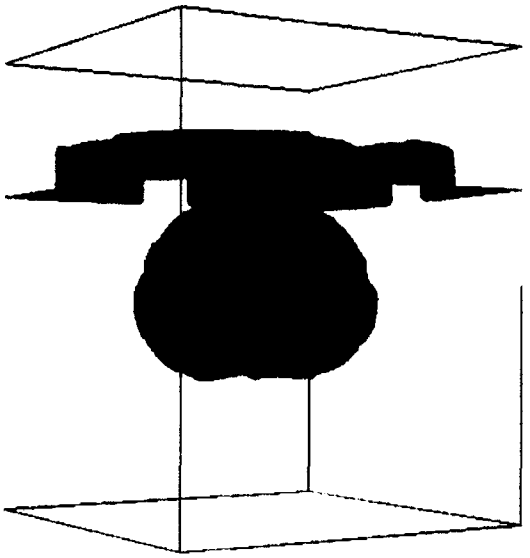

Fig. 4 — The 3-D underwater explosion bubble shortly after it has begun to rise. Light blue (green) is the air-water interface as seen through the water. Dark blue is the interface as seen through the air. Note the convoluted interface resulting from the Rayleigh-Taylor instability and the distorted lower surface of the bubble.

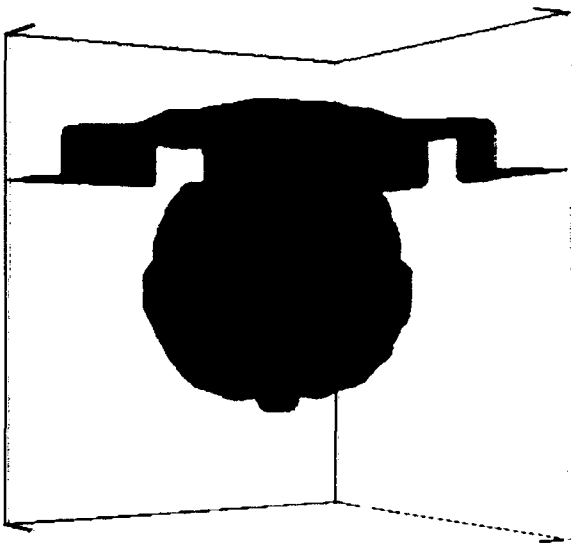

Fig. 5 — A cutaway view of the bubble at a slightly later time. The Rayleigh-Taylor induced ripples are apparent on the upper surface of the bubble.

Fig. 6 — The configuration of the 3-D underwater explosion bubble broaching the free surface. Here, light blue is the air-water interface seen through the air; dark blue is the same interface seen from the water side. The bubble has been sliced through to expose the inside.

center of the bubble. In this case, the bubble broaches the free surface before the water jet is completely formed. Figure 6 shows a cutaway view of the bubble-free surface after the bubble has broken through the water surface. Note the highly convoluted interface, which is being simulated accurately with this numerical algorithm.

Summary and Future Work: The numerical algorithm as outlined here has provided us with an accurate and efficient means of self-consistently modeling air entrainment, bubble production and collapse, and bubble- and free-surface interaction. As the actual interface between the air and water is not tracked

explicitly, modeling many bubbles is as simple as modeling a single bubble. The only criterion is sufficient grid resolution to represent bubbles of the size of interest. We are now developing a surface tension model and a vapor pressure model for the 3-D code. Both of these models are based on numerical techniques similar to that used to determine the mass fractions of the different fluids. The surface tension force is a continuumlike quantity, which is a function of the gradient of the mass fraction and is nonzero only at the interface between the two media. From the definition of the vapor pressure, a critical density is defined from which a second volume fraction can be extracted that permits an accurate determination of the amount of condensation and/or vaporization.

[Sponsored by ONR] ■

An Efficient Method for Solving Flows Around Complex Bodies

A.M. Landsberg and J.P. Boris
Laboratory for Computational Physics and Fluid Dynamics

Computational methods for efficiently solving the flow field around ships and submarines can aid the Navy in design and operation. However, the methods that are available require prohibitively large amounts of computer memory and CPU time. Therefore, the LCP&FD has developed an extremely efficient method to solve the unsteady, three-dimensional flows over complex bodies by using massively parallel computers. This method is being applied to solve the unsteady flow field and stack gas trajectories over the helo landing deck of the Navy's DDG51 destroyer.

Computational Method: The virtual-cell-embedding (VCE) method is a new capability for resolving complex geometries on a structured, orthogonal grid with little sacrifice in speed or memory. This method was incorporated into an efficient flux-corrected transport (FCT) algorithm [1] and packaged together in a parallel program, FAST3D. This program is a three-dimensional unsteady flow solver and runs on a vector computer (Convex C210) and a high performance parallel computer (32-node Intel iPSC/860 Touchstone) interchangeably.

In order to compute the unsteady flow field around complex three-dimensional geometries, an accurate method to resolve the body is required. Unstructured grid methods and adaptive gridding methods for structured grids are two common techniques to resolve complex geometries. These methods require large amounts of memory and are computationally expensive; however, in contrast, the VCE method requires little extra memory and CPU time to define the shape of a body accurately.

The VCE method greatly increases the accuracy of the flow solution around complex geometries when using a structured orthogonal grid. When using a structured orthogonal grid without the VCE method, a "staircase" effect is created on smooth bodies not aligned with the computational grid since a cell with rectangular edges must be either inside or outside of a body. However, with the VCE method, cells may be fully outside the body, fully inside the body, or partially inside the body. It is the partially obstructed cells that require special treatment. Thus, the VCE approach only refines or subdivides those cells next to the body. The term "virtual" is used since the subcells embedded within a cell are not stored in memory and therefore are not integrated in the flow solution. The VCE method incorporated into FCT produced accurate results when tested on a series of two- and three-dimensional problems to validate the approach.

DDG51 Computations: Development of a parallel, efficient method to solve complex three-dimensional flows allows a wide range of problems to be handled. The DDG51 computations are examples of a problem that currently uses FAST3D and could have been done no other way [2]. The DDG51 destroyer geometry is shown in Fig. 7. This geometry was obtained from a CAD package that constructed the shell of the ship with a series of plates. From this figure, some important features can be seen. The helicopter landing deck is the square aft section of the ship. There is a several meter

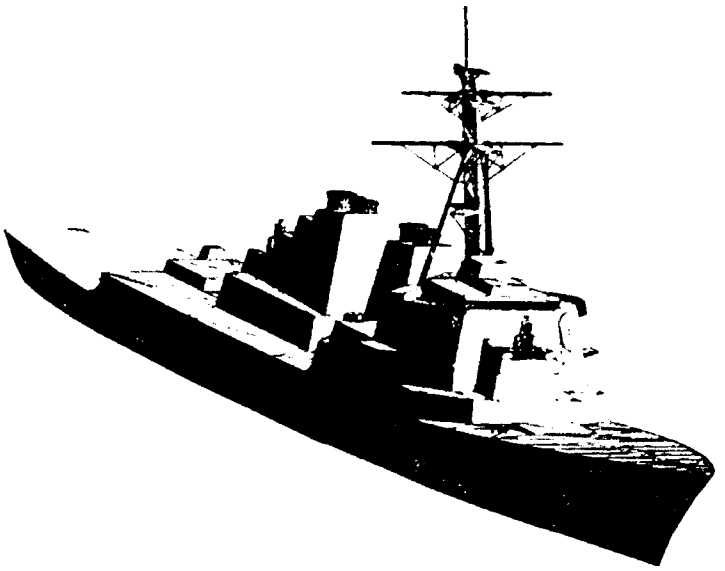

Fig. 7 -- Geometry of DDG51 destroyer

Fig. 8 Contours of temperature (top figure) and transverse velocity (bottom figure) over the DDG51 destroyer in a headwind. The high temperature regions are due to exhaust gases from the engine stacks. The unsteady flow solution with recirculation regions was computed on an Intel iPSC/860 parallel computer.

drop to the landing deck, which can lead to vortex shedding over the deck. Additional areas of interest are the engine stacks—approximately at midship—and one small stack near the helo landing deck. The exhaust gases from these stacks may possibly recirculate back towards the landing deck or prevent a possible approach to the landing deck. The revelant flow features, shown in Fig. 8, are the unsteady flow field with recirculation regions and the high temperature exhaust gas trajectories. As seen from the transverse velocity contours, large regions of

unsteadiness exist near the surface of the ship. However, the temperature contours for this test case do not indicate a problem with exhaust gases impinging on the landing deck. The effect of buoyancy on the stack gases and the effect of a nonuniform inflow velocity profile on the turbulence in the flow are also being analyzed. The results from these computations are being used to evaluate design alternatives and identify the existence of adverse flow conditions.

Summary: This new, efficient, parallel method solves the unsteady flow around truly complex three-dimensional geometries. By coupling this new computational method with high performance parallel computers, the time to solve these highly complex problems is reduced by over an order of magnitude, thus producing results literally overnight.

[Sponsored by DARPA and ONR]

References

1. E.S. Oran and J.P. Boris, **Numerical Simulation of Reactive Flow** (Elsevier, New York, 1987), Chap. 8.

2. A.M. Landsberg and J.P. Boris, *Naval Ship Superstructure Design: Complex Three-Dimensional Flows Using An Efficient, Parallel Method*, in preparation for High Performance Computing: Grand Challenges in Computer Simulation, sponsored by the Society for Computer Simulation, Arlington, Virginia (1993). ■

Ocean and Atmospheric Science and Technology

Real-Time SAR Processing for Polar Ice Applications and Research

I. Jurkevich, C.S. Lin, and S.A. Mango
Remote Sensing Division

A system called SARCOM, Synthetic Aperture Radar Communications System, has been developed by the NRL Remote Sensing Division for the Navy and the National Oceanic and Atmosphere Administration (NOAA) Joint Ice Center in Suitland, Maryland. SARCOM provides a real-time operational demonstration of the transmission of high-resolution microwave imagery of polar ice regions acquired by spaceborne Synthetic Aperture Radars (SAR) over a bandwidth-limited satellite communication link. System design, implementation, and testing are discussed. The system became fully operational in March 1992.

Background: Forecasting ice conditions in polar regions is of utmost importance on long- and short-time scales. On long-time scale, the global ice cover has a decisive influence on the Earth's climate. On the scale of a few days, detailed knowledge of ice state in a specific region is crucial for any human activity to be performed in that region. At the present time, the use of optical and infrared sensors for timely ice forecasting is limited by high cloud cover and long periods of darkness. The development of practical spaceborne SARs solves this problem because, at the appropriate radiated wavelengths, SARs are all weather, day/night sensors. However, SARs are also some of the highest data rate, data volume remote sensing systems in existence; therefore, timely distribution of SAR imagery to the forecasters and their customers is restricted by the limited bandwidth of conventional economical communication links. The solution to this problem is data compression, provided the imagery is not degraded in the process.

To investigate these problems and to assist the Navy ice forecasters, specifically the Navy/NOAA Joint Ice Center (JIC), in incorporating this new source of data into their established work, the NRL Imaging Systems and Research Branch undertook a project to provide a real-time applications demonstration of transmitting, over a T1 satellite link, imagery of the Arctic basin generated by spaceborne SARs.

To minimize cost, this effort makes use of the existing NOAA satellite communication link and takes advantage of an agreement between National Aeronautics and Space Administration (NASA) and three foreign space agencies (European, Japanese, and Canadian) whereby a portion of the data gathered by their polar orbiting SARs are, or will be, downlinked at a NASA sponsored facility at the University of Alaska in Fairbanks for exploration by the United States user community. The NASA Alaska SAR Facility (ASF), operated by the Geophysical Institute at the University of Alaska, was developed by the Jet Propulsion Laboratory to receive the raw observations, produce the initial images, and to archive them.

The SARCOM System, located at the ASF and interfaced to its equipment, captures data from ASF and then proceeds to operate autonomously. SARCOM is a special user of the ASF facility since it caters to quick-turn-around data, that is, data that are no older than 6 h from the time of acquisition. This requirement is driven by the needs of the short-time scale forecasting.

System Goals: The SARCOM goals were to provide SAR ice imagery to enhance and expand the ice forecasting capabilities and services of the Joint Ice Center. This imagery, especially the quick-turn-around imagery, would serve as quick forecasting and as synoptic databases for direct support to ships operating in these Arctic regions and for longer term sea ice database for ice modeling and research. These data will be used in research to determine ice concentration; to classify ice types; to determine ice motion and incorporate the kinematics into ice dynamics modeling; and to study the deformation of ice.

System Requirements: The SARCOM System has been designed to accommodate imagery from the following SARs: (1) E-ERS-1 (ESA, launched July 1991), (2) J-ERS-1 (Japan, launched February 1992), and (3) RADARSAT (Canada, to be launched 1994-1995). For these sensors the need for data compression in the SARCOM system is driven by two factors.

(1) the need to transmit in a real-time operation the high-resolution imagery of the SAR sensors with their high data rates of 40 to 60 megabits per second (Mbps); and (2) the constraint imposed by the bandwidth limitation of the communications satellite link, namely 1.33 Mbps maximum. These factors imply the need for data compression techniques with effective compression ratios in the range of 30-to-1 to 45-to-1. If the SARCOM system were to sustain equivalent real-time output image ratio of 10 to 80 Mbps, it had to perform the data compression at a sustained arithmetic rate of 160 to 200 Mflops (million floating point operations per second). The system implemented is now operating at a sustained rate of 260 Mflops.

System Implementation: As a first step in system implementation an exhaustive study was conducted of various data compression/reconstruction techniques in both the spatial and transform domains. For SAR ice imagery, when both the computational load and the fidelity of reconstructed imagery were considered, an adaptive Discrete Cosine Transform (ADCT) was adopted for SARCOM implementation. The transmit end was implemented in a hardware complex shown in Fig. 1. The SARCOM input image data source is an Ampex Digital Cassette Recorder (DCRSi). The system is designed around a high-speed input/output combined computer and bus (an APTEC IOC-24) while the very high-speed numerical processing function is carried out by an Active Memory Technologies distributed array of processors (DAP-610). The SARCOM system uses a DEC Microvax II as a control processor and a user software interface based on the Transportable Applications Executive (TAE). An IBIS 1.1 gigabyte high-speed disk drive (12.5 megabytes per second sustained transfer rates) is used for data staging.

The receiving end, located at the Joint Ice Center, uses a SUN 4/470 workstation and an embedded, specially modified, single board communication computer that, under software control, captures the data and stores it on the host disk. The captured data is subsequently reconstructed to form images using an embedded Sky Computer Skybolt floating point accelerator. These data/imagery are then used by the JIC to enhance ice forecasting activities and to provide ice operations mission support. The end-to-end system has been successfully tested by using the commissioning phase of ERS-1 observations.

Demonstration: Figure 2 shows an example of a polar ice application using SARCOM to provide a real-time demonstration of supporting ice mission activities and research at a campsite on the pack ice in the Arctic Basin. After the ERS-1 image formation processing at the Alaska SAR Facility, this scene was handled by SARCOM in real-time to get the imagery from the ASF to the JIC. The JIC was then able to satellite link and facsimile the scene to the LEADEX team at the camp on the pack ice so that they could *see* the ice formations in the immediate vicinity of the campsite as well as to *see* the ice camp in the context of the regional ice formations.

The full scene shown is from ESA's ERS-1 SAR that is a C-Band (5.66 cm wavelength) side-looking imaging radar operating in a stripmap mode with a strip center of 23° incidence angle. The scene is a nighttime image on March 26, 1992, 6:49 GMT, of multiyear pack ice in the Beaufort Sea. The region is off the continental shelf in deep water. The scene is displayed at a map scale of 500,00:1 and measures 100 km-by-80 km with a ground resolution of approximately 30 m.

The smaller inset image in the upper right corner of Fig. 2 is a 16 × 16 zoom of the 1.6 × 1.6 km ice region containing the LEADEX Ice Camp. The three, bright collinear *pixels*, along the direction from the upper left to the lower right, are the radar echoes from corner reflectors placed on the ice and designed to delineate the temporary runway established on the ice pack for the campsite. Each pair of corner reflectors is separated by an approximately 200 m area.

Summary: With the implementation of the SARCOM system, agencies responsible for forecasting ice conditions will, for the first time, have access to fresh observations on a very timely basis. Furthermore, they will have

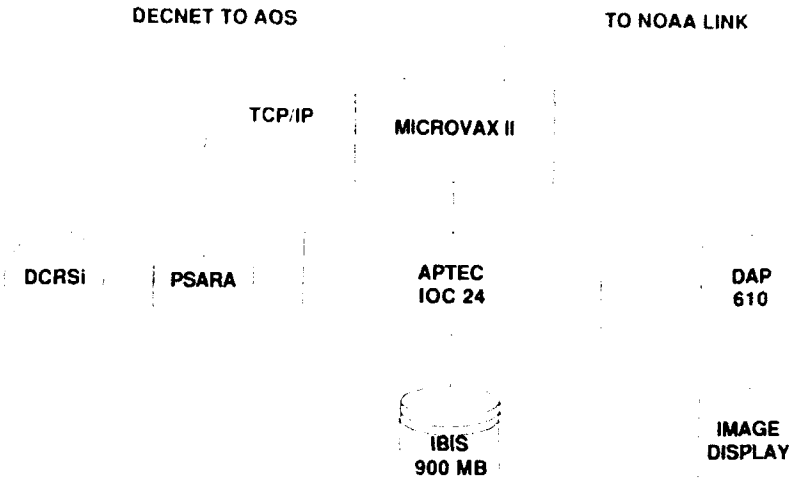

(a)

(b)

Fig. 1 — (a) SARCOM block diagram; (b) a view of the SARCOM system

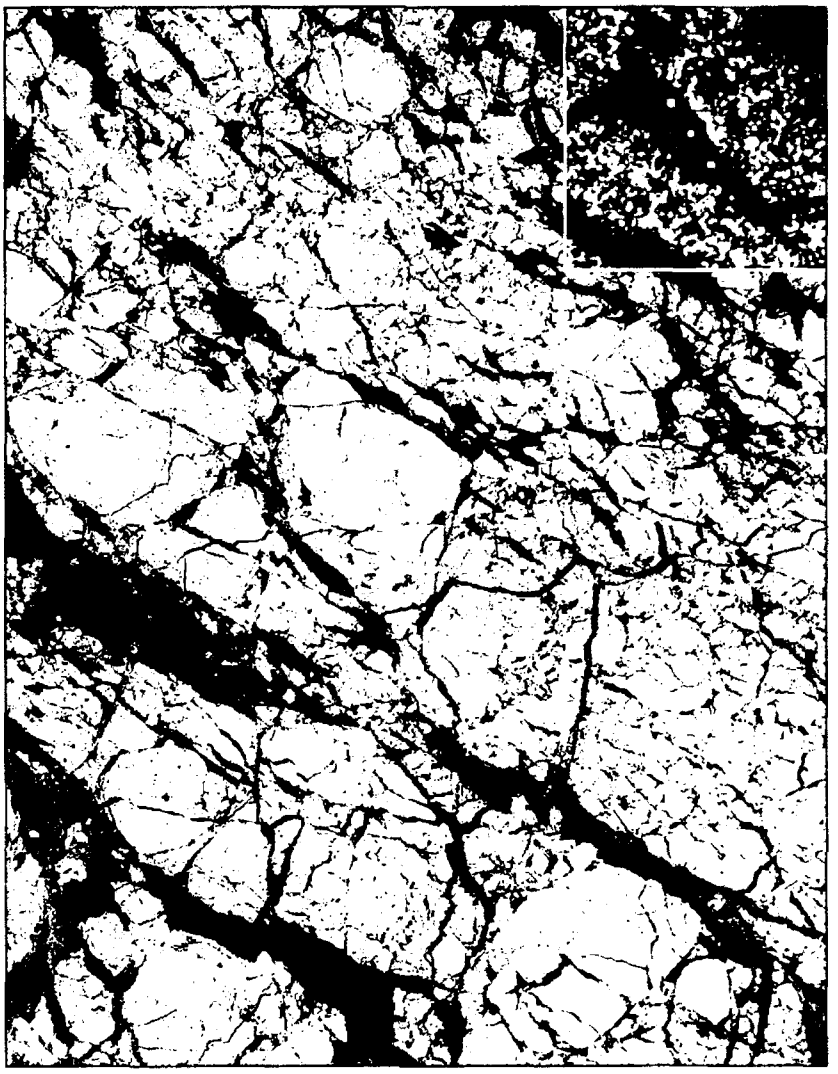

Fig. 2 — ERS-1 image of the LEADEX Ice Camp area

access to data under all weather conditions and at all times of the day. As a by-product of this project, sophisticated data compression techniques were developed that are usable for image communication under a variety of conditions.

Acknowledgments: The significant efforts of K. Hoppel and M. Grunes of the Bendix Field Engineering Corporation are gratefully acknowledged. As members of the NRL team, they implemented and validated the SARCOM system.

[Sponsored by the Office of the Oceanographer of the Navy, SPAWAR, and NOAA]

References

1. S.A. Mango, *Data Compression for Spaceborne SAR Imagery - The SARCOM System*, NRL Review, NRL Publication 123-2631, pp. 144-149, July 1989.

2. S.A. Mango, "Alaska SAR Facility (ASF) SAR Communications (SARCOM) Data Compression System," *Proc. of the NASA Scientific Data Compression Workshop*, Snowbird, Utah, May 1988, NASA Conference Publication 3025, pp. 393-417. ■

Ocean Wavenumber Spectra Measurements

J.A.C. Kaiser and G.J. Lindemann
Oceanography Division

High spatial resolution remote sensors of ocean features largely respond to surface roughness elements having length scales less than one meter. For research purposes this roughness should be characterized in a manner independent of the remote sensor, but techniques to do so in this spatial range are virtually nonexistent. One technique, pioneered at NRL [1] has occasionally been used and then in a linear approximate mode. Recently, by using digital image processing techniques, we have successfully extended the technique. This has been done by using a nearly exact algorithm to obtain wavenumber spectra and other rough-surface statistics. This has allowed us to actually reconstruct the rough surface for input to radar imaging models as weli as to ocean wave/current/surfactant interaction models.

The Technique: Waves on a water surface are visible because they reflect different portions of the variable sky brightness because of their changing slope; our technique quantifies this effect. Figure 3 shows the optical geometry and deployment. A video camera images the water surface from the bow of a ship with a 12-deg field-of-view (fov). Typically a two-to-four meter square is imaged. A second camera with an 8-deg fov images the sky, including the horizon. Also, a Ku-band (15.4 GHz) scatterometer is included to image the same area as the 12-deg fov camera. The video data is recorded on VHS or SVHS recorders, and 1-s averages of the scatterometer output are logged on a personal computer (PC). Later, the sky and wave video images are converted into two dimensional (2D) arrays by using a frame grabber having an 8-bit resolution.

Processing: The sky camera records the sky radiance field; at each pixel the water camera records the reflected sky radiance plus radiance scattered upward from the water below the surface. The sky radiance is azimuthally averaged and hence is a function of sky elevation angle only. The radiance incident on each pixel of the water camera is a function of sky elevation angle, slope of the water surface, and incidence angle (through the reflectivity). The upwardly scattered radiance is treated as a constant and can be estimated from the ocean optics literature for various water mass types [2].

These radiance balances are represented by two highly nonlinear equations; these are solved at each of the 64,000 pixels of the water image by an interactive technique on a Silicon Graphics Personal Iris 4D/35 that requires about 10 s/image. The solution yields the slope at each pixel and is calculated to within 0.17 mrad. The output is then a map of the slope in the look direction spanning the image. From this map, wavenumber spectra or slope histograms can be calculated, or the elevation map of the original surface can be reconstructed.

Sample Results: During the NRL High Resolution ARI Experiment, September 1991, we crossed an extensive surfactant slick and a current convergent front. Figure 4 illustrates the time series of Ku-band cross section measured as we crossed these features, typical slope cuts across the images, the slope histograms (uncorrected for geometrical distortion), and 20 individual slope spectra across each image. The sets of wave data are keyed into the proper points on the Ku-band data. Frame 4 is in the slick, 7 represents the "unaltered" ambient sea, 15 is in the roughest part of the front, and 21 is a smoother region adjacent to the front.

In the slicks (frames 4 and 21) the slope varies less across the images, and the slope histograms are clearly narrower and more peaked than in the "unaltered" ambient frame, and the slope spectra show less energy than in the ambient. In the rough part of the front the slope variability is the largest, hence the broadest slope histogram and the highest spectral energy. All of these observed behaviors are generally consistent with the theory of wave/current/surfactant interactions theory.

At the beginning of this article we referred to earlier work [1], which assumed the wave slope was nearly a linear function of the apparent wave brightness. We tested this assumption

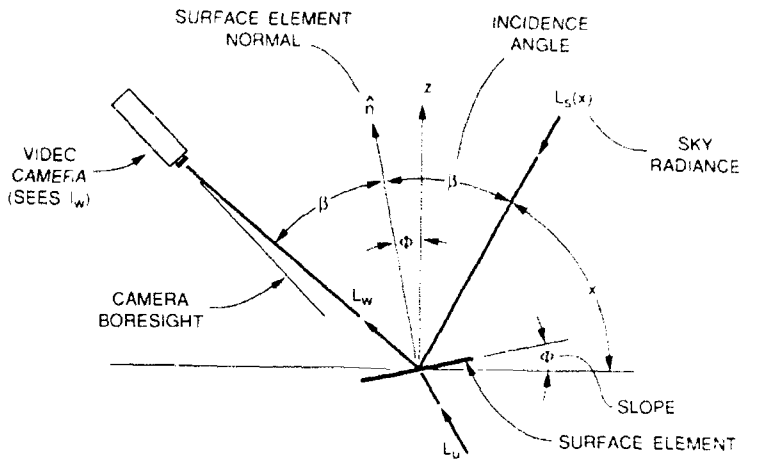

(a)

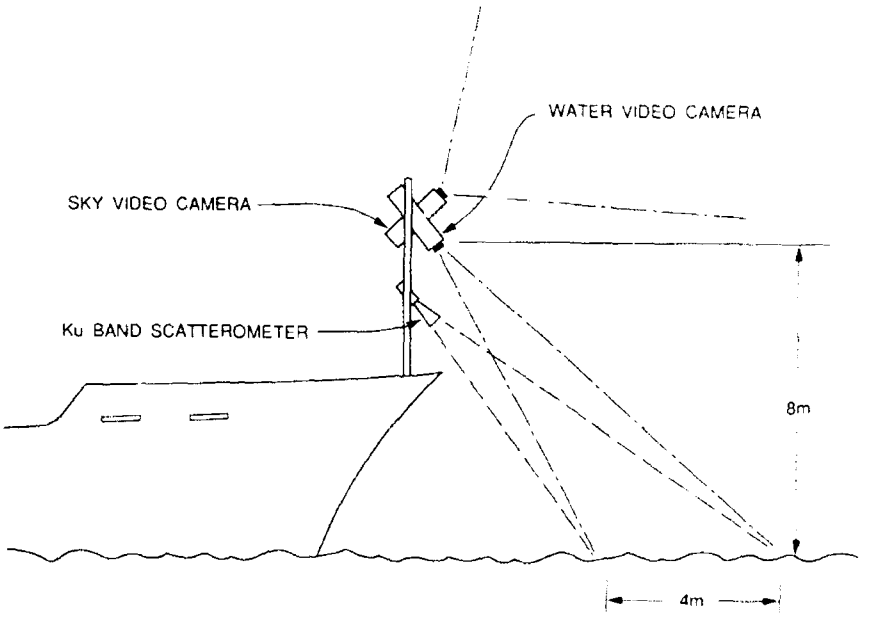

(b)

Fig. 3 – (a) Viewing geometry of the water imaging camera showing the path of the sky radiance and underwater radiance to the camera. (b) Deployment of the water and sky camera and Ku-band scatterometer on the bow of the research ship.

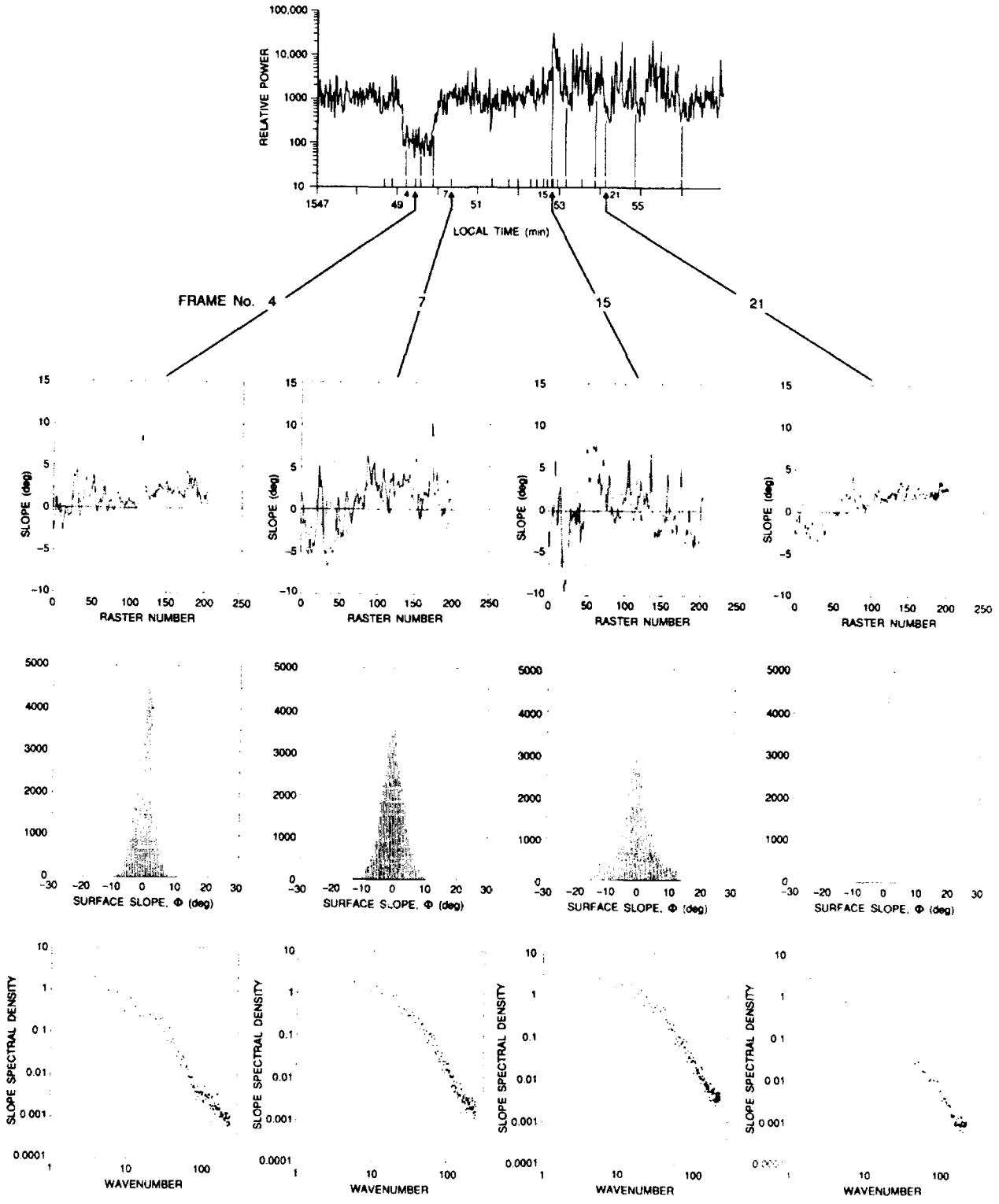

Fig. 4 — A time series of the Ku-band scatterometer output (relative cross section at 45° incidence and vertical polarization) as the slick (at frame 4) and the convergent front (frames 15 to 21) were crossed. Below are water slope cuts across an image, slope histograms, and slope wavenumber spectra at the slick, in an "unaltered" ambient sea, in the rough portion of the front and in the smoother region past the front.

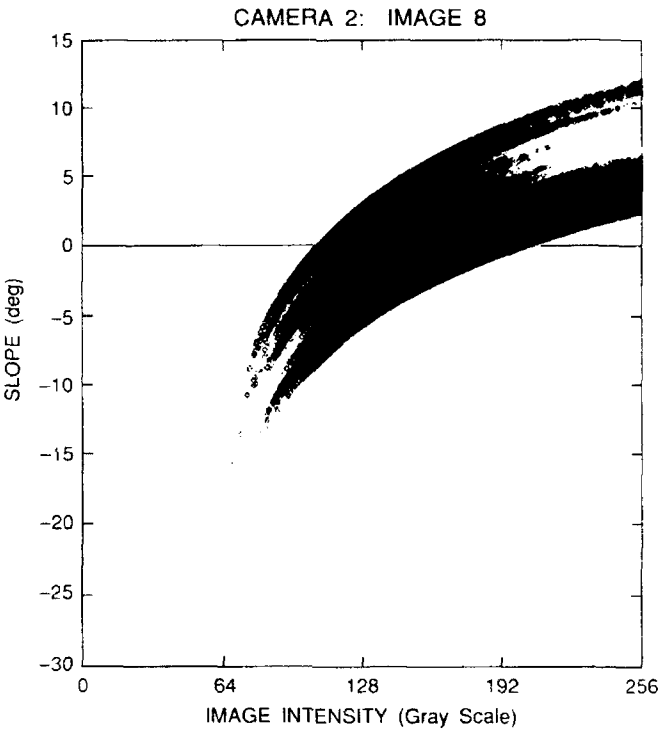

Fig. 5 — The original processing of data from this technique assumed that the wave image brightness at each point was nearly linearly proportional to the water slope at that point. This plot is the result of a more accurate solution of the radiance balance equations for one image and clearly shows that the linear assumption is not valid.

in Fig. 5 and as is evident, the slope is not a linear function of the apparent brightness.

This work has proven quite valuable in testing radar imaging models against "real world" data. We plan to extend this work by determining the directionality of the individual waves in the image by using the gradient of the brightness and calculating the two components of the slope vector at each pixel. This will allow directional histograms and directional wavenumber spectra to be determined.

[Sponsored by ONR]

References

1. D. Stilwell, "Directional Energy Spectra of the Sea from Photographs," *J. Geophys. Res.* **74**, 1974-1986 (1969).

2. R.W. Austin, "The Remote Sensing of Spectral Radiance from below the Ocean Surface," in *Optical Aspects of Oceanography*, N.G. Jerlov and E. Steemann Neilson, eds. (Academic Press, London and New York, 1974).

Numerical Modeling of the Atmosphere and Ocean

R.M. Hodur
Marine Meteorology Division

Many U.S. Navy operations require a detailed description of the present and future status of the atmosphere and of the ocean. Variations of such parameters as the wind, temperature, and moisture, for example, can be critical to mission planning and weapon performance. These variations are often quite local and can be caused by such phenomena as fronts, thunderstorms, sea breezes, and terrain. Other phenomena, such as hurricanes, can have a

profound influence on the atmosphere and can dramatically affect the ocean through exchanges of heat, momentum, and moisture across the air and ocean interface. Recent advances in computer technology, mesoscale meteorology, and numerical methods have allowed us to make realistic numerical simulations of many of these phenomena. Continued research will allow us to perform these types of simulations routinely and in a timely manner for support of military operations.

Computer models: Separate, three-dimensional (3-D) numerical models of the atmosphere and the ocean have been developed and integrated into the Coupled Ocean/Atmosphere Mesoscale Prediction System (COAMPS) by NRL. The atmospheric model solves the nonhydrostatic set of equations for the wind, temperature, pressure, moisture, and the turbulent kinetic energy (TKE) over a discrete grid. The treatment of moisture allows us to make forecasts of water vapor, cloud droplets, raindrops, ice crystals, and snowflakes. The TKE prediction allows for subgrid scale mixing of the prognostic variables, particularly important in the planetary boundary layer. The ocean model solves the hydrostatic equations of motion for the ocean currents, temperature, salinity, and the height of the free surface. The TKE is diagnosed for subgrid scale mixing processes. The models are fully coupled at the air and ocean interface. At every time step, the diagnosed surface fluxes as well as the precipitation reaching the surface are used to diagnose the changes of the near-surface momentum, temperature, moisture, and salinity fields.

Tropical Cyclone Simulation: Probably the most striking example of air and sea coupling takes place within a tropical cyclone. Vast amounts of heat and moisture are continuously drawn from the ocean to feed the convection associated with the storm. The atmospheric cyclonic circulation imparts a stress on the ocean that induces upwelling and very strong mixing within the upper few hundred meters of the ocean. The combination of these two effects leads to a strong cooling of the sea surface temperature (SST) in the vicinity of the eye of the tropical cyclone. This cooling is a result of relatively cold water being brought up to the surface by the mixing and upwelling. Figure 6 is a 3-D rendered image of the clouds and rain from a tropical cyclone simulation made with COAMPS. As it is often observed, relatively shallow convective clouds are found in the low levels at the outer periphery of the storm.

Fig. 6 — Three-dimensional rendering of cloud water, ice crystals (gray shades), and raindrops (red) for COAMPS tropical cyclone simulation. Green represents the ocean surface. Grid volume measures 600 km on each side and 18 km in the vertical.

Much deeper convective clouds producing heavy rainfall spiral in toward the eye while a flat cirrus canopy covers the system. Figure 7 shows the induced SST changes from the ocean model. A cooling of up to 8 K is found near the location of the eye. This cooling is found to have a negative impact on further storm development.

Simulation of Convective Storms: Strong convective storms are common in many parts of the world. These storms pose a particularly strong threat to aircraft because of the strong turbulence within the cloud and the strong wind shears they can create near the surface. Some of the most severe weather is associated with the strong downdrafts that are produced by heavy precipitation. Part of the precipitation evaporates as it falls below the cloud base and leaving a cold pool of air under the convective cloud. Figure 8 shows a 3-D rendered image of a COAMPS simulation of a convective storm

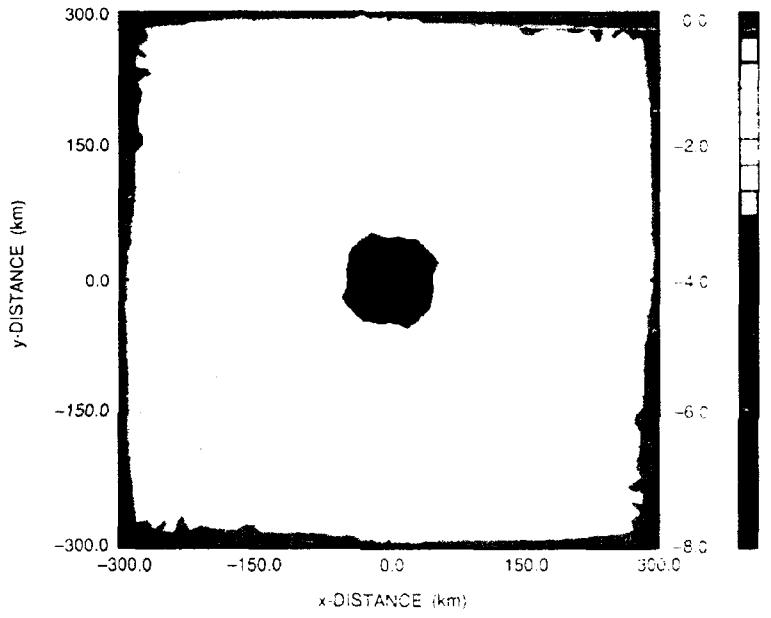

Fig. 7 – COAMPS forecast of sea-surface temperature cooling (K) induced by tropical cyclone fixed in center of grid

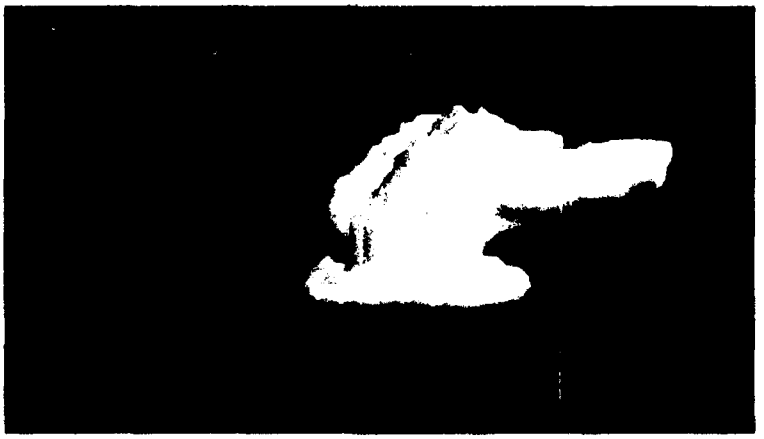

Fig. 8 – Three-dimensional rendering of cloud water, ice crystals (gray shades), and raindrops (red) for COAMPS convective storm simulation. Green represents the surface. Grid volume measures 40.5 km on each side and 13.2 km in the vertical.

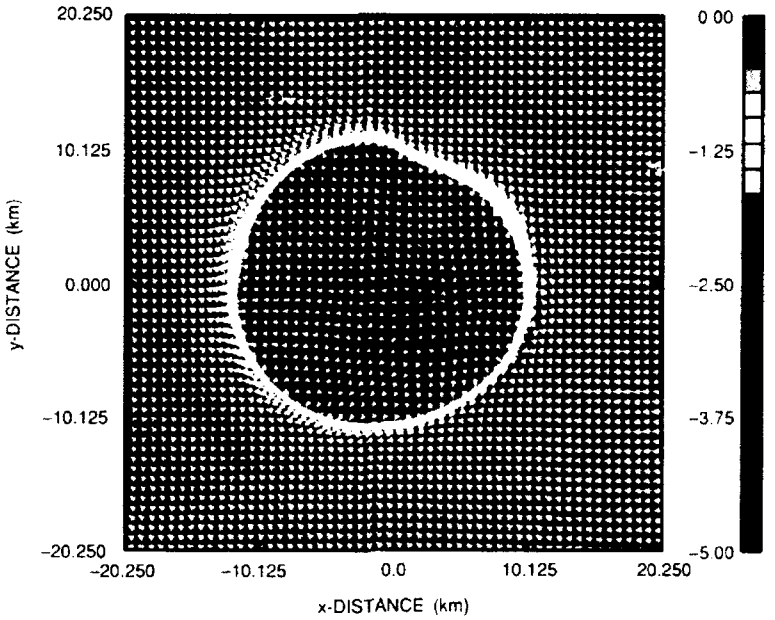

Fig. 9 — COAMPS forecast of 150 m potential temperature perturbation (K) and wind distribution for convective storm simulation. Wind vectors are scaled according to speed with the longest vector representing 14 m/s.

using only the atmospheric model. The cloud that has grown to a height of about 10 km, shows the characteristic flattening of the cloud top and a strong rainshaft falling from the cloud to the ground. The COAMPS forecast of the near-surface temperature and wind distribution for this system (Fig. 9) shows a pool of air under the storm up to 5 K colder than the surrounding air. There is also a strong horizontal wind shear at the leading edge of this cold pool. This is in excellent agreement with observations.

Summary: By using the most advanced computer technology and state-of-the-art numerical methods, we have developed a numerical prediction system capable of simulating many atmospheric and oceanic mesoscale phenomena. We are now working on implementing much of this technology developed for COAMPS into our operational prediction system for continued support of military operations.

[Sponsored by ONT and Oceanographer of the Navy] ■

Optical Science

Fiber-Optic Chemical Sensor for Copper(I) in Water

K.J. Ewing and I.D. Aggarwal
Optical Sciences Division

A.M. Ervin and R.A. Lamontagne
Chemistry Division

Introduction: Currently there is a great deal of interest in the use of optical fibers for remote, real-time measurement of chemical species [1]. Visible, infrared, and Raman spectra of samples that are inaccessible via standard techniques can be collected through the use of optical fibers. A remote sensor of this type has broad applications in the Navy as well as in the Department of Energy (DoE) and the Environmental Protection Agency (EPA) for both process and pollution control and monitoring. Due to heightened environmental awareness, both DoD and DoE are committing to the closing of many sites around the country where the ground and groundwater has been contaminated with hydrocarbons, chlorinated hydrocarbons, and heavy metals. The Navy is particularly interested in technologies that enable remote monitoring of pollutants in bays, rivers, and harbors frequented by Navy surface ships. Conceivably, fiber-optic chemical sensors offer the ability to monitor a variety of pollutants, such as heavy metals and hydrocarbons, which may be accidentally released by naval ships, thereby warning naval personnel of possible environmental contamination.

Source of Copper(I) Contamination: Select naval surface ships currently use a copper(I)-based paint on ship hulls to act as an antifouling agent, i.e., to keep attachment of sea growth on the ship hull to a minimum. A ship sitting in a harbor slowly releases copper(I) into the water, and, if there is a weak current or a large ship population in the area, the level of copper in the water can reach parts per billion (ppb) or higher levels. These low levels are significant since copper is known to exhibit toxic behavior towards marine organisms at concentrations as low as 1 ppb [2]. To correctly assess the environmental impact of naval vessels, it is important to be able to monitor the copper released by naval ships rapidly and with sufficient sensitivity.

Copper(I)-Specific Fiber-Optic Sensor: A copper(I)-specific fiber-optic sensor is being developed at NRL to monitor potential copper(I) contamination in the marine environment. The sensor is prepared by first immobilizing a colorimetric reagent called bathocuproine (bcp) onto porous polystyrene beads. A second polymer, Nafion, is then used to immobilize the bcp beads on the end of a bifurcated optical fiber. When the sensor is exposed to a copper(I) solution, the metal complexes with the immobilized bcp and an intense orange color is produced. By launching light from an argon ion laser (λ = 488 nm) down the fiber, the amount of light reflected from the polymer/reagent sensor ball can be monitored. As the copper(I)-bcp complex is formed, light from the laser is absorbed, resulting in a decrease in the amount of reflected light to the detector. Figure 1 plots the relative percent reflectivity vs time. This plot shows that after introduction of copper(I) into the equilibrated system, light is absorbed due to formation of the copper(I)-bcp complex with a concomitant decrease in the percent reflectivity. The data indicate that the rate of decrease in the percent reflectivity is proportional to the concentration, of copper(I), i.e., the lower the copper(I) concentration, the slower the rate of decrease in percent reflectivity. By plotting the slope of each line in Fig. 1 between 120 and 240 s vs the concentration of copper(I), a linear working curve is obtained as shown in Fig. 2. This curve indicates that the rate of decrease in the reflectivity is proportional to the concentration of copper(I) in solution, with a y-intercept value very close to zero at zero copper(I) concentration.

The aforementioned sensor exhibited a detection of approximately 1 ppm. In an effort to achieve a lower limit of detection, the sensor was modified. Visual examination of the previous sensor head revealed that approximately one-third of the copper-bcp complex formed was out of the optical path and therefore not detectable. To eliminate this problem, the size

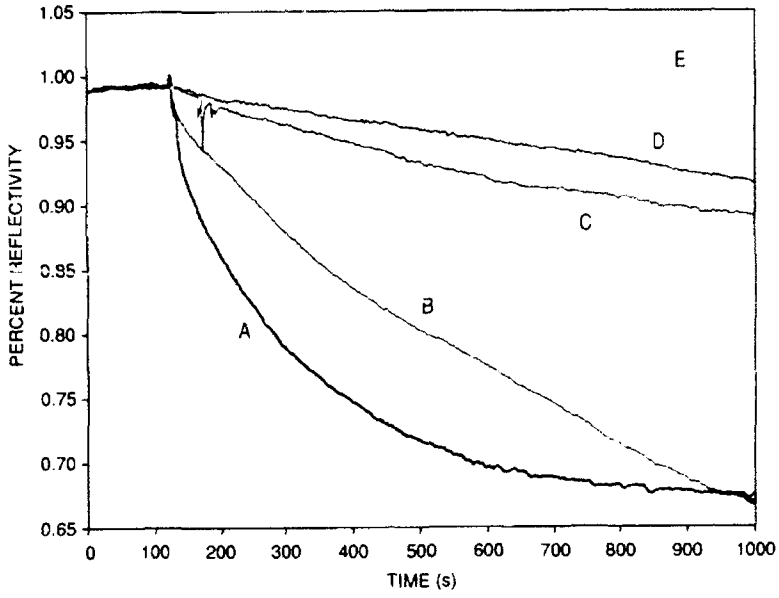

Fig. 1 — Plot of the percent reflectivity with respect to time for a series of different concentrations of Cu(I) (A-D) and Cu(II) (E). A = 43 ppm, B = 22 ppm, C = 6 ppm, D = 3 ppm, and E = 21 ppm (curve E was generated by monitoring the power change after sensor was exposed to a Cu(II) solution).

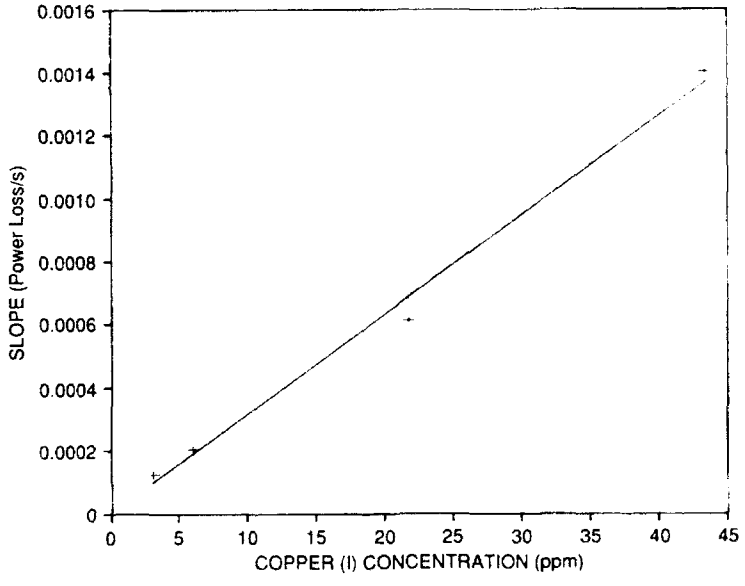

Fig. 2 — Plot of the slope of the percent reflectivity curve with respect to time between 120 and 240 s vs Cu(I) concentration. The line shown was calculated from the linear regression of the data points.

of the polymer/reagent ball was reduced to ensure that most of the copper(I)-bcp complex would be formed in the optical path. Figure 3 plots the percent reflectivity vs time curves for copper(I) concentrations of 325 and 650 ppb. Preliminary data suggest that the modified fiber-optic sensor can detect parts-per-billion concentrations of copper(I). The goals of continuing research on this sensor include acquisition of lower detection limits; establishment of methodology for the reproducible construction of the sensor head; investigation of potential interferences; and study of chemical stability and reversibility issues.

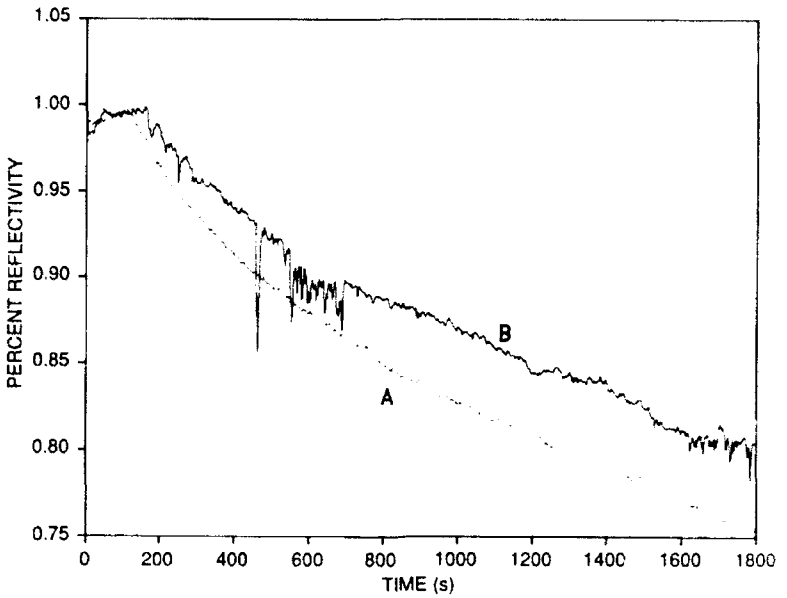

Fig. 3 — Plot of the percent reflectivity with respect to time for Cu(I) concentrations of A = 650 ppb and B = 325 ppb

Future Trends: As previously stated, DoD, DoE, and the EPA will be required to close a number of facilities around the country that currently contain hazardous materials in the ground and groundwater. To clean up these sites, identification, concentration, and exact location of chemical contamination needs to be accurately determined. Fiber-optic chemical sensors based on absorption, infrared, and Raman spectroscopic techniques are uniquely suited for determination of heavy metals as well as chlorinated hydrocarbons and fuels leached into the soil, groundwater, and marine environment.

[Sponsored by ONT]

References

1. O.S. Wolfbeis, ed., *Fiber Optic Chemical Sensors and Biosensors*, Vols. 1 and 2 (CRC Press, Boston, 1991).

2. E.W. Davey, M.J. Morgan, and S.J. Erickson, "A Biological Measurement of Copper Complexation Capacity of Sea Water," *Limnol. Oceanogr.* **18**, 993 (1973). ■

Nanochannel Glass Technology

R.J. Tonucci and A.J. Campillo
Optical Sciences Division

Nanochannel Glass Materials: We have developed a method of producing a submicron glass matrix [1], called nanochannel glass (NCG) that can be used as a mask or as a host for optoelectronic or semiconductor materials. The glass consists of large numbers ($> 10^6$) of uniform parallel pores or channels arranged in regular arrays, with packing densities as high as 10^{11} per square centimeter. The pores are highly uniform and can be made as small as tens of nanometers in diameter. The fabrication of these NCG materials is not unlike the way optic fibers and microchannel plates are made. As shown in Fig. 4(a), construction of an NCG array starts by insertion of an acid etchable core rod into an inert glass tube whose inner dimensions match the outer dimensions of the rod. The tube-rod composite is reduced to a fine filament by a high-temperature vacuum drawing process. The filaments are then stacked to form a large bundle and redrawn again into a fine

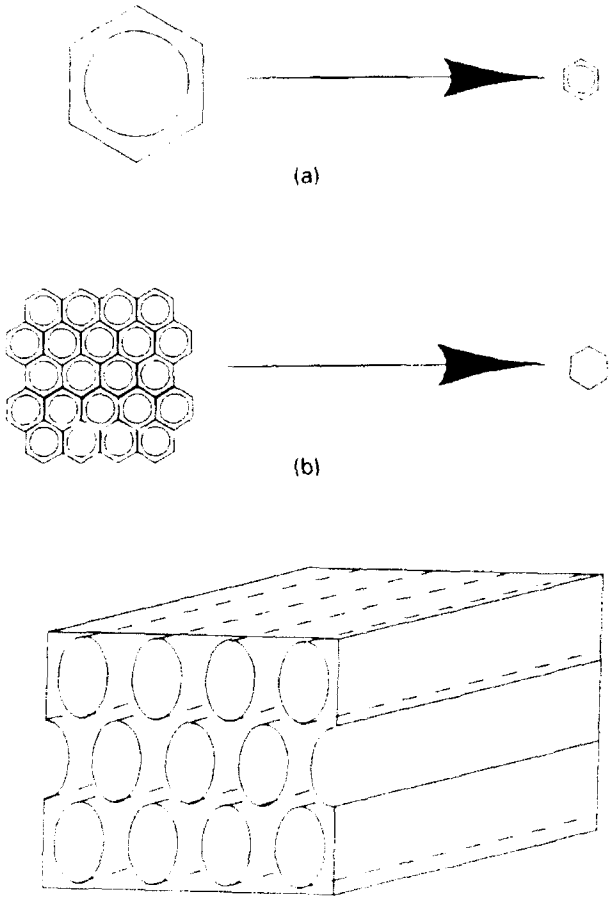

Fig. 4 — Schematic diagram for the fabrication of nanochannel glass arrays. (a) Reduction in diameter of cladding and core glass to a fine filament by vacuum draw process. (b) Stacking of filaments to form an array bundle. The bundle is then drawn, reducing the overall diameter to that of a filament again. The filament bundle can then be restacked and redrawn until the desired diameter of the core glass is achieved. (c) A magnified view of a channel array after acid etching.

filament (Fig. 4(b)). The process is continued until the desired channel diameter and total number of array elements is achieved. The core glass is then etched away leaving behind an array of hollow channels imbedded in a glass matrix as shown in Fig. 4(c). Wafers with 10^6/33 nm cores on 73 nm spacings have been fabricated, two orders of magnitude smaller than reported previously, and arrays with channel diameters of 10-15 nm are anticipated shortly. The nanochannels are consistently round and the array positioning/spacing is very regular (see Fig. 5). Nonuniform patterns and connected

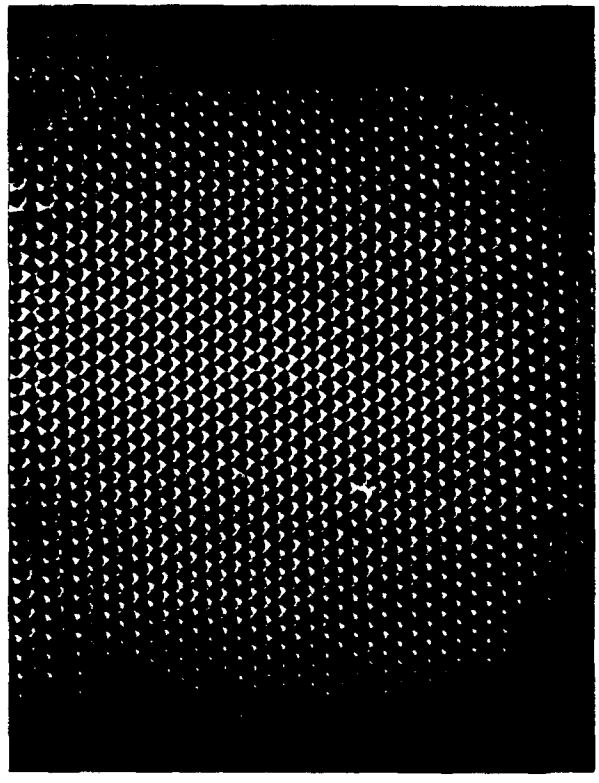

Fig. 5 — A scanning electron microscope micrograph of a 450 nm diameter channel array arranged in a hexagonal close packing configuration

structures can be fabricated by packing monofilaments of each type of glass prior to the first draw. This process greatly reduces the interdiffusion of glasses during the high-temperature draws since the bundling process essentially replaces the need for the first draw.

Research Efforts: Research efforts draw on a multidisciplinary base of technical expertise. NCG materials development and fabrication have been performed in the Optical Sciences Division at NRL and at Ni-Tec, a division of Varo Inc., located in Garland, Texas. Chemical vapor deposition and molecular beam epitaxy depositions of semiconductor materials into NCG arrays are accomplished with the collaborative efforts of the Chemistry and Electronics Science and Technology divisions at NRL. Lithographic techniques using electron cyclotron resonance etching, ion implantation, electron beams, and materials transport to define ultrasmall structures and potential devices require the facilities of the Nanoelectronics Processing

Facility, Condensed Matter and Radiation Sciences Division, and other divisions. In all, more than 21 people in 6 divisions are currently involved in research involving nanochannel glass materials.

Nanochannel Glass Applications: The high-temperature stability of NCG array structures makes them ideally suited as optically transparent templates for the deposition of semiconductor materials. The channels of the glass confine the volume of deposited semiconductor material into that of an ultrafine wire or dot. Because of the transparency of the glass array, linear and nonlinear direct optical measurements on a large variety of semiconductor and insulating materials can easily be made.

Electro-optic studies with liquid crystals in small diameter channel arrays take advantage of the insulating properties of the glass. The nonlinear optical properties of these systems and switching times as a function of channel diameter and applied fields are currently being studied.

The nanochannel glass has also been used as a lithographic mask to define regions for the formation and/or growth of semiconductor materials. When the mask is placed in front of a wide photon or particle beam, it produces an array of narrow beams capable of producing patterns with very small feature sizes. As the mask is translated relative to a resist-coated substrate, an array of millions of identical circuit elements are fabricated simultaneously. This represents a breakthrough in parallel patterning with nanometer resolution.

Quantum wells and superlattices can be laterally patterned with NCG structures. High-energy ion beams passing through the channels in NCG wafers are used to define both positive and negative masks. The ions pass into the quantum confined regions and stop where they transfer the pattern contained within the mask. Annealing of the samples after ion implantation removes the majority of the damage and returns the system to a lattice matched condition.

Research in magnetic materials, diamond patterning, and biological applications are but a few of the other areas currently being developed using the NCG. The rapid progress and diversity of research areas demonstrated above would not be possible without the support of personnel and utilization of the multidisciplinary environment and resources available at NRL.

[Sponsored by ONR and DARPA]

Reference

1. R.J. Tonucci, B.L. Justus, A.J. Campillo, and C.E. Ford, "Nanochannel Glass Arrays," *Science* **258**, 783 (1992). ■

Intermolecular Vibrational Dynamics in Liquids

D.P. McMorrow and J.S. Melinger
Condensed Matter and Radiation Sciences Division

Intermolecular dynamics of Raman-active modes in liquids traditionally have been investigated using the frequency-domain technique of spontaneous light-scattering (LS) spectroscopy. Because of the intense central Lorentzian feature present in the LS spectra of liquids, however, the extraction of detailed dynamical information on vibrational resonances below 100 cm^{-1} has proven difficult. Femtosecond nonlinear-optical (NLO) spectroscopies exhibit significant advantages over spontaneous scattering techniques for probing the Rayleigh-wing region of LS spectra. Using femtosecond NLO techniques in conjunction with Fourier-transform methods [1,2], we have developed a powerful spectroscopic tool for probing the low-frequency spectral region from $\sim 1 - 400$ cm^{-1}. This technique reveals previously unobserved vibrational features that provide important information regarding the microscopic molecular environment of liquids.

Femtosecond Fourier-Transform Raman (FFTR) Spectroscopy: Nonlinear-optical spectroscopies that are third order in the applied optical field are, in general, quadratic in the nonlinear-optical susceptibility $|\chi^{(3)}|^2$. The $\chi^{(3)}$ spectroscopies that use optical heterodyne detection (OHD), however, provide a significant exception to this rule. With OHD, the detected

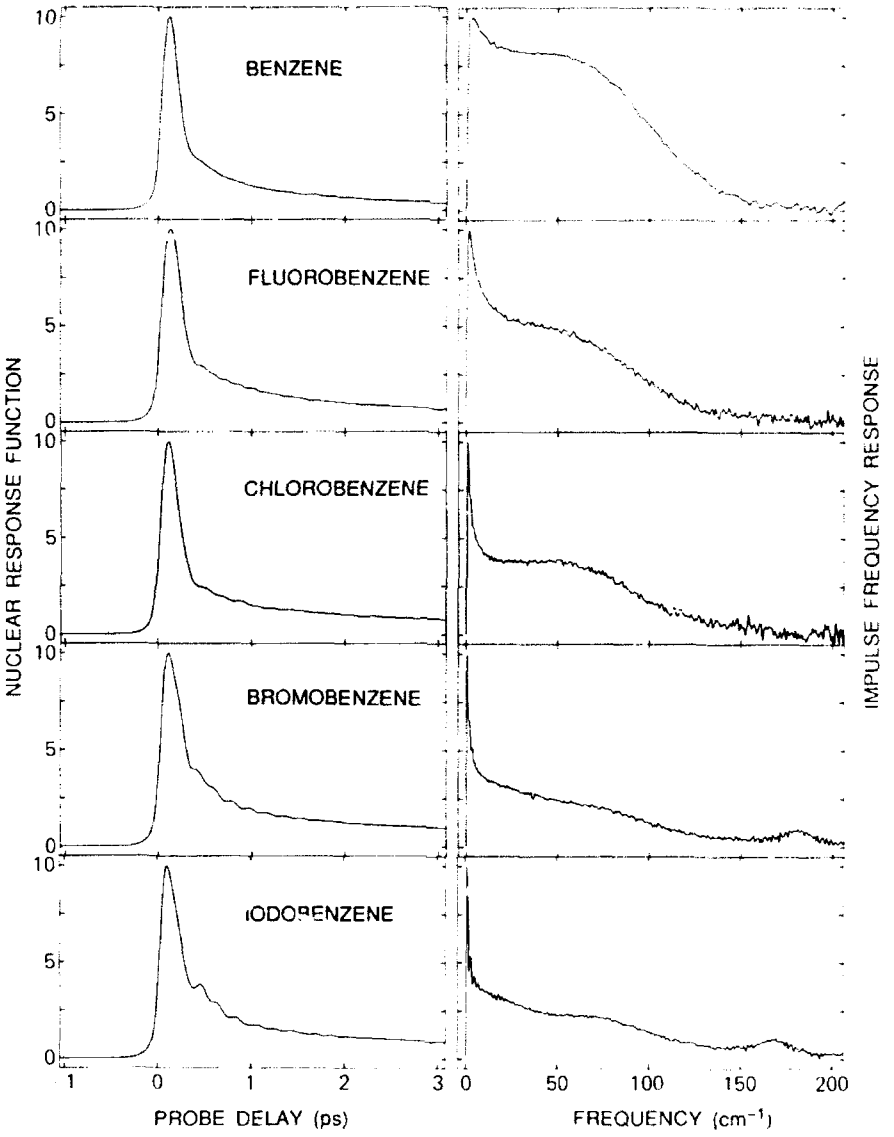

Fig. 6 -- *(left panel)* Nuclear part of the optical heterodyne detected optical Kerr effect transients for the liquids indicated. The nuclear and electronic contributions were separated using the FFTR methods described above [1,2]. *(right panel)* Frequency spectra corresponding to the transients shown. All intensity below $-150\ cm^{-1}$ is of intermolecular origin; the narrow features about $150\ cm^{-1}$ arise from intramolecular substituant wagging modes.

signal is rendered linear rather than quadratic in the NLO impulse response function, and it is linear in both the pump and the probe laser pulse intensities. Linearization of the signal permits the use of powerful Fourier-transform/deconvolution procedures that are generally not possible for $\chi^{(3)}$ spectroscopies. The FFTR method, in particular, results in separation of the nuclear and electronic contributions to the measured transients with no pulse-shape approximations or assumed models required [2] and generates directly the low-frequency NLO Raman spectrum of the material.

Figure 6 shows some typical FFTR results for benzene and several C_{2v} benzene derivatives. The left panel shows the nuclear part of the OHD optical Kerr effect (OKE) transients; the right panel shows the corresponding impulse frequency response functions. The nuclear response functions of Fig. 6 are quite similar in

many respects, with each exhibiting characteristics that are common to numerous molecular liquids investigated to date [1-3]: (1) a finite rise that arises from the molecular moment of inertia; (2) an initially rapid decay that is associated with the rapid dephasing of the inhomogeneously broadened vibrational (librational) ensemble; (3) an intermediate regime characterized by an ~500 fs relaxation: followed by (4) the slower relaxation of the orientational anisotropy.

Anisotropic Librational Motion in C_{2v} Benzenes: A significant advantage of a frequency-domain representation of temporal data is its interpretive value: it is often more straightforward to interpret spectral data than dynamical waveforms. While the transients of Fig. 6 show only subtle differences, transformation into the frequency domain more clearly reveals significant variations between the different liquids. While the benzene and fluorobenzene spectra appear fairly featureless about ~5 cm^{-1}, the bromobenzene and iodobenzene curves show complex structure in this spectral region: each appears to consist of a higher frequency band with a maximum in the 55 to 75 cm^{-1} region and a lower frequency feature around 15 cm^{-1}. Further analysis confirms the presence of two broad, overlapping bands that are not resolvable in the spontaneous LS spectra of these liquids. Figure 7 shows some results. To generate this figure, the diffusive reorientational contributions to the data have been removed, resulting in reduced spectra that are associated with the nondiffusive, inter- and intramolecular vibrational dynamics of the liquids. A distinct bimodal character is especially evident in the bromobenzene and iodobenzene spectra. For the C_{2v} molecules of Fig. 7, the observation of two intermolecular bands can be accounted for in terms of anisotropic librational motion: the higher frequency band is assigned to libration about the axis containing the substituant; the lower-frequency band to libration about an axis perpendicular to the substituant.

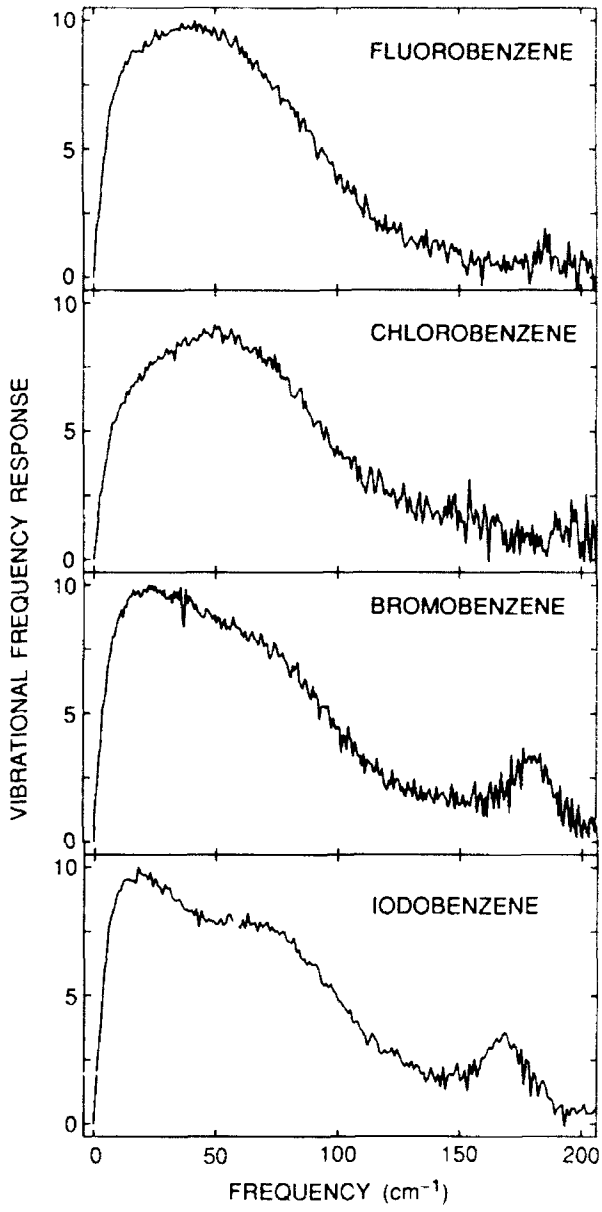

Fig. 7 — Nondiffusive (vibrational) contributions to the frequency spectra of Fig. 6, diffusive reorientational contributions were removed from the time-domain data by subtraction prior to the Fourier-transform analysis. These spectra reveal more clearly the low-frequency vibrational structure that is evident in Fig. 6. The bimodal structure evident in these spectra can be accounted for in terms of anisotropic librational degrees of freedom.

Perturbation of the Intermolecular Potential: Intermolecular dynamics that occur on the sub-500 fs timescale are determined in part by the details of the intermolecular potentials. The role of the local environment in shaping the intermolecular dynamics of liquids is revealed through dilution studies in which molecules of the neat liquid are systematically replaced by solvent molecules. This gives rise to an effectively continuous variation in the intermolecular

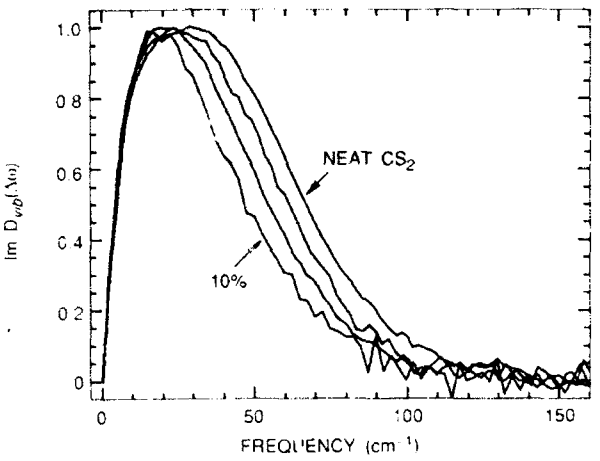

Fig. 8 — Nondiffusive (vibrational) part of the OHD OKE frequency response functions for CS_2 diluted in *n*-pentane solvent [3]. The spectra correspond to CS_2 volume fractions of 1.0 (*neat*), 0.75, 0.50, 0.10.

potential of the original species. Figure 8 illustrates the spectral evolution of the nondiffusive part of the frequency response function of CS_2 upon dilution in a weakly interacting alkane solvent [3]. The changes in the vibrational spectral density are clear: the intermolecular vibrational distribution narrows and shifts to lower frequency with increasing alkane concentration. The observed shift on dilution is consistent with the expected for an intermolecular vibrational mode as the curvature of the effective intermolecular potential is relaxed.

Conclusions: We have illustrated a powerful method for investigating the intermolecular dynamics of liquids. The FFTR spectra presented here reveal low-frequency, Raman-active intermolecular vibrational modes that previously have not been detected with conventional light-scattering techniques. The combination of time- and frequency-domain representations of the temporal data provides a compelling picture of the ultrafast dynamics and should be extremely useful in evaluation of vibrational contributions to the nonlinear-optical properties of material.

[Sponsored by ONR]

References

1. D. McMorrow and W.T. Lotshaw, "The Frequency Response of Condensed-Phase Media to Femtosecond Optical Pulses: Spectral Filter Effects," *Chem. Phys. Lett.* **174**, 85 (1990).

2. D. McMorrow, "Separation of Nuclear and Electronic Contributions to Femtosecond Four-Wave Mixing Data," *Opt. Comm.* **86**, 236 (1991).

3. D. McMorrow, S.K. Kim, J.S. Melinger, and W.T. Lotshaw, "Probing the Microscopic Molecular Environment in Liquids with Femtosecond Fourier-Transform Raman Spectroscopy," in *Ultrafast Phenomena VIII* (Springer Verlag, Berlin, 1992), in press. ■

Undersea Fiber-Optic Magnetometer System

F. Bucholtz, C.A. Villarruel, and G.B. Cogdell
Optical Sciences Division

Magnetic measurements are used for geomagnetic studies and for a variety of commercial and military applications. Certain applications require the magnetic sensors to be remotely located from the data collection station. In these cases, fiber-optic systems present a clear technological advantage because of their low attenuation characteristics and multiplexing capabilities. In 1991, a joint cooperative research and development program was initiated between NRL and the Norwegian Defence Research Establishment to construct, deploy, and test a fiber-optic magnetic array system (MARS). The final system to be deployed in 1993 will consist of eight sensors connected to shore and to each other with a cable containing both optical fibers and electrical wires. The basic system layout is shown in Fig. 9. The eight sensors will be housed in specially built, nonmagnetic, pressure-tolerant domes and will be fixed to the ocean bottom using nonmagnetic anchors.

Background: The fiber magnetic sensor is based on a physical phenomenon known as magnetostriction. Certain materials undergo a

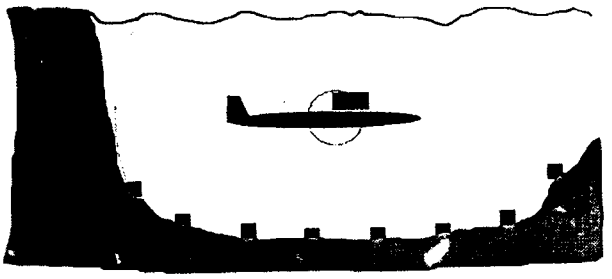

Fig. 9 — Concept for the fiber-optic MARS shows eight vector magnetometers at the bottom of a narrow channel or inlet. The system sends data to shore over a fiber-optic cable.

change in dimension in the presence of a magnetic field. Although the length change is very small (< 1 μm), it can easily be measured using a fiber-optic interferometer. This device compares the phases of light travelling in two distinct optical fibers, one reference fiber and one attached to the magnetostrictive material. Length changes less than atomic dimensions can be measured easily. The magnetostrictive material used in these sensors—an amorphous ferromagnetic alloy known as *Metglas* for metallic glass—responds strongly to magnetic fields. The relation between the normalized change in length $e = \Delta L/L$ and the magnetic field H is $e = CH^2$ where the magnetostriction parameter C depends on the magnetostrictive material and on details of the sensor's mechanical and electrical construction. NRL has developed a number of different fiber-optic magnetostrictive transducers for various applications including both low-frequency (< 10 Hz) and high-frequency (10 Hz to 50 kHz) sensing.

Sensor System: Each sensor for the MARS project consists of a fiber-optic vector magnetometer that measures the components of magnetic field along three orthogonal axes, a temperature sensor, tilt sensors, and an electro-optics package. This package converts optical signals to electrical signals, contains a microprocessor to handle data transfer, and provides excitation signals needed by the magnetometer. The tilt sensors are used to determine the orientation of each sensor. Software corrections are made to the data to *align* all the sensors along a common reference frame.

Figure 10 shows a simplified block diagram of the system. Light from the laser is transmitted to the sensor via a single-mode optical fiber. The single-mode optical fiber interferometer consists of a fiber optical coupler that divides the light into the two arms of the interferometer. The light is reflected by mirrors at the ends of each fiber, recombines at the coupler, and is transmitted to shore over a second fiber in the cable. Interference fringes are observed at the detector and converted to electrical signals, which are then stored and analyzed. A third fiber is used to transmit offsets and various command and control signals to the sensor.

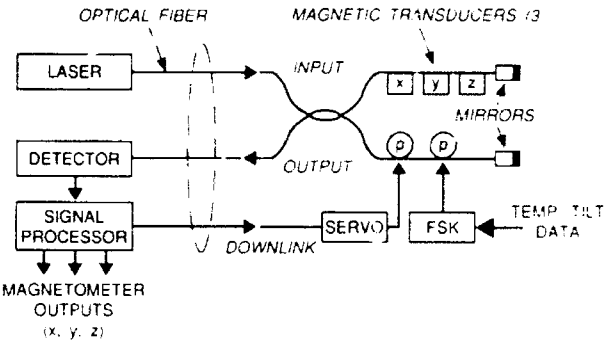

Fig. 10 — Schematic of the electro-optical signal processing

Undersea Prototype Tests: In 1992, tests were conducted of a two-sensor prototype system. The sensors were deployed in the Norwegian coastal waters at a depth in excess of 50 m. Figure 11 shows the three outputs from one of the sensor modules when a commercial vessel passed in the vicinity of the sensor. The curves have the characteristic shape of a magnetic dipole moving past a vector magnetometer.

The sensors were rigorously tested at NRL prior to shipment to Norway. Quality control techniques were implemented to improve transducer reliability and reproducibility. All sensor components were temperature cycled to ensure

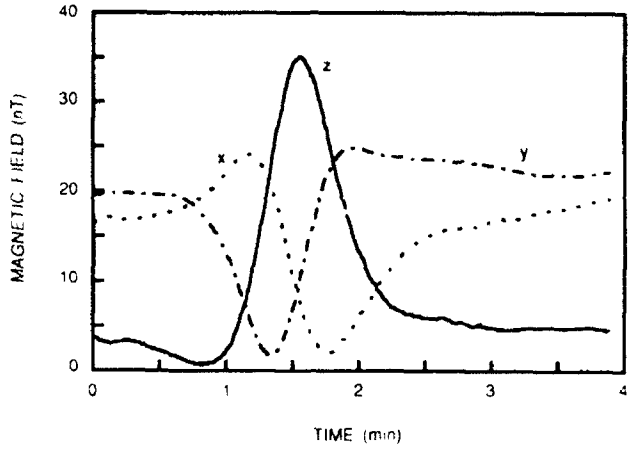

Fig. 11 — Outputs from the three channels of one vector magnetometer during the nearby passage of a commercial vessel

reliability and to induce infant mortality. The assembled sensors were also temperature cycled to verify operation and scale factor stability over the 0° to 30° C range.

Future: Future fiber-optic sensor arrays will likely include not only magnetic field sensors but also acoustic sensors and electric field sensors. Multi-influence systems of this type will offer improved detection reliability and will exploit the capabilities of fiber-optic technology.

Acknowledgments: The following individuals have made significant contributions to the results presented here: Anthony Dandridge and T.G. Giallorenzi of NRL; Dominique M. Dagenais, James A. McVicker, and Kee P. Koo of SFA, Inc.; Clay K. Kirkendall and Allen R. Davis of Maryland Research Foundation; Scott S. Patrick of Virginia Polytechnic and State University; and Kris. G. Wathen of Dynamic Systems.

[Sponsored by Navy International Programs Office and SPAWAR] ■

Space Research and Satellite Technology

Earth's Magnetospheric Field Lines

J.A. Fedder and S.P. Slinker
Plasma Physics Division

J.G. Lyon
Department of Physics and Astronomy
University of Iowa

C.M. Mobarry
NASA Center for Computational Sciences
Goddard Space Flight Center

The magnetosphere is the region of near-Earth space where the geomagnetic field has a dominant influence on the distribution and the dynamics of the plasma. Since the classic paper of Dungey [1], it has been widely recognized in the space physics community that electromagnetic coupling between the solar wind and Earth's magnetosphere is responsible for linking solar disturbances to the ionosphere and to the geomagnetic field. On many occasions, these disturbances, which are known as geomagnetic substorms and storms, are responsible for disrupting surface and transionospheric communications, navigation, and surveillance systems as well as Earth-based power transmission networks. Moreover, they are responsible for the creation of very active and widespread polar auroral displays. Understanding and modeling the structure of and physical processes influencing the Earth's magnetospheric field is critically important for studying the coupling of solar wind energy and momentum to the geosphere and for forecasting solar wind disturbances on man-made systems.

Magnetospheric Modeling: During recent years, NRL has developed numerical simulation techniques and codes for modeling the solar wind coupling to the magnetosphere and its effects on the near-Earth space environment. The basis of this modeling effort is the numerical solution of the magneto-hydrodynamic (MHD) equations. MHD describes the transport of mass, momentum, and energy in a global-scale space plasma. More importantly, it illuminates the conversion of energy from mechanical to electromagnetic form in dynamos and vice versa in motors and loads for scientific study. The global magnetospheric numerical simulation model is a key tool for investigating these conversion and transport processes. In these processes the energy of the solar wind, at distances from Earth greater than 64,000 km, is transported to the ionosphere, at 100 km altitude. This leads to aurora and other disturbances of near-Earth space. In the near term, these simulation techniques can lead to a real-time forecasting capability for the geospace environment.

Geomagnetic Structure: Certain features of the structure formed by the geomagnetic and the interplanetary magnetic field (IMF), which is carried by the solar wind, play a fundamental role in determining both the physics and the efficiency of the solar wind magnetosphere coupling process. These features, which are called magnetic neutral points or topological critical points, are regions where the magnetic field strength is very close to zero. At the critical points, the geomagnetic field can be joined to the IMF by a process known as magnetic reconnection, or merging as originally suggested by Dungey. The magnetic merging process not only changes the original geometry of the magnetic field but is also the primary process responsible for solar wind energy conversion and transport from regions more than 64,000 km away from Earth into all of the inner magnetosphere. As the IMF changes its direction, as the result of solar structure and solar activity, the solar wind magnetosphere interaction is markedly affected.

Magnetospheric Field Lines: The magnetic merging process between the IMF and the geomagnetic field has two extreme states (Fig. 1). Figure 1(a) shows the magnetic field structure, in the noon-midnight magnetic meridian plane, for a due-northward-directed IMF. In the figure, Earth is centered in the 45,000-km-diameter green ball, and the solar wind enters from the right. For this quasi-steady configuration, the yellow IMF lines and the pink geomagnetic lines are parallel to each other on their common boundary, which almost completely encloses Earth. Only a very few blue

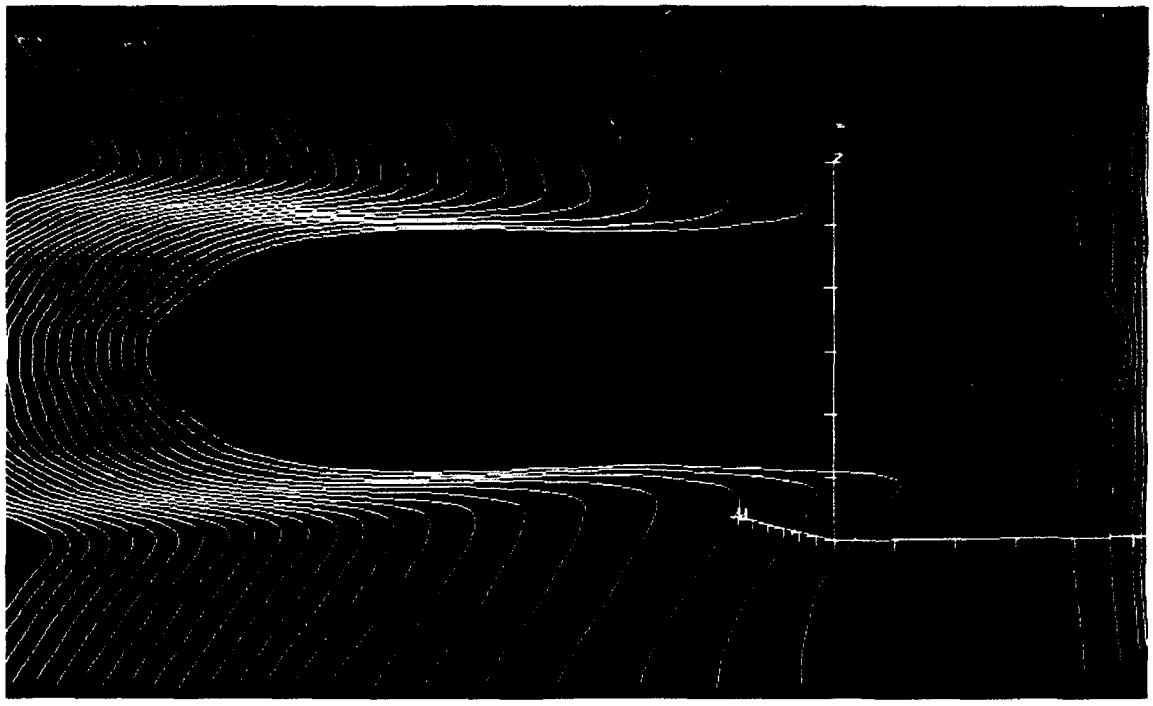

(a) North IMF

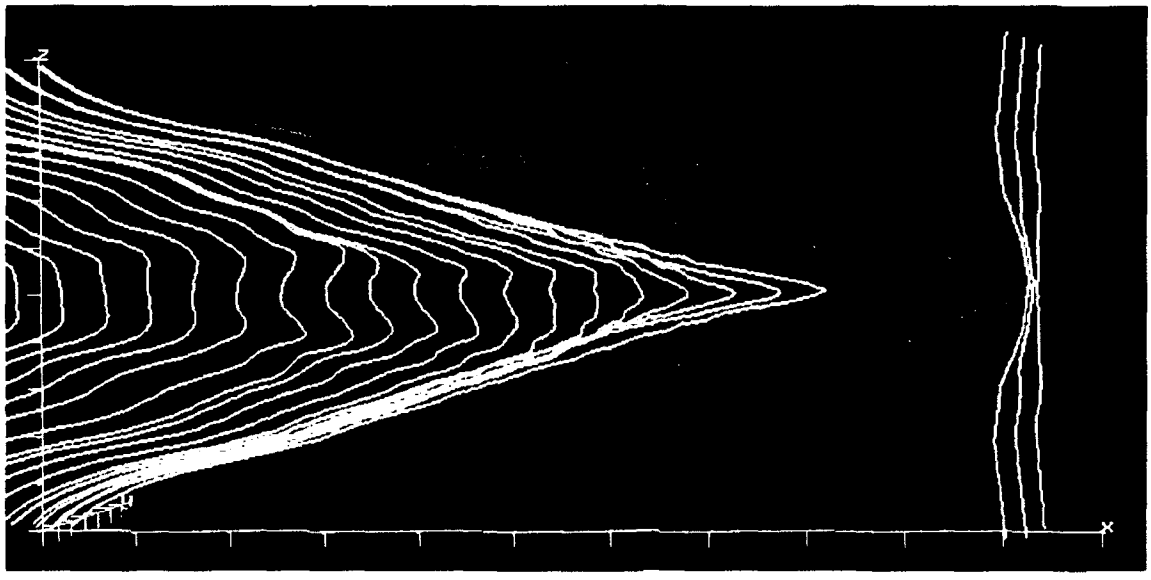

(b) South IMF

Fig. 1 — Earth's magnetospheric field lines. The images show computer generated magnetic field lines from the NRL Global Magnetospheric Simulation Code. The field lines were chosen to lie in the noon midnight meridian plane containing the geomagnetic poles. Pink lines show the geomagnetic field, yellow lines show the sun's field in the solar wind, and blue lines show magnetic field, which interconnects the two. These two images illustrate the only two quasi steady states for the solar wind magnetospheric coupling. The north IMF image is for a minimally interacting, ground state, magnetospheric configuration, the south IMF image is for a maximally interacting state. During periods when the solar wind magnetosphere interaction resembles the south IMF image Earth is subject to extensive and bright auroral displays at high latitudes. We also experience large, widespread electrical and magnetic disturbances on the ground.

merged field lines connect the geomagnetic field to the IMF through a small cone, the geomagnetic cusp, in the polar regions. The polar cusps contain the topological critical points where magnetic merging between the IMF and the geomagnetic field occurs. Even more remarkably, the magnetosphere, the region of influence of the geomagnetic field, is confined between 64,000 km upwind and 1,000,000 km downwind of Earth. In this ground state magnetosphere, the energy and momentum transfer from the solar wind to the geomagnetosphere is minimal, and auroral activity and geospace environmental disturbances are greatly reduced. Figure 1(b) shows the magnetic field structure for the other extreme state, which occurs when the IMF is directed due southward. In this quasi-steady configuration, the yellow IMF and the pink geomagnetic field lines touch only in the equatorial region, where they are antiparallel. The blue merged field lines interconnect the IMF with the geomagnetic field and now occupy a large volume of space in the polar regions. For this state, the topological critical region forms a closed curve, in the equatorial plane, with magnetic merging occurring along an appreciable length of the curve, both at the bow and in the magnetotail downstream. In this maximally coupled state, large amounts of solar wind momentum and energy are transferred to the inner magnetosphere and ionosphere. Indeed, the rate of energy transfer in the magnetosphere of Fig. 1(b) exceeds that of Fig. 1(a) by a factor larger than 100. The magnetospheric configuration of Fig. 1(b) is characteristic of periods when there are large geomagnetic, ionospheric, and space environmental disturbances. Under normal conditions, neither of the states shown above occur very often, because the solar wind and its imbedded IMF are continually changing. Ongoing research, using the global magnetospheric numerical simulation, is now directed toward studies of this continually changing solar wind magnetosphere coupling and energy transfer process. We are using actual measured solar wind parameters to study magnetospheric substorm processes and the creation of the aurora. The temporally resolved magnetospheric structure, dynamics, and aurora are then compared to measured data for verification and improvements to the model.

[Sponsored by NASA-SPTP and by ONR]

Reference

1. J.W. Dungey, "Interplanetary Magnetic Field and the Auroral Zone," *Phys. Rev. Lett.* **6**, 47-48 (1961). ■

NRL's Oriented Scintillation Spectrometer Experiment on NASA's Compton Gamma Ray Observatory

J.D. Kurfess and W.N. Johnson
Space Science Division

NRL's Oriented Scintillation Spectrometer Experiment (OSSE) was launched on NASA's Arthur Holly Compton Gamma Ray Observatory (GRO) on April 5, 1991. The 35,000 lb observatory, the largest unmanned scientific satellite ever launched, is the second of four *Great Observatories* covering the electromagnetic spectrum to be launched by the United States over a fifteen-year period (the Hubble Space Telescope was the first). Prior to its launch, the OSSE instrument was under development for over 13 years by a scientific team lead by the Naval Research Laboratory; the team included coinvestigators at Northwestern University, Clemson University, and the Defence Research Agency (DRA), Farnborough, England. The OSSE instrument is composed of four identical scintillation detector systems, each of which weighs about 800 lb [1]. Each detector has a 3.7° × 11.4° field of view, and the detectors are alternately pointed at sources of interest and nearby background regions of the sky. The OSSE instrument is shown in Fig. 2.

The OSSE team is undertaking a comprehensive research program in gamma ray astrophysics covering the energy region from 50 keV to 10 MeV. OSSE is investigating high-energy processes in solar flares, is studying exotic galactic sources such as neutron stars and black

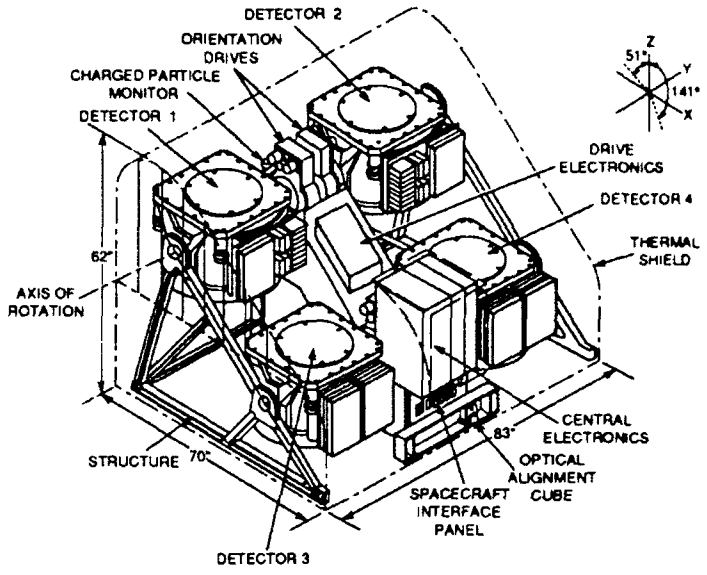

Fig. 2 — Schematic of the Oriented Scintillation Spectrometer Experiment

holes, and is also investigating the very energetic processes occurring in active galactic nuclei (AGNs) and quasars, which are the most distant objects observed in the universe. Highlights from the first year of the mission include the observation of several very large flares during a period of intense solar activity in June 1991; the detection of ^{57}Co radioactivity from supernova SN1987A; the investigation of positron annihilation radiation from the central region of our galaxy; targets of opportunity to observe several strong transient sources in the Galaxy; and the detection of active nuclei in distant galaxies that are presumed to harbor massive black holes [2].

Solar Flares: OSSE has obtained data on a large number of flares, including observations of four of the major Class X flares that occurred in June 1991. Class X flares are the most intense form of solar activity and may have significant impact on navigation and communications systems; they represent a radiobiological hazard to manned operations in space, and can even disrupt the national electrical power distribution system in extreme cases. The OSSE experiment operates in the energy region where the acceleration and interaction of nuclear particles in the flare region can be investigated through the gamma rays that are produced by these interactions. In late May 1991, sunspot region 6659 moved onto the solar disk and indicated potential for major activity. The OSSE viewing program was modified so that significant observing time could be given to the Sun. The Sun responded with major flares on June 1, 4, and 6. Figure 3 shows the energy spectrum and time history for the flare of June 4, 1991. Following these events, the entire GRO spacecraft was reoriented so that two other GRO experiments could also view the Sun. The Sun continued to cooperate with region 6659 producing three additional Class X flares on June 9, 11, and 15. Joint analysis of the OSSE and EGRET (Energetic Gamma-Ray Experiment Telescope) data for the June 11, 1991 flare has provided the first evidence for long-term (hours) particle storage in the flare region.

Galactic Sources: OSSE has observed a large number of discrete galactic gamma ray sources including the black hole candidates in the constellations Cygnus (Cyg X-1), Scorpius (GX 339-4), and Perseus (GRO J0422+32). Cygnus X-1 was one of the first celestial X-ray sources discovered and subsequently was the first to be suggested as a black hole based on a mass determination that exceeded the limit for neutron stars. These sources provide an opportunity to observe matter as it falls into the

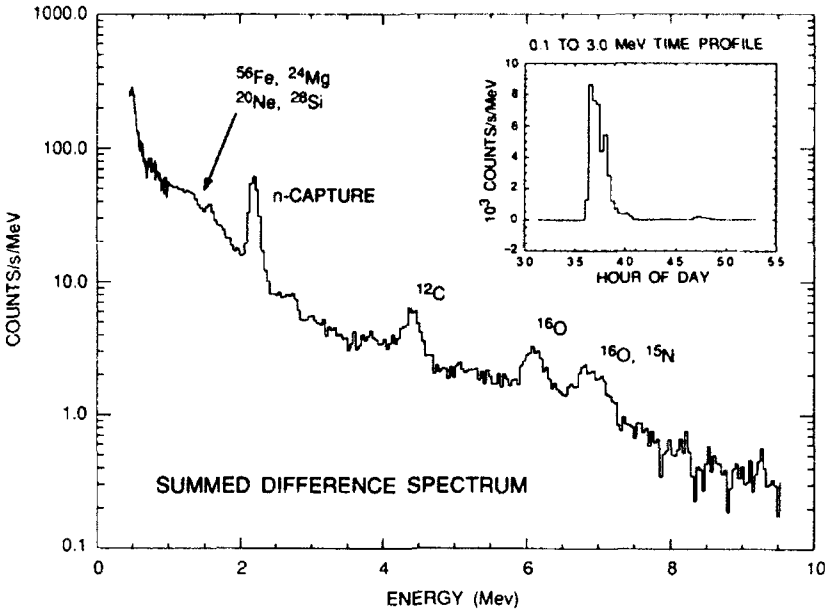

Fig. 3 — Time history of nuclear gamma ray emission and the gamma ray spectrum observed during the June 4, 1991 solar flare

intense gravitational fields associated with the black hole, and to use temporal and spectral characteristics to test models and thereby help confirm the reality of black holes. GX 339-4 and GRO J0422+32 were observed as targets of opportunity, in quick response to the outbursts reported by the BATSE experiment on GRO. Energy spectra for these three objects are shown in Fig. 4. All three objects exhibit spectra with characteristic temperatures of 500 to 1000 million degrees, which suggest that such spectra may be characteristic of stellar-mass black holes that are accreting matter from a companion star.

0.51 MeV Positron Annihilation Radiation: A goal of GRO is to produce a map of the galactic positron annihilation radiation. This radiation results when positrons, the antiparticle of electrons, are captured by electrons and often annihilated with the emission of two gamma rays with an energy of 0.51 MeV. There are several possible sources for the positrons, including galactic supernovae and novae, pulsars, and matter accreting onto galactic black holes. Previous experiments have discovered a strong source of 0.51 MeV emission in the general direction of our galactic center, but only by making detailed maps of this emission will it be possible to determine the sources and production mechanisms of the positrons. Detection of a time variable component would confirm earlier reports of a discrete source in the galactic center region.

The OSSE observations of the galactic center have provided a significant detection of the 511 keV line and associated positronium continuum, with a sensitivity ~10 times better than previous measurements. There has been no evidence for time variability of the 511 keV line flux, thus calling into question previous suggestions of time variability. The data from these observations have been used to test various models for the galactic distribution of the annihilation radiation. These studies indicate that the dominant sources of the observed emission are diffuse in nature. The limit on the flux from a discrete source near the galactic center is 2-3 $\times$ 10^{-4} gamma/cm^2-s. The distribution of the diffuse emission appears to be made up of two components—a galactic bulge component and a galactic disk component with the bulge component being more intense. This distribution appears to suggest that galactic supernovae are not the dominant source of positrons.

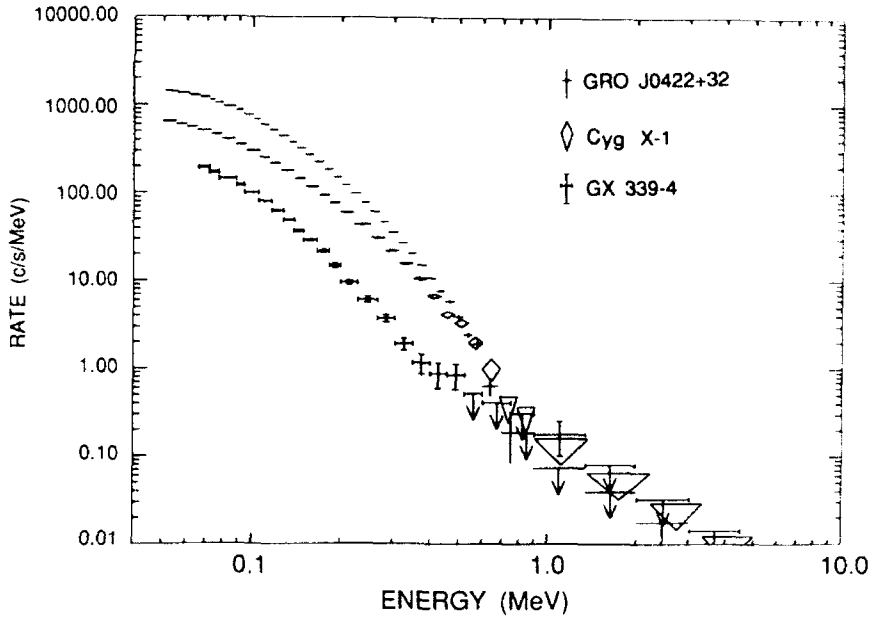

Fig. 4 — Gamma ray spectra for three galactic sources that are thought to be binary star systems where one of the objects is a black hole

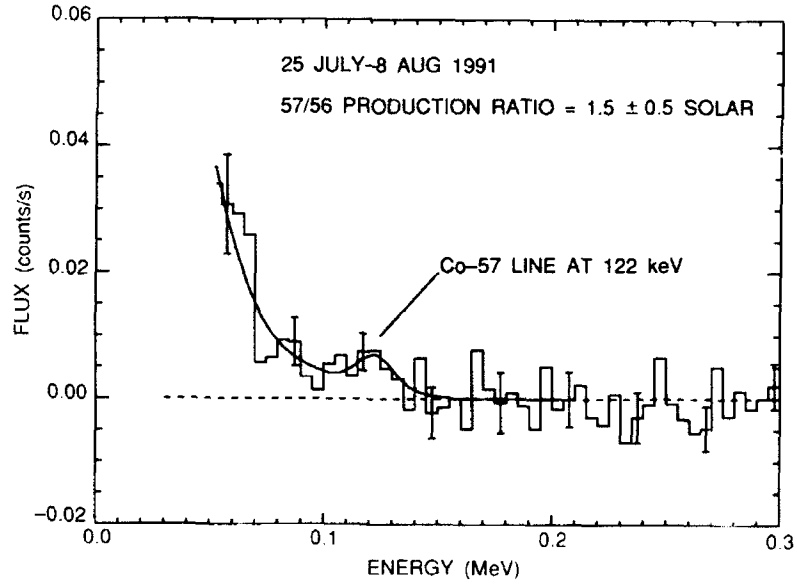

Fig. 5 — Spectrum of SN1987A showing the ^{57}Co line emission at 122 keV

Nucleosynthesis: OSSE has discovered ^{57}Co gamma radiation from SN1987A, the second radioactivity observed from a supernova [3]. Supernova remnants are thought to be powered by radioactivity from nuclei synthesized during the explosion. At the time of the OSSE observations, radioactive ^{57}Co was thought to be the dominant source of energy. Previous bolometric estimates suggested that the ^{57}Co production was about three times larger than theoretical models had predicted for the supernova explosion. The OSSE detection of ^{57}Co gamma radiation from SN1987A, shown in Fig. 5, has proven the nucleosynthetic origin for ^{57}Fe and is in good agreement with the theoretical models for ^{57}Co production. Therefore another source for the remainder of late-time bolometric power is required [4].

Active Galactic Nuclei: OSSE has observed about 30 AGNs with detections of 1/3 to 1/2 of them. High-quality data has been obtained on 3C273, Cen A, and NGC 4151 with sufficient sensitivity to address the temporal and spectral variability of these sources for the first time in the important energy range above 50 keV. The OSSE data provide a major new database to test models of AGNs and the possible unification of those models, and will significantly improve our knowledge of the contribution of AGNs to the diffuse high-energy cosmic background. For further information of OSSE results on AGN, the reader is referred to the article by Charles D. Dermer on pages 215-218 in this issue of the *Review*.

Conclusion: OSSE has worked exceptionally reliably since its launch by the space shuttle Atlantis. It is anticipated that the GRO mission will continue for another four to eight years, and the OSSE experiment should continue to provide important new information on the highest energy sources in the universe.

Acknowledgments: A major program such as OSSE represents the combined efforts of several hundred individuals who have contributed to its development. We wish to recognize contributions of other members of the OSSE science team: Drs. Mark Strickman, Bob Kinzer, Gerry Share, Ron Murphy, Eric Grove, and Dick Kroeger of NRL; Mel Ulmer, Bill Purcell, Steve Matz, and David Grabelsky of Northwestern University; Donald Clayton and Mark Leising of Clemson University; Greg Jung and Rob Cameron of Universities Space Research Association; Craig Jensen of George Mason University; and Clive Dyer of DRA, Farnborough.

[Sponsored by NASA]

References

1. W.N. Johnson, R.L. Kinzer, J.D. Kurfess, M.S. Strickman, W.R. Purcell, D.A. Grabelsky, M.P. Ulmer, D.A. Hillis, G.V. Jung, and R.A. Cameron, "The Oriented Scintillation Spectrometer Experiment Instrument Description," 1993, *Astrophys. J. Supp.* (in press.)

2. W.N. Johnson, J.D. Kurfess, M.S. Strickman, R.J. Murphy, R.L. Kinzer, G.H. Share, R.A. Kroeger, J.E. Grove, W.R. Purcell, S.M. Matz, M.P. Ulmer, D.A. Grabelsky, R.A. Cameron, G.V. Jung, M. Maisack, C.M. Jensen, D.D. Clayton, M.D. Leising, and C.S. Dyer, "Initial Results from OSSE on the Compton Observatory," 1992, *A&A Supp.* (in press.)

3. J.D. Kurfess, W.N. Johnson, R.L. Kinzer, R.A. Kroeger, M.S. Strickman, J.E. Grove, M.D. Leising, D.D. Clayton, D.A. Grabelsky, W.R. Purcell, M.P. Ulmer, R.A. Cameron, and G.V. Jung, "OSSE Observations of ^{57}Co in SN1987A," *Astrophys. J. Lett.* **399**, 137 (1992).

4. D.D. Clayton, M.D. Leising, L.-S. The, W.N. Johnson, and J.D. Kurfess, "The ^{57}Co Abundance in Supernova 1987A," *Astrophys. J. Lett.* **399**, 141 (1992). ■

Energetic Radiation from Black Holes

C.D. Dermer
Space Science Division

Suspected black holes in our galaxy and in the centers of other galaxies glow brilliantly at X-ray energies. The X rays are probably emitted when matter is heated to high temperatures while falling through the enormous gravitational potential of the black hole. Recent observations also show that black holes with radio jets pointed towards us are luminous gamma ray source that require new theories to explain the acceleration and outflow of gamma ray emitting particles.

Black Hole Signatures: By definition, a black hole is so dense and massive that even light cannot escape from it. We can therefore only look for one through its secondary effects

on the surrounding environment. One of the most promising methods for discovering a black hole is to find binary stellar systems with invisible companions. Using Kepler's laws to provide mass estimates, several systems in our galaxy have been discovered where the companion's mass exceeds several Solar masses. Since there is no known physical mechanism to support a degenerate star as massive as this against the force of gravitational collapse, we may conclude that these systems contain black holes.

Another method used to look for black holes is by observing their radiation signatures. Indeed, this may be the only way to study supermassive black holes that are thought to exist at the centers of our galaxy and other galaxies, since these objects are not members of binary systems. In the past 20 years, one of the most exciting astronomical discoveries is that a few percent of all galaxies contain active nuclei that emit as much energy as the combined output from all the stars in the galaxy. Much of the energy from these active galaxies is emitted in the form of X-ray photons. There have also been indications that some of these sources radiate enormous amounts of gamma radiation.

Theories about production of energetic radiation from black holes have mainly concentrated on a scenario where luminous energy is extracted from the gravitational potential of the infalling material. The acceleration mechanism for the radiating particles is uncertain: some theories use the thermal heating of material that accretes in a disk geometry; some consider energetic particle injection followed by Compton upscattering and electron-positron pair production; and others treat acceleration through standing shocks formed by the infalling fluid.

New Observations: Our knowledge of active galaxies and galactic black-hole candidates has undergone a profound change with the launch of the Compton Gamma Ray Observatory on 5 April 1991. The Oriented Scintillation Spectrometer Experiment (OSSE), one of the four gamma ray telescopes on the Compton, is dedicated to viewing the extreme conditions of temperature, density, and gravitational field thought to occur in the vicinity of collapsed stars and supernovae (see the article by James D. Kurfess and W. Neil Johnson on pages 211-215 in this issue of the *Review*). NRL is the principal investigator institution for OSSE, which has made the most sensitive measurements to date of Active Galactic Nuclei (AGN) in the energy range between 50 keV and 10 MeV.

More than eleven AGN have now been detected with OSSE [1]. Many are radio-quiet objects known as Seyfert galaxies, and a few others are radio-loud objects known as blazars or quasars. OSSE finds that the Seyfert galaxies have spectra that display a spectral softening at energies greater than ≈ 100 keV. So far, no observations have been made of features near 500 keV that reveal the telltale sign of positron production. This is shown most clearly in Fig. 6 for NGC 4151. The absence of these features places strong constraints on nonthermal models for these sources, which predict intense gamma ray emission and electron-positron pair generation.

On the other hand, observations with OSSE and the Energetic Gamma Ray Experiment Telescope (EGRET), another telescope on the Compton Observatory, show that the radio-loud AGN can be intense sources of X rays and gamma rays [2]. The evidence indicates that in those rare cases where we are observing nearly down the axis of the radio jet, an intense flux of highly beamed gamma radiation is emitted, extending to GeV and, in one case, TeV energies. The intensity of the radiation is so great that we are able to peer at some gamma ray blazars whose radiation, prior to being detected, has been redshifted by the expansion of the universe by a factor of ~ 3. Figure 6 also shows the OSSE data for the quasar 3C 273, a source whose radio axis is evidently aligned along our observing direction. Figure 7 shows a radio image of the radio galaxy Cygnus A, which may be similar to how 3C 273 would appear if we could view it at a large angle with respect to its jet axis [3].

Significance of Energetic Radiation from Black Holes: The gamma ray observations are providing a new perspective on the AGN unification scenario, whereby different classes of AGN merely reflect different orientations of the observer with respect to the galaxy. We [4] are

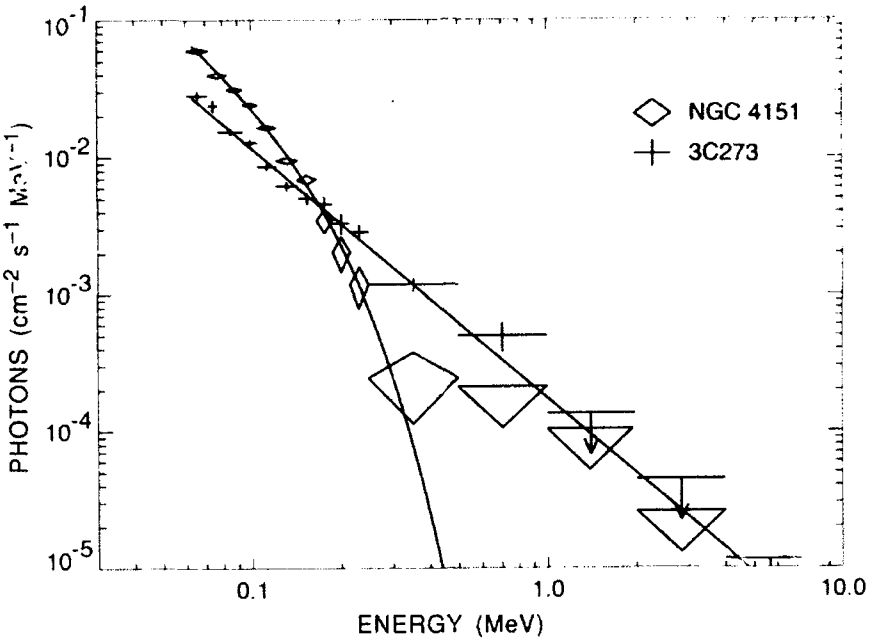

Fig. 6 — OSSE data for the nearby Seyfert galaxy NGC 4151 and the radio quasar 3C 273, at distances of about 30 million light-years and 3 billion light-years, respectively. The weak gamma ray emission above several hundred keV in NGC 4151 constrains models involving prolific positron production, and may support a thermal accretion model. Gamma rays from 3C 273 are probably produced in association with a radio jet.

Fig. 7 — The radio galaxy Cygnus A at a distance of about 1 billion light-years. One of the major discoveries of the Compton Observatory is that intense gamma ray emission discovered by OSSE and EGRET apparently originate from radio galaxies such as Cygnus A that have radio jets aligned nearly along our line of sight.

performing numerical simulations of jets in which energetic electrons Compton-scatter accretion disk radiation to gamma ray energies. This model can explain the multiwavelength continuum of blazars, and the fact that most of the bolometric luminosity appears in gamma rays. Moreover, the appearance of AGN depends sensitively on the observing direction, in agreement with the AGN unification scenario (see Fig. 8).

Besides providing a laboratory of physical extremes unavailable here on Earth, black holes accomplish tasks that require monumental human ingenuity: accelerating particles to ultra-high energies. Our effort to understand particle acceleration near black holes may be put to use

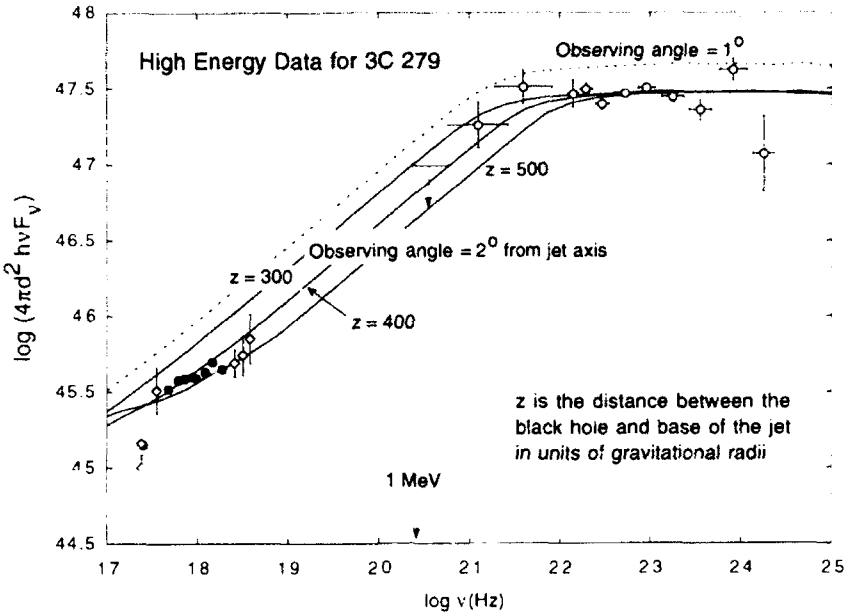

Fig. 8 — Simulation [4] of the multiwavelength emission produced by beamed electrons in an outflowing jet that produce gamma rays by Compton scattering accretion disk radiation and radio radiation by the synchrotron process. Note the strong dependence of the gamma ray intensity on observer direction. Also shown is the high-energy data [2] from the quasar 3C 279.

in other astrophysical scenarios as well as in terrestrial particle acceleration schemes. The plasma physics required to understand particle beams and gamma ray production in the radio jets of AGN parallels the work done in beam and jet physics, but in a new regime. Black holes may also play a significant role in the production of the highest energy cosmic rays. Most important, perhaps, is the increased knowledge gained of the role that supermassive black holes play in the formation of galaxies and the structure of our universe.

[Sponsored by ONR and NASA]

References

1. R.A. Cameron, J.E. Grove, W.N. Johnson, J.D. Kurfess, R.L. Kinzer, R.A. Kroeger, M.S. Strickman, M. Maisack, C.H. Starr, G.V. Jung, D.A. Grabelsky, W.R. Purcell, and M.P. Ulmer, "OSSE Observations of Active Galaxies and Quasars," *Proc. of the Compton Observatory Symposium*, N. Gehrels, ed. (in press, 1992).

2. R.C. Hartman, D.L. Bertsch, C.E. Fichtel, S.D. Hunter, G. Kanbach, D.A. Kniffen, P.W. Kwok, Y.C. Lin, J.R. Mattox, H.A. Mayer-Hasselwander, P.F. Michelson, C. von Montigny, H.I. Nei, P.L. Nolan, K. Pinkau, H. Rothermel, E. Schneid, M. Sommer, P. Sreekumar, and D.J. Thompson, "Detection of High-Energy Gamma Radiation from Quasar 3C 279 by the EGRET Telescope on the Gamma Ray Observatory," *Astrophys. J. Lett.* **385**, L1-L4 (1992).

3. C.D. Dermer and R. Schlickeiser, "Quasars, Blazars, and Gamma Rays," *Science* **257**, 1642-1647 (1992).

4. C.D. Dermer and R. Schlickeiser, "Quasars, Blazars, and Gamma Rays," *Astrophys. J.* **257**, 2642-1647 (1992). ■

Parallel Processing for Space Surveillance

L.M. Healy and S.L. Coffey
Spacecraft Engineering Department

Background: Space surveillance is concerned with tracking, cataloging, and analyzing the orbital motion of more than 7000 Earth-orbiting objects. The quantity of objects motivated a parallel processing approach to deal with the massive number of mostly independent computations required to update the catalog and perform associated analysis. One of the most important functions is to predict close conjunctions of objects, particularly to support manned missions such as the shuttle and the Space Station Freedom. Our objective was to investigate the ability of parallel processing to perform this function COMBO named after the software that runs at the two space surveillance centers NAVSPASUR (Naval Space Surveillance Center) and the U.S. Space Command.

Close Orbit Detection (COMBO): The surveillance centers currently run programs called COMBO, which finds all satellites that come close to a particular satellite. However, with parallel processing we can be more ambitious: to find all close contacts between objects in the catalog, that is, an all-to-all comparison. On a parallel processor such as the Connection Machine comparing the Cartesian positions between all members in the catalog is performed in a series of shift-compare steps. To prepare for the comparison, a copy of the catalog is made. All possible combinations can then be examined by shifting the copy relative to the original. In each shift the difference in positions is calculated in parallel.

However, instead of comparing every possible pair of satellites, about 24.5 million comparisons, which would take a long time even on a parallel computer, we can rearrange the data so that one axis (say the Z axis) is sorted. Then, the shifting may stop when the minimum of the Z differences is greater than the designated contact distance. This reduces the number of comparisons to about 350,000, or about 50 serial steps, for a contact distance of 50 km.

Figure 9 is a snapshot of the objects in the catalog and those objects that were within 2.5 km of another object. This image was taken from a sequence of images generated by the COMBO program.

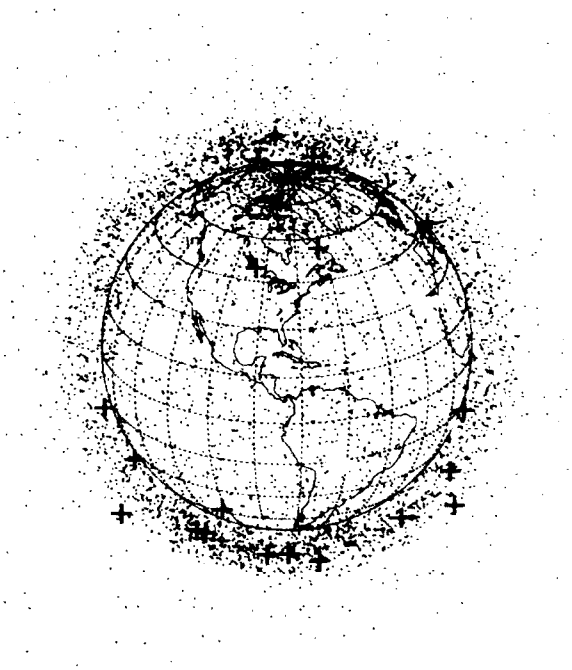

Fig. 9 — Satellite distribution on March 12, 1992. Black dots, whose size do not reflect actual object size, indicate positions of the objects in the catalog. Red crosses mark positions of objects that are within 2.5 km of another object.

Propagation: To find the position at each time step, we must propagate the orbits—that is, from the initial conditions, compute the future position. A variety of ways can be used to do this, but we have concentrated on analytic methods. These techniques are particularly well suited to parallel processing since the new position is a function of the time and thus can be computed without iteration.

Based on the pioneering work of Brouwer [1], NAVSPASUR and the U.S. Space Command run analytic orbit propagators, called PPT2 and SGP4 respectively, on their serial computers. The analytic propagators work, by averaging away the short-period orbital variations, leaving only the long-period variations, because of the deviations of the Earth's mass

distribution from a homogeneous sphere. We have adapted these programs to run on the Connection Machine and incorporated them into the close-orbit detection code. Preliminary work has begun on improved propagators using advanced analytic techniques.

Debris: We can use this program to aid in the study of the effects of space debris. Instead of comparing all-to-all within the catalog, we can compare all-to-all between the catalog and another collection of element sets, those computed from the simulation of the explosion of a satellite. Debris can be simulated by assuming that the fragments are isotropically dispersed from the center of mass, with a speed distribution that follows a Maxwell gas distribution law. Although this debris model is very simple, it shows qualitative agreement with observed breakups as they evolve over time [3].

Status and Plans: We are now able to do a propagation, all-to-all comparison and produce a graphical display in any one of three projections in about one second per time step. NAVSPASUR plans to begin evaluating the applicability of this program to their operations. In cooperation with NASA, we will be studying orbital debris, particularly as it affects the space station, with this program.

This is the first of several planned investigations of parallel processing to space surveillance. Orbit determination, the process of updating orbital elements, is now being pursued. Here the space surveillance centers must process 70,000 observations coming from the Space Surveillance Network to produce the updated element sets that make up the catalog.

Orbit propagation is another application that we will be pursuing. It is now recognized that improved orbit prediction is necessary for many applications. However, the computational burden of better accuracy applied to the 7000 object catalog will require substantially more computer resources than are now available. Both advanced analytic algorithms and numerical integrators will be devised to take advantage of the parallel architecture.

After maintaining catalog of satellites whose primary purpose is to facilitate the defense of the country, the advent of a U.S. space station has reawakened an interest in all the techniques used in space surveillance. In particular, during last year an effort has been made by NASA to catalog space debris, which may number as many as 25,000 objects, down to a size of 1 cm. We expect our work to be an essential part of this effort.

[Sponsored by ONR]

References

1. D. Brouwer, "Solution of the Problem of Artificial Satellite Theory Without Drag," *Astron. J.* **64**, 378-397 (1959).

2. L. Healy, S. Coffey, "Parallel Computing for Space Surveillance," *Proc. of the 1992 Space Surveillance Workshop*, MIT, Lincoln Laboratory Project, Report STK-193, April 1992.

3. R. Jehn, "Fragmentation Models," MAS Working Paper Nr. 312, European Space Operations Centre, Dec. 1990.

Awards and Recognition

Special Awards and Recognition

NRL is proud of its many distinguished scientists and engineers. A few of these have received exceptional honors for their achievements.

Dr. Isabella Karle
Laboratory for the Structure of Matter

1992 VINCENT DU VIGNEAUD AWARD

Dr. Karle was recognized for establishing "experimental procedures used worldwide for molecular structure analysis using electron and X-ray diffraction techniques. She has pioneered in elucidating the crystal structures of numerous biologically active molecules, including complex peptides containing many residues." The award is named for Vincent du Vigneaud, a Nobel prize-winning American biochemist who was an early leader in peptide chemistry.

Dr. Herbert Friedman
Chief Scientist Emeritus of NRL's E.O. Hulburt Center for Space Research

1992 MASSEY AWARD FROM THE ROYAL SOCIETY OF LONDON

The award, which honors the memory of British physicist, Sir Harrie Massey, was presented to Dr. Friedman at the 29th Plenary Meeting of the Committee on Space Research (COSPAR), "in recognition of his distinguished contributions to rocket and satellite astronomy, particularly X-ray astronomy, and for his long-standing service to COSPAR."

Dr. Stuart Searles
Optical Sciences Division

1992 RANK PRIZE FUND AWARD (Presented at the Royal College of Surgeons in London, England)

Dr. Searles was cited for "his discoveries leading to the development of the rare gas halide excimer laser." Dr. Searles' developments leading up to the rare gas halide excimer laser include: several flashlamp pumped chemical lasers, a free burning flame laser, and the electron beam pumped Argon-Nitrogen laser.

Dr. Bhakta Rath
Associate Director of Research
Materials Science and Component Technology Directorate

1992 MINERALS, METALS, AND MATERIALS SOCIETY (TMS) FELLOWS AWARD

Dr. Rath was cited for "outstanding research contributions in physical metallurgy and for visionary leadership in research planning and administration." According to TMS, this is the society's most prestigious award, and the highest honor that recognizes an individual for a lifetime of outstanding contributions to the practice of metallurgical and materials science.

1991 GEORGE KIMBALL BURGESS MEMORIAL AWARD

Dr. Rath was recognized for his "outstanding contributions to materials research during the period 1986-1991 through his research and administration of materials research at the Naval Research Laboratory."

Dr. Robert R. Meier
Space Science Division

1991 E.O. HULBURT ANNUAL SCIENCE AND ENGINEERING AWARD

Dr. Meier was recognized for his "investigation and discovery of the many complex mechanisms and influences in the near-Earth space environment that cause emission of ultraviolet (UV) radiation in all its forms." He was also cited for developing "comprehensive theory to follow UV radiation scattering and propagation through the atmosphere and for the development of space UV monitoring concepts that hold the promise of rapid synoptic imaging and assessment of ionospheric 'weather' from space."

Dr. Warren E. Pickett
Condensed Matter and Radiation Sciences Division

1990 E.O. HULBURT ANNUAL SCIENCE AND ENGINEERING AWARD

Dr. Pickett was recognized for "his major contributions in the area of theoretical studies of high-temperature superconductivity...Under his leadership, detailed studies of properties, such as Fermi surfaces, lattice dynamics, structural stability, transport behavior, and effects of alloying in these systems have been accomplished."

Francis J. Campbell
Condensed Matter and Radiation Sciences Division

IEEE 1992 ERIC O. FORSTER DISTINGUISHED SERVICE AWARD

Mr. Campbell was cited for his "outstanding contributions to the IEEE's Dielectrics and Electrical Insulation Society." He is the tenth member of the society to receive this award for "recognition of sustained leadership, support and for contributions to the advancement of the field of dielectrics and electrical insulation that have enhanced the goals and growth of the society."

Dr. Cha-Mei Tang
Plasma Physics Division

1992 WOMEN IN SCIENCE AND ENGINEERING AWARD FOR SCIENTIFIC ACHIEVEMENT

In the area of free electron lasers, Dr. Tang was the first to publish on two very important topics: efficiency enhancement schemes and radiation focusing and guiding. She has also made many contributions for the advancement of women in science. She is one of the founders of the NRL Scientific and Technical Women's Network. In addition to her contributions to women's activities at NRL, she also encourages young women to enter scientific fields.

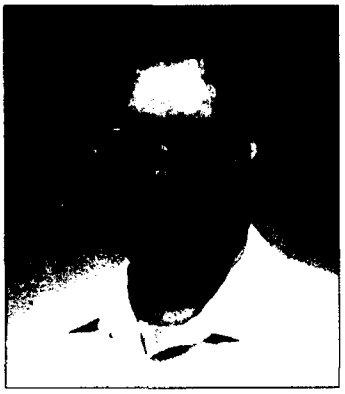

Dr. Moshe Friedman
Plasma Physics Division

SIGMA XI 1992 APPLIED SCIENCE AWARD

Dr. Friedman was cited for "sustained creativity, original scientific foresight, and pioneering research in the physics of intense relativistic electron beams and its applications, such as high-power microwave generation from the relativistic klystron amplifier and compact Wakefield accelerators."

Dr. Edward McCafferty
Materials Science and Technology Division

SIGMA XI 1992 PURE SCIENCE AWARD

Dr. McCafferty was recognized for his "published research that has significantly advanced the fundamental understanding of localized corrosion in an approach that has been innovative, interdisciplinary, and multidivisional, bringing new tools, people, and ideas to the age-old problem of corrosion."

Dr. Gerald H. Share
Space Science Division

SIGMA XI 1992 PURE SCIENCE AWARD

Dr. Share was cited for his "outstanding achievements in gamma-ray astrophysics using the Solar Maximum Mission Gamma-Ray Spectrometer, including the detection of cobalt-56 radioactivity in SN1987a, investigations of positron annihilation radiation and aluminum-26 radioactivity of galactic origin, studies of solar flares and cosmic gamma-ray bursts, and investigations of radiation associated with nuclear reactors in space."

David L. Pettit
Naval Center for Space Technology

NAVY SUPERIOR CIVILIAN SERVICE AWARD

Mr. Pettit was cited for "outstanding service...in the design, development, acquisition, and performance verification of several major systems for the Navy space effort and for solving difficult technical and managerial problems in the development of robust dynamic first-of-a-kind system...."

Dr. Frances Ligler
Center for Bio/Molecular Science and Engineering

1992 OFFICE OF NATIONAL DRUG CONTROL POLICY TECHNOLOGY TRANSFER AWARD FOR DRUG ENFORCEMENT

Dr. Ligler was recognized for her initiative in transferring the technology for the NRL-developed flow immunosensor, a novel system to detect drugs of abuse, to the commerical sector. The flow immunosensor is a highly sensitive, drug-screening device that is expected to be both timesaving and cost-efficient.

Anne Kusterbeck
Center for Bio/Molecular Science and Engineering

1992 OFFICE OF NATIONAL DRUG CONTROL POLICY TECHNOLOGY TRANSFER AWARD FOR DRUG ENFORCEMENT

Ms. Kusterbeck was recognized for her initiative in transferring the technology for the NRL-developed flow immunosensor, a novel system to detect drugs of abuse, to the commerical sector. The flow immunosensor is a highly sensitive, drug-screening device that is expected to be both timesaving and cost-efficient.

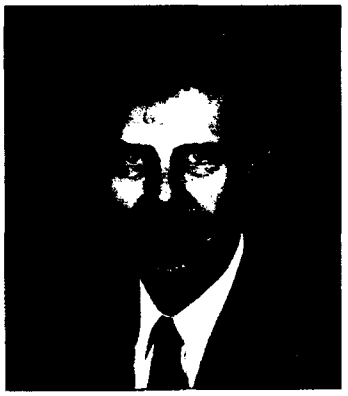

Dr. Teddy Keller
Chemistry Division

1992 FEDERAL LABORATORY CONSORTIUM AWARD FOR EXCELLENCE IN TECHNOLOGY TRANSFER

Dr. Keller was cited for his "exceptional creativity and initiative in the effective technology transfer (to industry) of phthalonitrile monomer/prepolymer technology for a broad spectrum of applications... These novel polymeric materials have the potential to bridge the gap between currently used high-temperature polymers and metals/ceramics."

Maria T. Kalcic
Marine Geosciences Division

INDUCTED INTO THE SPACE TECHNOLOGY HALL OF FAME

Ms. Kalcic was inducted into the Space Technology Hall of Fame by the U.S. Space Foundation for her work on the National Aeronautics and Space Administration's Earth Resources Laboratory Applications Software (ELAS). Ms. Kalcic's selection to the Hall of Fame was based on experiments and products originally developed for applications in space programs, but which have made significant contributions to the benefit of people on Earth. Ten programs were nominated for this distinguished award and ELAS was one of the two selected.

Dr. Richard H. Rein
Office of Technology Transfer

NAVY TECHNOLOGY TRANSFER LIFE ACHIEVEMENT AWARD FOR 1991

According to the Office of Naval Research nomination, "Dr. Rein, who joined NRL in 1990, has been extremely effective in attracting the interest of nongovernmental organizations in the use of NRL-developed technology...Dr. Rein has been instrumental in publicizing the benefits and advantages of government scientist/engineer participation within the NRL community...."

Dr. Paul F. Ottinger
Plasma Physics Division

IEEE 1992 PLASMA SCIENCE AND APPLICATIONS COMMITTEE AWARD

Dr. Ottinger was cited for "his contributions to plasma science in intense light-ion-beam transport, stability, and focusing for inertial confinement fusion, and in the theory of the plasma-erosion-switch for applications to pulsed-power generators." Dr. Ottinger is the first winner of this award who is not affiliated with a university.

Dr. Noel Turner
Chemistry Division

1991 CHEMICAL SOCIETY OF WASHINGTON (CSW) CHARLES L. GORDON AWARD

Dr. Turner was recognized for his "many contributions to the smooth operation of the CSW and his contributions to the science of chemistry. As stated in the nomination, "Dr. Turner has had a productive career in applying surface analysis techniques to polymer coatings, charcoal adsorbents, lubrication surfaces, and electrodes...."

David K. Woodington
Research and Development Services Division

NAVY MERITORIOUS CIVILIAN SERVICE AWARD

Mr. Woodington was cited for achieving "an unequaled record of excellence in efficiency and productivity in the management of the Public Works Division." Furthermore, "in less than eighteen months, Mr. Woodington reorganized the Division and instituted management goals and objectives that turned the Public Works Division into one of the most productive and efficient support divisions at the Laboratory."

Dr. Barry M. Klein
Condensed Matter and Radiation Sciences Division

NAVY MERITORIOUS CIVILIAN SERVICE AWARD

According to the award citation, "as head of the Complex Systems Theory Branch (which he also established), Dr. Klein recruited scientists of world-class caliber. The scope of their work under his leadership is remarkable...The productivity and impact of the branch program under Dr. Klein's leadership has attracted national and international recognition, in keeping with the highest traditions of the United States Navy."

Nelson M. Head, Jr.
Information Technology Division

OFFICE OF THE CHIEF OF NAVAL RESEARCH EQUAL EMPLOYMENT OPPORTUNITY AWARD
(Supervisory Category)

Mr. Head was recognized for demonstrating a total commitment to encouraging opportunities for minorities. He was cited for his "dedication and strong leadership...devoting many off-duty hours as a participant in career fairs designed to attract affirmative employment candidates."

NRL COMMANDING OFFICER'S AWARD FOR ACHIEVEMENT IN THE FIELD OF EQUAL OPPORTUNITY
(Supervisory Category)

Mr. Head is credited with promoting equal employment opportunites at NRL for a number of years utilizing existing hiring programs to hire candidates from underrepresented groups. Through these programs, he has employed minority summer students, minorities in professional fields, and mobility-impaired college students.

Saurabh F. Dalal
Tactical Electronic Warfare Division

NRL COMMANDING OFFICER'S AWARD FOR ACHIEVEMENT IN THE FIELD OF EQUAL OPPORTUNITY
(Nonsupervisory Category)

Mr. Dalal was recognized for his work as the volunteer chairman of the Asian Pacific American (APA) subcommittee in NRL's EEO program. Under his chairmanship, the subcommittee examined employee training and development courses offered at NRL and proposed additional courses for APAs and other employees, with a desire to improve their oral and written communications skills.

Patrick W. Theriot
Marine Geosciences Division

OFFICE OF THE CHIEF OF NAVAL RESEARCH'S OUTSTANDING EMPLOYEE WITH DISABILITIES AWARD

Mr. Theriot was cited for his positive attitude and friendly spirit that serves as a shining example for all who work with him. The award reads, in part, "Your community involvement with spinal cord patients through lectures and television commercials is outstanding. Your dedication and inspirational courage are a credit to the Office of the Chief of Naval Research and the Department of the Navy."

DEPARTMENT OF THE NAVY AWARD OF MERIT FOR GROUP ACHIEVEMENT

Scientists and engineers of the Naval Center for Space Technology were honored for their contributions to the Low-Power Atmospheric Compensation Experiment (LACE) Program Management Team. From l to r: D. Penn, W. Adkins, P. Regeon, J. Schaub, R. Palma, D. Horan, and H. Smathers.

DEPARTMENT OF THE NAVY AWARD OF MERIT FOR GROUP ACHIEVEMENT

Researchers from the Space Systems Technology Department were recognized for "exceptional meritorius service in the development, planning, and performance of a critically important series of special experiments." From l to r: S. Catania, P. Nicholson, and D. Fritz.

DEPARTMENT OF THE NAVY AWARD OF MERIT FOR GROUP ACHIEVEMENT

A team of researchers in the Space Science Division were recognized for their development of the Oriented Scintillation Spectrometer Experiment (OSSE). The nomination stated that "the instrument integration and test phases were conducted with remarkable success...the spacecraft integration and test, and the prelaunch operations went exceptionally well, and OSSE's performance in orbit has been outstanding." Front row: (l to r) J. Kurfess, R.Rubin, J. Lyon, P. Sandora, G. Kowalski, and M. Strickman. Back row: (l to r) Dr. T. Coffey, E. Simson, W. Marlin, R. Kroeger, W. Johnson, and CAPT P. Gaffney. Not pictured is R. Kinzer.

DEPARTMENT OF THE NAVY AWARD OF MERIT FOR GROUP ACHIEVEMENT

Researchers from the Naval Center for Space Technology were recognized for their "exceptional contributions in the design, development, and integration of the instrumentation package for NRL's first High Temperature Superconductivity Space Experiment (HTSSE-1)." Front row: (l to r) A. Marderness, L. Oliver, K. Alexander, A. Peltzer, A. Hall, J. Freitas, B. Kleindienst, and T. Kaweeki. Back row: (l to r) D. Spencer, B. Parker, C. Lichtenberg, M. Johnson, R. Harry, J. DeCamp, J. Cleveland, M. Bahrain, and R. Balduaf. G. Wiedemann is not pictured.

POINT DEFENSE DEMONSTRATION SYSTEM RADAR TEAM:(l to r) J. Alter, E. Maine, G. Trunk, Dr. P. Selwyn (ONT), R. Beattie, S. Brockett, P. Hughes, J. Wilson, M. Kim, and F. Caherty. Not pictured are M. Siegert and A. March.

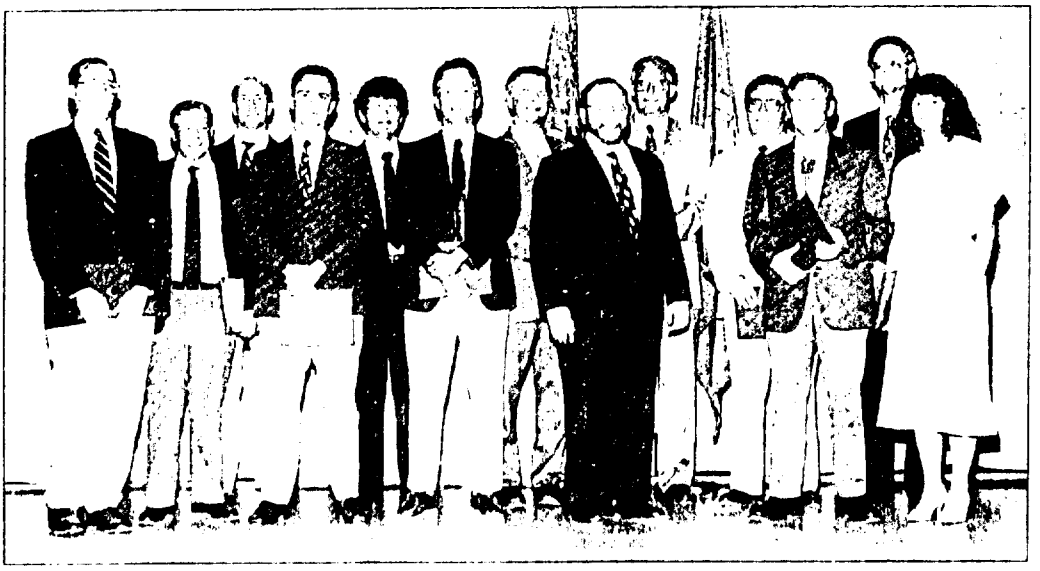

SPACE BASED IR SURVEILLANCE TEAM: (l to r) W. Shaffer, J. Hornstein, M. McHugh, R. Rhodes, B. Sweeney, A. Schaum, J. Michalowicz, Dr. P. Selwyn (ONT), T. Giallorenzi, G. Hoskins, R. Lucke, J. Kershenstein, and S. Hicks. Not pictured is E. Stone.

OFFICE OF NAVAL TECHNOLOGY SPECIAL GROUP AWARD

Twenty four NRL employees received awards from the Office of Naval Technology (ONT) for their contributions to Space Based Infrared (IR) Surveillance and the development of a Point Defense Demonstration System Radar. NRL was recognized by ONT for extraordinary accomplishment as evidenced by its successful demonstration of major advances in radar technology needed for countering the threat of modern antiship missiles.

Individual Honors

Laboratory employees received numerous scientific medals, military service awards, academic honors, and other forms of recognition, including election and appointment to offices in technical societies. The following is an alphabetical list of persons who received such recognition in fiscal year 1992.

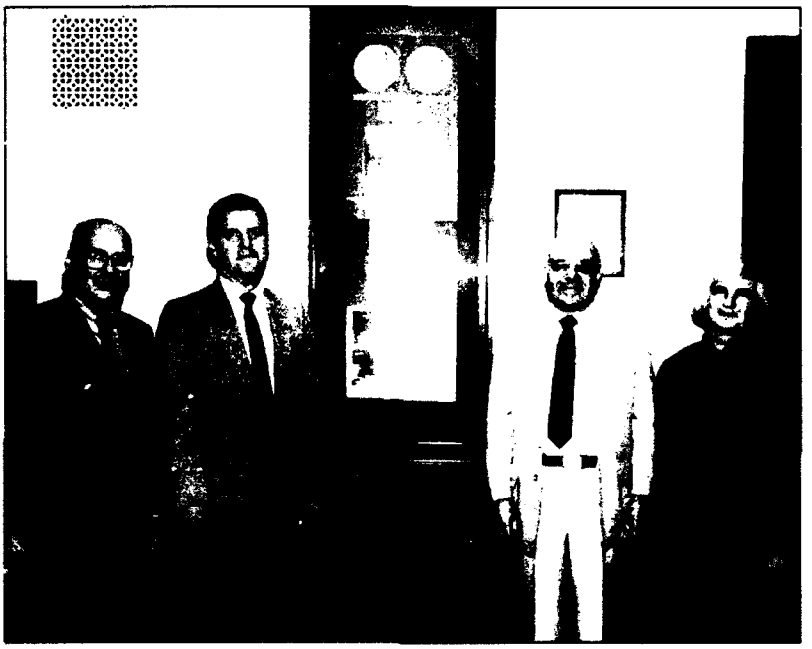

From l to r: The Honorable Gerald A. Cann, Assistant Secretary of the Navy (Research, Development, and Acquisition); The Honorable Dan Howard, Under Secretary of the Navy; and Dr. Jerome Karle and Dr. Isabella Karle of NRL's Laboratory for Structure of Matter, stand before the 1985 Nobel Prize display installed recently at the Pentagon. Dr. Jerome Karle was the recipient of the Nobel Prize in Chemistry.

Abrams, R., Chairman, Vacuum Electronics Subcommittee, International Electronic Devices Meeting.

Aggarwal, I.D., Program Committee Member, 9th International Symposium on Halide and Non-Oxide Glasses.

Ahn, S., Chairman, Editorial Committee of Korean Scientists and Engineers Association in America.

Anderson, W.T., Coordinator, Tri-Service MIMIC Reliability and Radiation Effects Program; Technical Program Chairman, GaAs Reliability Workshop; Member, Scientific Steering Committee of the Expert Evaluation and Control of Compound Semiconductor Materials and Technologies Workshop (EXATEC); Member, Technical Program Committee of the International Reliability Physics Symposium; Member, Technical Program Committee of the Advanced Microelectronics Qualification, Reliability, and Logistics Workshop; Member, Technical Program Committee of the European Symposium on Reliability of

Electron Devices, Failure Physics, and Analysis (ESREF); and Member, Technical Program Committee of VLSI Test Symposium.

Andreadis, T.D., Member, OUSD Microwave Effects Panel; Member, OUSD HPM System Effects Assessment Team; and Member, OUSD HPM Foreign Asset Assessment Team.

Apruzese, J.P., Guest Editor, *Applied Optics*, feature issue on ultrashort wavelength lasers; Member, Program Committee, SPIE Conference, "Ultrashort Wavelength Lasers II;" and Member, Program Committee, Lasers '92 Conference.

Au, B.D., 1992 NASA Group Achievement Award, Upper Atmosphere Research Satellite (UARS) Instrument Development Group.

Bachmann, C.M., Appointed to the Program Committee of the 1993 IEEE Workshop on Neural Networks for Signal Processing; Member of Sigma Xi; and Member, International Neural Network Society.

Barker E.B., Member, Data Assimilation Working Group, Stormscale Operational and Research Meteorology Program.

Barone, F.R., Chairman, Infrared Information Symposia Specialty Group on Infrared Countermeasures (a DoD-sponsored organization for the dissemination of classified information on Military Infrared Technology and its applications).

Batra, N.K., Associate Technical Editor, *Materials Evaluation*; Senior Member of IEEE; Member, IEEE UFFCS Technical Committee; Chaired a technical session on "IMAGING," at 1992 QNDE Conference; and Chaired a technical session on "NDE of Anisotropic Materials," IEEE Ultrasonic Symposium, December 1991.

Bernhardt, P.A., Appointed to the Arecibo Science Advisory Council; Vice Chairman, URSI-USNC (U.S. National Committee of the International Radio Science Union), Commission H — Waves in Plasmas; Editor, American Geophysical Union Books Board; and Editor, Committee on Space Research issue of *Advances in Space Science on Active Experiments in Space*.

Dr. Kenneth Dere is congratulated by CAPT Paul G Gaffney II, USN, NRL's Commanding Officer, for winning a 1992 Alan Berman Research Publication Award

Bielecki, D.J., "Choke Point Ocean Surveillance (U)," Proceedings of the 5th National Symposium on Sensor Fusion, 21-23 April 1992, Orlando, Florida.

Binari, S.C., Member, GaAs IC Symposium Technical Program Committee.

Blue, J.E., Fellow, Acoustical Society of America; and Chairman, Membership Committee, Acoustical Society of America.

Bogar, F., Elected Second Vice Chairman, National Capital Section of the Electrochemical Society for 1992-1993.

Boos, J.B., Chair, Electron Devices Area, 1993 International Conference on InP and Related Materials; and Secretary, Steering Committee, International Conference on InP and Related Materials.

Brady, Jr., R.F., Fellow, Royal Society of Chemistry (London); Technical Editor, *Journal of Coatings Technology*; Won Roon Foundation Award for best paper presented at the 1992 meeting of the Federation of Societies for Coatings Technology; and U.S. Navy Representative to The Technical Cooperation Program (TTCP), Panel P-3 on Organic Materials.

Brown, D., Session Chairman, 1991 Hardened Electronics and Radiation Technology Conference; Short Course Chairman, 1991 Nuclear and Space Radiation Effects Conference; and Technical Program Chairman, 1993 Nuclear and Space Radiation Effects Conference.

Brueckner, G.E., 1992 NASA Group Achievement Award, Upper Atmosphere Research Satellite (UARS) Instrument Development Group.

Bultman, J.D., Member, Committee on Creosote and Creosote Solutions; Member, Committee for the Evaluation of Wood Preservatives of the American Wood-Preservers' Association; Associate Editor and Member of the Editorial Board of *El Guayulero* (published by the Association for the Advancement of Industrial Crops); Associate Editor, *Biotropica* (published by the Association for Tropical Biology); and Associate Science Editor (NRL) for *Naval Research Reviews* (published by the Office of Naval Research).

Buot, F.A., Member, Editorial Board, Transport Theory and Statistical Physics; Member, Advisory Committee, International Workshop on Computational Electronics; Member, International Electron Devices Meeting (IEDM) Program Committee; and Session Chairman, IEDM Session on "Advanced Device Modeling."

Butler, J.W., Member, Organizing Committee and Session Chair for the Twelfth International Conference for Application of Accelerators in Research and Industry, Denton, Texas, November 1992.

Campbell, F.J., Fellow, Institute of Electrical and Electronics Engineers; Fellow, American Institute of Chemists; Member, Naval Aerospace Vehicle Wiring Action Group; Member, Sigma Xi; listed in *Who's Who in America*, 47th Edition (1992); listed in *Who's Who in Science and Engineering*, 1st Edition (1992); and received the Eric O. Forster Award for Distinguished Service from the Dielectrics and Electrical Insulation Society of the Institute of Electrical and Electronics Engineers.

Carruthers, G.R., Editor, *National Technical Association Journal*.

Carter, W.H., Invited to write the chapter on "Coherence Theory," for the book, *The Optical Society of America Handbook of Optics*, edited by M. Bass (McGraw-Hill, New York, 1993); Member, Fellows and Awards Committees for the SPIE International Society for Optical Engineering.

Cherkis, N.Z., National Fellow, the Explorers Club; Committee Member, U.S. Board on Geographic Names (Advisory Committee on Undersea Features); Invited expert to 4th-9th General Bathymetric Chart of the Oceans (GEBCO) Subcommittee for Digital Bathymetry (IOC/IHO); Scientific Advisor, GEBCO Guiding Committee; Bathymetric Advisor, Coordinating Committee for Circum-Atlantic Project (IUGS/USGS); and Invited expert, U.S.-Japan Cooperative Program in Natural Resources (UJNR)-Joint Sea Bottom Surveys Panel.

CAPT J.R. Love, USN, NRL's Chief Staff Officer, presents Mr. Nelson M. Head, Jr., of the Information Technology Division, with the Office of the Chief of Naval Research's Command Award for EEO achievements in the supervisory category

Chin-Bing, S.A., Thesis adviser to master of science degree recipient from the University of New Orleans, Department of Physics; biography listed in *American Men and Women of Science*, 17th Edition; appointed to the Technical Committee on Underwater Acoustics of the *Acoustical Society of America*; appointed to the graduate faculty of the University of New Orleans, appointed as National Research Council Postdoctoral adviser; invited contributor of the chapter, "The Effects of Large-Scale and Small-Scale Ocean Environmental Changes on

Underwater Acoustic Propagation Forecasting," for the book *Coupled Ocean Prediction and Acoustic Propagation Models*, A.R. Robinson and D. Lee (editors), American Institute of Physics, 1993; invited contributor of the chapter, "Sound Propagation in the Ocean Environment," for a book by the Computational Science Education Project — a project of the U.S. Government's Grand Challenges: High Performance Computing and Communications; appointed as a Member of the International Editorial Board for the proposed journal *Modeling and Scientific Computing*, to be published by Kluwer Academic Publishers, The Netherlands; and organized and chaired the Second Parabolic Equation Workshop.

Collins, M.D., Invited organizer of Special Session on Wave Propagation at SIAM Meeting of Society of Industrial and Applied Mathematicians in June 1992, Los Angeles.

CAPT Gaffney presents the Navy Achievement Medal to LT Mark Null, USN, pictured here with his wife. LT Null, a geophysicist at NRL-SSC, was recognized for his scientific acumen that "led to the development of new technology in the bathymetric and geoacoustic characterization of the oceans."

Commisso, R.J., Member, Plasma Science and Applications Executive Committee of the IEEE Nuclear and Plasma Sciences Society.

Conroy, D.J., 1992 NASA Group Achievement Award, Upper Atmosphere Research Satellite (UARS) Instrument Development Group.

Cooper, K.P., Invited to present a seminar on "Rapidly Solidified Cu-Cr Alloys," at the 26th Annual Materials Science Colloquium Series, University of Virginia, Charlottesville, Virginia, November 18, 1991; invited to contribute a chapter on "Laser Surface Processing," in *ASM Handbook, Vol 18, Friction Lubrication and Wear Technology*, American Society for Metals, International, Materials Park, Ohio, 1992; Reviewer, NASA's Microgravity Science and Applications Division Solidification Review Panel, May 28-29, 1992; Honorary Treasurer, Washington, DC Chapter of American Society for Metals, International; and continuing Member, ASM International, the Metallurgical Society, and Sigma Xi.

Cooperstein, G., Fellow, American Physical Society; Technical Program Committee Member, 1993 IEEE International Pulsed Power Conference; and Co-chairman, 9th International Conference on High Power Particle Beams, Washington, DC, May 1992; invited to serve as a member of the 1993 Program Committee at the Conference on Lasers and Electro-Optics (sponsored by the Optical Society of America).

Davis, L.C., Chair, Artificial Intelligence Technical Section, Operations Research Society of America.

Decina, B., Secretary, IEEE Oceanic Engineering Society Washington/Northern Virginia Chapter; and Guest Editor, *IEEE Journal of Oceanic Engineering*, April 1993.

DeVore, C.R., Newsletter Editor and ex officio Member, Executive Committee, Division of Computational Physics, American Physical Society.

Dobisz, E.A., Member of Program Committee, American Vacuum Society National Symposia; and Member of Program Committee, SPIE Conference on Electron-Beam, X-ray, & Ion Beam Submicrometer Lithographies for Manufacturing in March 1992 and appointed for 3rd consecutive year for 1993.

Elam, W., Fellow, American Institute of Physics Congressional Science.

Elton, R.C., Member, Program and Organizing Committees for 4th International Collo-

quium, Atomic Spectra and Oscillator Strengths Astrophysics and Laboratory Plasmas, National Institute of Standards and Technology, September 1992; Member, International Advisory Board, 3rd International Conference on X-ray Lasers, Germany, May 1992; and Member, International Advisory Board, 10th International Conference on Vacuum-UV Physics, Paris, July 1992.

Farwell, R.W., Member, Administrative Committee, IEEE Oceanic Engineering Society; Associate Editor, IEEE Oceanic Engineering Society; Chairman, Underwater Acoustic Technology, Technical Committee, IEEE Oceanic Engineering Society; and Member, Acoustical Society of America, Technical Committee on Acoustical Oceanography.

Fedder, J.A., Member, NSF Geospace Environment Modeling Steering Committee.

Feuillade, C., Fellow, Institute of Acoustics (UK).

Fischer, K.M., Elected Secretary, Gulf Coast Section of Marine Technology Society.

Fitzgerald, J.W., Member, Committee on Nucleation and Atmospheric Aerosols of the International Commission on Cloud Physics; and Chairman of the session "Condensation," at the Thirteenth International Conference on Nucleation and Atmospheric Aerosols, 24-28 August 1992, Salt Lake City, Utah.

Fleischer, P., Executive Committee, Sigma Xi, Gulf Coast Chapter.

Ford, R.T., Board of Directors and Treasurer, Electromagnetic Compatibility Society (EMCS) of the Institute of Electrical and Electronics Engineers (IEEE); recipient of the IEEE EMCS's 1993 Lawrence G. Cumming Award; appointed EMCS delegate to the Defense R&D Policy Subcommittee of the IEEE United States Activities Board; and appointed to the IEEE Technical Activities Board's New Technology Directions Committee.

Friebele, E.J., Chairman, NATO Panel IV, Research Study Group 12, Nuclear Effects Task Group; Fellow, American Ceramic Society; Member, DARPA Eye and Sensor Protection Steering Committee; and Member, Tri Service Fiber Optics Coordinating Committee.

Friedman, H., Massey Gold Medal of the Royal Society of London, "In Recognition of His Distinguished Contributions to Rocket and Satellite Astronomy, Particularly X-ray Astronomy;" and Elected to Council American Philosophical Society.

CAPT Gaffney presents the Navy Commendation Medal and certificate to CAPT Warren W. Schultz, USN, NRL's Biotechnology Program Manager, for his contribution to Operations Desert Shield and Desert Storm

Giallorenzi, T.G. Member, National Academy of Engineering; Vice President for Publications, IEEE Laser and Electro-optics Society; Associate Editor for *OSA Applied Optics*, *IEEE Proceedings*, and *IEEE Lightwave Telecommunications Systems*; Member, Board of Governors, IEEE Laser and Electro-optics Society; Editorial Board, *Laser Focus Magazine*, *OSA Optics and Photonics Magazine*; and Member, Steering Committees—IEEE/OSA Conference on Lasers and Electro-optics and IEEE/OSA Optical Fiber Conference.

Gibson, J., Chairman, 1992 Tri-Service/NASA Cathode Workshop; and Chairman of a Session, Program Committee Member; and Invited Speaker at the International Symposium SID '92.

Glembocki, O.J., Conference Chairman, SPIE Symposium on "Spectroscopic Characterization Techniques for Semiconductor

Technology IV;" and Member, Advisory Committee, SPIE Symposium on Compound Semiconductor Physics and Devices.

Goerss, J.G., Member, American Meteorological Society Committee on Weather Forecasting.

Gold, S.H., Continuing elected membership on Executive Committee of the Plasma Science and Applications Committee of the IEEE Nuclear and Plasma Sciences Society and Chairman of its Membership Subcommittee; continuing service as Associate Editor of the *IEEE Transactions on Plasma Science*; Session Organizer and Session Chairman, "Intense Beam Microwave Sources Session," at the Nineteenth IEEE International Conference on Plasma Science, 1-3 June 1992, Tampa, Florida; and Member, Program Committee, Twentieth IEEE International Conference on Plasma Science to be held 7-9 June 1993 in Vancouver, B.C., Canada.

Grabowski, K.S., Chairman, Symposium on Materials Modification by Energetic Atoms and Ions, held at the Spring Materials Research Society Meeting, April 1992.

Grinstein, F.F., Associate Fellow, American Institute of Aeronautics and Astronautics.

Griscom, D.L., Chairman, Glass & Optical Materials Division, American Ceramic Society; Fellow, American Ceramic Society; and Symposium Organizer, 1993 PAC RIM Meeting, American Ceramic Society.

Grun, J., Fellow, American Physical Society.

Gursky, H., Appointed to the Advisory Board, Institute for Computational Sciences and Informatics, George Mason University.

Hawkins, J.H., Member, NOAA/NESDIS Sea Surface Temperature Research Panel; Member, of U.S. National Research Council for Ocean Remote Sensing, U.S.-U.S.S.R. Workshop, June 1991.

Hembree, L.H., Member, Environmental Technology Working Group, Defense Modeling and Simulation Office.

Holst, R.W., Appointed Senior Field Officer, Naval Reserve Technology Mobilization Program.

Hoppel, W.A., Member of Working Group, "Aerosol Physics and Chemistry," of the International Aerosol Climatology Project of the World Meteorological Organization; and Member, editorial Board (American Association for Aerosol Research), *Aerosol Science and Technology*.

Hovermale, J.H., Fellow, American Meteorology Society.

CAPT Gaffney presents the Navy Commendation Medal and certificate to LCDR James Campbell, USN, a research microbiologist in NRL's Center for Bio/Molecular *Science and Engineering*, along with his wife, Patricia. LCDR Campbell was recognized for his contribution to Operations Desert Shield and Desert Storm.

Huba, J.D., Fellow, American Physical Society; and awarded Editori Citation for Excellence in Refereeing (*Journal of Geophysical Research: Space Physics*).

Hubler, G.K., Member, International Committee, Conference on Surface Modification of Metals by Ion Beams; Co-editor, SMMIB Proceedings; and Program Committee, Ion Beam Modification of Materials Conference.

Hughes, H.L., Member of the Steering Committee, Nuclear and Space Radiation Effects Conference.

Jacob, R.J.K., Vice-chair, Association for Computing Machinery, Special Interest Group on Computer-Human Interaction (ACM SIGCHI); Associate Papers Chair, CHI '92 Conference; Editorial Board, ACM Transactions on Computer-Human Interaction; and Advisory Board, University of Maryland Human-Computer Interaction Lab.

Jacobs, V., Fellow, American Physical Society; and Editor, *Coherent Radiation Processes in Strong Fields* (Gordon and Breach, Great Britain, 1991).

Jordan, A.K., Visiting Scientist, Research Laboratory of Electronics, Massachusetts Institute of Technology, Cambridge, Massachusetts.

Joyce, G.R., Fellow, American Physical Society.

Kabler, M.N., Fellow, American Physical Society; and Spokesperson for Participating Research Team, Beam Line X24C, at National Synchrotron Light Source, Brookhaven National Laboratory.

Kailasanath, K., Associate Fellow, American Institute of Aeronautics and Astronautics (AIAA); Program Chairperson, The Combustion Institute (Eastern Section); Member, Program Subcommittee, 24th International Symposium on Combustion; and Member, AIAA Propellants and Combustion Technical Committee.

Kalcic, M.T., Inducted into the Space Technology Hall of Fame (April 2, 1992) by the U.S. Space Foundation for her work on NASA's Earth Resources Laboratory Applications Software.

Kaufman, B., Fellow, American Astronautical Society (AAS); and Deputy Director of Aerospace Sciences Group of the AIAA.

Keller, T.M., Recipient of 1992 Federal Laboratory Consortium (FLC) Award for Excellence in Technology Transfer.

Kelner, G. Chairperson of the panel discussion at Sic Review, September 9-11, 1992, Charlottesville, Virginia.

Kershenstein, J.C., Office of Naval Technology (ONT) best accomplishment award for contributions to Space-Based Infrared (IR) Surveillance.

Killiany, J.M., Navy Member on Subgroup B of the Advisory Group on Electron Devices; and Chairman, Infrared Detector Specialty Group.

King, S.E., Member, Superconducting Super Collider BaF_2 Review Panel.

Klein, B.M., Received the Navy Superior Civilian Service Award, September 1992.

Dr. Susan Numrich of NRL's Information Technology Division was selected a Fellow to the Council for Excellence in Government. Dr. Numrich was recognized for her "technical capability and her potential for increased managerial responsibility."

Lackie, K.W., CNR Navy Superior Civilian Service Award for performance as Assistant Chief of Naval Research and Deputy Assistant Chief of Naval Research

Landwehr, C., Silver Core Award for Distinguished Service to International Federation for Information Processing (IFIP), September 1992; Chairman and U.S. National Leader, TTCP XTP-1 (Trustworthy Computing Technologies); Chairman, Working Group 11.3 (Database Security), IFIP; Program Co-chair, Third Working Conference on Dependable Computing for Critical Applications; Invited panelist, NASA Langley Peer Review on Formal Methods Research; and Editorial Board Member, *Journal of Computer Security*.

Lavoie, D., Executive Committee, Sigma Xi, Gulf Coast Chapter; and Editor (with R. Rezak of Texas A&M University), *Carbonate Microfabrice* (Springer-Verlag, Heidleburg).

Lean, J.L., 1992 NASA Group Achievement Award, Upper Atmosphere Research Satellite (UARS) Instrument Development Group.

Lee, T.L., Member, American Meteorological Society Committee on Satellite Meteorology and Oceanography.

Linder, N.R., 1992 NASA Group Achievement Award, Upper Atmosphere Research Satellite (UARS) Instrument Development Group.

Dr. David L. Bradley, superintendent of NRL's Acoustics Division, was elected to the executive council of the Acoustical Society of America

Long, J.P., Chairman, Time Resolved Spectroscopy Special Interest Group of the National Synchrotron Light Source.

Marks, C.J., Vice President for Compliance, Federally Employed Woman, Inc. (1991-1992); and Vice President for Policy and Long Range Planning, Federally Employed Women, Inc. (1992-1993).

Marrian, C.R.K., Vice Chair, Program Committee, 38th National Symposium of the American Vacuum Society, Seattle, Washington, November 11-15, 1992; and Editor, SPIE Institute of Advanced Technologies Volume entitled, "The Technology of STM Lithography."

Marsh, S.P., Elected Member of the Physical Metallurgy Technical Committee of the Minerals, Metals, and Materials Society (TMS); elected TMS Solidification Committee representative to the *Journal of Metals*; and elected to the Editorial Board of *Metallurgical Transactions B*.

McCafferty, E., Member, Corrosion Monograph Committee, the Electrochemical Society; and NRL Sigma Xi Award in Pure Science.

McCollum, M.D., Co-editor, "Transducers for Sonics and Ultrasonics," Proceedings of the Third International Workshop on Transducers for Sonics and Ultrasonics, June 1992.

McLean, J.D., Program Chair, IEEE Symposium on Research in Security; Privacy Chair, NSA Technical Exchange Working Group for High Assurance Systems; and Associate Editor, *Journal of Computer Security*.

Meadows, C., Associate Editor, *Journal of Computer Security*.

Mehl, M.J., Member, American Geophysical Union; Member, American Physical Society; and Member, Sigma Xi.

Michel, D.J., Fellow, ASM International; Member, Technical Program Committee, Fourth International Symposium on Environmental Degradation in Nuclear Power Systems—Water Reactors; Member, Nuclear Materials Committee, ASM International and TMS; and Professorial Lecturer, the George Washington University.

Middour, J.W., Member, Astrodynamics Technical Committee, American Institute of Aeronautics and Astronautics.

Morris, G.B., District Representative to the Voting Council, Society of Exploration Geophysicists.

Mosher, D., Fellow, American Physical Society; and Scientific Secretary and Proceedings Editor, 9th International Conference on High Power Particle Beams, Washington, DC, May 1992.

Mueller, G.P., Co-chairman, Eighth DoD Conference on Directed Energy Warfare, Vulnerability, Survivability and Effects; Editor, *Proceeding of the First DoD Workshop on Liquid Cell Power Limiters*, Volumes 1 and 2; O.S. Chairman, Subpanel 5, IEP U.S./U.K.-3.

Nagel, D.J., Member, Proposal Review Committee, X-ray Lithography Program, Defense Advanced Research Projects Agency (DARPA); Member, NRL Management Training Committee; and Member, DOE Nuclear Radiography Review Panel.

Namenson, A.T., Member, DNA Hardness Assurance Committee.

Natishan, P.M., Councillor, National Capital Section of the Electrochemical Society; Trustee, Baltimore-Washington Section of the National Association of Corrosion Engineers; Chairman, National Capital Section of the Electrochemical Society; and Representative to the Individual Membership Committee, the Electrochemical Society.

Nero, R.W., Member, Acoustical Society of America, Technical Committee on Acoustical Oceanography.

Ngai, K.L., International Advisory Committee and Program Committee, International Conference on Defects in Insulating Materials, Nordkirchen, Germany, August 16-22, 1992; and Co-organizer, 2nd International Discussion Meeting on Relaxations in Complex Systems, Alicante, Spain, June 28-July 8, 1993.

Oran, E.S., Fellow, American Institute of Aeronautics and Astronautics; Publications Committee, Chair of Journals Subcommittee, and Pendray Award Selection Committee of American Institute of Aeronautics and Astronautics; Past Chair, Division of Computational Physics, American Physical Society; Board of Directors, Combustion Institute; Associate Editor, *Journal of Computational Physics*; Advisory Board, Computer in Physics; Editorial Board, *Combustion and Flame*; Editorial Board, *Progress in Energy and Combustion Science*; Secretary of Board of Directors, International Colloquium on Dynamics of Energetic and Reactive Systems; and Program Chair, 25th Symposium (International) on Combustion, August 1994.

Ottinger, P.F., Received 1992 Plasma Science and Applications Award from IEEE Nuclear and Plasma Sciences Society.

Pande, C.S., Chairman, Physical Metallurgy Committee of the Metallurgical Society; and Member, International Committee of Electron Microscopy Society of America.

Parker, J.T., 1992 NASA Group Achievement Award, Upper Atmosphere Research Satellite (UARS) Instrument Development Group.

Patel, V., Fellow, American Physical Society; Member, National Academy of Sciences Task Group for Geomagnetic Studies; Chair and Organizer, Session for AGU Chapman Conference on ULF Waves, Williamsburg, Virginia, September 1992; Member, NSF Interagency Committee on Solar-Terrestrial Research; and Board Member, Institute for Advanced Physics Studies, La Jolla, California.

Petersen, E.L., Member-at-Large on IEEE Nuclear and Space Radiation Effects Conference Steering Committee.

Phillips, G.W., Appointed to DNA RUOSI Technology Study Team.

Pickett, W.E., Editorial Board, *Journal of Superconductivity* (published by Plenum Publishing Company); Fellow, American Physical Society; and received the E.O. Hulburt Award.

Piquette, J.C., Elected to *American Men and Women of Science*, January 1992.

Preller, R., JGR Associate Editor; and Member, AMS Polar Meteorology and Oceanography Committee.

Price, G.E., "Choke Point Ocean Surveillance (U)," Proceedings of the 5th National Symposium on Sensor Fusion, 21-23 April 1992, Orlando, Florida.

Prokes, S.M., Vice Chair, Materials Research Society Publications Committee; Subcommittee Chair, MRS Committee on books; and Member, MRS Bulletin Publication Committee.

Qadri, S.B., Invited to speak at the XIII AIRAPT International Conference on High Pressure Science and Technology, "Pressure Induced Crystalline Transformations of Diluted Magnetic Semiconductors," October 7-11, 1991.

NRL's Chesapeake Bay Detachment (CBD) was recognized by the Calvert County Commissioners in Maryland for the mutual aid support provided by the CBD Fire Department. The commissioners presented a proclamation of appreciation to LCDR B.K. Jones, USN, (right), the officer in charge at CBD, and CBD Fire Chief Joseph Garner.

Rath, B.B., Fellow, Minerals, Metals and Materials Society (TMS of AIME); received George Kimball Burgess Memorial Award of American Society for Materials International (ASM) and Charles S. Barrett Medal of the Rocky Mountain Chapter of ASM International; Member, External Review Board for the Institute of Materials, University of Connecticut; Member, Materials Research Center Advisory Board, University of Pittsburgh; Member, Engineering Advisory Council, Florida Atlantic University; Member, Advisory Board, Materials Science, Colorado School of Mines; Member, Guidance and Evaluation Board, Department of Energy; Member, Committee on Materials Task Group on Materials Planning, Office of Science and Technology Policy; Member, Engineers Public Policy Council, American Association of Engineering Societies; Member, Technical Division Board, ASM International; Chairman, Materials and the Environments Subcommittee of the Government Public Affairs Committee; Member, International Advisory Committee, Conference on Physics of Semiconductor Devices; Member, Program Committee, Conference on New and Alternative Materials; Member, Organizing Committee, Pacific Rim Conference on the Role of Shear and Diffusion in the Formation of Plate-Shaped Transformation Products; Chairman, Organizing Committee, Conference on Materials and Global Environment; Member, Organizing Committee, Fundamental Aspects of Dislocation Interactions; Member, Editorial Board, *Bulletin of Materials Science*, Indian Academy of Sciences; Member, International Editorial Board, *Materials and Design*; and Member, Editorial Committee, *International Materials Review*.

Reinecke, T.L., Fellow, American Physical Society.

Richardson, M.D., Naval Advisor to Environmental Parameters Group, MCM Technology Study, Naval Studies Board, National Research Council, and National Academy of Sciences; and Editor (with J.M. Hovem and R.D. Stoll), *Shear Waves in Marine Sediments* (Kluwer Academic Publishers).

Ripin, B.H., Appointed to DOE Fusion Energy Advisory Committee; elected to APS Council and Executive Board; appointed to DOE E.O. Lawrence Awards Committee; appointed to APS Committee on International Freedom of Scientists; Fellow, American Physical Society; Senior Member of the IEEE; and appointed Chairman, APS Publication Oversight Committee.

Mr. Bernard Kaufman of NRL's Naval Center for Space Technology was elected a Fellow of the American Astronautical Society. Mr. Kaufman is a recognized authority in astrodynamics who, over the past three decades, has made significant contributions in astrodynamics.

Rosen, M., Member, SDIO Threat Working Group.

Rose-Pehrsson, S.L., Technology Transfer Award for Hydrazine Dosimetry, July 1992.

Rudgers, A.J., Fellow, Acoustical Society of America; and Member, Membership Committee, Acoustical Society of America.

Saks, N.S., Technical Chairman, 1992 Nuclear and Space Radiation Effects Conference.

Sartwell, B.D., Received special award in April 1992 from the American Vacuum Society for outstanding service as General Chairman of the International Conference on Metallurgical Coatings and Thin Films in

1989 and 1991; Senior Editor, *Proceedings of the 1992 International Conference on Metallurgical Coatings and Thin Films*; Editor, *Journal Surface and Coatings Technology*, published by Elsevier Sequoia; and Member, Program Committee and Session Chairman for the 1991 Annual Symposium of the American Vacuum Society, Seattle, Washington.

Schmidt-Nielsen, A., Charter Fellow, American Psychological Society; Fellow, American Psychological Association; Secretary/Treasurer, Division 21 of the American Psychological Association; Membership Chair, Division 21 of the American Psychological Association; and Speech Communications Representative to the Acoustical Society of America Committee on Standards.

Shanabrook, B.V., Appointed to the International Advisory Committee of the 10th International Conference on Electronic Properties of Two Dimensional Systems.

Share, G.H., Bruno Rossi Prize awarded by the High Energy Astrophysics Division of the American Astronomical Society; and Sigma Xi Award for Pure Research.

Shepler, E.L., 1992 NASA Group Achievement Award, Upper Atmosphere Research Satellite (UARS) Instrument Development Group.

Skelton, E.F., Commissioned as spokesperson for Beamline X17C at Brookhaven National Laboratory; elected Energy-Dispersive Diffraction Special Interest Group Representative to the Users' Executive Committee at National Synchrontron Light Source, Brookhaven, New York; and invited to serve on the International Advisory Committee, Second International Conference on Semiconductor Materials, New Delhi, India.

Sleger, K.S., Chairman, RF Components Subpanel of JDL Reliance Electronic Devices; Navy Deputy Member, Advisory Group on Electron Devices (AGED) Working Group A; and Member of Steering Committee, 1993 International Conference on Silicon Carbide and Related Materials.

Smidt, F.A., Edited *Proceedings of International Conference on Surface Modification of Metals by Ion Beams*; Member, U.S. Government-TTG-A, Sub-Group C (Technology Export Control Advisory Group on Coatings); Fellow, ASM International; Member, Böhmische Physikalische Society (Honorary); Member, International Committee of Surface Modification of Metals by Ion Beams Conference; Senior Editor, ASM, *International Handbook on Surface Engineering* (Vol. 5 revision); and Member, ASM International Awards Committee.

Snow, A.W., Editorial Board, *Journal of Applied Polymer Science*.

Sohl, D.W., 1992 NASA Group Achievement Award, Upper Atmosphere Research Satellite (UARS) Instrument Development Group.

Dr. Phillip Sprangle of NRL's Plasma Physics Division was elected a senior member of the Institute of Electrical and Electronics Engineers (IEEE)

Sprangle, P.A., Fellow, American Physical Society; Member, Sigma Xi; appointed to Editorial Board of *Physics of Fluids B*; elected Senior Member, Institute of Electrical and Electronics Engineers; and Member, DARHT Feasibility Assessment Independent Consultants.

Stahlbush, R., Best Paper Award, 1992 Nuclear and Space Radiation Effects Conference.

Summers, G.P., Chairman, Department of Physics, University of Maryland Baltimore County; and invited Short Course Presenter, Nuclear and Space Radiation Effects Conference, New Orleans, Louisiana, July 1992.

Tang, C.M., Fellow, American Physical Society; and received the Women in Science and Engineering Award for the most outstanding woman scientist in the Federal government.

Temes, C.L., Served on Technical Review Group for Military Critical Technologies List; and served on Anti-Air Warfare Study Team for 21st Century Destroyer.

Tolstoy, A., Approved as NRC/NRL Post Doc Advisor; served on the following committees: ASA Acoustical Oceanography, ASA Standards, Chair of ASA Committee on Status of Women, National Standing Committee on Tomography, and NRL Sigma Xi (Vice President); invited to sit on NSF Panel to review Small Business Proposals; invited panelist on "Research in Government," at SIAM Meeting; author of Invited Review Paper, "Review of Matched Field Processing for Environmental Inverse Problems," *International Journal Modern Physics C*, 3(4), 691-708 (1992); invited talks: "Low Frequency Acoustic Tomography Using Matched Field Processing: Experimental Plan," presented at IEEE Oceans 91 Conference, October 1991; "Applied Mathematics in Underwater Acoustics," presented at SIAM Conference, July 1992; and "Ocean Acoustic Tomography via Matched Field Processing," presented at local IEEE Ocean Science Chapter, September 1992.

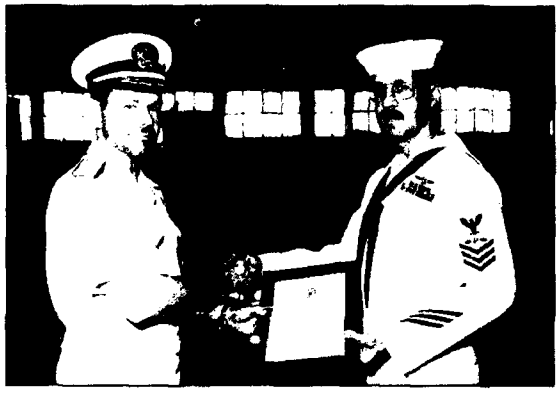

RADM William Miller, Chief of Naval Research (CNR), presents a certificate to AT1 William Lesnock of NRL's Flight Support Detachment. AT1 Lesnock was named 1991 OCNR Sailor of the Year. He was also presented with a Navy Achievement Medal.

Trunk, G.V., Chairman of KTP-2, a technical exchange panel on radar data processing under the auspices of subgroup K (radar) within The Technical Cooperation Program (TTCP).

Turner, N.H., Elected Member-at-Large to the Applied Surface Science Division of the American Vacuum Society; received Charles L. Gordon Award of the Chemical Society of Washington (Washington section of the American Chemical Society) in December 1991; Alternate Councillor, Chemical Society of Washington (Washington section of the American Chemical Society); and Membership Secretary, Division of Colloid and Surface Chemistry of the American Chemical Society.

Van Buren, A.L., Fellow, Acoustical Society of America; Member, Acoustical Society of America Committee on Standards; and Technical Program Chairman, Third International Workshop on Transducers for Sonics and Ultrasonics.

VanHoosier, M.E., 1992 NASA Group Achievement Award, Upper Atmosphere Research Satellite (UARS) Instrument Development Group.

Venezky, D.L., Appointed to the American Chemical Society Council Committee on International Activities.

Wagner, R.I., Program Committee, 1992 International Conference on Narrow Gap Semiconductors; and Program Committee, 1992 Meeting of IRIS Specialty Group on Infrared Material.

Wang, H.T., Chairperson, 11th International Conference on Offshore Mechanics and Arctic Engineering, Calgary, Canada; Member, Advisory Committee for ONR URI (University Research Initiative), "Fundamental Dynamics of Ocean Structures," at Oregon State University; and Courtesy Professor, Ocean Engineering Program, Oregon State University.

Waterman, J.R., Editor, *Proceedings of the 1992 HgCdTe Workshop*.

Werby, M.F., Appointed as National Research Council Postdoctoral adviser (completed assignment as Adviser to an ONT Postdoctoral Recipient in 1992); Fellow, Acoustical

Society of America; and Invited contributor of a chapter on acoustic scattering algorithms for a book by the Computational Science Education Project—a project of the U.S. Government's Grand Challenges: High Performance Computing and Communications.

Whitlock, R.R., Invited speaker, XIII AIRAPT Conference, Bangalore, India, 7-11 October 1991.

Wieting, T.J., Member, OUSD Microwave Effects Panel; Member, OUSD HPM Systems Effects Assessment Team; Member, OUSD Team on Project Tiger Grip; Member, OUSD HPM Foreign Asset Assessment Team; Navy representative, NATO AC243 Panel I Research Study Group; and Member, Program Committee and Session Chairman, Sixth HPM Conference.

Williams, E.G., Fellow, Acoustical Society of America; and Member, DARPA/ONR Numerical Modelling Committee.

Wilsey, N.D., Member, Editorial Board, *Journal of Materials Science: Materials in Electronics*.

Young, F.C., Chairman, Executive Committee, IEEE Plasma Science and Applications Committee; and Senior Member, IEEE.

CAPT Gaffney presents *1992 NRL Review* awards to Drs. Peter Ogden (left) and Fred Erskine

Alan Berman Research Publication and Edison Patent Awards

The Annual Research Publications Awards Program was established in 1968 to recognize the authors of the best NRL publications each year. These awards not only honor individuals for superior scientific accomplishments in the field of naval research, but also seek to promote continued excellence in research and in its documentation. In 1982, the name of this award was changed to the Alan Berman Research Publications Award in honor of its founder.

There were 442 separate publications published in 1992 that were considered for recognition. Of those considered, 39 were selected. These selected publications represent 131 authors, each of whom received a publication awards certificate, a bronze paperweight, and a booklet listing the publications that received special recognition. In addition, NRL authors share in their respective division's monetary award.

The winning papers and their respective authors are listed below by their research units. Non-Laboratory coauthors are indicated by an asterisk.

NRL also recognizes patents as part of its annual publication awards program. The NRL Edison (Patent) Awards were established in January 1991 to recognize NRL employees for outstanding patents issued to NRL by the U.S. Patent and Trademark Office during the preceding calendar year. The award recognizes significant NRL contributions to science and engineering as demonstrated by the patent process that are perceived to have the greatest potential benefit to the country. Of the 60 patents considered for 1992, two were selected, representing nine inventors. They are listed under the Edison Patent Awards.

Radar Division

AN/SPS-49 Digital Coherent Sidelobe Cancellation Study
Michael J. Steiner, Feng-Ling Lin, Karl R. Gerlach, James P. Hansen, and Ben H. Cantrell

Radar Countermeasures to Unintentional Modulation Exploitation
George J. Linde and Carl V. Platis

Information Technology Division

Direct Manipulation and Intermittent Automation in Advanced Cockpits
James A. Ballas, Constance Heitmeyer, and Manuel Pèrez

Algorithms for Multiple-Target Tracking
Jeffrey K. Uhlmann

Optical Sciences Division

Dual Difference Filtering: A Replacement for Interpolation and Subtraction to Detect Changes in Misregistered Signals
Alan Schaum

Nanochannel Array Glass
Ronald Tonucci, Brian Justus, Anthony Campillo, and Charles Ford*

Tactical Electronic Warfare Division

Tactical Proforma Signal Exploitation
Andrew M. Findlay, Joseph G. Crnkovich, Jr., Lawrence K. Ruffin, David Chau, and Steven A. Webb*

Transmission-Line Amplifiers
Gerald A. Chayt and Sidney T. Smith*

Underwater Sound Reference Detachment

Method for Transducer Transient Suppression. I: Theory
Jean C. Piquette

Method for Transducer Transient Suppression. II: Experiment
Jean C. Piquette

Direct Measurement of the Temperature-Dependent Piezoelectric Coefficients of Composite Materials by Laser Doppler Vibrometry
Kurt M. Rittenmyer and Pieter S. Dubbelday

Laboratory for the Structure of Matter

Implications for an Ion Channel in Leu-zervamicin: Crystal Structure of Polymorph B
Isabella L. Karle, Judith L. Flippen-Anderson, Sanjay Agarwalla,* and Padmanabhan Balaram*

Chemistry Division

NMR Imaging of Anisotropic Solid-State Chemical Reactions Using Multiple-Pulse Line-Narrowing Techniques and ^1H T_1 Weighting
Leslie G. Butler,* David G. Cory, * Kerry M. Dooley,* Joel B. Miller, and Allen N. Garroway

Molecular Dynamics Simulations and Experimental Studies of the Formation of Endohedral Complexes of Buckminsterfullerene
Richard C. Mowrey, Mark M. Ross, and John H. Callahan

Materials Science and Technology Division

Structural Origins of Magnetic Anisotropy in Sputtered Amorphous Tb-Fe Films
Vincent G. Harris, Kevin D. Aylesworth, Badri N. Das,
William T. Elam, and Norman C. Koon

Abstract Zwanzig Model Reduction Theory with Application to Discretized Linear Systems
Luther D. Flippen, Jr.

Laboratory for Computational Physics and Fluid Dynamics

The Stability of Imploding Detonations in the Geometrical Shock Dynamics (CCW) Model
C. Richard DeVore and Elaine S. Oran

Chemical Energy Release and Dynamics of Transitional, Reactive Shear Flows
Fernando F. Grinstein and K. Kailasanath

Condensed Matter and Radiation Sciences Division

Fermi Surfaces, Fermi Liquids, and High-Temperature Superconductors
Warren E. Pickett, Henry Krakauer,* Ronald E. Cohen,* and David J. Singh

Pulsed Laser Deposition of Epitaxial $BaFe_{12}O_{19}$ Thin Films
Carmine A. Carosella, Douglas B. Chrisey, Peter Lubitz, James S. Horwitz,
Paul Dorsey,* Randel Seed,* and Carmine Vittoria*

Plasma Physics Division

Electron Beam Tracking in a Preformed Density Channel
Donald P. Murphy, Robert E. Pechacek,* Daniel P. Taggart,* Richard F. Fernsler,
Richard F. Hubbard, Steven P. Slinker, and Robert A. Meger

Propagation and Guiding of Intense Laser Pulses in Plasmas
Phillip Sprangle, Eric Esarey, Jonathan Krall, and Glenn Joyce

Electronics Science and Technology Division

Electron and Hole Trapping in Irradiated SIMOX, ZMR, and BESOI Buried Oxides
Robert E. Stahlbush, George J. Campisi, John B. McKitterick,*
Witek P. Maszara,* Peter Roitman,* and George A. Brown*

Interface Phonons of Quantum Wires
Peter A. Knipp* and Thomas L. Reinecke

Center for Bio/Molecular Science and Engineering

Coplanar Molecular Assemblies of Amino- and Perfluorinated Alkylsilanes: Characterization and Geometric Definition of Mammalian Cell Adhesion and Growth
David A. Stenger, Jacque H. Georger,* Charles S. Dulcey, James J. Hickman,* Alan S. Rudolph, Thor B. Nielsen,* Stephen M. McCort,* and Jeffrey M. Calvert

Acoustics Division

A Self-Starter for the Parabolic Equation Method
Michael D. Collins

Anderson Localization of One-Dimensional Wave Propagation on a Fluid-Loaded Plate
Douglas M. Photiadis

Remote Sensing Division

Principal Components Transformation of Multifrequency Polarimetric SAR Imagery
Jong-Sen Lee and Karl W. Hoppel*

Assessment of National Technical Means for Oceanographic Data Collection and Marine Compliance
Ralph L. Fiedler, Albert E. Pressman, Peter A. Mitchell, Davidson T. Chen, Philip R. Schwartz, Ronald J. Holyer, Bazil E. Arthur, Jr., Robert A. Arnone, Kenneth J. Johnston, Stephen A. Mango, and John C. Daley

Oceanography Division

Development, Testing, and Operation of a Large Suspended Ocean Measurement Structure for Deep-Ocean Use
Martin G. Fagot, Richard C. Swenson,* Timothy A. Howell, Glen D. McCardle, and Dexter L. Walton

Rotating Modons Over Isolated Topographic Features
Richard P. Mied, Albert D. Kirwan,* and Gloria J. Lindemann

Marine Geosciences Division

Airborne Gravimetry
John M. Brozena

Marine Meteorology Division

Potential Refractivity as a Similarity Variable
B. John Cook and Stephen D. Burk

Design of the Navy's Multivariate Optimum Interpolation Analysis System
Edward Barker

Space Science Division

The Hydrogen Coma of Comet P/Halley Observed in Lyman α Using Sounding Rockets
Robert McCoy, Robert R. Meier, Horst Uwe Keller,*
Chet B. Opal,* and George B. Carruthers

X-ray Variability of Scorpius X-1 During a Multiwavelength Campaign
Paul L. Hertz, Brian A. Vaughn,* Kent S. Wood, Jay P. Norris,*
Kazuhisa Mitsuda,* Peter F. Michelson,* and T. Dotani*

Space Systems Development Department

A Fault-Tolerant Solid State Memory for Spaceborne Applications
Kenneth A. Clark and Barry W. Johnson*

NRL/USNO Two Way Time Transfer Modem Design and Test Results
G. Paul Landis and Ivan J. Galysh

Spacecraft Engineering Department

Ground-Based Ladar Measurements of Satellite Vibrations
K.I. Schultz* and Shalom Fisher

NRL Edison (Patent) Awards

High Resolution Patterning on Solid Substrates

Martin C. Peckerar and Christie R. Marrian
ELECTRONICS SCIENCE AND TECHNOLOGY DIVISION

Joel M. Schnur, Paul E. Schoen, Jeffrey Calvert,
and Jacque H. Georger, Jr.*
CENTER FOR BIO/MOLECULAR SCIENCE AND ENGINEERING

Pulsed X-ray Lithography

David J. Nagel
CONDENSED MATTER AND RADIATION SCIENCES DIVISION

Martin C. Peckerar
ELECTRONICS SCIENCE AND TECHNOLOGY DIVISION

Edward F. Miles
OFFICE OF COUNCIL

Awards for *NRL Review* Articles

Awards for *NRL Review* articles were established during 1990 to recognize authors who submit outstanding research articles for this scientific publication. The articles are judged on the relevance of the work to the Navy and the DoD, readability to the college-graduate level, and the use of graphics that are interesting and informative. The following awards were presented for articles that appeared in the *1992 NRL Review*.

FEATURED RESEARCH ARTICLE

Understanding Superconductivity in the Cuprates: Theory and Experiment
Stuart A. Wolf, Mark E. Reeves, and Joshua L. Cohn
MATERIALS SCIENCE AND TECHNOLOGY DIVISION
and
Vladimir Z. Kresin
LAWRENCE BERKELEY LABORATORY

DIRECTORATE AWARDS FOR SCIENTIFIC ARTICLES

General Science and Technology Directorate

Far Ultraviolet Cameras Experiment on STS-39: Observations of the Far UV Space Environment
George R. Carruthers
SPACE SCIENCE DIVISION

Warfare Systems and Sensors Research Directorate

Acoustic Backscattering from the Sea Surface
Peter M. Ogden and Fred T. Erskine
ACOUSTICS DIVISION

Materials Science and Component Technology Directorate

Buckminsterfullerene: Building Blocks for New Materials
Mark M. Ross, John H. Callahan, and Steven W. McElvany
CHEMISTRY DIVISION
and
Mark R. Pederson, Larry L. Boyer, and Warren E. Pickett
CONDENSED MATTER AND RADIATION SCIENCES DIVISION

Naval Center for Space Technology

Ground-based Laser Measurements of Vibration of the LACE Satellite

Shalom Fisher
SPACECRAFT ENGINEERING DEPARTMENT,
Donald Augenstein
UNIVERSITY OF MARYLAND,
and
Kenneth I. Schultz
MASSACHUSETTS INSTITUTE OF TECHNOLOGY LINCOLN LABORATORY

CAPT Paul Gaffney presents the featured research article award for the *1992 NRL Review* to (l to r) Drs. Stuart Wolf, Mark Reeves, and Joshua Cohn

Dr. George Carruthers of the Space Science Division accepts a *1992 NRL Review* award from CAPT Gaffney

Professional Development

Programs for NRL Employees

During 1992, under the auspices of the Employee Development Branch, NRL employees participated in about 5000 individual training events. Many of these were presented as either videotaped or on-site instructed courses on diverse technical subjects, management techniques, and enhancement of such personal skills as efficient use of time, speed reading, memory improvement, and interpersonal communications. Courses are also available by means of computer-based training (CBT) and live television courses for monitoring nationwide.

One common study procedure is for employees to work full time at the Laboratory while taking job-related scientific courses at universities and schools in the Washington area. The training ranges from a single course to full graduate and postgraduate programs. Tuition for training is paid by NRL. The formal programs offered by NRL are described here.

Dr. Astrid Schmidt-Nielsen of the Information Technology Division participated in the Advanced Graduate Research Program. She recently spent six months at the University of Minnesota.

GRADUATE PROGRAMS

• The **Advanced Graduate Research Program** (formerly the Sabbatical Study Program, which began in 1964) enables selected professional employees to devote full time to research or pursue work in their own or a related field for one year at an institution or research facility of their choice without the loss of regular salary, leave, or fringe benefits. NRL pays all educational costs, travel, and moving expenses for the employee and dependents. Criteria for eligibility include professional stature consistent with the applicant's opportunities and experience, a satisfactory program of study, and acceptance by the facility selected by the applicant. The program is open to paraprofessional (and above) employees who have completed 6 years of Federal Service, 4 of which are required at NRL.

• The **Edison Memorial Graduate Training Program** enables employees to pursue advanced studies in their fields at local universities. Participants in this program work 24 hours each workweek and pursue their studies during the other 16 hours. The criteria for eligibility include a minimum of 1 year of service at NRL, a bachelor's or master's degree in an appropriate field, and professional standing in keeping with the candidate's opportunities and experience.

• To be eligible for the **Select Graduate Training Program**, employees must have a college degree in an appropriate field and must have demonstrated ability and aptitude for advanced training. Students accepted in this program devote a full academic year to graduate study. While attending school, they receive one half of their salary; and NRL pays for tuition, books, and laboratory expenses. During the summer, they work at the Laboratory and receive normal pay and fringe benefits.

Lilimar Z. Avelino of the Acoustics Division participates in the Edison Memorial Graduate Training Program. She is pursuing a master of *science degree in electrical engineering at* Johns Hopkins University.

• The **Naval Postgraduate School** (NPS), located in Monterey, California, provides graduate programs to enhance the technical preparation of Naval officers and civilian employees who serve the Navy in the fields of science, engineering, operations analysis, and management. It awards a master of arts degree in national security affairs and a master of science degree in many technical disciplines. In addition, a doctor of philosophy degree may be earned in select fields of science and engineering.

NRL employees desiring to pursue graduate studies at NPS may apply for a maximum of six quarters away from NRL, with thesis work accomplished at NRL. Specific programs are described in the NPS catalog. Participants will continue to receive full pay and benefits during the period of study.

• Under the **Foreign Liaison Scientist Program**, assistance is provided to the Chief of Naval Research (CNR), the Chief of Naval Operations (CNO), and the Commandant of the Marine Corps (CMC) in discharging their responsibilities on matters of general scientific and technical interest to the United States in the United Kingdom, Europe, and Far East in foreign liaison offices that are maintained in several areas of the world. Foreign liaison scientists serve in these offices to establish relationships with overseas scientists and scientific activities, to monitor contract and treaty agreements, and to promote the exchange of information and research results between foreign sources and the U.S. Navy R&D establishment. Each year NRL will make assignments to the Office of Naval Research Europe (London, England), and the Office of Naval Research Asia (Tokyo, Japan). The purpose of such assignments is to acquaint a limited number of NRL's technical professionals with the functions of international operations, including such activities as developing productive liaisons with foreign scientists and research activities, representing the interests of the U.S. Navy in multinational conferences and scientific meetings, and preparing technical reports and papers with editorial interpretation for appropriate audiences in the United States.

• In addition to NRL and university offerings, application may be made to a number of noteworthy programs and fellowships. Examples of such opportunities are the **Alfred P. Sloan Fellows Program**, **Brookings Institute Advanced Study Program**, The **Fellowship in Congressional Operations**, and the **Women's Executive Leadership Program**. These and other programs are announced from time to time as schedules are published.

Mark T. Soyka of the Space Systems Development Department participates in the Select Graduate Program at the University of Texas

• Research conducted at NRL may be used as **thesis material for an advanced degree**. This original research is supervised by a quali-

John Traylor of the Spacecraft Engineering Department participated in the Naval Postgraduate School Program in a space system engineering curriculum

fied employee of NRL who is approved by the graduate school. The candidate should have completed the required course work and should have satisfied the language, residence, and other requirements of the graduate school from which the degree is sought. NRL provides space, research facilities, and supervision but leaves decisions on academic policy to the cooperating schools.

CONTINUING EDUCATION

• Local colleges and universities offer **undergraduate and graduate courses** at NRL for employees interested in improving their skills and keeping abreast of current developments in their fields. These courses are also available at many other DoD installations in the Washington, DC area.

• The Employee Development Branch at NRL offers to all employees **short courses** in a number of fields of interest including technical subjects, computer operation, supervisory and management techniques, and clerical/secretarial skills. Laboratory employees may attend these courses at nongovernment facilities as well. Interagency courses in management, personnel, finance, supervisory development, and clerical skills are also available.

For further information on any of the above programs, contact the Employee Development Branch (Code 1840) at (202) 767-2956.

TECHNOLOGY TRANSFER

• The **Office of Research and Technology Applications Program** (ORTA) ensures the full use of the results of the Nation's federal investment in research and development by transferring federally owned or originated technology to state and local governments and the private sector.

• The **Navy Science Assistance Program** (NSAR) establishes an information loop between the Fleet and the R&D shore establishments to expedite technology transfer to the user. The program addresses operational problems, focuses resources to solve specific technical problems, and develops a nucleus of senior scientific personnel familiar with the impact of current research and system performance on military operations.

• The **Scientist-to-Sea Program** (STSP) provides increased opportunities for Navy R&D laboratory/center personnel to go to sea to gain first-hand insight into operational factors affecting system design, performance, and operations on a variety of ships.

Inquiries concerning NRL's programs should be made to Dr. Richard Rein (Code 1003.1) at (202) 767-3744. Inquiries concerning NSAP or STSP programs should be made to Dr. George Abraham (Code 1003.1) at (202) 767-3521.

PROFESSIONAL DEVELOPMENT

NRL has several programs, professional society chapters, and informal clubs that enhance the professional growth of employees. Some of these are listed below.

• The **Counseling Referral Service** (C/RS) helps employees to achieve optimal job performance through counseling and resolution of problems such as family, stress and anxiety.

behavioral, emotional, and alcohol- or drug-related problems that may adversely impact job performance.

C/RS provides confidential assessments and short-term counseling, as well as training workshops and referrals to additional resources in the community. (Contact Robert Power, Code 9012 at (202) 767-6857.)

• A chartered chapter of **Women in Science and Engineering** (WISE) was established at NRL in 1983. Informal monthly luncheons and seminars are scheduled to inform scientists and engineers of women's research at NRL and to provide an informal environment for members to practice their presentations. WISE also sponsors a colloquium series to feature outstanding women scientists. (Contact Dr. Wendy Fuller at (202) 767-2793, Dr. Debra Rolison at (202) 767-3617, or Dr. Cha-Mei Tang at (202) 767-4148.)

• **Sigma Xi**, the Scientific Research Society, encourages and acknowledges original investigation in pure and applied science. As an honor society for research scientists, individuals who have demonstrated the ability to perform original research are elected to membership in local chapters. The NRL chapter, comprised of approximately 600 members, recognizes original research by presenting awards annually in pure and applied science to outstanding NRL staff members. The chapter also sponsors lectures at NRL on a wide range of scientific topics for the entire NRL community. These lectures are delivered by scientists from all over the nation and the world. The highlight of the Sigma Xi lecture series is the Edison Memorial Lecture, usually featuring a Nobel laureate. (Contact Dr. Robert Pellenbarg at (202) 767-2479 or 2202.)

• The **NRL Mentor Program Pilot Project** for NRL scientists and engineers was established to explore the feasibility of instituting a laboratory wide mentoring program. The Pilot Project is managed by a steering committee formed by the NRL Women's Science and Technology Network. The program offers a personal approach to career development and personal training. NRL mentors are identified as successful, experienced scientists and engineers.

Dr. Sally Ride, the first woman astronaut to go into space on a NASA mission, spoke at a Plasma Physics Division colloquium. Her visit was sponsored by WISE and the FWP Subcommittee.

Mentorees, who are colleagues with less developed technical and/or managerial skills, are paired with selected mentors. The program's focus is on imparting knowledge and expertise necessary for the professional and career growth and development of the mentorees. NRL NOTICE 12400 established the Pilot Project and provides the policy and procedures for the program. (Contact Zakya Kafafi at (202) 767-4871 or Kay Howell at (202) 767-3884.)

• Employees interested in developing effective self expression, listening, thinking, and leadership potential are invited to join either of two NRL chapters of **Toastmasters International**. Members of these clubs, who possess diverse career backgrounds and talents, meet three times a month in an effort to learn to communicate not by rules but by practice in an atmosphere of understanding and helpful fellowship. NRL's commanding officer endorses Toastmasters (see NRLINST 12410.11), and the Employee Development Branch pays for membership and educational materials for those employees whose supervisors see a need for their active training in public speaking or communication skills. (Contact Mrs. Kathleen Parrish at (202) 767-2782.)

EQUAL EMPLOYMENT OPPORTUNITY (EEO) PROGRAMS

Equal employment opportunity is a fundamental NRL policy for all persons, regardless of race, color, sex, religion, national origin, age, or physical/mental handicap. The EEO office's

major functions include affirmative action in employment; discrimination complaint process; EEO training of supervisors, managers, and EEO collateral duty personnel; advice and guidance to management on EEO policy; and the following special emphasis programs:

• The **Federal Women's Program** (FWP) supports and enhances employment and advancement opportunities for women and addresses issues that affect women in the workplace. It provides counseling and referral services and sponsors a chapter of Women in Science and Engineering to recognize outstanding female scientists and engineers. Distinguished women scientists are guest lecturers at quarterly presentations.

• The **Hispanic Employment Program** (HEP) focuses on working with supervisors, managers, and subcommittees to recruit and place qualified Hispanics. The program is involved with Hispanic community organizations and local schools and provides activities specifically designed to offer employment opportunities to Hispanics. "El Ingeniero" (The Engineer), which encourages Hispanic youth to pursue a career in engineering, is one such program.

Entertainer Tony Melendez tells his story while playing an instrumental song during NRL's celebration of National Hispanic Heritage Month and National Disabilities Month

The **Black Employment Program** (BEP) concentrates on recruiting, placing, developing, and advancing African American employees throughout NRL. It also encourages them to achieve their maximum potential.

• The **Individuals with Handicaps Program** (IHP) assists management to improve employment and advancement opportunities for qualified handicapped and disabled veteran employees. It also advises on accommodations necessary for handicapped persons. It recruits handicapped summer students from colleges and universities for technical positions in engineering and science and paraprofessional positions in accounting and administration; it also seeks Cooperative Education Program (Co-op) candidates who are pursuing degrees in engineering, computer sciences, or the physical sciences.

• The **Asian-American/Pacific Islander Program** (API) identifies areas of concern regarding the recruitment, selection, advancement, retention, and utilization of API employees throughout NRL. The program interacts with API professional/community organizations to address employment concerns.

• The **American Indian/Alaskan Native Employment Program** (AI/ANEP) focuses on the employment concerns of AI/ANEP employees. The program provides counseling and referral services on recruitment, hiring, placement, promotion, retention, and other areas of employee interest.

• The **Federal Employment Opportunity Recruitment Program** (FEORP) is designed to establish, maintain, and update targeted recruitment programs to reduce the conspicuous absence or manifest imbalance categories of NRL employment through innovative internal and external recruitment. In addition, it fosters relationships with minority and women's institutions and organizations.

Special programs are held during the year to promote an awareness of the contributions and capabilities of women and minorities. (Contact the EEO office at (202) 767-2486 for all EEO programs.)

OTHER ACTIVITIES

• The **Community Outreach Program** traditionally has used its extensive resources to foster programs that provide benefits to students and other community citizens. Volunteer employees assist with and judge science fairs, give lectures, tutor, mentor, coach, and serve as classroom resource teachers. The program also sponsors Black History Month art and essay contests for local schools, student tours of NRL, a student Toastmasters Youth Leadership Program, an annual Christmas party for neighborhood children, and an annual collection for Children's Hospital. Through this program NRL has active partnerships with four District of Columbia public schools. (Contact the Public Affairs Office at 767-2541.)

NRL's Community Outreach volunteer, Levi Daniels of the Plasma Physics Division, works with Leckie Elementary School students on an electricity project

• Other programs that enhance the development of NRL employees include four computer user groups (**IBM PC**, **Mac**, **NeXT**, and **Sun**), the **Microcomputer Software Support Center**, and the **Amateur Radio Club**. The **Recreation Club** accommodates the varied interests of NRL's employees with its numerous facilities, such as a 25-yard, 6-lane indoor swimming pool; a gymnasium with basketball and volleyball; a weight room and exercise area; table tennis; meeting room; softball and basketball leagues; jacuzzi whirlpool; saunas; classes in five different martial arts groups, aerobics exercise, swimming, and water walking; and specialized sports clubs (running, skiing, biking, and golfing). The **Showboaters**, a nonprofit drama group that presents live theater for the enjoyment of NRL and the community, performs two major productions each year in addition to occasional performances at Laboratory functions and benefits for local charities. The most recent productions were "You Can't Take it With You" and "The Murder Room." Though based at NRL, membership in Showboaters is not limited to NRL employees.

NRL employees annually sponsor a Christmas party for 150 children from nearby schools. Shown here are the Clauses (Kathy Parrish of the Technical Information Division and Frank Clarke, former NRL employee) and students as they join Ronald McDonald in McRocking Kid's concert.

Programs for Non-NRL Employees

Several programs have been established for non-NRL professionals. These programs encourage and support the participation of visiting scientists and engineers in research of interest to the Laboratory. Some of the programs may serve as stepping-stones to federal careers in science and technology. Their objective is to enhance the quality of the Laboratory's research activities through working associations and interchanges with highly capable scientists and engineers and to provide opportunities for outside scientists and engineers to work in the Navy laboratory environment. Along with enhancing the Laboratory's research, these programs acquaint participants with Navy capabilities and concerns.

RECENT Ph.D., FACULTY MEMBER, AND COLLEGE GRADUATE PROGRAMS

• The **National Research Council (NRC)/ NRL Cooperative Research Associateship Program** selects associates who conduct research at NRL in their chosen fields in collaboration with NRL scientists and engineers. The tenure period is 2 years. The Office of Naval Research offers the associate post-tenure research grants tenable at an academic institution.

• The American Society for Engineering Education (ASEE) administers the **Office of Naval Research (ONR) Postdoctoral Fellowship Program** that aims to increase the involvement of highly trained scientists and engineers in disciplines necessary to meet the evolving needs of naval technology. Appointments are for 1 year (renewable for a second and sometimes a third year). These competitive appointments are made jointly by ONR and ASEE.

• The American Society for Engineering Education also administers the Navy/ASEE **Summer Faculty Research Program** for university faculty members to work for 10 weeks with professional peers in participating Navy laboratories on research of mutual interest.

• The **NRL/United States Naval Academy (USNA) Cooperative Program for Scientific Interchange** allows faculty members of the U.S. Naval Academy to participate in NRL research. This collaboration benefits the Academy by providing the opportunity for USNA faculty members to work on research of a more practical or applied nature. In turn, NRL's research program is strengthened by the available scientific and engineering expertise of the USNA faculty.

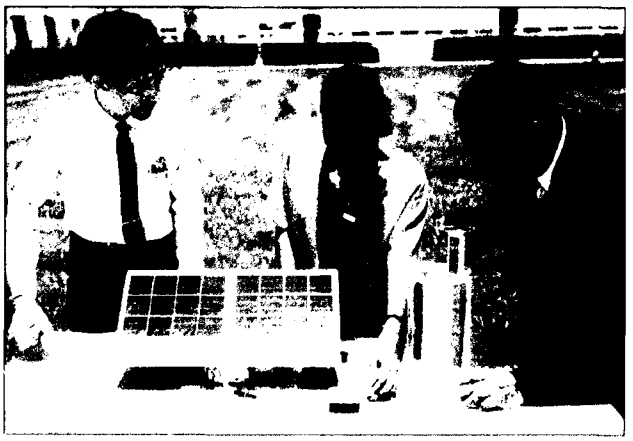

Ballou High School student, Jessica Peterson demonstrates the use of solar energy to produce hydrogen and oxygen from water, to chemistry teacher Clarence Taylor (right) and mentor Dr. George Carruthers (left) of NRL's Space Science Division. The project won first place in chemistry at Ballou's science fair.

• The **Office of Naval Research Graduate Fellowship Program** helps U.S. citizens obtain advanced training in disciplines of science and engineering critical to the U.S. Navy. The 3-year program awards fellowships to recent outstanding graduates to support their study and research leading to doctoral degrees in specified disciplines such as electrical engineering, computer sciences, material sciences, applied physics, and ocean engineering. Award recipients are encouraged to continue their study and research in a Navy laboratory during the summer.

For further information about the above five programs, please contact Mrs. Jessica Hileman at (202) 767-3865.

• The **United States Naval Academy Ensign Program** assigns Naval Academy graduates to NRL to work in areas of their own choosing commensurate with their academic qualifications. These graduates provide a fruitful summer of research assistance, while gaining valuable experience in the Navy's R&D program. (Contact CDR Bob Young at (202) 767-2103.)

PROFESSIONAL APPOINTMENTS

• **Faculty Member Appointments** use the special skills and abilities of faculty members for short periods to fill positions of a scientific, engineering, professional, or analytical nature.

• **Consultants and experts** are employed because they are outstanding in their fields of specialization, or because they possess ability of a rare nature and could not normally be employed as regular civil servants.

• **Intergovernmental Personnel Act Appointments** temporarily assign personnel from the state or local government or educational institution to the federal government (or vice versa) to improve public services rendered by all levels of government.

UNDERGRADUATE COLLEGE STUDENT PROGRAMS

Several programs are tailored to the undergraduate that provide employment and work

NRL-Stennis Space Center's Curtis B. Favre, Jr. (left), a physical science technician in the Acoustics Division, and Dr. Herbert C. Eppert, Jr. (right), Head, Marine Geosciences Division, discuss projects with students at the Region VI Science and Engineering Fair held in Biloxi, Mississippi

experience in naval research. These are designed to attract applicants for student and full professional employment in the Laboratory's shortage category positions, such as engineers, physicists, mathematicians, and computer scientists. The student employment programs build an understanding of NRL job opportunities among students and educational personnel, so that educators can provide students who will meet NRL's occupational needs. The employment programs for college students include the following:

• The **Cooperative Education Program** alternates periods of work and study for students pursuing bachelor degrees in engineering, computer science, or the physical sciences. Several universities participate in this program.

• The **Clerical Cooperative Education Program** employs students interested in pursuing careers in the clerical occupation. Students work part time during the school year and full time during school breaks.

• The **Federal Junior Fellowship Program** hires needy students entering college to be assistants to scientific, professional, or technical employees.

• The **Summer Employment Program** employs students for the summer in paraprofes-

sional and technician positions in engineering, physical sciences, and computer sciences.

• The **Student Volunteer Program** helps students gain valuable experience by allowing them to voluntarily perform educationally related work at NRL.

• The **1040-Hour Appointment** employs students on a half-time basis to assist in scientific work related to their academic program.

For additional information, contact Cindy Stiles at (202) 767-3030.

HIGH SCHOOL PROGRAMS

• The **DoD Science & Engineering Apprentice Program** (SEAP) employs high school juniors and seniors to serve for 8 weeks as junior research associates. Under the direction of a mentor, students gain a better understanding of research, its challenges, and its opportunities through participation in scientific programs. Criteria for eligibility are based on science and mathematics courses completed and grades achieved; scientific motivation, curiosity, and capacity for sustained hard work; a desire for a technical career; teacher recommendations; and achievement test scores. The NRL program is the lead program and the largest in DoD.

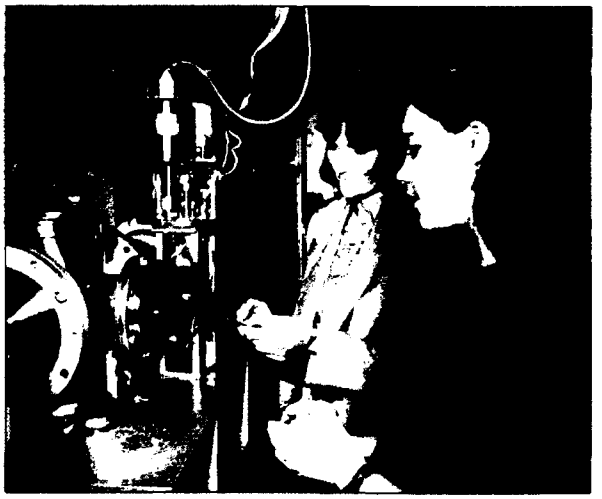

Dr. Catherine Cotell of the Condensed Matter and Radiation Sciences Division looks on as SEAP student Cecelia Sheridan loads a sample for coating with a bonelike ceramic into the pulsed laser deposition chamber

For additional information on these programs, please contact the Employee Development Branch (Code 1840) at (202) 767-2956.

General Information

Technical Output

The Navy continues to be a pioneer in initiating new developments and a leader in applying these advancements to military requirements. The primary means of informing the scientific and engineering community of the advances made at NRL is through its technical output—reports, articles in scientific journals and books, papers presented to scientific societies, and topical conferences, patents, and inventions.

This section lists a portion of NRL's output for FY 1992. The omitted parts are oral presentations (about 1860), reports that carry a military security classification, and letter reports to sponsors.

A complete listing of the publications by NRL authors, including reports, articles in scientific journals and books, patents, and SIRs appear in the *Bibliography of NRL Publications* as a separate publication.

Type of Contribution	Unclass.	Class.	Total
Papers in periodicals, books, and proceedings of meetings	792	0	792
NRL Reports	33	17	50
NRL Memorandum Reports	90	29	119
Books	1	0	1
Patents granted			59
Statutory Invention Registrations (SIRs)			2

Key Personnel

Code	Office	Direct-in-Dialing (202)76 & (202)40; Autovon 29-	Extension
	EXECUTIVE DIRECTORATE		
1000	Commanding Officer	CAPT P.G. Gaffney II, USN	73403
1001	Director of Research	Dr. T. Coffey	73301
1000.1	Scientific Staff Assistant	Mr. K.W. Lackie	72880
1002	Chief Staff Officer/Inspector General	CAPT J.R. Love, USN*	73621
1003	Associate Director of Research for Strategic Planning	Dr. W.M. Tolles	73584
1005	Head, Office of Management and Administration	Ms. M. Oliver	73086
1010	Deputy for Space Systems	Dr. R. LeFande*	73324
1200	Head, Command Support Division	CAPT J.R. Love, USN*	73621
1220	Head, Security	Mr. J.C. Payne	73048
1230	Public Affairs Officer	Mr. J. Gately, Jr.*	72541
1240	Head, Safety Branch	Mr. K.J. King*	72232
1280	Officer in Charge, Pax River Flight Support Detachment	CDR S.S. Smith, USN	301-863-3751
1800	Director, Human Resources Office	Ms. B. Duffield	73421
1803	Deputy EEO Officer	Ms. D. Erwin*	72486
3008	Legal Counsel	Ms. H. Halper*	72244
	BUSINESS OPERATIONS DIRECTORATE		
3000	Associate Director of Research	Mr. R.E. Doak	72371
3030	Head, Management Information Systems Staff	Mr. R.L. Guest	72030
3200	Head, Contracting Division	Mr. J.C. Ely	75227
3300	Comptroller, Financial Management Division	Mr. D.T. Green	73405
3400	Supply Officer, Supply Division	Mr. W.E. Ralls, Jr.	73446
3500	Director, Research and Development Services Division	Mr. D.K. Woodington	73371
	GENERAL SCIENCE AND TECHNOLOGY DIRECTORATE		
4000	Associate Director of Research	Dr. R.A. LeFande	73324
4003	Consultant for Critical Technology Assessment	Mr. L.M. Winslow	72887
4006	Technology Base Manager	Dr. S. Sacks	73666
4040	Scientific Consultant	Dr. P. Mange	73724
4050	Signature Technology Office	Dr. D.W. Forester	73116
	WARFARE SYSTEMS AND SENSORS RESEARCH DIRECTORATE		
5000	Associate Director of Research	Mr. R.R. Rojas	73294
5200	Head, Technical Information Division	Mr. P.H. Imhof	73388
5300	Superintendent, Radar Division	Dr. M.I. Skolnik	72936
5500	Superintendent, Information Technology Division	Dr. R.P. Shumaker	72903
5600	Superintendent, Optical Sciences Division	Dr. T.G. Giallorenzi	73171
5700	Superintendent, Tactical Electronic Warfare Division	Dr. J.A. Montgomery	76278
5800	Head, Research Computation Division	Mr. R.F. Saenger	72751
5900	Superintendent, Underwater Sound Reference Detachment	Dr. J.E. Blue	407-857-5230
	MATERIALS SCIENCE AND COMPONENT TECHNOLOGY DIRECTORATE		
6000	Associate Director of Research	Dr. B.B. Rath	73566
6030	Head, Laboratory for Structure of Matter	Dr. J. Karle	72665
6100	Superintendent, Chemistry Division	Dr. J.S. Murday	73026
6300	Superintendent, Materials Science & Technology Division	Dr. D.U. Gubser	72926
6400	Director, Lab. for Computational Physics and Fluid Dynamics	Dr. J.P. Boris	73055
6600	Superintendent, Condensed Matter & Radiation Sciences Division	Dr. D.J. Nagel	72931
6700	Superintendent, Plasma Physics Division	Dr. S. Ossakow	72723
6800	Superintendent, Electronics Science & Technology Division	Dr. G.M. Borsuk	73525
6900	Center for Bio/Molecular Sciences and Engineering	Dr. J. Schnur	73344
	OCEAN AND ATMOSPHERIC SCIENCE AND TECHNOLOGY DIRECTORATE		
7000	Associate Director of Research	Dr. E.O. Hartwig	48690
7030	Head, Systems Support and Requirements	Dr. R.M. Root	601-688-4010
7100	Superintendent, Acoustics Division	Dr. D.L. Bradley	73482
7200	Superintendent, Remote Sensing Division	Dr. K. Johnston	72351
7300	Superintendent, Oceanography Division	Dr. W.B. Moseley	601-688-4670
7400	Superintendent, Marine Geosciences Division	Dr. H.C. Eppert, Jr.	601-688-4650
7500	Superintendent, Marine Meteorology Division	Dr. J.B. Hovermale	408-656-4721
7600	Superintendent, Space Science Division	Dr. H. Gursky	76343
	NAVAL CENTER FOR SPACE TECHNOLOGY		
8000	Director	Mr. P.G. Wilhelm	76547
8100	Superintendent, Space Systems Development Department	Mr. R.E. Eisenhauer	70410
8200	Superintendent, Spacecraft Engineering Department	Mr. R.T. Beal	76407

*Additional Duty

ORGANIZATIONAL CHART
EXECUTIVE DIRECTORATE

COMMANDING OFFICER
Code 1000
CAPT P.G. Gaffney II, USN

DIRECTOR OF RESEARCH
Code 1001
Dr. T. Coffey

ASSOCIATE DIRECTORS OF RESEARCH

OFFICE FOR STRATEGIC PLANNING
Code 1003
Dr. W.M. Tolles

BUSINESS OPERATIONS DIRECTORATE
Code 3000
R.E. Doak

GENERAL SCIENCE AND TECHNOLOGY DIRECTORATE
Code 4000
Dr. R.A. LeFande

WARFARE SYSTEMS AND SENSORS RESEARCH DIRECTORATE
Code 5000
R.R. Rojas

MATERIALS SCIENCE AND COMPONENT TECHNOLOGY DIRECTORATE
Code 6000
Dr. B.B. Rath

OCEAN AND ATMOSPHERIC SCIENCE AND TECHNOLOGY DIRECTORATE
Code 7000
Dr. E.O. Hartwig

NAVAL CENTER FOR SPACE TECHNOLOGY
Code 8000
P.G. Wilhelm

ORGANIZATIONAL CHART (Continued)
EXECUTIVE DIRECTORATE

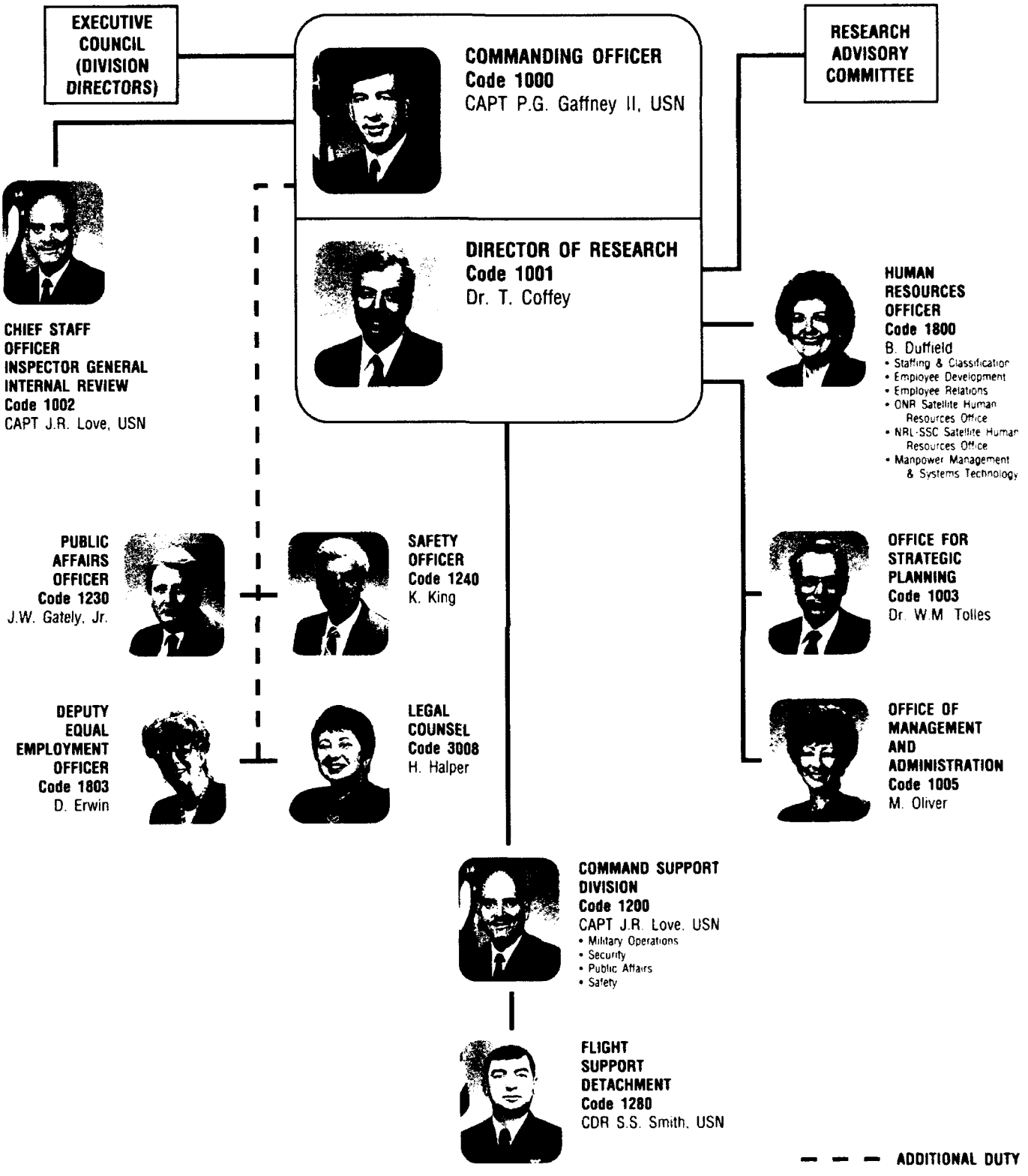

BUSINESS OPERATIONS DIRECTORATE
Code 3000
R.E. Doak

CONTRACTING DIVISION
Code 3200
J. Ely
- Policy & Analysis
- Contract Negotiations
- Acquisition Strategies/Training
- Advance Acquisition Planning
- Contractual Execution
- Contract Administration
- Acquisition Policy Interpretations & Implementation

FINANCIAL MANAGEMENT DIVISION
Code 3300
D.T. Green
- Budget
- Systems Operations
- Accounting
- Financial
- Disbursing

SUPPLY DIVISION
Code 3400
W.E. Ralls, Jr
- Purchasing
- Technical
- Customer Liaison
- Credit Card
- Material Control
- Supply Stores
- *Delivery & Storage*

RESEARCH AND DEVELOPMENT SERVICES DIVISION
Code 3500
D.K. Woodington
- Project Management
- Chesapeake Bay Detachment
- Operations
- Services
- Administrative
- Engineering

GENERAL SCIENCE AND TECHNOLOGY DIRECTORATE/ DEPUTY FOR SPACE SYSTEMS
Code 4000/1010
Dr. R.A. LeFande

CRITICAL TECHNOLOGY ASSESSMENT
Code 4003
L.M. Winslow

TECHNOLOGY BASE MANAGER
Code 4006
Dr. S. Sacks

SCIENTIFIC CONSULTANT/SDI
Code 4040
Dr. P. Mange

SIGNATURE TECHNOLOGY OFFICE
Code 4050
Dr. D.W. Forester

WARFARE SYS AND SENSORS RESEARCH DIRECTORATE
Code 5000
R.R. Rojas

TECI DIVI
Code
P. Ir
- Tect
- Pub
- Grat
- Syst

RAD
Code
Dr.
- Rad
- Adv
- Sea
- Tar
- der
- Aro

INFO
Code
Dr
- Nav
- Con
- Hun

OPT
Code
Dr
- Adv
- Apd
- Las
- Elec
- Det

TAC
Code
Dr
- OH
- EW
- Air
- Shi
- Int

RES
Code
R.F.
- So
- Us
- Co

UNI
DET
Coo
Dr.
- Ac
- Ac
- Te
- Mi

ORGANIZATIONAL CHART (Continued)

ARFARE SYSTEMS
D SENSORS
SEARCH
RECTORATE
de 5000
R. Rojas

TECHNICAL INFORMATION DIVISION
Code 5200
P. Imhof
- Technical Library/Software Support
- Publications
- Graphic Design Services
- Systems/Photographic

RADAR DIVISION
Code 5300
Dr. M.I. Skolnik
- Radar Analysis
- Advanced Radar Systems
- Search Radar
- Target Characteristics
- Identification Systems
- Airborne Radar

INFORMATION TECHNOLOGY DIVISION
Code 5500
Dr. R.P. Shumaker
- Navy Center for Applied Research in Artificial Intelligence
- Communication Systems
- Human-Computer Interaction
- Center for Computer High Assurance Systems
- Transmission Technology
- Advanced Information Technology

OPTICAL SCIENCES DIVISION
Code 5600
Dr. T.G. Giallorenzi
- Advanced Concepts
- Applied Optics
- Laser Physics
- Electro-optical Technology
- Optical Techniques

TACTICAL ELECTRONIC WARFARE DIVISION
Code 5700
Dr. J.A. Montgomery
- Off-Board Countermeasures
- EW Support Measures
- Airborne EW Systems
- Ships EW Systems
- Integrated EW Simulation

RESEARCH COMPUTATION DIVISION
Code 5800
R.F. Saenger
- Software
- User Services
- Computer Operations & Communications

UNDERWATER SOUND REFERENCE DETACHMENT
Code 5900
Dr. J.E. Blue
- Acoustical Materials & Transduction
- Acoustical Systems
- Technical Services
- Measurements

MATERIALS SCIENCE AND COMPONENT TECHNOLOGY DIRECTORATE
Code 6000
Dr. J.B. Rath

LABORATORY FOR THE STRUCTURE OF MATTER
Code 6030
Dr. J. Karle

CHEMISTRY DIVISION
Code 6100
Dr. J.S. Murday
- Chemical Dynamics & Diagnostics
- Materials Chemistry
- Surface Chemistry
- Navy Technology Center for Safety & Survivability

MATERIALS SCIENCE AND TECHNOLOGY DIVISION
Code 6300
Dr. D.U. Gubser
- Physical Metallurgy
- Materials Physics
- Composites & Ceramics
- Mechanics of Materials

LABORATORY FOR COMPUTATIONAL PHYSICS AND FLUID DYNAMICS
Code 6400
Dr. J.P. Boris
- Center for Reactive Flow & Dynamical Systems
- Center for Computational Physics Developments
- Reactive Flow Physics

CONDENSED MATTER AND RADIATION SCIENCES DIVISION
Code 6600
Dr. D.J. Nagel
- Radiation Effects
- Directed Energy Effects
- Surface Modification
- Dynamics of Solids
- Complex Systems Theory

PLASMA PHYSICS DIVISION
Code 6700
Dr. S. Ossakow
- Radiation Hydrodynamics
- Laser Plasma
- Charged Particle Physics
- Pulsed Power Physics
- Space Plasma
- Beam Physics

ELECTRONICS SCIENCE AND TECHNOLOGY DIVISION
Code 6800
Dr. G.M. Borsuk
- Nanoelectronics
- Solid State Devices
- Vacuum Electronics
- Microwave Technology
- Surface & Interface Sciences
- Electronic Materials

CENTER FOR BIO/MOLECULAR SCIENCE AND ENGINEERING
Code 6900
Dr. J. Schnur
- Biosystems
- Biosensors
- Advanced Materials

OCEAN AND
ATMOSPHE
AND TECHN
DIRECTORA
Code 7000
Dr. E.O. Ha

OCEAN AND ATMOSPHERIC SCIENCE AND TECHNOLOGY DIRECTORATE
Code 7000
Dr. E.O. Hartwig

SYSTEMS SUPPORT AND REQUIREMENTS
Code 7030/NRL-SSC
Dr. R.M. Root

ACOUSTICS DIVISION
Code 7100
Dr. D.L. Bradley
- Center for Environmental Acoustics
- Acoustic Signal Processing
- Physical Acoustics
- Acoustic Systems
- Ocean Acoustics
- Acoustic Simulation & Tactics

REMOTE SENSING DIVISION
Code 7200
Dr. K. Johnston
- Special Projects Office
- Radio/IR/Optical Sensors
- Remote Sensing Physics
- Imaging Systems & Research
- Remote Sensing Applications

OCEANOGRAPHY DIVISION
Code 7300/NRL-SSC
Dr. W.B. Moseley
- Ocean Dynamics & Prediction
- Ocean Sciences
- Small Scale Phenomenology
- Ocean Technology

MARINE GEOSCIENCES DIVISION
Code 7400/NRL-SSC
Dr. H.C. Eppert, Jr.
- Tactical Oceanography Warfare Support
- Marine Physics
- Seafloor Sciences
- Mapping, Charting, and Geodesy

MARINE METEOROLOGY DIVISION
Code 7500/NRL-MRY
Dr. J.B. Hovermale
- Support
- Prediction Systems
- Forecast Support

SPACE SCIENCE DIVISION
Code 7600
Dr. H. Gursky
- Office of Strategic Phenomena
- Engineering Management
- Ultraviolet Measurements
- X-Ray Astronomy
- Upper Atmosphere Physics
- Gamma & Cosmic Ray Astrophysics
- Solar Physics
- Solar Terrestrial Relationships
- E.O. Hulburt Center for Space Research

NAVAL CENTER FOR SPACE TECHNOLOGY
Code 8000
P.G. Wilhelm

SPACE SYSTEMS DEVELOPMENT DEPARTMENT
Code 8100
R.E. Eisenhauer
- SDI Office
- Mission Development
- Advanced Systems Technology
- Space Electronic Systems Development
- Command Control Communications Computers & Intelligence
- Space Applications

SPACECRAFT ENGINEERING DEPARTMENT
Code 8200
R.T. Beal
- Design Test & Processing
- Systems Analysis
- Control Systems

Contributions by Divisions, Laboratories, and Departments

Radar Division (Code 5300)

Beyond the Horizon Radar Technique
Edward E. Maine, Jr.
Polarimetric Radar Studies of Laboratory Sea Spikes
Mark A. Sletten, Dennis B. Trizna, and Jin Wu

Information Technology Division (Code 5500)

Tripod Operators for the Efficient Object Recognition
Frank J. Pipitone
Direct Manipulation in the Modern Cockpit: A "Workstation" with Multiple, Concurrent Tasks
James A. Ballas, Constance L. Heitmeyer, and Manual A. Pérez
A High-Fidelity Network Simulator for SDI
Edwin L. Althouse, Dennis N. McGregor, Radhakrishman R. Nair, and Stephen G. Batsell

Optical Sciences Division (5600)

Fiber-Optic Chemical Sensor for Copper(I) in Water
Kenneth J. Ewing, Ishwar D. Aggarwal, Angela M. Ervin, and Robert A. Lamontagne
Nanochannel Glass Technology
Ronald J. Tonucci and Anthony J. Campillo
Undersea Fiber-Optic Magnetometer System
Frank Bucholtz, Carl A. Villarruel, and Gary B. Cogdell

Tactical Electronic Warfare Division (Code 5700)

CRUISE_Missiles Electronic Warfare Simulation
Allen J. Goldberg and Robert J. Futato
Flying Radar Target (FLYRT) Technology Development
Kevin G. Ailinger, Harvey E. Chaplin, Kenneth G. Limparis, and Steven K. Tayman
Optimal Resource Allocation Using Genetic Algorithms
Karen E. Grant

Underwater Sound Reference Detachment (Code 5900)

Electroacoustic Transducer Transient Suppression
Jean C. Piquette
Development of Polyurethane/Epoxy Based Interpenetrating Polymer Networks for Damping Applications
Rodger N. Capps and Christopher S. Coughlin

The Laboratory for the Structure of Matter (Code 6030)

Opioid Peptides—X-ray Characterization of Two Potent Enkephalin Analogs
Judith L. Flippen-Anderson and Clifford George

Chemistry Division (Code 6100)

Ultrafast Photochemical Processes
Andrew P. Baronavski and Jane K. Rice
Chemical Adhesion Across Composite Interfaces
Arthur W. Snow and J. Paul Armistead
Fiber-Optic Chemical Sensor for Copper(I) in Water
Kenneth J. Ewing, Ishwar D. Aggarwal, Angela M. Ervin, and Robert A. Lamontagne

Materials Science and Technology Division (Code 6300)

Ultrathin Magnetic Film Research at NRL
James J. Krebs
Communicating with Chaos
Thomas L. Carroll and Louis M. Pecora
Development of New Concepts for Fatigue Crack Thresholds
Kuntimaddi Sadananda and A.K. Vasudevan
Utilization of Empty Space to Enhance Material Properties
M. Ashraf Imam, Virgil Provenzano, and Kuntimaddi Sadananda

Laboratory for Computational Physics and Fluid Dynamics (Code 6400)

Numerical Simulation of Bubble-Free Surface Interaction
Mark H. Emery and Jay P. Boris
An Efficient Method for Solving Flows Around Complex Bodies
Alexandra M. Landsberg and Jay P. Boris

Condensed Matter and Radiation Sciences Division (Code 6600)

Nanocapillarity in Fullerine Tubules
Jeremy Q. Broughton and Mark R. Pederson
Risk Assessment and Directed Energy Weapons
Arthur I. Namenson, Terence J. Wieting, and Nathan Seeman
Intermolecular Vibrational Dynamics in Liquids
Dale P. McMorrow and Joseph S. Melinger

Plasma Physics Division (Code 6700)

A Plasma Mirror for Microwaves
Anthony E. Robson, Wallace A. Manheimer, and Robert A. Meger
Earth's Magnetospheric Field Lines
Joel A. Fedder, Steven P. Slinker, John G. Lyon, and Clark M. Mobarry

Electronics Science and Technology Division (Code 6800)

The Mechanisms of Visible Photoluminescence in Porous Silicon
S.M. Prokes and O.J. Glembocki
Superconductivity of Layered Superconductors: An Interlayer Coupling Model
Attipat K. Rajagopal

Center for Bio/Molecular Science and Engineering (Code 6900)

Neuronal Patterning
David A. Stenger

Acoustics Division (Code 7100)

Trans-Oceanic Acoustic Propagation and Global Warming
B. Edward McDonald, William A. Kuperman, Michael D. Collins, and Kevin D. Heaney
BiKR—A Range-Dependent, Normal-Mode Reverberation for Model for Bistatic Geometries
Stephen N. Wolf, David M. Fromm, and Bradley J. Orchard
Predicting Acoustic Signal Distortion in Shallow Water
Robert L. Field and James H. Leclere

Remote Sensing Division (Code 7200)

Real-Time SAR Processing for Polar Ice Applications and Research
Igor Jurkevich, Chung S. Lin, and Stephen A. Mango

Oceanography Division (Code 7300)

Ocean Wavenumber Spectra Measurements
Jack A.C. Kaiser and Gloria J. Lindemann

Marine Geosciences Division (Code 7400)

Airborne Electromagnetic Hydrographic Techniques
Edward C. Mozley, Timothy N. Kooney, and Daniel E. Fraley

The U.S. Navy's Compressed Aeronautical Chart Database
Maura C. Lohrenz

Marine Meteorology Division (Code 7500)

Numerical Modeling of the Atmosphere and Ocean
Richard M. Hodur

Space Science Division (Code 7600)

NRL's Oriented Scintillation Spectrometer Experiment on NASA's Compton Gamma Ray Observatory
James D. Kurfess and W. Neil Johnson
Energetic Radiation from Black Holes
Charles D. Dermer

Space Systems Development Department (Code 8100)

The High Temperature Superconductivity Space Experiment (HTSSE)
Amey R. Peltzer, Christopher L. Lichtenberg, and George E. Price
Satellite Laser Ranging for Platform Position Determination and Ephemeris Verification
G. Charmaine Gilbreath, James E. Pirrozoli, Thomas W. Murphy, Wendy L. Lippincott, and William C. Collins

Spacecraft Engineering Department (Code 8200)

Parallel Processing for Space Surveillance
Liam M. Healy and Shannon L. Coffey

Employment Opportunities for Entry-Level and Experienced Personnel

The *NRL Review* illustrates some of the exciting science and engineering carried out at NRL as well as the potential for new personnel.

The Naval Research Laboratory offers a wide variety of challenging positions that involve the full range of work from basic and applied research to equipment development. The nature of the research and development conducted at NRL requires professionals with experience. Typically, there is a continuing need for electronics, mechanical, aerospace, ceramic, and materials engineers; metallurgists and oceanographers with bachelor's and/or advanced degrees; and physical and computer scientists with Ph.D. degrees. Opportunities exist in the areas described below.

Ceramic Engineers and Materials Scientists/Engineers. These employees are recruited to work on materials, microstructure characterization, electronic ceramics, solid-state physics, fiber optics, electro-optics, microelectronics, fracture mechanics, vacuum science, laser physics technology, and radio frequency/microwave/millimeter wave/infrared technology.

Electronics Engineers and Computer Scientists. These employees may work in the areas of communications systems, electromagnetic scattering, electronics instrumentation, electronic warfare systems, radio frequency/microwave/millimeter wave/infrared technology, radar systems, laser physics technology, radiowave propagation, electron device technology, spacecraft design, artificial intelligence, information processing, signal processing, plasma physics, vacuum science, microelectronics, electro-optics, fiber optics, solid state, software engineering, computer design/architecture, ocean acoustics, stress analysis, and expert systems.

Mechanical Engineers. These employees may be assigned to spacecraft design, remote sensing, propulsion, experimental fluid mechanics, experimental structural mechanics, solid mechanics, elastic/plastic fracture mechanics, materials, finite-element methods, nondestructive evaluation, characterization of fracture resistance of structural alloys, combustion, and CAD/CAM.

Chemists. Chemists are recruited to work in the areas of combustion, polymer science, bioengineering and molecular engineering, surface science, materials, fiber optics, electro-optics, microelectronics, electron device technology, and laser physics.

Physicists. Physics graduates may concentrate on such fields as materials, solid-state physics, fiber optics, electro-optics, microelectronics, vacuum science, plasma physics, fluid mechanics, signal processing, ocean acoustics, information processing, artificial intelligence, electron device technology, radiowave propagation, laser physics, ultraviolet/X-ray/gamma ray technology, electronic warfare, electromagnetic interaction, communications systems, radio frequency/microwave/millimeter wave/infrared technology, and computational physics.

Oceanographers, Meteorologists, and Marine Geophysicists. These employees work in the areas of ocean dynamics, air-sea interaction, upper ocean dynamics, oceanographic bio-optical modeling, ocean and atmosphere numerical modeling and prediction, artificial intelligence applications for satellite analysis, benthic processes, aerogeophysics, marine sedimentary processes, and advanced mapping techniques. Oceanographers and marine geophysicists are located in Washington, DC, and the Stennis Space Center, Bay St. Louis, Mississippi.

Meteorologists are located in Washington, DC, and Monterey, California.

FOR FOREIGN NATIONALS

U.S. citizenship is required for employment with NRL.

APPLICATION AND INFORMATION

Interested applicants should submit an Application for Federal Employment (SF-171), which can be obtained from local offices of the Office of Personnel Management and personnel offices of Federal agencies, to the address below.

Direct inquiries to:

Naval Research Laboratory
Civilian Personnel Division, Code 1812 RV 93
Washington, DC 20375-5324
(202) 767-3030

Location of NRL in the Capital Area

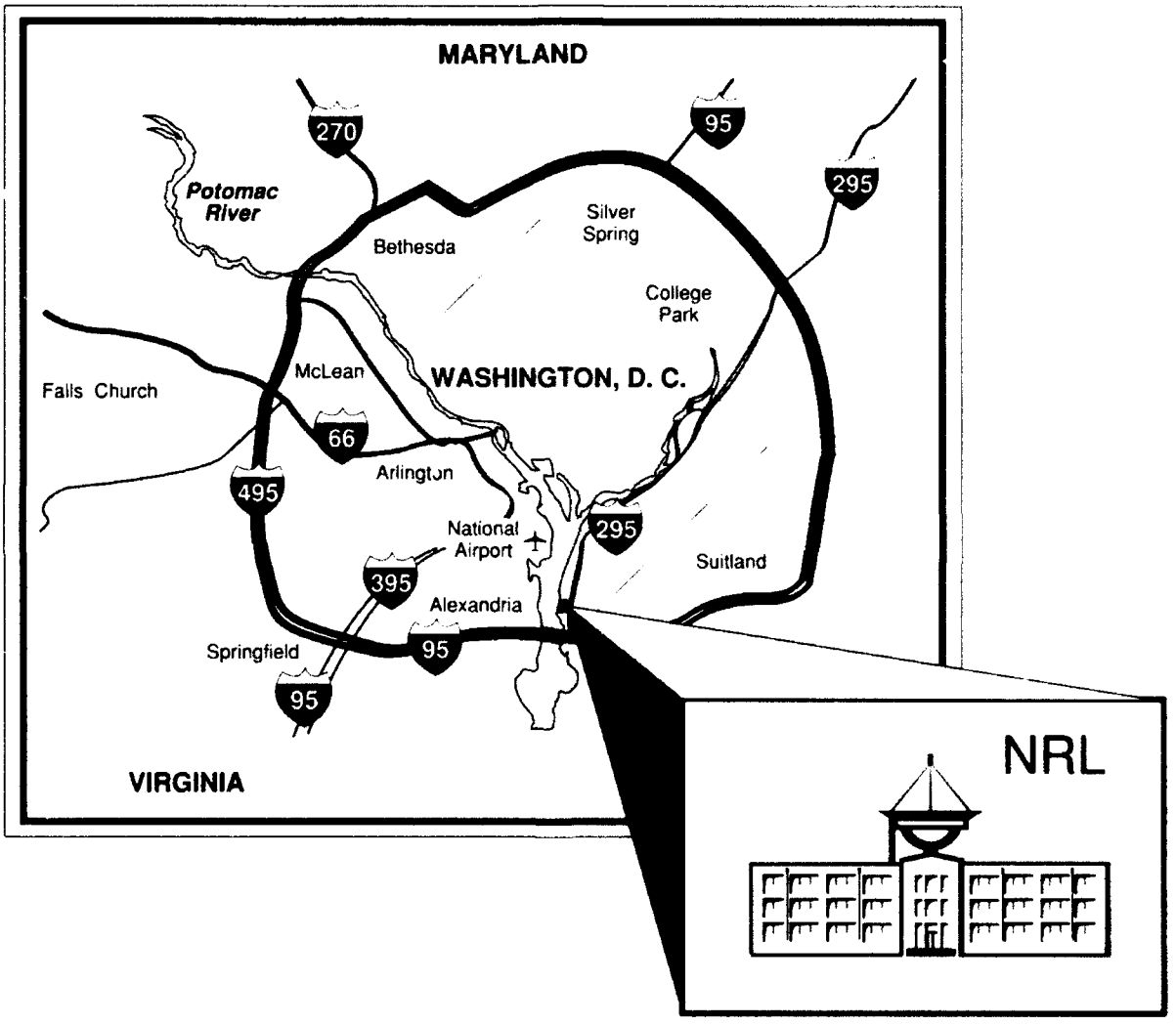

Subject Index

Author Index

NRL Review Staff

Senior Science Editor: Dr. John D. Bultman
Senior TID Editor: Beba Zevgolis
TID Consultants: Kathleen Parrish and Patricia Staffieri

Graphic design: Tazewell Rufty

Graphic support: Susan Guilmineau, Carol Hambric, Micheal McMullin, and Jan Morrow

Photographic production: Richard Bussey, Gayle Fullerton, James Marshall, Chris Morrow, Barbara Padgett, Ray Reynolds, Michael Savell, Christine Savoy, and Paul Sweeney

Computerized composition and design production: Donna Gloystein, Judy Kogok, and Dora Wilbanks

Editorial assistance: Irene Barron, Maureen Long, Saul Oresky, Kathleen Parrish, Patricia Staffieri, and David van Keuren

Production coordination: Timothy Calderwood

Production assistance: Rosie Bankert, Diltricia Montgomery, and Leona Sprankel

Distribution: Joyce Harris and Barbara Jolliffe

Head, Technical Information Division: Peter H. Imhof

Further Information: Information on the research described in this *NRL Review* may be obtained by contacting Dr. Richard Rein, Head, Technology Transfer and Special Programs, Code 1003.1, (202) 767-3744. General information about NRL may be obtained from the Public Affairs Office, Code 1230, (202) 767-2541. The sources of information on the various nonresearch programs at NRL are listed in the *NRL Review* chapter entitled "Programs for Professional Development."

The NRL *Fact Book* gives details about the Laboratory and its operations. It lists major equipment, current fields of research, field sites, and outlying facilities. It also presents information about the responsibilities, organization, key personnel, and funding. A copy may be obtained by contacting the Technical Information Division, Publications Branch, Code 5231, (202) 767-2782.

REVIEWED AND APPROVED
May 1993

Paul G. Gaffney II
Captain, USN
Commanding Officer